INVESTIGATION OF THE SAFETY PROFILE OF POLYMERIC NANOMEDICINES *IN VITRO* VIA ASSESSMENT OF MACROPHAGE AND HEPATOCYTE RESPONSES

Leagh G. Powell

Submitted for the degree of Doctor of Philosophy

Heriot-Watt University
Institute of Biological Chemistry, Biophysics and Bioengineering
Engineering and Physical Sciences
April 2019

Abstract

Nanoparticles (NPs) can be used in clinical applications (e.g. for drug delivery or bioimaging) in order to better treat and diagnose disease. Many nanomedicines are made from polymers, and improvements in polymer NP synthesis methods have made it easier to design and synthesise complex and diverse polymer NPs (PNPs) for clinical use. However, investigation into PNP safety has lagged behind their development, resulting in uncertainties regarding the safety of these PNPs. *In vitro* studies conducted to date have focused on assessment of cytotoxicity and cytokine production to screen the toxicity of nanomedicines.

Micelles are one of the most attractive PNPs for medical use as they have a hydrophobic core that can carry cargo and a hydrophilic shell that interacts with the exterior environment. A panel of micellar PNPs of varying complexity were selected for investigation in this study. In the first instance, a novel polymer was used to generate poly (decamethylene succinate-co-pheylsuccinate) (PDP) NPs to investigate the influence of an adsorbed pluronic acid (PF68) coating on the toxicity of NPs. Next, the impact of poly-lactic-co-glycolic acid (PLGA) chain length (4K, 15K and 55K) on PNP toxicity was investigated. Finally, the toxicity of redox-reactive (RR)-NPs, composed from PLGA, was compared to NPs which lacked this element (nRR-NP). All NPs tested had a polyethylene glycol (PEG) element in the shell.

PNP safety was investigated via assessment of cytotoxicity, cytokine production, cellular uptake, genotoxicity, reactive oxygen species (ROS) production, urea and albumin production and intracellular calcium concentration ($[Ca^{2+}]_i$). The toxicity of the PNP panel to the C3A hepatocyte cell line was assessed *in vitro* as it is established that NPs administered via various routes (e.g. inhalation, ingestion, intravenous injection) accumulate in the liver.

There was little to no cytotoxicity observed for all PNPs. Uptake of the PDP NPs by C3A cells was greatest, but low for 4K, 15K, 55K, RR and nRR NPs. PDP-PF68 PNPs and nRR-NPs induced genotoxicity via an oxidative mechanism, whereas the other NPs did not. Production of the anti-inflammatory cytokine interleukin (IL)-1ra, was elevated. No change in the production of the other cytokines (e.g. IL-8. Tumour necrosis factor

(TNF)α, IL-1β) was observed. ROS production was elevated by all PNPs investigated. Liver-specific markers of toxicity (urea and albumin production) were decreased for all PNPs investigated, with the greatest effect observed for nRR-NPs. A slight increase in $[Ca^{2+}]_i$ was observed for cells exposed to RR-NPs.

The findings obtained allowed the physicochemical properties of the PNPs which conferred toxicity to be identified; this can inform the design of PNPs in the future. More specifically, the addition of a PF-68 shell or a redox-responsive linker increased the safety of the PNPs. However, increasing chain length enhanced PNP toxicity. This study could also aid in developing evidence-based *in vitro* approaches to screen PNP safety, and therefore contribute to the development of a tiered testing strategy to facilitate assessing the toxicity of future generations of PNPs. By using a battery of tests to screen the toxicity of the PNP panel in this study a comprehensive assessment of PNP safety was performed, and the findings provided insight into their mechanism of action.

Acknowledgements

I would like to sincerely thank my supervisor, Dr Helinor Johnston, without her patience, encouragement and support I would not have been able to have completed my PhD. I'd also like to thank Prof Vicki Stone for her positivity and support. Both my supervisors have been amazing role models for what women in science can achieve. I would especially like to thank Dr David Brown for all the help he provided to me and countless other students , he is one of a kind. I would also like to thank and acknowledge the James Watt Scholarship whose funding has made this research project possible.

I would like to thank, my collaborators who have provided enthusiasm and support including Prof Cameron Alexander, Dr Claudia Conte and Dr Deepak Kakde from the University of Nottingham, as well as Dr Lea Ann Dailey and Dr Thais Fedatto Abelha from King's College London, you have all provided me with inspiration to look further.

There are many people in EPS and EGIS I would like to thank for their ear, support and an endless supply of coffee, without these fantastic people this time would not have been half as fun. I'd like to especially thank the Nano lunch crew for a lot of 'interesting' conversations and laughs.

I would like to thank my parents, Tina and Emmet, for their much needed and valued support and belief though out my long long education, I am sure we owe Antony a lot. Of course, I'd like to thank my husband Mitch, who has supported me with kindness and time to take this chance with a dream, I am forever grateful. I would like to thank all my oldest friends that have been with me throughout this time with a calming word and a cold beverage Anna, Sarah, Tara, Carolyne and Ciara. I am so lucky to have you all in my life.

"Sometimes the fall kills you. And sometimes, when you fall, you fly."-Neil Gaiman

ACADEMIC REGISTRY

Research Thesis Submission

Name*:*	Leagh Powell		
School:	EPS		
Version:	Final submission	Degree Sought:	Doctor of Philosophy

Declaration

In accordance with the appropriate regulations, I hereby submit my thesis and I declare that:
1) the thesis embodies the results of my own work and has been composed by myself
2) where appropriate, I have made acknowledgement of the work of others and have made reference to work carried out in collaboration with other persons
3) the thesis is the correct version of the thesis for submission and is the same version as any electronic versions submitted*.
4) my thesis for the award referred to, deposited in the Heriot-Watt University Library, should be made available for loan or photocopying and be available via the Institutional Repository, subject to such conditions as the Librarian may require
5) I understand that as a student of the University I am required to abide by the Regulations of the University and to conform to its discipline.
6) I confirm that the thesis has been verified against plagiarism via an approved plagiarism detection application e.g. Turnitin.

** Please note that it is the responsibility of the candidate to ensure that the correct version of the thesis is submitted.*

Signature of Candidate*:*		Date	

Submission

Submitted By *(name in capitals):*	LEAGH POWELL
Signature of Individual Submitting:	
Date Submitted:	

For Completion in the Student Service Centre (SSC)

Received in the SSC by *(name in capitals):*			
Method of Submission *(Handed in to SSC; posted through internal/external mail):*			
E-thesis Submitted (mandatory for final theses)			
Signature:		Date:	

Table of Contents

List of Figures

Table of Tables

Abbreviations

AB	Alamar Blue
Ag	Silver
ANOVA	Analysis of variance
Au	Gold
BUN	Blood urea nitrogen
$[Ca^{2+}]_i$	Intracellular calcium concentration
CFDA-AM	AM (5-Carboxyfluorescein Diacetate, Acetoxymethyl Ester)
CLF	Cholyl lysyl fluorescein
CN-PPV	poly(2,5-di(hexyloxy) cyanoterephthalylidene)
CO_2	Carbon dioxixde
CuO	Copper oxide
DCFH-DA	2', 7'-Dichlorodihydrofluorescein diacetate
DiL	1,1′- dioctadecyl-3,3,3′,3′-tetramethyl indocarbocyanine perchlorate
DiO	3,3'-dioctadecyloxacarbocyanine perchlorate
DLS	Dynamic light scattering
DMSO	Dimethyl sulfoxide
DPH	Dose per hepatocyte

EC_{20}	Effective concentration where 20% of cells die
EDTA	Ethylenediaminetetraacetic acid
EGFR	Epidermal growth factor receptor
ELISA	Enzyme-linked immunosorbent assay
EMA	European Medicine Agency
Ex/Em	Excitation/emission
FBS	Foetal bovine serum
FDA	The Food and Drug Administration
Fe_3O_4	Iron(II, III) oxide
FLARE	Fragment length analysis using repair enzymes
Fpg	Formamidopyrimidine DNA glycosylase
GPx	Glutathione peroxidase
Gro-α	Growth-regulated α
GSH	Glutathione
H_2O_2	Hydrogen peroxide
HBSS	Hanks Balanced Salt Solution
HEPES	4-(2-hydroxyethyl)-1-piperazineethanesulfonic acid)
IL-1ra	IL-1 receptor antagonist
IL-6/8/1/1β	Interleukin-6/8/1/1β
KC	Keratinocyte chemoattractant
LPS	Lipopolysaccharide
MCP-1	Monocyte chemoattractant protein 1
MDA	Malondialdehyde
MEM	Minimum Essential Medium
MFSD	Microfluidic solvent displacement
MnSOD	Mitochondrial antioxidant manganese superoxide dismutase
MTS	3-(4,5-dimethylthiazol-2-yl)-5-(3-carboxymethoxyphenyl) -2-(4-sulfophenyl)-2H-tetrazolium)
MTT	3-(4,5-dimethylthiazol-2-yl)-2,5-diphenyltetrazolium bromide
ND	Non-detectable
NPs	Nanoparticles
NR	Neutral Red
nRR-NPs	Non-redox reactive NPs

PAMAM	Polyamidoamine
PBMC	Peripheral blood mononuclear cells
PBS	Phosphate-buffered saline
PDP	poly (decamethylene succinate-co-pheylsuccinate)
PDI	Polydispersity index
PEG	Polyethene glycol
PEI	Polyethyleneimine
PEO	Poly (ethyl oxide)
PF68	Pluronic F68
PFR	Phenol red free
PLA	Poly(dl-lactide)
PLGA	Poly-lactic-co-glycolic acid
PNP	Polymeric NP
PPE	Poly(2,5-di(3′,7′-dimethyloctyl) phenylene-1,4-ethynylene)
PPO	Propyl oxide
QD	Quantum dots
RES	Reticuloendothelial system
ROS	Reactive oxygen species
RR-NPs	Redox reactive NPs
RT	Room temperature
SCM	Standard curves midpoint
SEM	Standard error mean
SiO_2	Silicon dioxide
SOD	Superoxide dismutase
TDA	Total dose administration
TDAI	Total dose administered per individual
TEM	Transmission electron microscopy
THF	Tetrahydrofuran
TiO_2	Titanium dioxide
TNF-α	Tumour necrosis factor alpha
UFCB	Ultrafine carbon black
(v/v)	Volume (of solute) per volume (of solvent)
ZnO	Zinc oxide

3Rs	Replace, refine, reduce
4K NPs	PEG2K-PLGA4K
15K NPs	PEG2K-PLGA15K
55K NPs	PEG5K-PLGA55K

Publications

•Kermanizadeh A, Powell LG, Stone V, Møller P. Nano delivery systems and stabilized solid drug nanoparticles for orally administered medicine – current landscape International Journal of Nanomedicine 2018 (Accepted for publication).

•Kakde D*, Powell LG*(* joint first authors), Bansal KK, Howdle S, Irvine D, Mantovani G, Millar G, Dailey LA, Stone V, Johnston HJ, Alexander C. Synthesis, characterization and evaluation of in vitro toxicity in hepatocytes of linear polyesters with varied aromatic and aliphatic co-monomers. J Control Release. 2016. pii: S0168-3659(16)30504-1.

•Boyles MSP, Powell LG, Kermanizadeh A, Johnston HJ, Rothen-Rutishauser B, Stone V, Clift MJD. An overview of nanoparticle biocompatibility for their use in nanomedicine, in pharmaceutical nanotechnology: innovation and production. 2016. Wiley-VCH Verlag GmbH & Co. KGaA, Weinheim, Germany.

Conference presentations

•Powell LG, Conte C, Monteiro P, Alexander C, Stone V and Johnston HJ. An *in vitro* investigation of redox reactive polymer nanoparticle safety using macrophage and hepatocyte cell lines. European Nanomedicine Meeting 2017. Poster, Kings College London.

•Powell LG, Kakde D, Alexander C, Stone V and Johnston HJ. An *in vitro* investigation of novel polymer nanoparticles safety using a macrophage cell line. Academy of Pharmaceutical Sciences Conference 2016. Poster, Strathclyde University, Glasgow.

•Oral: Powell LG, Kakde D, Alexander C, Stone V and Johnston HJ Are plastic nanomedicines safe? Imaging's Got Talent 2016 IGMM. Prize won for oral presentation 2016, The University of Edinburgh.

•Powell LG, Kakde D, Alexander C, Stone V and Johnston HJ. An in vitro investigation of polymer nanoparticle safety using a hepatocyte cell line Scottish Microscopy Group Symposium 2016. Poster, Heriot Watt, Edinburgh.

•Powell LG, Johnston HJ and Stone V. Investigating cytotoxicity and cellular uptake of polymer nanomedicines in hepatocytes in vitro. Postgraduate Research Conference, Heriot Watt 2015. Poster, Heriot Watt, Edinburgh.

Chapter 1. Introduction

1.1 Nanoparticles and nanomedicines

Engineered nanoparticles (NPs) are defined as a population of particles where 50% or more have one or more dimension in the nanoscale (1-100 nm) (Potočnik 2011). NPs are currently being used in many different industries including electronics, cosmetics, food and pharmaceuticals (Lin et al. 2006; Erickson 2009; Kong et al. 2011; Athinarayanan et al. 2014). With growing use and exposure to NPs, a comprehensive understanding of their impacts on human health and the environment is required (Donaldson et al. 2004; Maynard et al. 2006; Oberdörster et al. 2007; Maynard & Aitken 2016). The properties of NPs can be strikingly altered compared to those observed for the bulk material they are composed from, allowing NPs to have new and useful properties which as exploited by industry (Edwards-Jones 2009; Zhang et al. 2016).

The low solubility, instability and untargeted nature of many pharmaceuticals such as chemotherapies can make it challenging to administer them without adverse (side) effects (Guo et al. 2011; Li et al. 2014). Therefore, there is a call for new and improved drug delivery systems that can contain these challenging cargos as well as target their delivery to specific diseased cells. Nanomedicine is an exciting, relatively new field that uses NPs for medical applications and has the potential to address unmet clinical needs in diagnosing and treating a wide range of diseases (Fangueiro et al. 2015). Indeed, it is hoped that NPs can provide improved efficacy and targeting of pharmaceuticals, while decreasing adverse effects (Chen et al. 2001; Constantin et al. 2017).

However, investigations into NP safety have lagged behind NP production. As a result, many uncertainties linger regarding the potential adverse health effects of these materials. Nanotoxicology investigates the potential detrimental impacts of NPs on human health and the environment (Donaldson et al. 2004; Maynard et al. 2006; Oberdörster et al. 2007; Maynard & Aitken 2016). The uncertainty regarding NP toxicity can result in industries finding it difficult to assess NP safety (Kermanizadeh et al. 2015).

1.2 Designing nanomedicines

When designing a NP for medical use, physiochemical characteristics can be selected that could aid in achieving the desired clinical outcome. However, the physicochemical properties of NPs (e.g. composition, shape, size, charge and surface properties) also influence their toxicity (Hoshino et al. 2012). It is therefore important to understand which physicochemical properties influence the toxicity of nanomedicines. Accordingly, the physicochemical properties of NPs are commonly characterised in parallel to NP hazard assessments.

A decrease in NP size can result in a larger surface-to-volume ratio, as the rate of reactions can depend on surface area, an increase in area could increase the probability of chemical interactions, therefore potentially increasing surface reactivity; this can give NPs desirable qualities such as increased interaction with target cells and therefore improved cellular targeting and internalisation (Win & Feng 2005). However, the same characteristics that make NPs appealing for medical applications can contribute to their toxicity. For example, silver (Ag) NPs have been used successfully to inhibit bacterial growth and have great potential for use in wound dressings (Rennukka et al. 2014). However, previous *in vitro* research has observed that a decrease in the size of Ag NPs (4.7 to 42 nm) can result in an increase in cell death in hepatoma and leukaemia cells (Avalos et al. 2014).

Also, a NP's surface charge can help overcome the challenge of cellular internalisation of low solubility, unstable medical treatments. Previously a positively charged tri bock polymeric NP (PNP), meaning it is composed of 3 blocks (lengths) of connection polymers, poly(ethylene glycol)-block-poly(e-cap-rolactone)-block-poly(2-aminoethyl ethylene phosphate) has been shown to have increased cellular uptake compared with neutral or negatively charged PNPs and therefore, has the potential to be utilised in the delivery of negatively charged genetic material such as small interfering RNA for the treatment of cancer (Mao et al. 2011). However positively charged NPs had been observed to elicit higher levels of toxicity than neutral or negative NPs. For example, positively charged NPs were more toxic to human brain cells (1321N1) *in vitro* which could hinder their medical usefulness (Bexiga et al. 2014).

NPs can differ in shape, such as spheres, nanotubes or rods (Boyles et al. 2015; Sato et al. 2017). Previously, spherical gold (Au) NPs have been observed to be internalised by cervical cancer cells (HeLa) more readily than rod-shaped Au NPs of a similar size (Chithrani et al. 2006). This pattern of preferential NP uptake has led to many NPs for medical use being spherical (Zhang & Eisenberg 1995; Li et al. 2011).

Nanomedicines are a diverse population of materials, with NPs composed of lipids, polymers, metals and metal oxides (Haldemann et al. 1995; Seyednejad et al. 2011; Hutter & Maysinger 2013; Bozzuto & Molinari 2015; Liu et al. 2016). The composition of NPs can influence their toxic potency. For example, previous research using human neutrophils cells (HL60) comparing the toxicity of a panel of NPs including titanium dioxide (TiO_2) NPs and zinc oxide (ZnO) NPs of similar size range and shape showed that composition was capable of influencing toxicity, with TiO_2 eliciting lower toxicity, as observed in previous studies using different endpoints (Joshi-Barve et al. 2007; Kermanizadeh et al. 2013; Johnston et al. 2015)

Liposomes are spherical NPs composed of a phospholipid bilayer similar to that of the cell's membrane (Bozzuto & Molinari 2015). Doxil, a liposomal NP, was one of the first nanomedicines to gain approval over 2 decades ago from the Food and Drug Administration (FDA) of the United States of America. This liposome NP encapsulates the chemotherapeutic doxorubicin. Doxil has successfully been used in the treatment of ovarian cancer and has shown increased site-specific delivery as well as decreased toxicity when compared to doxorubicin in a non-nano form (James et al. 1994).

1.3 Polymer nanomedicines

Thanks to improvements in controlled polymer synthesis techniques, it has become easier to design a range of polymers such as polyesters, polyethers or polyamides for clinical use. Polymers are made up of repeating monomers that can either all be the same to form homopolymers such as polyethene glycol (PEG) or Poly(lactide) PLA, or a combination of these units can be generated to produce heteropolymers such as poly-lactic-co-glycolic acid (PLGA) (Menemse 1999; De Oliveira Tiera et al. 2010). The unique characteristics

and freedom in the design process of PNPs makes them an attractive candidate to generate simple and complex NPs for drug delivery and diagnostics for diseases such as arthritis and cancer (Wuelfing et al. 1998; Peracchia et al. 1999; Kanaras et al. 2002; Koole et al. 2008; Muthu et al. 2014; Niemirowicz et al. 2016).

Increasing interest in PNPs is also attributed to PNPs having several factors that are useful for medical applications including biocompatibility; biodegradability; increased circulation time and an ability to protect sensitive or challenging to formulate cargo (Conde et al. 2014). Additionally, PNPs are relatively quick and inexpensive to produce, leading to the rapid development of a diverse array of PNPs.

In nanomedicine, when using polymer-based NPs, micellar PNPs are predominantly utilised. Micelles are formed when copolymers, composed of two or more different polymers, are added to an aqueous solution. These NPs self-assemble into spherical NPs with a core-shell structure, where the hydrophobic portion of the polymer is driven inside the micelle to form the core and the hydrophilic portion faces the outside to form the shell. When hydrophobic therapeutics such as low solubility drugs are present in the aqueous solution, these will become trapped at the core of these PNPs (Figure 1.1) (Kataoka et al. 2001; Kim et al. 2010; Pamujula et al. 2012). The preparation of micellar NPs can be relatively quick, cost-effective and straightforward (Mura & Couvreur 2012; Hare et al. 2017). A potential advantage of loading drugs within the core of a micellar PNP, is that the toxicity of the administrable drug may be decreased, for example, formulations of paclitaxel as a free drug usually requires excipients. However, the excipient Cremophor used to formulate free drug paclitaxel into Taxol™ can elicit toxicity, while the paclitaxel-containing PNPs do not require Cremophor and has been shown to elicit lower adverse effects *in vivo* (Kim et al. 2007).

The first and currently only micelle PNP to be approved by the FDA, Estrasorb (over 15 years ago), is a micellar NP used to encapsulate the pharmaceutical, Estrodiol, a menopause hormone therapy (Simon et al. 2006). However, the translation of nanomedicines from preclinical development to medical use has been slow (Maynard & Aitken 2016). Over 2210 patents have been applied for, and 320 nanoforms are in clinical trial. However, only 25 clinical trials for NPs have progressed beyond small-scale safety

focused trials, also known as phase I trials (epo.org, clinicaltrials.gov). Additionally, it can be challenging to upscale the production of PNPs for use in the pharmaceutical industry due to multiple chemical reactions and purification steps required, making upscaling PNP production time and resource consuming (Lammers et al. 2012). Also, PNP production can have a large number of variables that affect size or stability such as the specific polymer used; preparation method or storage conditions, therefore possibly leading to batch to batch variation (Sharma et al. 2015). These factors may make it difficult to produce the uniform PNPs that are required for consistent medical outcomes and to conform to appropriate regulations (EMA 2013a; EMA 2013b; Hatton et al. 2014).

Nanomedicine toxicity studies commonly compare the free cargo to the cargo within the NPs, but often fail to investigate the toxicity associated with the NP delivery system alone or with a non-medical cargo such as a dye (Yoo & Park 2001; Khalil et al. 2013; Arunkumar et al. 2015; Vasconcelos et al. 2015; Jin et al. 2017; Radwan et al. 2017). Therefore, it is essential to fill this knowledge gap. This is especially relevant for *in vivo* studies where there has been limited investigation of the toxicity of PNPs such as PLGA-PEG NPs not containing drugs or therapeutic genetic material (Lin et al. 2016).

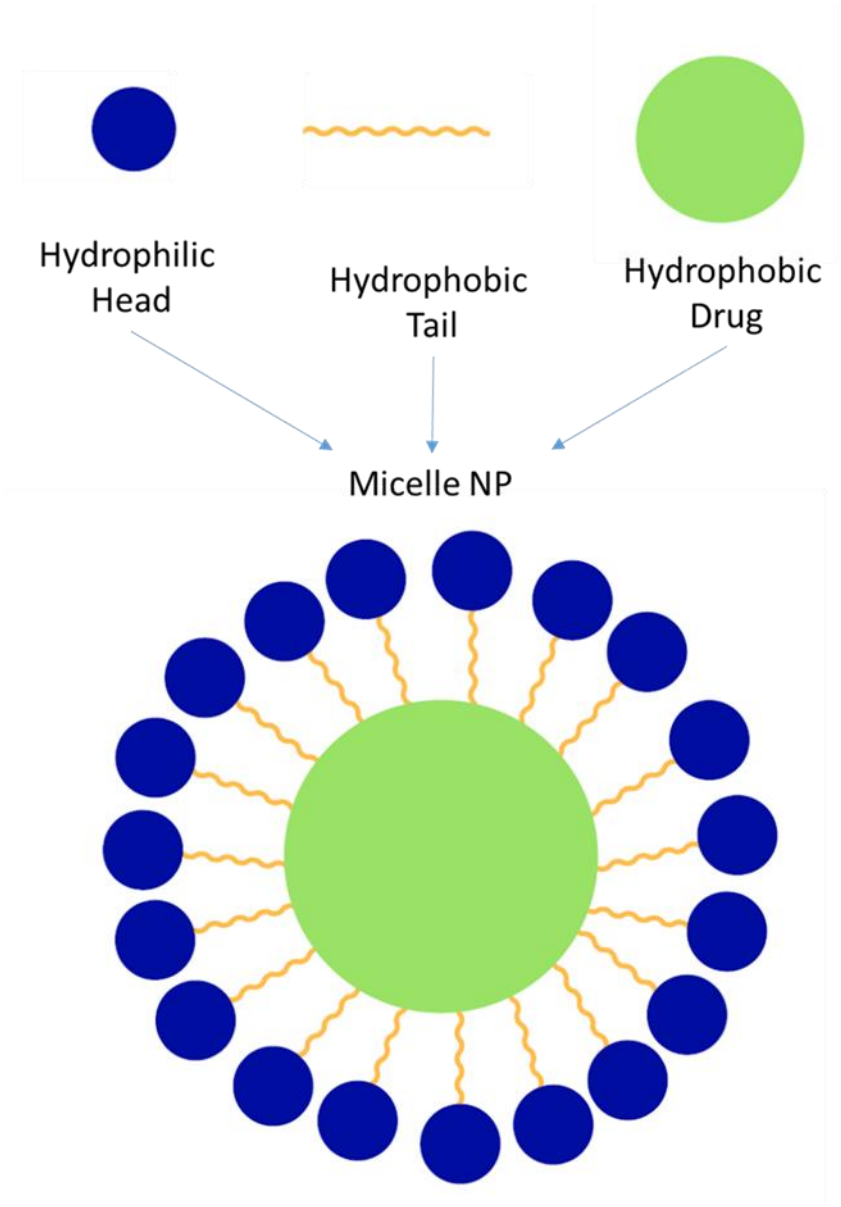

Figure 1.1 Micelle NP.

Representation of polymer micellar NP used in nanomedicine made up of polymer consisting of hydrophilic head (blue) and hydrophobic tail (orange) containing hydrophobic drug as the cargo (green).

1.4 Passive and active targeted nanomedicines

Although NPs have the potential to treat many diseases, cancer treatment has been the focus of many nanomedicines, to date. This focus on cancer may be in part attributed to the enhanced permeability and retention (EPR) effect, where the leaky vasculature of tumours allows NPs under 200 nm to passively target cancer cells (Matsumura & Maeda 1986; Yokoyama et al. 1990; O'Neal et al. 2004). Indeed, the EPR effect has been exploited with clinically approved PNPs, such as intravenously administered Genexol, a copolymer of PEG and PLA to deliver the broad-spectrum chemotherapy Paclitaxel (Werner et al. 2013).

Active targeting can be achieved via functionalisation of the NP surface, for example with peptides or antibodies. The epidermal growth factor receptor (EGFR) is overexpressed on tumour cells making it a promising target for nanomedicines (Laskin & Sandler 2004). In previous studies to promote targeted delivery of the chemotherapeutic, doxorubicin PLGA–PEG NPs were conjugated to a peptide that targets the EGFR. When ovarian adenocarcinoma cells (SKOV) were exposed to these PNPs; cellular uptake increased 300% compared to PLGA-PEG NPs lacking the peptide (Hou et al. 2011). Furthermore, in 2013, the federal agency in the United States of America that is responsible for health and human services, the food and drug administration (FDA) approved Kadcyla, a PNP with a monoclonal antibody for EGFR-2 on its surface. These antibodies target metastatic breast cancer cells over-expressing EGFR-2 to deliver therapy directly to the diseased cell, reducing widespread damage to healthy cells (Chung et al. 2014; Weissig et al. 2014).

1.5 Controlled targeting of nanomedicines

PNPs can be generated that release their cargo in response to one or several intracellular or extracellular stimuli such as temperature, pH or redox potential (Han et al. 2015; Constantin et al. 2017; Yeh et al. 2018). Previously PEGylated liposomal PNPs sensitive to both pH and temperature were used for vaginal administration of potential anticancer drug Arctigenin. The pH sensitivity was conveyed by an acid cleavable linker between the core of the NP and the PEG coating, while the temperature sensitive element allowed

the PNPs to transform from a solid to gel allowing for prolonged drug contact (Chen et al. 2012).

Previous research has shown that a high redox environment of thiols such as glutathione (GSH) levels within cancer cell intracellular compartments as well as in the tumour cells microenvironment are present (Russo et al. 1986; Raghavendra et al. 2008; Sun & Davis 2010; Brülisauer et al. 2014). The ability to include redox sensitive elements, such as disulphide bonds in NPs which respond to differences in redox potential are promising as they could enable effective targeting of cancer cells (Tobío et al. 2000; Wang et al. 2010). To date, redox reactive NPs have been used for the delivery of cancer drugs and gene therapy *in vitro* using human cervical cells (HeLa) using polymer and liposomal-based NPs (Petros et al. 2008; Takae et al. 2008).

Furthermore, disulphide linkers have been utilised in the development of FDA approved PNPs such as Gemtuzumab ozogamicin, used in the treatment of myeloid lymphoma (Lehner et al. 2012). Additionally, the presence of disulphide linker has previously been seen to increase NP stability within biological media (Sun & Davis 2010). This increased stability could influence the safety profile of these NPs as they may circulate in the body for longer, possibly leading to differential NP-cell interactions.

1.6 Coatings of nanomedicines

When nanomedicines are administered intravenously, orally, dermally or via inhalation an exposure route specific layer of proteins adhere to the outer surface of the NP, known as the protein corona (Kreyling et al. 2002; Kreyling et al. 2014). There is evidence that the protein corona can affect NP size and can influence NP interactions with cells and thus affect the safety of the NPs (Fischer & Chan 2007; Lazarovits et al. 2014). When administering NPs *in vivo* one of the biggest challenges to be overcome is clearance by the reticuloendothelial system (RES). The RES is found in macrophage rich organs such as the liver and spleen, and the internalisation of NPs by these macrophages reduces their circulation time, to reduce their interaction with target cells/tissues (Singh et al. 2006; Shubayev et al. 2009).

NP coatings can help reduce the interaction of NPs with the RES. One of the most common coatings for nanomedicines is PEG, which is FDA approved and is generally regarded as safe for medical use (Gref et al. 2000; Cruz et al. 2011; Svenson 2015). Previous research with PEGylated poly (n-butyl cyanoacrylate) PNPs showed a reduction of surface protein-binding to the NP, that altered the NP fate by providing a "stealth" like property as it prevented RES recognition and reduced clearance by macrophages *in vivo*, therefore increasing circulation time (Chaudhari et al. 2012; Bertrand et al. 2017). The increase in circulation time with PEG coating of PNPs may be attributed to PEG's hydrophilic nature resulting in less protein opsonisation; meaning that when the NP is administered *in vivo*, fewer proteins bind to the NP surface (Alexis et al. 2008; Sheng et al. 2009; Li et al. 2011). This increased circulation time, could potentially reducing drug administration frequency, which may reduce adverse effects and enhance patient adherence to treatment (Li & Huang 2011). PEG also reduces NP aggregation/agglomeration (Murali et al. 2015). It is desirable to inhibit NP aggregation/agglomeration as it will reduce their usefulness in a clinical setting due to aggregation/agglomeration making it challenging to maintain the even dispersion necessary for administration and treatment (Cao et al. 2016).

Furthermore, PEG has already been used for protein-PEG conjugated drugs that are FDA and the European Medicine Agency (EMA) approved such as Adagen, a PEGylated adenosine deaminase used to treat immunodeficiency disease (Hershfield et al. 1987). PEG, is often used to coat NPs composed of other materials such as metals, for example, superparamagnetic iron oxide nanoparticles used for bioimaging (Yu et al. 2012). Additionally, there are PEGylated lipid NPs FDA/EMA approved and in clinical use such as the doxorubicin containing, Doxil, used in the treatment of breast cancer (Barenholz 2012).

Studies investigating the impacts of PNP coating on safety have been performed predominantly with PLGA NPs. The addition of PEG to PLGA NPs can improve the NPs usefulness as a nanomedicine as PEG increases drug loading capability, solubility and stability (Danhier et al. 2009). Interestingly PEGylation of PLGA NPs can change the pharmacokinetic and biodistribution of NPs, for example, paclitaxel-loaded PLGA-PEG

NPs were observed to specifically target tumour cells unlike PLGA NPs lacking PEG (Senthilkumar et al. 2008; Danhier et al. 2009).

Another way of decreasing opsonisation and reducing NP aggregation/agglomeration and increasing NP stability is to absorb surfactants to the surface of NPs such as block copolymer Poloxamine 188, also known as Pluronic F68 (PF68) (Morales et al. 2005; Santander-Ortega et al. 2006; Gref et al. 2012). Previous research suggests that PF68-coated NPs degrade more rapidly within the cell than uncoated NPs, to enhance the release of cargo and potentially impacting on PNP safety (Astete & Sabliov 2006; Anderson & Shive 2012; Narayanan et al. 2013).

1.7 Nanomedicine accumulation in the liver

Currently, the use of *in vitro* models is promoted for safety testing of NPs by the EMA (EMA 2013a) for ethical, financial and time reasons (EMA 2013b). Furthermore, there have been concerns about rodent (mouse and rat) use in toxicology testing due to species differences between rodents and humans and poor reproducibility (Bale et al. 2014; Johnston et al. 2018). Previous studies have shown that polymer and metal-based NPs accumulate within the liver after intravenous injection, oral administration, and inhalation, suggesting that circulating NPs could enter the liver independently of the route of exposure (Figure 1.2) (Ogawara et al. 1999; Park et al. 2010; Schleh et al. 2012; Hirn et al. 2011; Sharma et al. 2012).

Hepatocytes are the main cell population in the liver, making up over 65% of the volume (Racanelli & Rehermann 2006). In addition, hepatocytes are responsible for many of the liver's functions such as albumin production, one of the most abundant serum proteins. Albumin is responsible for essential functions in hepatocytes including maintaining the osmotic pressure of the cell, scavenging of reactive oxygen species (ROS) and transport of different ligands as well as drugs (Lepedda et al. 2014; Larsen et al. 2016). Therefore, investigation of impacts of NPs on hepatocytes *in vitro* is an appropriate model to assess NP toxicity to the liver.

Previously *in vitro* 2-D hepatocyte cell lines have been used to assesse a range of engineered nanomaterials such as TiO_2, Ag, ZnO and multi-walled carbon nanotubes. Observations have primarily been via single exposure, at 24-72 hours post exposure for the potential effects on viability, cytokine production, ROS production, uptake, genotoxicity, intracellular calcium concentration as well as urea and albumin production (Kermanizadeh et al. 2012; Kermanizadeh et al. 2012; Gaiser et al. 2013; Kermanizadeh et al. 2013; Nguyen et al. 2015). However, few studies have investigated the toxicity of PNPs to hepatocytes *in vitro*.

Previous cytotoxicity studies have been performed to assess the toxicity of (clinically relevant) NPs to hepatocytes *in vitro*. For example, highly fluorescent Au nanoclusters stabilized with dihydrolipoic acid (DHLA) are intended for biomedical imaging, and drug delivery stimulated a decrease in cell viability and an increase reactive oxygen species production in human hepatocyte cells (HepG2) (Shang et al. 2011; Yang et al. 2014). However, when superparamagnetic Fe_3O_4 NPs, proposed to improve magnetic resonance imaging were exposed to hepatocyte cells (HepG2) using the MTS (3-(4,5-dimethylthiazol-2-yl)-5-(3-carboxymethoxyphenyl)-2-(4-sulfophenyl)-2H-tetrazolium) assay low cytotoxicity was observed at concentrations up to 10 mg/mL (Solar et al. 2015). Additionally, PLGA NPs containing a near-infrared dyes intended as a contrast agents for molecular imaging were observed to have no effect on the viability or mitochondrial activity of hepatocyte cells (HepG2) (Kohl et al. 2011). Furthermore, although PNPs poly(6-O-methacryloyl-D-galactopyranose)-b-poly(L-lactide)-b-poly(6-O-methacryloyl-D-galactopyranose), were observed to accumulate in hepatocyte cells (HepG2) these PNPs were observed to not affect cell viability up to 10 µg/ml using the MTT (3-(4,5-dimethylthiazol-2-yl)-2,5-diphenyltetrazolium bromide) assay (Wang et al. 2016).

Quantification of urea and albumin production can be used as a specific indicator of liver function (Watts et al. 1995). Urea is formed when ammonia is detoxified predominantly in the liver (Gong et al. 2015). A decrease in urea or albumin production by the liver suggests a loss of hepatic function. Therefore, quantification of urea and albumin production can be used as indicators of liver or hepatocyte function (Watts et al. 1995). Previous studies have indicated a decrease in urea and albumin production following

exposure of primary hepatocytes to TiO_2 NPs *in vitro* (Natarajan et al. 2015). These results reflected earlier *in vivo* findings where a decrease in blood urea nitrogen (BUN), the *in vivo* equivalent of urea concentration, and a decrease in liver function was observed in mice following oral administration of TiO_2 NPs (Xu et al. 2013). Additionally, hepatocytes (C3A) exposed to ZnO NPs showed decreased albumin production *in vitro* that did not affect urea production (Kermanizadeh et al. 2012). To date, this endpoint has not been commonly used in the safety screening of PNPs *in vitro*.

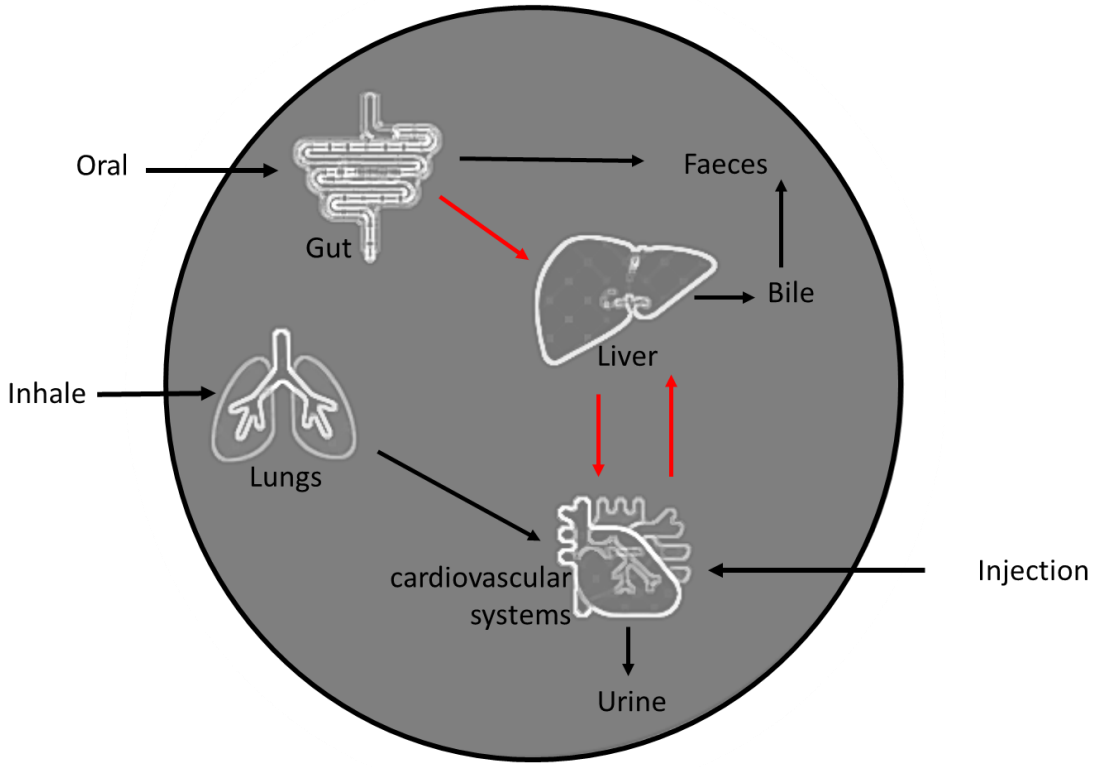

Figure 1.2 Exposure routes: Nanomedicines.

Poly nanomedicines in this study have been designed to be administered orally, via inhalation or via injection. The black arrows indicate possible fate of nanomedicines with in the body following exposure. The red arrows indicate how nanomedicine may enter and exit the liver following administration.

1.8 Safety profiling

Employing a tiered testing strategy to assess nanomedicine toxicity could speed up nanomedicine progression to clinical application, and save time and resources (Figure 1.3) (Johnston et al. 2018). More specifically, using this type of approach testing progresses from consideration of toxicity within the design of NPs, to characterisation of physicochemical properties to predict toxicity before performing *in vitro* testing to screen toxicity and then finally progressing to *in vivo* investigations and human studies. Using this type of approach, it is intended that *in vivo* testing is minimised, making testing more ethical.

Another way to reduce *in vivo* investigations in the future could be to utilise read-across, which enables a prediction of the safety of novel NPs by using existing data from similar NPs (Arts et al. 2015). Additionally the use of *in silico* (computational) tools such as Lazar, a free web-based platform that uses read-across to predict potential NP toxicity based on descriptors for the NP core (current database: Ag or Au cores) and the NP coating (current database: 30+ coatings e.g. citrate to polyvinyl alcohol) (Helma et al. 2017; nano-lazar.in-silico.ch/predict). Applying these principles would be in line with the 3Rs (replace, refine, reduce) which advocates the replacement of *in vivo* methods with alternatives where possible, refinement of current *in vivo* methods and reduction of animal numbers (Burden et al. 2017; Johnston et al. 2018).

Ideally, the safety testing of PNPs would be performed using standardised methods, were possible rely on alternative models. However, due to the complexity of PNPs under development and use, the testing strategy used to assess toxicity may need to be tailored to specific PNPs, until the level of understanding of nanotoxicity and the impact of physiochemical properties on NP safety improves.

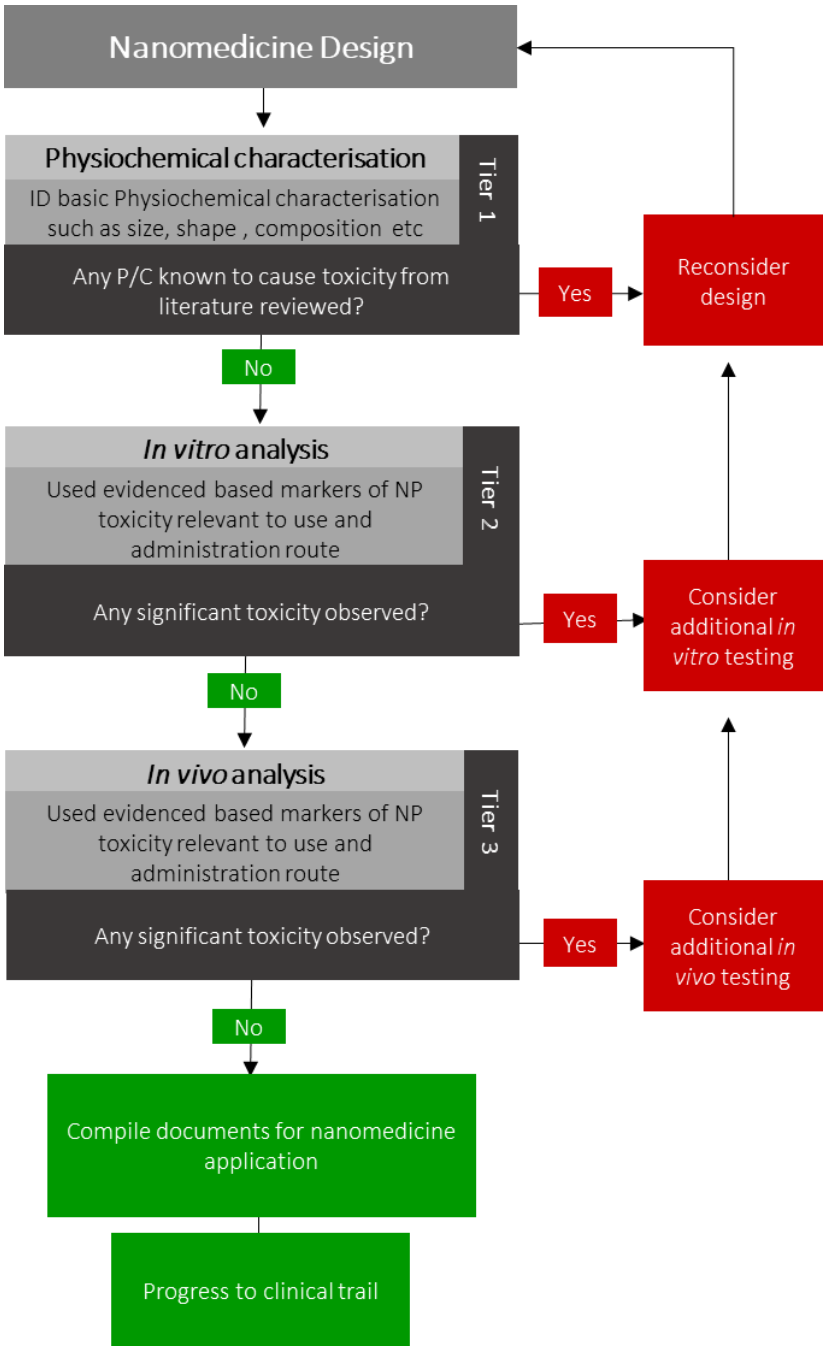

Figure 1.3 Tiered testing strategy for assessment of nanomedicine safety.

A tiered testing approach for screening PNP toxicity from NP design progressing to assessment of physiochemical characteristic, then *in vitro* analysis, then only progressing with suitable NPs to *in vivo* analysis before progressing to clinical trials. Information gained from each step in the tiered testing strategy can feed back into the safer design of NPs in the future. This approach has the potential to reduce the resources required for testing PNPs toxicity.

1.9 Cytotoxicity

Endpoints used to investigate the toxicity of PNPs can be selected based on the large body of evidence for engineered NPs (metal, metal oxides and carbon NPs) (Brown et al. 2004; Huang et al. 2010; Kermanizadeh et al. 2012; Arai et al. 2015). The first step of assessing NP toxicity *in vitro* is commonly the investigation of cytotoxicity. It is crucial to establish the cytotoxicity of these PNPs *in vitro* initially, so that further testing can then be performed at non-lethal concentrations and more can be learned about the mechanism of nanotoxicity. When assessing the toxicity of nanomedicines it is also important to consider relatively realistic concentrations when assessing safety (Section 2.2.4).

Several studies assessing PNP cytotoxicity use a single assay, primarily the MTT assay in a range of cells such as alveolar epithelial cells (A549), human breast adenocarcinoma (MCF-7 and MDA-MB-23), mouse fibroblasts (L929) and red blood cells (Fischer et al. 2003; Esfandyari-manesh et al. 2016). The MTT assay evaluates cell viability via the assessment of mitochondrial function. However, a variety of alternative assays such as Alamar Blue (AB), AM (5-Carboxyfluorescein Diacetate, Acetoxymethyl Ester) (CFDA-AM) and Neutral Red (NR) assays can be used to gather data on metabolic activity, membrane integrity and lysosomal function respectively to assess cytotoxicity/cell viability simultaneously (Figure 1.4) (Yuan 2014; Connolly et al. 2015). The AB assay measures cell metabolic activity based on the reduction of non-fluorescent Resazurin to fluorescent Resorufin by metabolically active cells. The CFDA-AM assay assesses plasma membrane integrity based on the conversion of non-fluorescent CFDA-AM to fluorescent 5-carboxyfluorescein by esterases within living cells. Thus, dye retention occurs only in cells with an intact plasma membrane. The NR assay can determine lysosomal function based on the uptake and retention of fluorescent 3-amino-7 dimethylamino-2-methyl phenazine hydrochloride in functional undamaged lysosomes (Cenni et al. 2008). Of benefit is that these cytotoxicity assays are amenable to high throughput testing which is ideal for nanomedicine screening as they are rapid, and cost-effective.

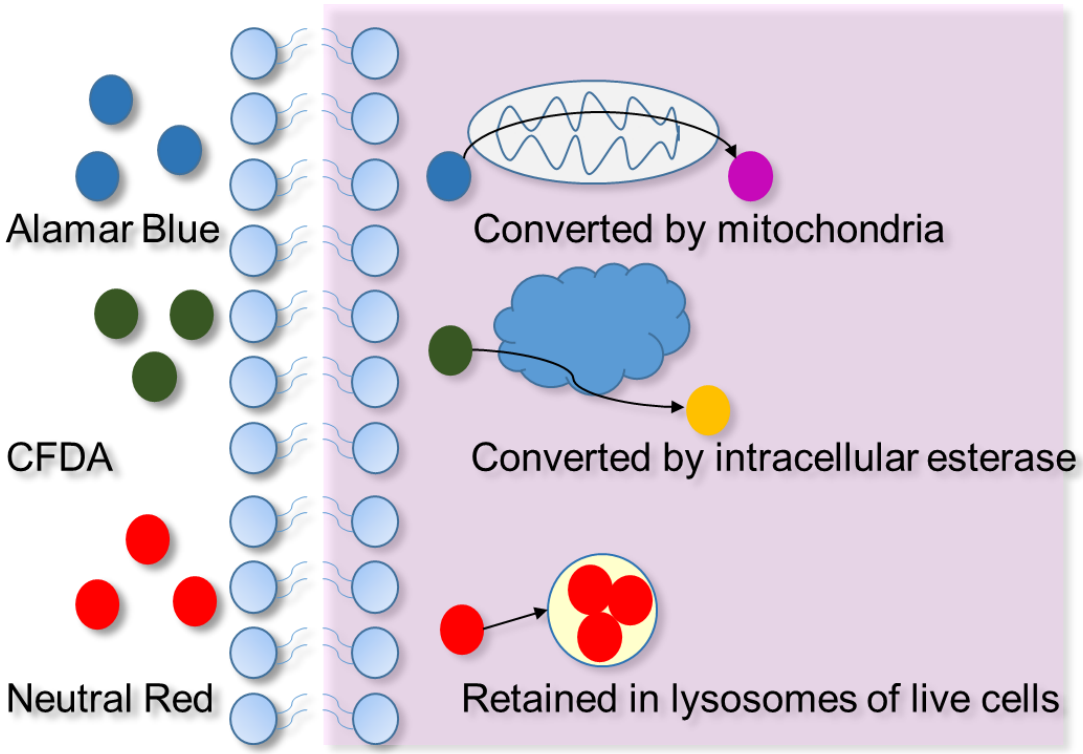

Figure 1.4 Cytotoxicity assays.

The AB assay measure cell metabolic activity when non-fluorescent Resazurin (blue) is converted to fluorescent Resorufin (purple). The CFDA-AM assay measures plasma membrane integrity when non-fluorescent CFDA-AM (green) is converted to fluorescent 5-carboxyfluorescein (orange) by esterases. The NR assay measures lysosomal function when undamaged lysosomes.

1.9.1 Uptake

Assessing PNP uptake when investigating the toxicity of PNPs is crucial, as it can influence the efficacy and toxicity of PNPs (Nie et al. 2011; Zhao et al. 2011). The uptake of PNPs by target and non-target cells can be investigated *in vitro* or *in vivo*. Lower internalisation by non-target cells can be beneficial for nanomedicines, in order to reduce side effects. Within studies conducted to date, visualisation and quantification of the uptake of fluorescent PNPs by cells is the most common means of assessment. Uptake has been quantified for fluorescent polystyrene and PLGA NPs in macrophage, kidney, epithelial, fibroblast, and endothelial cell lines using predominately microscopy and flow cytometry (Davda & Labhasetwar 2002; Firdessa et al. 2014). Additionally, electron microscopy such as transmission electron microscopy (TEM) possesses a high enough resolution to image individual NPs; and can be a useful tool to investigate NP uptake and intracellular fate (Zhang et al. 2014; Niemirowicz et al. 2016).

Quantification of NP uptake by cells can be challenging but essential to help understand the mechanism of nanotoxicity. There can be vast differences in the level of NP uptake between cell types. For example, Firdessa et al. showed that macrophages internalised 100% of 200 nm polystyrene NPs using flow cytometry, whereas kidney epithelial cells internalised approx. 5-10% (Firdessa et al. 2014; Oh & Park 2014).

Particles can enter cells via different routes, that are either active (energy dependent) or passive (energy independent). NPs can enter the cell passively through the cell membrane. However, this is not often observed and is dependent on the physiochemical properties of the NP (e.g. lipophilicity) (Underhill & Ozinsky 2002). To investigate the uptake of NPs via passive transport red blood cells are a useful model as they cannot perform energy dependent uptake (Underhill & Ozinsky 2002). Previous studies have observed that red blood cells passively internalise D-penicillamine-coated quantum dots (QD) (8 nm) with no damage to the cell's membrane observed (Wang et al. 2012).

Energy-dependent uptake of NPs by cells occurs predominantly via phagocytosis or pinocytosis (Figure 1.4). Phagocytosis is mostly performed by specialised cells (phagocytes) such as macrophages, that engulf particles into membrane-bound

phagosomes (Conner & Schmid 2003). Macrophages internalise cell debris, particles and bacteria ranging from 100 nm to 6 µm, via phagocytosis, (Shu et al. 2005; Tsai & Discher 2008; Rodriguez 2013). Macrophages are found in a range of tissues such as the liver and lungs and are known to accumulate NPs *in vivo* (Ruge et al. 2012; Jemnit et al. 2017). Furthermore, macrophage cells (J774) *in vitro* have been observed to readily internalise polystyrene PNPs of 20-200 nm diameter (Clift et al. 2008). Once internalised, the phagosome fuses with lysosomes containing hydrolytic enzymes which at a low pH digest the contents of the phagolysosome (Conner & Schmid 2003; Qiu et al. 2013).

Knowledge of the uptake mechanism can be essential for assessing downstream toxicity, as uptake can determine intracellular localisation. Pinocytosis is performed by most cells and occurs mostly via invagination of the cell membrane to form a membrane-bound vesicle (endosome), that can then be transported to a range of organelles within the cells such as lysosomes, mitochondria or even the nucleus (Conner & Schmid 2003; Sahay et al. 2010). Pinocytosis can be further divided into clathrin-dependent and independent endocytosis for NPs ~100-200 nm and under 100 nm respectively. Clathrin-independent endocytosis can also include caveolae-dependent (<80 nm) and clathrin/caveolae independent endocytosis known as macropinocytosis (Conner & Schmid 2003; Sahay et al. 2010; Kasper et al. 2013).

The mechanism of PNP uptake into cells can be investigated using specific inhibitors of endocytic processes such as Wortmannin, which prevents phagocytosis and macropinocytosis, or chlorpromazine hydrochloride, which inhibits clathrin-mediated endocytosis (Firdessa et al. 2014). PNPs such as poly(methacrylic acid-co-cholesteryl methacrylate) containing the chemotherapy doxorubicin have been observed to be internalised by hepatocyte cells (HepG2) via caveolae-dependent and clathrin-mediated endocytosis using pharmacological inhibitors (Sevimli et al. 2015). Moreover, hepatocyte cells (HepG2) have been observed *in vitro* to endocytose cholesterol-modified pullulan (a natural polymer) PNPs via both macropinocytosis and clathrin-mediated endocytosis (Jiang et al. 2013). These results highlight that hepatocytes internalise PNPs via several mechanisms of uptake. However as the inhibitors used to determine the uptake mechanisms can themselves cause alterations to the cells, it can be challenging to make definitive conclusions regarding PNP uptake mechanisms (Iversen et al. 2011).

Fluorescent probes (to identify specific organelles) and TEM have also been used to investigate the mechanism of uptake and fate of internalised NPs (Johnston et al. 2015).

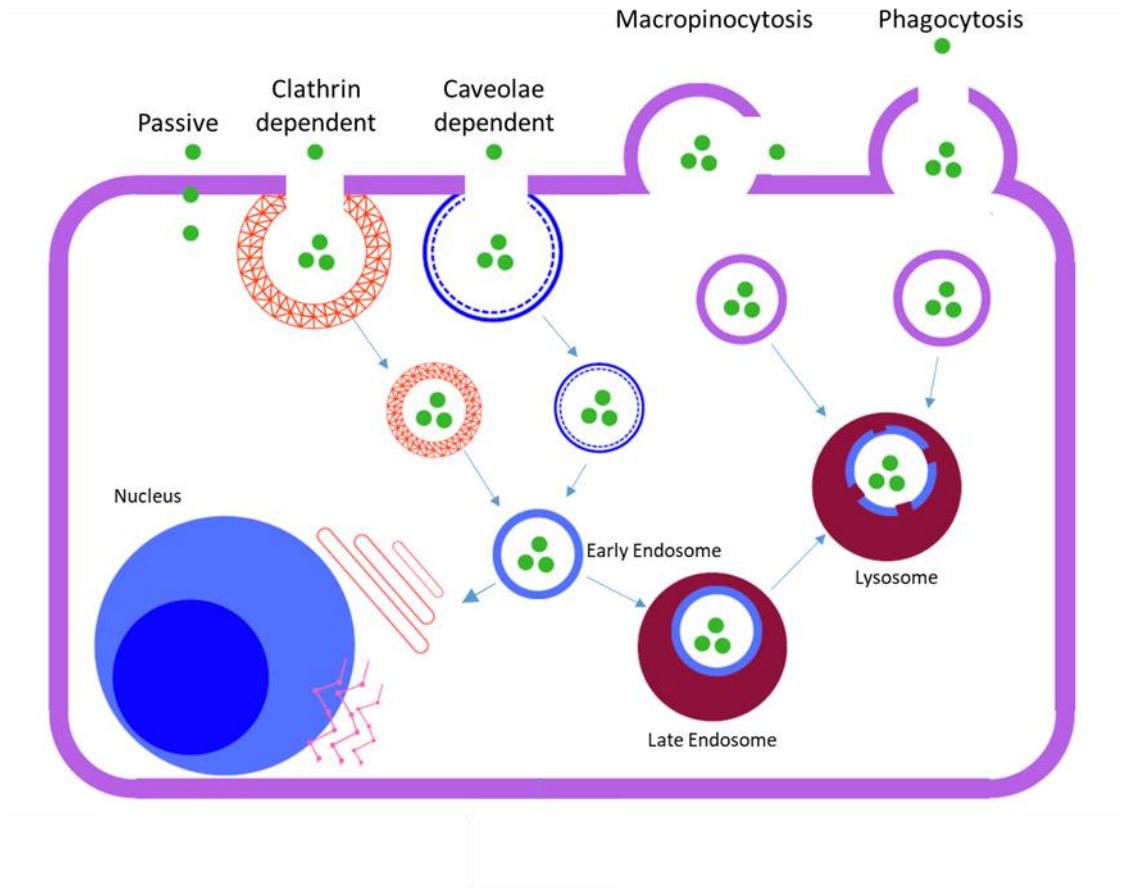

Figure 1.5 Schematic of the NP-cell interaction.

NPs can enter the cells through a range of mechanisms passive, clathrin-dependent endocytosis, caveolae-dependent endocytosis, micropinocytosis and phagocytosis. Once inside the cell NPs (green) are transported either directly to the lysosome for degradation or indirectly via the early and late endosome. NPs can also be transported to the nucleus, endoplasmic reticulum, Golgi apparatus or mitochondria via endosomes.

1.9.2 Cytokine production

Activation of an inflammatory response by NPs is commonly observed *in vivo,* with inflammatory responses typically monitored via assessment of immune cell accumulation or cytokine production (e.g. (Park et al. 2010; Yukawa et al. 2014), reviewed by (Johnston et al. 2018)). For example, exposure of mice to cobalt NPs (50 μg/ animal) via intratracheal installation resulted in an increase in the infiltration of neutrophils and macrophages in the alveolar space indicating acute lung inflammation (Wan et al. 2017). Additionally, when mice were exposed via the murine air pouch model to polyamidoamine (PAMAM) dendrimer PNPs, an increase in the infiltration of leukocytes, the majority of which were neutrophils, was observed indicating these PNPs had proinflammatory activities (Durocher & Girard 2016)

Investigation of cytokine production is also commonly used as an indicator of NP toxicity *in vivo* and *in vitro* (Stone et al. 2009). Interleukin-8 (IL-8) is a chemokine that can initiate a pro-inflammatory response via activation and migration of immune cells, and in particular neutrophils (Larsen et al. 1989). Cationic polyethyleneimine (PEI) NPs caused an increase in keratinocyte chemoattractant (KC) levels (the mouse homolog of IL-8), following intraperitoneal injection of mice bearing tumours (Cubillos-Ruiz et al. 2009). *In vitro,* several studies have indicated that NPs of diverse physicochemical properties stimulate an increase in IL-8 production by hepatocytes (Cho et al. 2012; Dobrovolskaia & McNeil 2013; Elsabahy et al. 2013). Interestingly, low-toxicity NPs such as TiO_2, as well as high-toxicity NPs including Ag NPs, can stimulate IL-8 production by hepatocytes (e.g. C3A cells and primary human hepatocytes) (Joshi-Barve et al. 2007; Kermanizadeh et al. 2013). Tumour necrosis factor alpha (TNF-α) is a cytokine that plays a role in acute phase response as well as tissue repair and upon upregulation can promote systemic inflammation (Natanson et al. 1989; Marino et al. 1997; Goeddel 1999). TNF-α has previously been seen to be produced by hepatocytes following inflammation *in vivo* in mice (Spencer et al. 2013).

IL-6 is a proinflammatory cytokine that plays a role in the acute phase response as well as liver regeneration following injury (Ferguson-Smith et al. 1988 ; Cressman et al. 1996). Previously *in vitro* and *in vivo* studies using primary rat hepatocytes and rats have

observed to induce IL-6 expression and production when challenged by lipopolysaccharide (LPS), a bacterial hepatotoxin (Norris et al. 2014). Additionally, respiratory epithelial cells (A549) had elevated IL-6 production when exposed to PNPs such as PEI NPs and PLGA/ polyvinyl alcohol NPs. However these NPs failed to increase production of IL-8 (Robbens et al. 2010; Grabowski et al. 2013). Furthermore, PNPs made up of N-isopropylacrylamide, vinylpyrrolidone and acrylic acid have been seen to elicit a cytokine response in hepatocyte cell lines (HSC-T6), with an increase in the production of both IL-6, and TNF-α observed (Bisht et al. 2011).

IL-1β is a proinflammatory cytokine that is expressed by many cell lines such as macrophages and hepatocytes (Saklatvala & Dingle 1980 ; Negrin et al. 2014; Chen & Xu 2018). Mice instilled intratracheally with TiO_2 NPs had increased IL-1β mRNA expression observed in the kidneys (Huang et al. 2015), while *in vitro* macrophage cell lines have been seen to increase production of IL-1β when exposed to Ag or silicon dioxide (SiO_2) NPs (Carlson et al. 2008; Park & Park 2009). The IL-1 inhibitor, IL-1 receptor antagonist (IL-1ra), is an anti-inflammatory cytokine that has previously been suggested to have a protective role during liver inflammation (Gabay et al. 2010). Additionally, previous studies suggest *in vivo* in mice that hepatocytes can produce high levels of IL-1ra in response to LPS (Lamacchia et al. 2012). There are limited studies assessing IL-1ra production by PNP exposure *in vitro* and *in vivo*. Although for NPs composed of other materials IL-1ra production in response to NPs has been studied, *in vitro*. For example, a significant increase in IL-1ra production was observed from THP-1 cells (human monocyte) exposed to TiO_2 NPs (Kim et al. 2007). While, *in vivo* when osteoporosis patients were treated with 100 mg/day of sodium alginate NPs (approx. 200 nm), this also induced an increase in circulating levels of IL-1ra (Qu et al. 2017).

TiO_2 NPs in relation to nanotoxicity are much like PNPs as they are assumed to have relatively low toxicity due to relatively low reactivity, however proinflammatory cytokines (TNF-α, IL-1β and IL-6) have been elevated in cells (e.g. hepatocytes) following exposure to TiO_2 NPs (Cui et al. 2011; Kermanizadeh et al. 2012) as well as IL-1ra (Bale et al. 2014). However, several studies suggest that PNPs do not elicit a potent cytokine response. For example, monocytes and polymorphonuclear cells were exposed to PLGA-PEG NPs *in vitro*, and it was observed there was no increase in IL-1β, IL-6,

TNF-α or IL-8 cytokine production (Segat et al. 2011). While, alveolar epithelial cells (A549) exposed to cationic polystyrene NPs (57 nm), observed a slight reduction in IL-8 production (Thach & Finkelstein 2013). Investigation of the capacity of PNPs to stimulate an inflammatory response is essential to screen during nanomedicine safety profiling as prolonged inflammation could result in adverse effects in the clinic.

1.9.3 Oxidative stress

ROS such as hydrogen peroxide, superoxide and hydroxyl radical are normal by-products of metabolism and can have essential physiological functions. However, they can also compromise cell function by damaging lipids, protein and DNA. When ROS levels are raised within cells, this can lead to oxidative stress, a potential detrimental state for the cell which is characterised by an increase in ROS production and depletion in protective antioxidants (Sims et al. 2017). In the liver (as well as other cell types), an increase in intracellular ROS could result in an imbalance of ROS and antioxidants, which favours ROS, leading to indirect downstream effects such as DNA damage and metabolism changes to the hepatocytes (Filippi et al. 2014; Evans et al. 2017). ROS generation can also decrease mitochondrial membrane potential resulting in unhealthy mitochondria and potentially cells (George et al. 2009).

ROS production has been studied for engineered NPs (e.g. copper oxide (CuO), Ag) in hepatocytes *in vitro* as well as macrophages (e.g. Liu et al. 2016; Ahmad et al. 2016). Additionally, an increase in ROS production was observed following cadmium selenide/zinc sulfide QD exposure in rat pheochromocytoma cells (PC12), primary human umbilical vein endothelial cells (HUVEC) and murine neural progenitor cells (C17.2) (Soenen et al. 2014). Interestingly, the addition of a polymer coating to a metal or metal oxide NPs has previously been seen to reduce NP induced ROS production, for example, mice orally administered poly-vinyl-pyrrolidone coated Au NPs had a lower level of ROS production in the liver in comparison to the uncoated Au NPs (Iswarya et al. 2016). Similarly, when superparamagnetic iron oxide NPs were coated with PEG and administered *in vitro* to porcine aortic endothelial cells less ROS production was observed for the coated NPs than the uncoated NPs (Yu et al. 2012).

Previous research shows low levels of ROS production elicited by PNPs, such as cervical cancer cells (HeLa) exposed to natural chitosan PNPs (< 30 nm) or macrophages (RAW264.7) and human lung cells (BEAS-2B) exposed to PLGA NPs < 200 nm (Benito-Miguel et al. 2015; Zheng et al. 2015). However, studies using hepatic cells (HuH7), as spheroid cultures, have indicated that PEGylated and non-PEGylated PAMAM dendrimer NPs could produce a ROS response (Chen et al. 2016). Also, PLGA NPs coated with PEI have been observed to increase ROS production in hepatocytes *in vitro* (HepG2) (Yu et al. 2014). Interestingly this response was not seen to change with increasing concentration (25-250 µg/mL) indicating that ROS production can occur at relatively low concentrations without affecting cell viability (Yu et al. 2014).

1.9.4 Genotoxicity

DNA damage (genotoxicity) can lead to mutations, which may promote disease development such as cancer. Therefore testing of NP genotoxicity is an integral part of nanomedicine safety profiling, as the adverse effects of genetic damage may out weight the therapeutic benefits (Vidal et al.2001). Previous studies have shown that NPs of different physicochemical properties may be able to stimulate genotoxic effects directly via NP-DNA interactions (An et al. 2010; Tang et al. 2012), indirectly via NP-induced ROS production (Sharma et al. 2012) or via interactions with proteins relevant to cell division or DNA repair (Huang et al. 2009). Direct NP-DNA interactions may correlate with uptake and be size-dependent, with smaller NPs potentially entering the nucleus via nuclear pores and directly interacting with the DNA (Barillet et al. 2010; Jin et al. 2012). For example, silicon carbide NPs of approx. 10 nm have been shown to enter the nucleus of alveolar epithelial cells (A549) (Barillet et al. 2010). Also, NPs could potentially interact directly with DNA or nuclear proteins during mitosis (Frohlich 2012).

NPs generated ROS may potentially induce oxidative damage leading to DNA strand breaks or base lesions (Cooke et al. 2003). In a previous study, ZnO NPs were observed to cause DNA damage mediated via oxidative stress in hepatocyte cells (HepG2) (Kermanizadeh et al. 2014). This study used the alkaline comet assay that allows for the detection of single and double DNA strand breaks as well as the contribution of oxidative

stress with the addition of formamidopyrimidine DNA glycosylase (Fpg), repair enzyme that recognises oxidised bases in damaged DNA (Collins 2004; Sharma et al. 2012).

As highlight by the EMA, genotoxicity is a crucial safety assent endpoint when assessing PNP nanomedicines (EMA 2012). When genotoxicity is observed for PNP nanomedicines, this can hinder progression of these PNPs to the clinic as genotoxicity can be related to the deployment of cancers. However to date, there are relatively limited publications on ROS-mediated genotoxicity for PNPs, compared to publications based on genetic damage mediated by metal and metal oxide NPs (Deng et al. 2017). However, in a prior comparative study, PLGA- poly (ethyl oxide) (PEO) NPs, at therapeutically relevant concentrations, were seen to be genotoxic to hepatocytes as well as Kupffer cells 4 hours and 24 hours post exposure *in vitro* in rat hepatocytes (Cowie et al. 2015). Interestingly, using eight different cell lines, hepatocytes were the most sensitive cell line to DNA strand breaks when exposed to iron (II, III) oxide (Fe_3O_4), TiO_2 and SiO_2 NPs at concentrations up to 80 $\mu g/cm^2$, highlighting the sensitivity of hepatocytes to NP toxicity (Cowie et al. 2015).

Several *in vitro* studies investigating genotoxicity of polymer-based nanomedicines at more realistic non-cytotoxic concentrations showed limited genotoxicity. Studies investigating the cytotoxicity and genotoxic capability of thermo-responsive dendritic polymer nanogels (polyglycerol-poly(glycidyl methyl ether-co-ethyl glycidyl ether) designed as novel drug delivery systems for dermal application indicated that in primary normal human keratinocytes (NHK), adult human skin (HaCaT) and dendritic (XS52) cell lines, neither cytotoxic and genotoxic effects were observed (Edlich et al. 2017; Gerecke et al. 2017). Additionally, using human isolated peripheral blood mononuclear cell the cytotoxicity and genotoxicity of PLGA-PEO NPs were investigated. While, there were indications of cytotoxicity above 75 mg/cm^2, assessment of genotoxicity at non-cytotoxic concentrations revealed that there was no genotoxic observed by DNA strand breaks, oxidised bases or chromosomal aberrations (Tulinska et al. 2015).

Although, there have been studies that point towards PNPs having the capabilities to induce genetic damage using different endpoints. Previously investigating DNA stand breaks poly(methyl- methacrylate) NPs were observed to be non-genotoxic *in vitro* using

human T lymphocyte cells (Jurkat) (Acosta- et al. 2012). Genotoxicity was also explored in fibroblast cells (L929) using poly(methyl- methacrylate) NPs, although there was limited internalisation of these NPs, genotoxicity was as chromosol damage (Graça et al. 2017). These studies show the importance of using multiple endpoints to investigate genotoxicity.

Also, the physicochemical characteristic of the PNPs along with the sensitivity of different cell lines has been investigated. The effects of NP surface charge on *in vitro* genotoxicity were investigated using both using PLGA NPs with three different cell lines (mouse lymphoma (L5178Y), human B-lymphoblastoid (TK6) and human bronchial epithelial (16HBE14o-)). Interestingly no genotoxicity was observed for negatively or neutral PNPs however, PLGA NPs with a positive charge on their surface were cytotoxic and capable of inducing chromosomal damage in 16HBE14o- cells but not induce DNA strand breaks (Platel et al. 2016).

Importantly *in vitro* and *in vivo* models are being used to assess genotoxicity of PNPs. Both *in vitro* and *in vivo* investigations were performed for the biodegradable copolymer (ethyl vinyl ether and maleic anhydride) intended for oral drug delivery (Iglesias, Cerain, et al. 2017)(Iglesias, Dusinska, et al. 2017)(Iglesias, Irache, et al. 2017). *In vitro* studies showed that these copolymer NPs did not induced genotoxicity in Caco-2 cells up to 2 mg/mL or mouse lymphoma cells up to 600 µg/mL (Iglesias, Cerain, et al. 2017)(Iglesias, Dusinska, et al. 2017). However, *in vivo* studies in mice, using these copolymer NPs indicated, these NPs were capable of induction DNA strand breaks and oxidised bases in the duodenum at a dose of 2000 mg/kg (Iglesias, Irache, et al. 2017). Although 2000 mg/kg is a relatively high does, these results do highlight the importance of though genotoxicity assessment of PNPs for medical use.

1.9.5 Intracellular calcium

Intracellular calcium concentration ($[Ca^{2+}]_i$) is strictly regulated and has essential roles in cell metabolism and gene expression. An increase in $[Ca^{2+}]_i$ can lead to membrane damage, apoptosis, cytokine production as well as DNA damage (Florea et al. 2005; Brown et al. 2002). Elevation of $[Ca^{2+}]_i$ in hepatocytes can occur as a response to cellular

injury and has potential as a marker for nanomedicine induced hepatotoxicity (Trump et al. 1984; Tolosa et al. 2012; Jemnitz et al. 2017). Previous studies have seen an increase in $[Ca^{2+}]_i$ in a variety of cell types following NP exposure, including Ag NPs (Johnston et al. 2015), TiO_2 NPs, (Simon et al. 2011), ZnO NPs (Huang et al. 2010), polymer NPs (Jemnitz et al. 2017) and ultrafine carbon black (UFCB) (Stone et al. 2000; Möller et al. 2005). *In vitro* studies have demonstrated that increased $[Ca^{2+}]_i$ following NP exposure can be associated with decreased cell viability in neuroblasts (Meindl et al. 2015) and membrane repair in cervical cancer cells (HeLa) (Shareia et al. 2009). Additionally, an increase in $[Ca^{2+}]_i$ in rat pulmonary artery smooth muscle cells was linked to an increase in cell proliferation which can be an indicator of a damaged cell, following acute SiO_2 NP exposure (Dubes et al. 2017).

Limited studies have assessed the impact of PNPs on $[Ca^{2+}]_i$. However, there is evidence that polystyrene NPs of <100 nm are capable of inducing an increase in $[Ca^{2+}]_i$ in macrophages and neuroblasts (Brown et al. 2001; Meindl et al. 2015). Furthermore, PLGA NPs <100 nm increased intracellular calcium influx in both macrophage cells (RAW264.7) and human lung cells (BEAS-2B) (Zheng et al. 2015). Interestingly, hepatocytes derived from rats have shown an increase $[Ca^{2+}]_i$ when exposed to polymer PAMAM dendrimers NPs. However this increase in $[Ca^{2+}]_i$ did not occur when cells were exposed to PEGylated PAMAM dendrimers NPs (Jemnitz et al. 2017). These results indicate that polymer NPs can elicit an increase in $[Ca^{2+}]_i$ in a range of cell lines and that NP physicochemical properties such as shell/coatings may impact upon the magnitude of the response observed.

It is uncommon to assess $[Ca^{2+}]_i$, however, the addition of this endpoint could provide valuable insight into the effects of shorter NP-cell interaction times that are not examined in routine assays that are predominantly performed at 24 hours such as following intravenous administration. This shorter NP-cell interaction times may have clinical relevance for nanomedicines that are administered intravenously.

1.10 Project aims and objectives

The overall aim of this project is to guild the development of evidence-based *in vitro* approaches to screening the toxicity of PNPs of various physiochemical properties. This information could be used in a tiered testing approach which enables a screening of PNP toxicity using a battery of *in vitro* tests before progressing with *in vivo* testing. This approach has the potential to reduce the resources required for testing these PNPs such as time, financial investment and animal number, therefore becoming more in line with the principles of the 3Rs (Burden et al. 2017).

Therefore, this study aims to investigate the toxicity of a panel of PNPs to the liver *in vitro* via investigation of:

1. The role of a polymer coating (PF68) on the toxicity of PNPs to hepatocyte and macrophage cells *in vitro.*

2. The role of polymer composition (PLGA and PEG chain length) on the toxicity of PNPs to hepatocyte cells *in vitro.*

3. The role of controlled targeting elements (redox sensitive PLGA PNPs) on the toxicity of PNPs to hepatocyte cells *in vitro.*

Existing knowledge of the mechanism of NP toxicity informed endpoint selection in this study. More specifically, a range of tests will be employed to investigate the cellular and molecular events underlying the potential toxicity of PNPs to hepatocytes *in vitro*. The following endpoints have been prioritised for investigation:

I. Cytotoxicity

II. Cytokine production

III. ROS production

IV. Cellular uptake

V. Genotoxicity

VI. Albumin and urea production

VII. Intracellular calcium concentration

It is hypothesised that the physicochemical properties of PNPs (e.g. composition, size, surface coating) will influence their uptake by cells and their ability to stimulate cytotoxicity, cytokine production, ROS production, genotoxicity, urea and albumin production and intracellular calcium concentration.

Chapter 2. *In vitro* assessment of the influence of Pluronic coating on polymer NP safety using C3A hepatocytes and J774 macrophage

2.1 Introduction

2.1.1 Designing safe novel PDP PNP for nanomedicine

Polymer-based NPs can be relatively quick and inexpensive to produce, leading to the rapid development of a diverse array of polymeric NPs. However, investigations into polymer NP safety have lagged-behind their production. As a result, many uncertainties linger regarding the potential adverse health effects of these materials and how the polymer characteristics vary, highlighting an urgent need to assess polymer NP safety. With the growing use of and exposure to NPs, a comprehensive understanding of NP safety is necessary to ensure their safe use.

For this study, a linear polyester with phenyl containing side chains that could form micelles was generated by collaborators at the University of Nottingham that could form micelles. These NPs were designed as nanomedicines. Previous studies have demonstrated that an increase in phenyl content in the side chain of polymers can increase the polymers' biodegradability, a highly desirable trait for nanomedicines (Jin et al. 2000).

Cancer treatment has been the focus of many nanomedicines. The PNPs in this study (section 2.2.1) were designed to be under 200 nm in diameter to take advantage of the EPR effect, which allows NPs to accumulate passively within tumours (Matsumura & Maeda 1986; Yokoyama et al. 1990; O'Neal et al. 2004). Additionally, the PNPs prepared for this study contained the hydrophobic fluorescent dye coumarin-6 to mimic hydrophobic drug loading and to allow for NP visualisation using fluorescent microscopy. Micellar PNPs were generated using the novel block-copolymer poly (decamethylene succinate-co-pheylsuccinate) (PDP) with 70% succinic acid, and 30% phenylsuccinic acid as this composition was found to have the highest loading capability (Figure 2.1) (Kakde et al. 2016). With safety at the forefront, these PNPs were produced to have a negative charge, as earlier studies have shown that positively charged NPs can be more toxic, although positively charged NPs have the advantage that they can be taken up more readily by cells than negatively charged NPs (Yu et al. 2011; Hühn et al. 2013).

In this study, PF68, was adsorbed onto the PNP surface, this surfactant introduces "stealth" like properties, decreases polymer NP aggregation/agglomeration and increases stability due to steric stabilisation (Moghimi et al. 1994; Reich et al. 1997). PF68 is a triblock copolymer, meaning it is composed of 3 blocks (lengths) of connection polymers, e.g. PF68 composed of PEO connected to poly (propyl oxide) (PPO) with in turn is connected to an additional PEO (PEO-PPO-PE). PF68 containing 80% poly PEO and 20% PPO (Mei et al. 2009). PEG and PEO are similar as they are composed of the same polymer, with differing molecular weights (Moghimi et al. 2004). Adsorbance of the surfactant PF68 to the NP's surface could change the safety profile of the NP by decreasing aggregation/agglomeration and increasing NP stability (Morales et al. 2005; Santander-Ortega et al. 2006). Using these NPs, it was possible to compared the toxicity of coated and non-coated NPs, allowing for the assessment of how coating (PF68) of polymer based nanomedicines could influence overall PNP toxicity.

2.1.2 The effect of PF68 coating on PNP safety

PF68 is a surfactant used as a coating to increase the stability of NP suspensions and has previously been shown to decrease PNP uptake in macrophage and hepatocyte cell lines (Zhang et al. 1998). Studies investigating the impacts of PF68 coating on PNP safety have been performed predominantly with PLGA NPs. For example, Grabowski investigated the interaction of PF68-coated PLGA NPs with THP-1 (macrophage) cells and showed that exposing cells to concentrations as high as 100 µg/mL of PF68-coated PLGA NPs, induced no change in cytotoxicity or cytokine production (IL-8, IL-6, monocyte chemoattractant protein 1 (MCP-1) or TNF-α) when compared with uncoated PLGA NPs following 24 hours exposure (Grabowski et al. 2013; Grabowski et al. 2015).

However, alveolar epithelial cells (A549) treated with PF68-coated PLGA NPs at 100 µg/mL, did result in increased production of IL-8, IL-6 and MCP-1 in comparison to cells exposed to medium alone. There was also increased PNP internalisation, resulting in granulation of the cells when compared with PNPs coated with polyvinyl alcohol and chitosan, as well as PF68 alone (Grabowski et al. 2013; Grabowski et al. 2015). Interestingly, when a different lung cell model, Calu-3, (lung epithelial) was exposed to similar PLGA NPs coated with PF68, cytotoxicity was only observed at extremely high

concentrations (5 mg/mL), with no increase in cytokine production observed (IL-6 and IL-8) following 24 hour exposure (Mura et al. 2011).

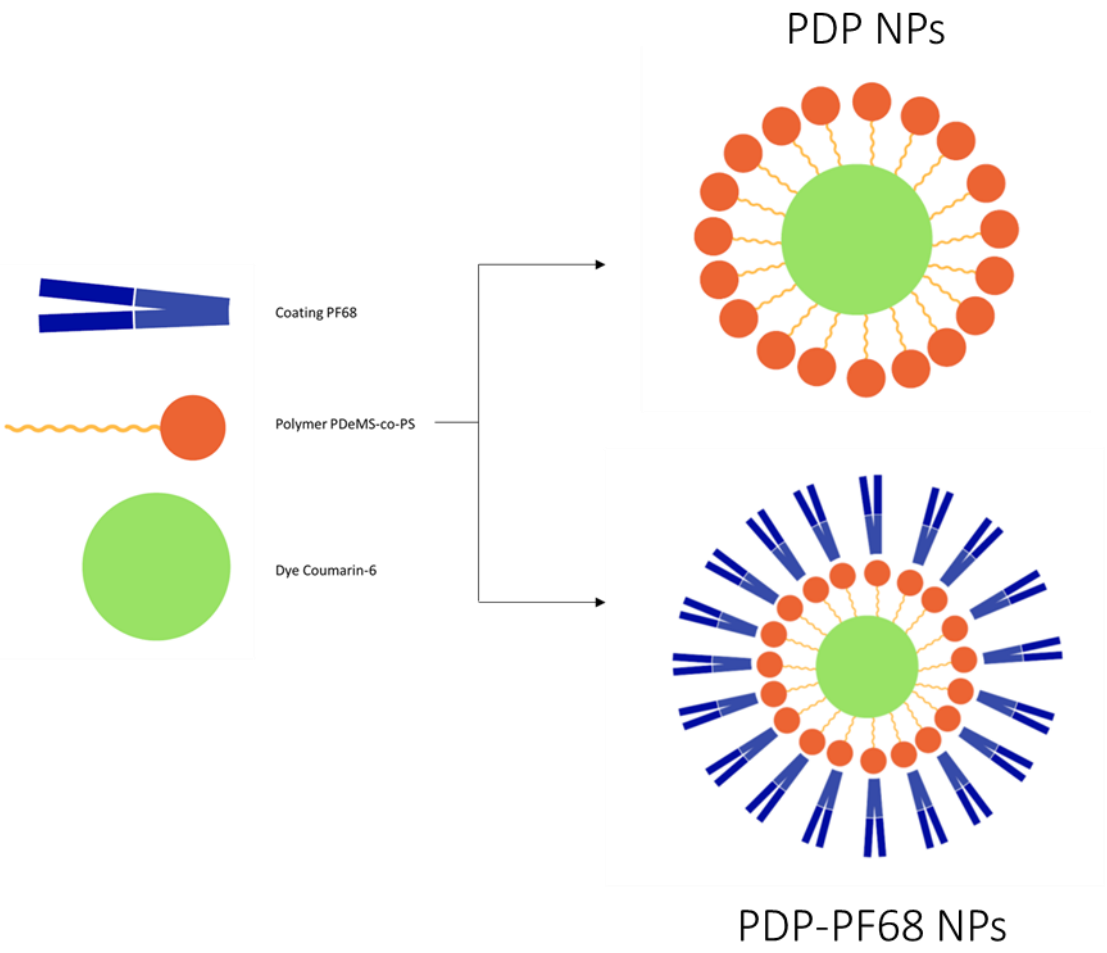

Figure 2.1 Scheme of micellar PDP and PDP-PF68 NPs.

Representation of NPs used in this study made of polymer PDP (orange), coumarin-6 dye (green) and PF68 coating (blue).

2.1.3 Study aims and hypothesis

This study aimed to evaluate the impact of a PF68 coating on PDP NP toxicity. Initially, after 24-hours exposure, cytotoxicity was assessed in C3A hepatocytes as it is established that NPs administered via various routes accumulate in the liver. C3A cells are clonally derived from of human hepatocyte cells, HepG2. The C3A cells can be more suitable for semi-high throughput assays than HepG2 as C3A cells have stronger contact inhibition of growth, promoting a single cell layer, resulting in more reliable assay results (Kelly 1994). Next, the uptake of NPs was visualised using fluorescent microscopy and quantified using a fluorescence plate reader, followed by measurement of cytokine production. The genotoxicity was assessed via the Comet assay and the contribution of ROS to DNA damage evaluated. A brief investigation of cytotoxicity and uptake of NPs in the macrophage cell line J774 was performed to compare target sites and the usefulness of different cell lines as predictive models of PNP toxicity. Due to these batch produced NPs having short stability, low volume and low NP concentration, it was not always possible to perform all desired endpoints or for a full complement of concentrations to be used for applied endpoints.

It was hypothesised that

1. PDP and PDP-PF68 NPs, at pharmacologically relevant concentrations would stimulate minimal cytotoxicity in both C3A hepatocyte cells and J774 macrophage cells.

2. PF68-coated NPs would be internalised to a lesser extent than uncoated PDP NPs and stimulate less cytokine production in both cell lines.
    a. J774 macrophage cells would internalise more NPs that C3A hepatocyte cells.
    b. With lower uptake of PDP-PF68 compared to PDP NPs.

3. PDP-PF68 would be less genotoxic than PDP NPs.
    a. DNA damage observed would be via an oxidative mechanism.

2.2 Materials and methods

2.2.1 NP preparation

NPs were prepared from a novel polyester, by collaborators (Prof Cameron Alexander and Dr Kakde) from the University of Nottingham. The polymer, PDP was synthesised using succinic acid, phenylsuccinic acid and 1, 10-decandiol (Figure 2.2).

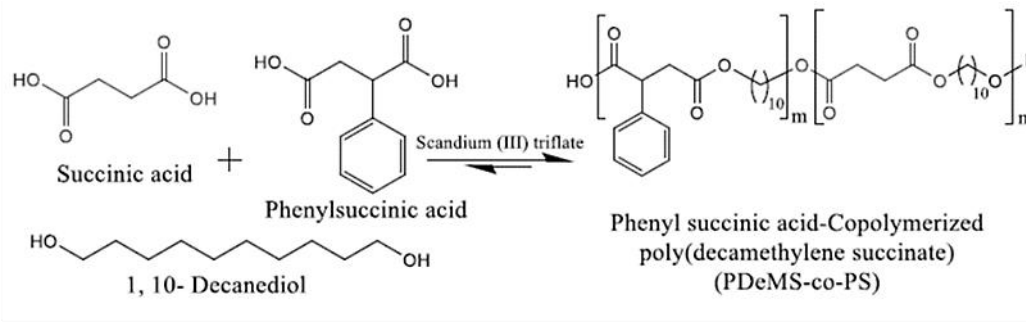

Figure 2.2 Polymer synthesis of PDP NPs.
Chemical structure and synthesis scheme of the block copolymer, PDP, used to formulate PF68 coated and uncoated NPs (adapted from Kakde et al. 2016).

NPs composed of poly (decamethylene succinate-co-pheylsuccinate) termed PDP, containing coumarin-6 dye were prepared using a nanoprecipitation method without and with a PF68 coating termed PDP-PF68. In brief, at room temperature (RT) PDP (20 mg) and coumarin-6 (1 mg) were dissolved in acetone (5 mL), and then this polymer dye solution was added dropwise to high-performance liquid chromatography water (10 mL) using a syringe pump, with or without the addition of 0.5% PF68. To help acetone evaporation, the suspension was stirred without a lid for four hours and then allowed to evaporate overnight without stirring.

Any evaporated water was replaced before the suspensions were filtered through a membrane syringe filter (pore size: 220 nm) (Millipore) and passed through PD10 Desalting Column (GE Healthcare Life Sciences) to separate the free dye from the suspensions and remove any contaminants. Suspensions were transported at RT and

immediately stored at stored at 4°C upon arrival. Stability was determined by monitoring changes in hydrodynamic diameter and identified to be one month (Kakde et al. 2016). For use in experiments, NPs were freshly diluted in cell culture medium and briefly vortexed.

2.2.2 NP characterisation

NPs were characterised by dynamic light scattering (DLS) and TEM. Using DLS, NPs were prepared in a phenol-red free Minimum Essential Medium Eagle cell culture medium containing 10% heat-inactivated foetal bovine serum (FBS), 2 mM L-glutamine (Gibco, Invitrogen), 100 U/mL penicillin/streptomycin (Gibco, Invitrogen), 1 mM sodium pyruvate (Sigma-Aldrich) and 1% non-essential amino acids (Sigma-Aldrich) termed PRF-Complete Medium at a NP concentration of 125 µg/mL. Hydrodynamic diameter, polydispersity index (PDI- an unitless value that reflects size distribution and stability of NP suspensions, (section 2.5.2)) and zeta potential were measured using a Zetasizer Nano ZS (Malvern) at the time of preparation (T0) and 24 hours post-incubation at 37°C and 5 % carbon dioxide (CO_2) (T24). Data are expressed as mean ± standard error mean (SEM).

TEM was used to verify the shape and size of the NPs, which were prepared at a concentration of 125 µg/mL in PRF-Complete Medium, then suspended on 200 mesh Formvar/Carbon Copper Grids (TAAB). These grids were air-dried for 30 minutes and imaged using a JEM-1400 Plus (JEOL) transmission electron microscope equipped with GATAN Oneview Camera and Gatan -GMS3 software operating at 80 kV. Images were processed and analysed using ImageJ/Fiji software.

2.2.3 Cell culture and cell treatment with NPs

Human C3A hepatocellular carcinoma cells and mouse J774 macrophage cells were obtained from the American Type Culture Collection. C3A cells were cultured in Minimum Essential Medium (MEM) supplemented with 10% heat-inactivated FBS, 2 mM L-glutamine (Gibco, Invitrogen), 100 U/mL penicillin/streptomycin (Gibco, Invitrogen), 1 mM sodium pyruvate (Sigma-Aldrich) and 1% non-essential amino acids

(Sigma-Aldrich), termed Complete Medium. J774 cells were cultured in RPMI Medium supplemented with 10% heat-inactivated FBS, 100 U/mL penicillin/streptomycin (Gibco, Invitrogen), termed Complete J774 Medium.

Both cell lines were maintained at 37°C and 5% CO_2 in 75 cm^2 tissue culture flasks (Corning). C3A cells were sub-cultured using 0.25% trypsin, in phosphate-buffered saline (PBS) (Gibco, Invitrogen). J774 cells were sub-cultured using a cell scraper. For use in experiments, cells were counted, and their viability assessed using 0.4% trypan blue (Gibco, Invitrogen) and a Bright-Line Haemocytometer (Sigma-Aldrich). Cells were seeded into microplates and incubated at 37°C and 5% CO_2 for 24 hours before exposure to NPs.

2.2.4 Identification of relevant NP concentrations for testing

To determine the appropriate concentrations of NPs for *in vitro* experiments the dose of Genexol ™, a polymeric micellar nanomedicine currently used in the treatment of cancer was used as a model nanomedicine (Yang et al. 2011). Genexol is typically administered to human patients at dosages of 300 mg/m^2 (m^2 is area of the human patients), every 3 weeks for 5 cycles for recurrent breast cancer, resulting in a total dose administration (TDA) of 1500 mg/m^2 (Kim et al. 2004). To convert mg/m^2 to mg/kg for human consumption, K_m (37 for humans) was used to convert surface area to weight ratio, based on guidance from the FDA (FDA 2005).
K_m is a conversation factor, calculated as follows, $K_m=100/KxW^{0.33}$, were K is a dimensionless factor used to adjust for animal body shapes differences that result in different surface area to weight ratios and W is body weight in kg (FDA 2005).

A TDA in mg/kg of 40 mg/kg was calculated by dividing the TDA in mg/m^2 by the human K_m. The total dose administered per individual (TDAI) of 2838 mg was calculated by dividing the average weight of a human male (70 kg) by the mg/kg calculated above. Next, to estimate the possible clinially relevant maxium NP exposure of each heptocyte in a liver the following assumptions were made, that 100% of administered NPs accumulate in the liver and that the NPs distribute equally amongst all hepatocytes. The average liver has approximately 171 million hepatocytes per gram, and the average

minimal weight of a healthy human male liver is 986 g, resulting in $1.686x10^{11}$ hepatocytes in the average male liver (Molina & DiMaio 2012). An *in vivo* dose per hepatocyte (DPH) of 1.68×10^{-5} µg/hepatocyte was calculated by dividing the TDAI by the number of hepatocytes in an average male liver.

It was essential to have an *in vitro* exposure range containing concentrations similar to those expected for *in vivo* dosing to reflect the application of these NPs in the clinic. For *in vitro* experiments, a concentration ranging from 1-300 µg/mL was used. Assuming the concentration was distributed equally among all the C3A hepatocytes, a concentration per cell *in vitro* of 6.0×10^{-4} µg/hepatocyte was calculated by dividing the top concentration of NPs (300 µg/mL) by the number of C3A hepatocyte cells ($5x10^5$ cells/mL). Therefore, 300 µg/mL gave µg/hepatocytes one order of magnitude higher than that seen *in vivo*; it was determined that serial dilution from this maximum value would, therefore, generate useful data.

2.2.5 Cytotoxicity Assay: AB, CFDA-AM, NR

A 96-well plate fluorescent-based assay which simultaneously assessed the viability of C3A cells following exposure to NPs using AB, CFDA-AM and NR assays was applied (Connolly et al. 2015).

Cells were seeded at a concentration of $1.56x10^5$ cells/cm^2 in 96-well plates and incubated for 24 hours at 37°C and 5% CO_2. Cells were then exposed to NPs (4.6, 9.3, 18.7, 37.5, 75.0, 150 and 300 µg/mL) (100 µL/well) or MEM Complete Medium (control), 1% Triton X100 (positive control) or sterile water diluted in medium (vehicle control) in triplicate for 24 hours at 37°C and 5% CO_2.

Following NP treatment, the cell supernatant was collected and frozen at -80˚C, and cells were washed twice using PBS. Next, a solution containing 1.25% v/v AB (TREK Lab Services) and 4 µM CFDA-AM (Sigma-Aldrich) was prepared in PRF Complete Medium and added (100 µL/well), and cells were incubated at 37°C and 5% CO_2 for one hour. Fluorescence was measured on a SpectraMax M5 Microplate Reader (Molecular Devices) at excitation/emission (Ex/Em) of 532/590 nm for AB and 485/535 nm for CFDA-AM.

Cells were then washed twice using PBS, and NR solution (33 µg/mL) in PRF Complete Medium added to each well (100 µL) (Sigma-Aldrich) and incubated at 37°C and 5% CO_2 for one hour. Following incubation, cells were washed three times with PBS. Then 50% ethanol and 1% acetic acid was prepared in water (Baxter) and added (100 µL) before shaking the plates at RT for 20 minutes. Fluorescence was measured in a SpectraMax M5 Microplate Reader at an Ex/Em of 532/645 nm. All experiments were repeated three times, with some concentrations changed between each repetition to fill in the gaps in the concentration-response curve, according to the benchmark concentration approach (De Jong et al. 2013). The benchmark concentration approach here refers to building on the previous experiment replicates to form a complete concentration-response curve by addressing additional doses between replicates, this can allow for independence in concentration choice and concentration spacing as well as allow for comparison between different NPs (Wignall et al. 2014). Data are expressed as mean % cell viability (i.e. % of untreated control) ± SEM.

To determine the interference potential of the NP with the assay parameters, NPs (4.6, 9.3, 18.7, 37.5, 75.0, 150 and 300 µg/mL) where prepared in triplicate, in PRF Complete Medium alone (100 µL/well) and fluorescence was measured on a SpectraMax M5 Microplate Reader at excitation/emission (Ex/Em) of 532/590 nm for AB, 485/535 nm for CFDA-AM and 532/645 nm for NR immediately following preparation (T0) and following 24 hours at 37○C and 5% CO^2 (T24). To assess if NPs interfered with the assay reagents, NPs (4.6, 9.3, 18.7, 37.5, 75.0, 150 and 300 µg/mL) where prepared in triplicate, in PRF Complete Medium containing 1.25% v/v AB, 4 µM CFDA-AM or 33 µg/mL NR solution (33 µg/mL) (100 µL/well) and fluorescence was measured on a SpectraMax M5 Microplate Reader at excitation/emission (Ex/Em) of 532/590 nm for AB, 485/535 nm for CFDA-AM or 532/645 nm for NR immediately following preparation (T0) and following 1 hour at 37○C and 5% CO^2 (T1). To establish if the NPs interference with the assays end product that is to be measured fluorescently , NPs (4.6, 9.3, 18.7, 37.5, 75.0, 150 and 300 µg/mL) where prepared in triplicate, in PRF Complete Medium containing the end product of AB, Rescurufin (2uM) or the end product of CFDA-AM, 5-CF(4uM) (100 µL/well) and fluorescence was measured on a SpectraMax M5 Microplate Reader at excitation/emission (Ex/Em) of 532/590 nm for AB or 485/535 nm for CFDA-AM

immediately following preparation (T0) and following 1 hour at 37○C and 5% CO^2 (T1). Inference results were only reported when positive.

2.2.6 Uptake assay: Confocal microscopy

Cells were seeded onto 12 mm uncoated glass coverslips at a concentration of $6.58x10^4$ cells/cm^2 at 37°C and 5% CO_2 in 24-well plates for 24 hours. Next, they were exposed to a sub-lethal concentration of NPs (equivalent to 100 µg/mL in 96 well plate set up determined during cytotoxicity assays, section 2.2.5) or control (MEM Complete Medium) for 10, 60, 240 and 1440 minutes at 37°C and 5% CO_2. All steps were performed in subdued lighting at RT. Equivalent concentration calculated here and in all following experiments by: Mass Dose at 100 µl in 96 well plate = 31.25 µg/cm^2 (Concentration x Volume)/Surface Area ((100 x 0.1)/0.32). Therefore, concentration needed in 24 well plate = 118.75 µg/mL (Mass Dose x Surface Area)/Volume ((33.43 x 1.9)/0.5).

Cells were then washed twice with PBS following exposure and fixed in 3% formaldehyde (in PBS) (Sigma-Aldrich) for 30 minutes at 4°C. Subsequently; the cells were washed twice with PBS and incubated with 50 mM ammonium chloride (Sigma-Aldrich) to quench unreacted aldehyde groups, for 10 minutes. Cells were then washed a further three times with PBS followed by permeabilisation with 0.1% Triton for 20 minutes. Cells were further washed twice with PBS, before the addition of the primary antibody monoclonal anti α tubulin mouse ascites fluid clone DM1A (Molecular Probes) (1:200 in PBS) for one hour. After incubation, cells were washed twice with PBS and incubated with the secondary antibody Rhodamine Red goat anti-mouse Immunoglobulin G (Molecular Probes) (1:100 in PBS) for one hour. Cells were washed twice and incubated for five minutes with 1 µg/mL DAPI (4′,6-diamidino-2-phenylindole) (Sigma-Aldrich) prepared in PBS.

Finally, cells were washed twice with PBS and coverslips were mounted onto glass slides with Vector shield (Vector) and edges sealed with nail varnish. Slides were stored at 4°C before imaging using A Zeiss LSM880 confocal microscopy and the Zeiss Zen program.

2.2.7 Uptake Assay: Plate method

A 96-well plate fluorescence-based uptake assay was developed used to determine the uptake of fluorescently loaded NPs by C3A cells. Cells were seeded in 96-well plates as in section 2.2.5 and were exposed to NPs at sub-lethal concentrations (4.6-300 µg/mL) or MEM Complete Medium (control) in duplicate for 10, 60 and 1440 minutes at 37°C and 5% CO_2 or 1440 minutes at 4°C. All steps were performed in the subdued lighting at RT.

Following NP treatment, cells were washed twice using PBS, then incubated for 10 minutes in 50 µL of 0.4% volume (of solute) per volume (of solvent) (v/v) Trypan Blue to quench extracellular fluorescence. Cells were washed three times using PBS. To lyse cells, a working solution of 0.2% Triton X100 was added (100 µL) and the plates were shaken for 20 minutes. Fluorescence of the cell lysate was measured in SpectraMax M5 Microplate Reader at Ex/Em 488/550 nm. Standard curves were prepared in cell lysate at concentrations of 4.6-300 µg/mL for each NP and used to calculate µg/mL of NPs retained following NP exposure; fluorescence was measured at an Ex/Em of 488/550 nm. Data are expressed as µg/mL retained (from appropriate standard curves) ± SEM.

2.2.8 Genotoxicity assessment: Comet assay

A six-well-based assay was used to assess specific oxidative DNA damage and DNA strand breaks using the Fpg modified Comet assay. The % DNA tail was measured using electrophoresis as cleaved DNA will produce a longer DNA tail than the intact nucleus (Bulcão et al. 2014; Annangi et al. 2014). Although guidance documents on genetic toxicology testing put forward by the Organisation for Economic Co-operation and Development (OECD), advice a minimum of three concentrations be used, due to the limited volume and concentration of the NPs for these high-volume genotoxic assays the number of concentrations was limited to two, although these results can give insight in to the genotoxicity of these NPs, results most be considered preliminary (OECD 2015).

Following 24 hours growth at 37°C and with 5% CO_2 in 6-well plates (Costar) (1.56×10^5 cells/cm^2), C3A cells were washed twice with Hanks Balanced Salt Solution (HBSS) (Sigma-Aldrich) then exposed to NPs (75 and 150 µg/mL), HBSS (control) or 60 µM

hydrogen peroxide (H_2O_2, positive control) (Sigma-Aldrich) in duplicate for 240 minutes at 37°C and 5% CO_2.

Cells were washed twice with HBSS and treated with trypsin (section 2.2.3) and then resuspended in Complete Medium and centrifuged at 850 g for two minutes. Subsequently, the supernatant was discarded, and cells resuspended in HBSS (1 mL). The cells were then added (20 μL) to low melting point agarose (240 μL). The cell-agarose suspension (125 μL) was then deposited on pre-coated agarose slides in duplicate. Slides were incubated on ice for 10 minutes then transferred to a lysis buffer (66.75 mL lysis buffer base (Sigma-Aldrich), 7.5 mL dimethyl sulphoxide (Sigma-Aldrich), 750 μL Triton-X (Sigma-Aldrich)), for 24 hours at 4°C.

After incubation, the slides were washed in a buffer; 400 mM HEPES (4-(2-hydroxyethyl)-1-piperazineethanesulfonic acid), 1 M potassium chloride, 5 mM ethylenediaminetetraacetic acid (EDTA) and 2 mg/mL bovine serum albumin at pH8 (Sigma-Aldrich). Slides were then incubated with Fpg enzyme (Sigma-Aldrich) (1:500 in Fpg buffer), or the buffer alone at 37°C for 30 minutes. Slides were then transferred to an electrophoresis solution (300 mM sodium hydroxide, 200 mM EDTA, 2 L distilled water at pH 13) and incubated for 20 minutes at 4°C. Electrophoresis was carried out for 20 minutes at 24 V and 270 mA. Next, slides were transferred to a neutralisation buffer (48.5 g Tris base, 900 mL distilled water pH7.5 (Sigma-Aldrich)) for 15 minutes at 4°C. Slides were then dried for 15 minutes at RT before being fixed with 100% ethanol and stored at 4°C.

Samples were stained with GelRed (Biotum) to visualise DNA. They were imaged using a fluorescence microscope (Zeiss AX10 with Allied Vision Technologies Stingray camera) connected to the image-analysing software (Comet Assay IV, Perceptive Instruments, UK). Fifty measurements were taken for each slide per experiment. The % DNA in the tail can be used as a proportional measurement of DNA damage. The software above used the ratio of the intensity of the comet tail and intensity of the comet head and tail together to calculated % DNA in the tail. Data are expressed as mean % Tail DNA ± SEM.

The above experiment, section 2.2.8 was performed by Gavin Millar, School of Engineering and Physical Sciences, Nano Safety Research Group, Heriot-Watt University as part of his undergraduate research project under supervision by Leagh Powell and Dr David Brown of the NanoSafety Research Group.

2.2.9 Measurement of cytokine production

A multiplex sandwich enzyme-linked immunosorbent assay (ELISA) was used to measure secretion of IL-8, IL-1ra, growth-regulated α protein (Gro-α) and TNF-α from C3A cells exposed to NPs. Supernatants obtained from the cytotoxicity experiments were thawed and analysed using a Human Magnetic Luminex Assay kit (R&D Systems) as per the manufacturer's instructions. All steps using cell supernatant were carried out at RT and in reduced light. Sublethal NP concentrations (75, 150 and 300 µg/mL as determined in section 2.2.5) were assessed as well as Complete Medium (negative control).

Briefly, the microbead cocktail (25 µL) was added to appropriate wells in a 96-well plate, followed by samples, negative controls and standards (0-2000 pg/mL prepared in Complete Medium) (50 µL) and incubated for two hours shaking at RT. After incubation, wells were washed three times with wash buffer (100 µL), before adding biotin antibody cocktail (25 µL) and incubation of one hour while shaking at RT. Wells were washed three times with wash buffer, followed by the addition of 50 µL of streptavidin-PE, and incubated 30 minutes at RT with constant shaking. Before measuring, the wells were washed three times with wash buffer, and finally, samples were resuspended in 100 µL wash buffer and read using Bio-Plex MAGPIX Multiplex Reader (Bio-Rad). The concentration of cytokines present in the samples was calculated from the linear regression obtained from the standard curves. Data are expressed as average pg/mL ± SEM.

Additionally, NPs' interference with this assay was established by adding the standard curves midpoint (SCM) concentration to 300 µg/mL NPs prepared in the same medium as the standard curve. Any interference observed was presented in results, if not presented interference was not observed.

2.2.10 Statistical analysis

Experimental data were analysed using GraphPad Prism software. One-way analysis of variance (ANOVA) using Tukey post-test or two-way ANOVA, followed by the Bonferroni post-test were used to test significance which was set at $p< 0.05$. All experiments were repeated three times on different days unless otherwise stated.

2.3 Results

2.3.1 PDP and PDP-PF68 NPs: Physiochemical characterisation

Measurements of hydrodynamic diameter, zeta potential and the PDI of NPs prepared in PRF Complete Medium were performed using DLS immediately after preparation and following 24 hours' incubation at 37°C and with 5% CO_2, to reflect assay conditions (Figure 2.3). Immediately following preparation, the hydrodynamic diameters of PDP-PF68 NPs were observed to be significantly ($p< 0.05$) higher (145.93±1.41 nm) than those of the PDP NPs, albeit a small increase in size of ~6 nm (139.50±0.90 nm), no difference was seen following 24 hours of incubation (Figure 2.3A).

The zeta potentials of both PDP-PF68 and PDP NPs were slightly negative, ranging from -10.7 to -12.7 mV (Figure 2.3C). No significant differences were seen for zeta potential between PDP-PF68 and PDP NPs at both time points investigated. The PDI values for both PDP-PF68 and PDP NPs were low, 0.13 for PDP NPs and ranging from 0.20-0.22 for PDP-PF68 NPs. PDI values were significantly higher ($p< 0.05$) for PDP-PF68 when compared to PDP NPs at both time points (Figure 2.3B). The PDI was significantly lower ($p < 0.05$) for PDP-PF68 NPs after 24 hours incubation.

TEM images of PDP-PF68 and PDP NPs suspended in PRF Complete Medium are shown in Figure 2.4. TEM images suggest that there are low levels of agglomeration/aggregation for both NPs investigated. PDP NPs appeared spherical and monodispersed with evidence of a visibly denser core when compared to PDP-PF68 NPs (Figure 2.4A/B). PDP-PF68 NPs also appear spherical, although there seems to be a small increase in aggregation/agglomeration, compared with PDP NPs, reflected in the PDI data (Figure 2.4 B). The diameter of NPs according to TEM images ranges from ~50-80 nm.

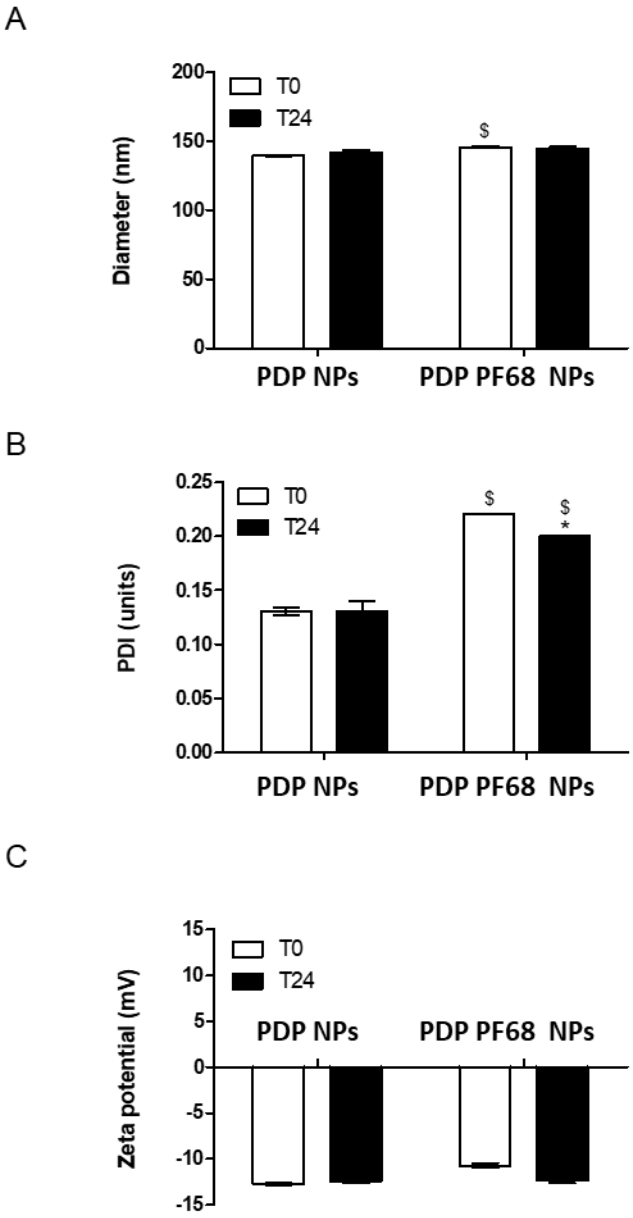

Figure 2.3 Characterisation of PDP and PDP-PF68 NPs properties: DLS.

NPs (PDP and PDP-PF68) suspended in Complete Medium (125 µg/mL), hydrodynamic diameter (A), PDI (B) and zeta potential (C) were assessed at 0 hours (T0) and 24 hours (T24) post incubation at 37°C and 5% CO_2, using DLS. Significant difference indicated by *= $p < 0.05$ comparing T0 and T24. Significance indicated by $ = $p < 0.05$ comparing PDP to PDP-PF68 NPs. Data are expressed as mean ± SEM (n=3).

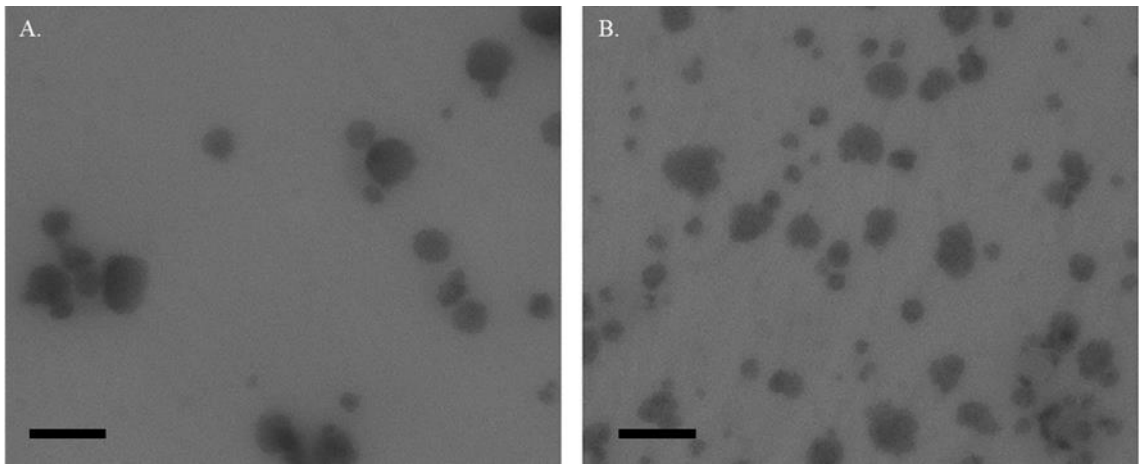

Figure 2.4 TEM Characterisation of PDP and PDP-PF68 NPs.

Images of PDP (A) and PDP-PF68 (B) NPs, suspended in PRF Complete Medium at 125 µg/mL and imaged using TEM. Representative images (n=3), scale bar, represents 200 nm.

2.3.2 PDP and PDP-PF68 NPs: Cytotoxicity in C3A cells

Cells were exposed to NPs using a benchmark concentration approach at concentrations ranging from 4.6-300 µg/mL for 24 hours to determine the impact of PDP and PDP-PF68 NPs on C3A cell viability using three simultaneous fluorescent assays; AB; CFDA-AM and NR. Measurement of metabolic activity using the AB assay showed no significant reduction in viability for cells exposed to PDP NPs when compared with the control (Complete Medium), at the tested concentrations (Figure 2.5A). PDP-PF68 NPs induced a significant decrease ($p < 0.05$) in cell viability at concentrations of 62.5, 250 and 300 µg/mL, although, cell viability was not reduced to below 80% at the concentrations tested and therefore is unlikely to be biologically relevant (Figure 2.5A).

No significant effect on cell viability was observed following exposure of C3A cells to PDP NPs at all concentrations tested when the CFDA-AM assay was used (Figure 2.5B). At concentrations >150 µg/mL, PDP-PF68 NPs were seen to stimulate a significant decrease ($p < 0.05$) in the viability of C3A cells. Again, cell viability did not fall below 80% (Figure 2.5B). Using the NR assay, it was observed that PDP NPs had a statistically significant effect ($p < 0.05$) at the two highest concentrations tested (250 and 300 µg/mL), with viability falling to 88.4 and 94.6% respectively. The PDP-PF68 NPs had a similar effect as PDP NPs at concentrations of 250 and 300 µg/mL with viability seen to be 86.6% at 250 µg/mL and 97.1% at 300 µg/mL (Figure 2.5C).

An EC_{20} value (effective concentration where 20% of cells die), indicating the concentration at which NP exposure causes 20% cell death, could not be calculated within the range of concentrations used for either NPs with the above assays.

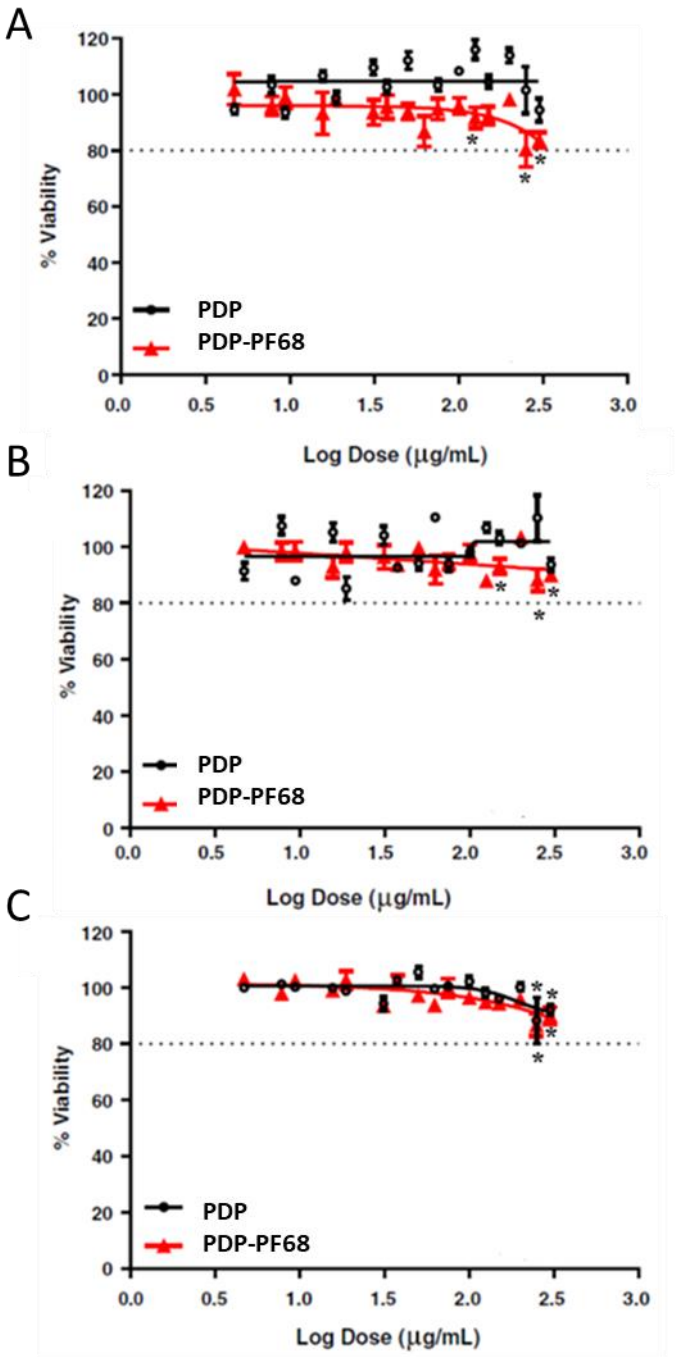

Figure 2.5 Cytotoxicity of PDP and PDP-PF68 NPs to C3A cells.

C3A cells were exposed to PDP (black) or PDP-PF68 (red) NPs, 4.6-300 µg/mL for 24 hours. Percentage viability was measured via AB (A), CFDA-AM (B) and NR (C) assays. Data are expressed as mean % cell viability (i.e. % of untreated control) ± SEM (n=3). Significance indicated by * = $p < 0.05$, compared with control.

2.3.3 PDP and PDP-PF68 NPs: Uptake confocal using C3A cells

Cells where exposed to PDP-PF68 and PDP NPs at a sub-lethal concentration (100 µg/mL) to allow examination of the NPs' internalisation by C3A cells over time using confocal microscopy. Cell structure was visualised by labelling tubulin (red), while DAPI was used to stain the nucleus (blue). The PDP and PDP-PF68 NPs were loaded with a fluorescent green dye, coumarin-6 (green), to mimic pharmaceutical or bioimaging product. A yellow colour was used to indicate points where tubulin and NPs colocalised. When DNA and NPs colocalised, a green-blue colour was used.

Both NPs appear to be readily taken up by C3A cells after 10 minutes (Figure 2.6A). Internalisation increases progressively from 10 to 1440 minutes for both NPs. Confirmation of NP internalisation in the interior of the cell was apparent in xy-yz micrographs generated from z-stacks (Figure 2.7). A change in subcellular distribution over time was observed. NPs were compartmentalised at 10-240 minutes, potentially within the cells' organelles such as endosomes, lysosomes or mitochondria (Figure 2.7B/C). Additionally, there was evidence that NPs are localised between cells at 60 and 240 minutes, which could suggest accumulation in bile canaliculi (Figure 2.6B/C). Colocalisation of both NPs with tubulin was evident within the perinuclear region of the cells at 60 and 240 minutes (Figure 2.6B/C).

At 240 minutes, both NPs appears to be diffusely accumulated within the nucleus of some cells, evident by a green-blue colour (Figure 2.7C). There were vacuoles in the perinuclear region which contain PDP NPs at all time points, and for PDP-PF68 NPs this was apparent up to 240 minutes. There were changes to the nucleus morphology of cells treated with PDP-PF68 NPs. More specifically, at 10, 240 and 1440 minutes there was possible nuclear fragmentation or blebbing (Figure 2.6B/C/D indicated by arrow). After 1440 minutes' exposure, the pattern of internalised NPs diverged for the PDP-PF68 NPs and PDP NPs. The PDP NPs were diffuse throughout the cytoplasm of the cell at 1440 minutes, with some NP compartmentalisation. For the PDP-PF68 NPs, a diffuse pattern was also apparent, but with no NP compartmentalisation. While cells exposed to PDP-PF68 NPs for 1440 minutes had vacuoles located adjacent to the nucleus that appeared more abundant and lacked NPs. At 1440 minutes evidence of nuclear damage was

observed for cells treated with both NPs (highlighted by white arrows in Figures 2.6D and 2.7D)

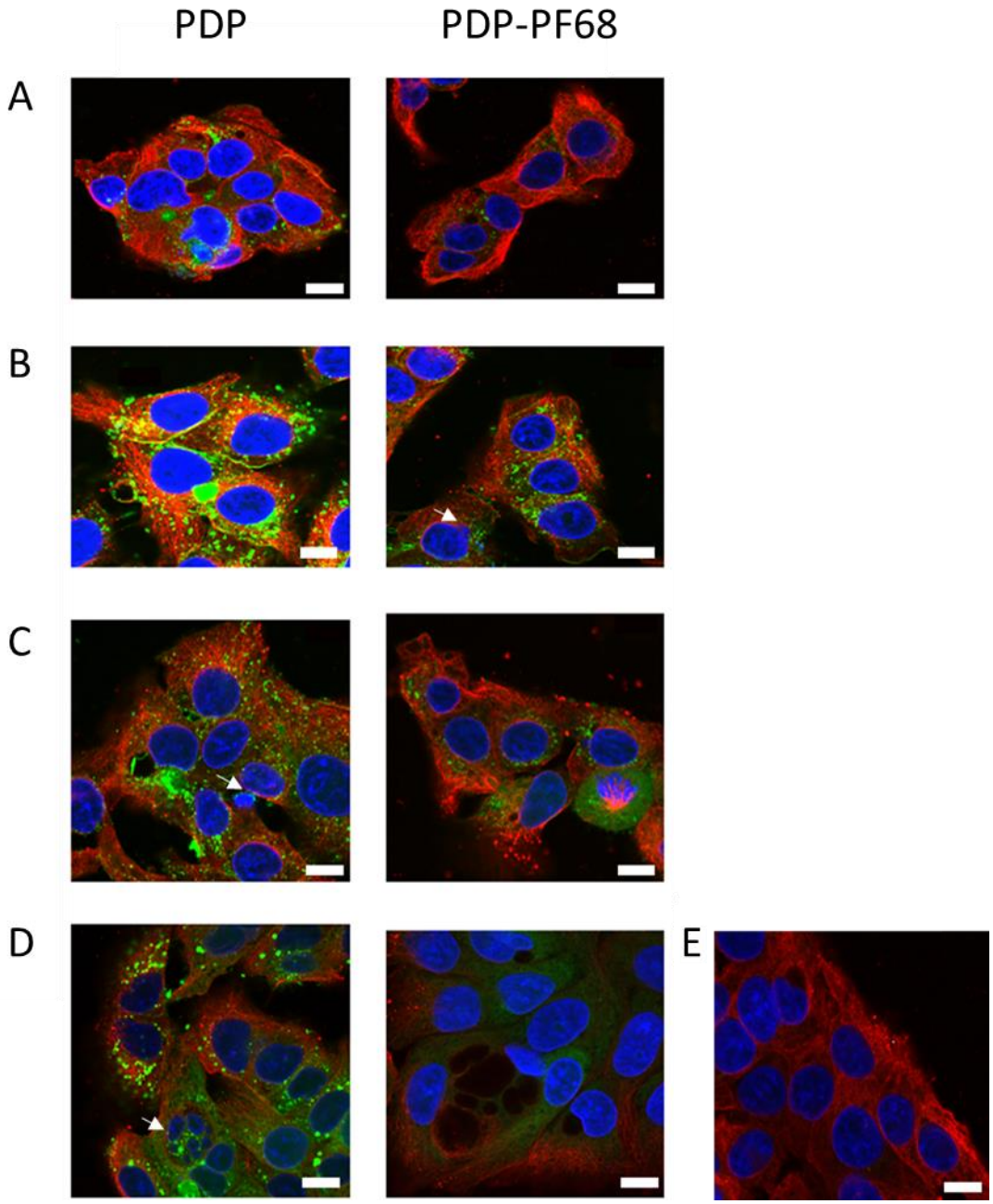

Figure 2.6 Uptake of PDP and PDP-PF68 NPs over time by C3A cells.

Cells were treated with 100 µg/mL PDP NPs or PDP-PF68 (green) for 10 (A), 60 (B), 240 (C) or 1440 (D) minutes or Complete Medium as a control (E). Tubulin (red), DNA (blue), representative image (n=3) scale bar =10 µm. Arrows point towards nucleus damage.

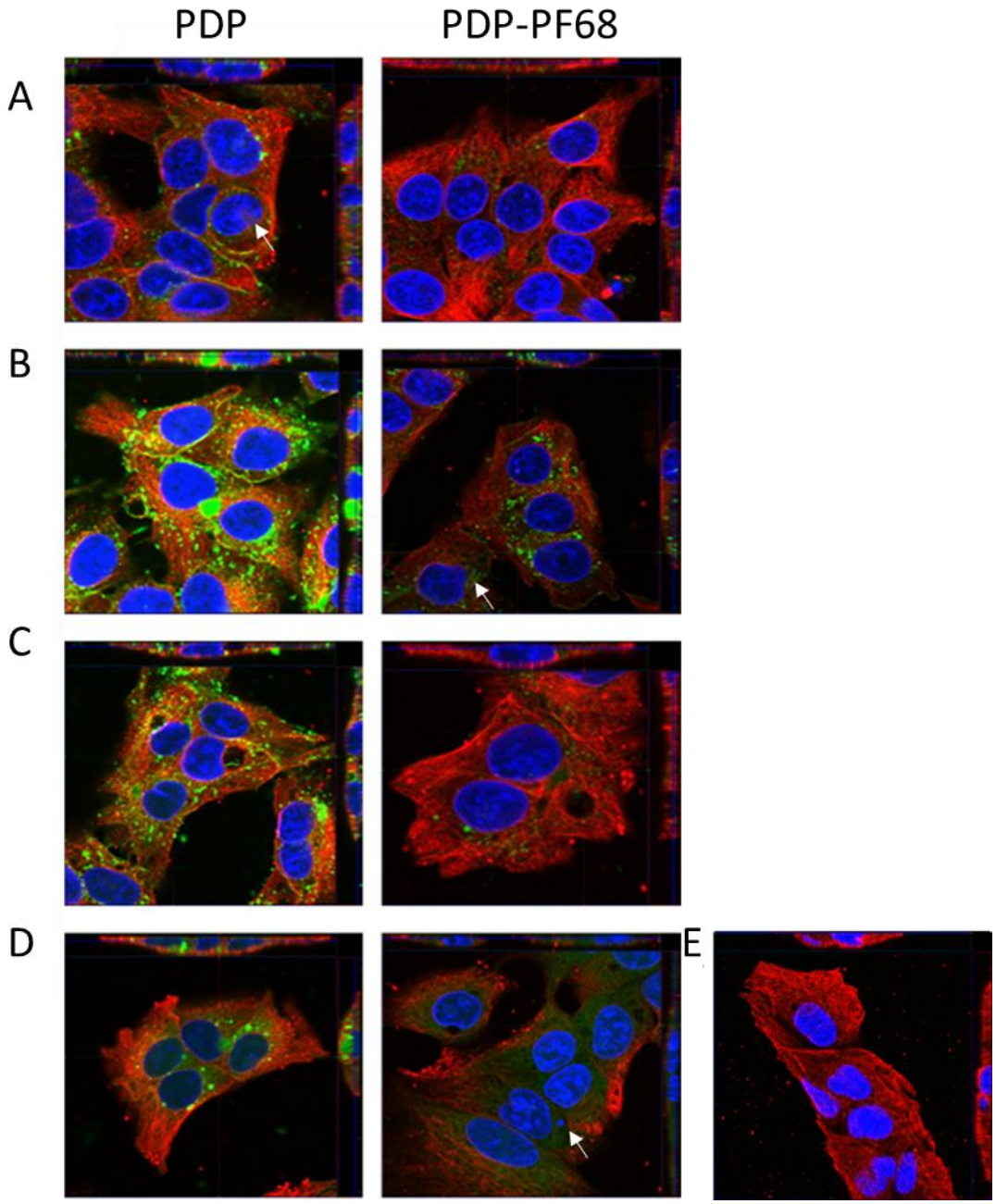

Figure 2.7 Uptake of PDP and PDP-PF68 NPs over time by C3A cells: Z stacks. Cells were treated with 100 µg/mL PDP NPs or PDP-PF68 NPs (green) for 10 (A), 60 (B), 240 (C) or 1440 (D) minutes or Complete Medium as a control (E), xy and yz micrographs generated from Z-stacks. Tubulin (red), DNA (blue), representative images (n=3), scale bar = 10 µm. Arrows point towards nucleus damage

2.4.2 PDP and PDP-PF68 NPs: Uptake, plate using C3A cells

The µg/mL retained of the applied NP concentration by the C3A cells following exposure was calculated over a range of concentrations (4.6-300 µg/mL). PDP NPs had a significant increase ($p < 0.001$) in uptake at early time points (10 minutes) with a concentration-dependent increase (Figure 2.8). At 60 and 1440 minutes significant increases ($p < 0.001$) in uptake were observed at concentrations up to 37.5 and 75 µg/mL respectively. While there was less NP internalisation above these concentrations. There appears to be no significant internalisation of either NPs at 4°C (Figure 2.9).

More specifically, the µg/mL retained increased with time (Figure 2.8). The PDP NPs had the highest level of uptake, 13.8 µg/mL at a NP concentration of 75 µg/mL after 1440 minutes. Significant uptake ($p < 0.001$) for PDP-PF68 NPs was only observed at 1440 minutes, with 2.4 µg/mL retained at a NP concentration of 150 µg/mL. Quantifying uptake of PDP-PF68 and PDP NPs using a fluorescence 96-well plate-based method confirmed the confocal microscopy observations (section 2.3.3).

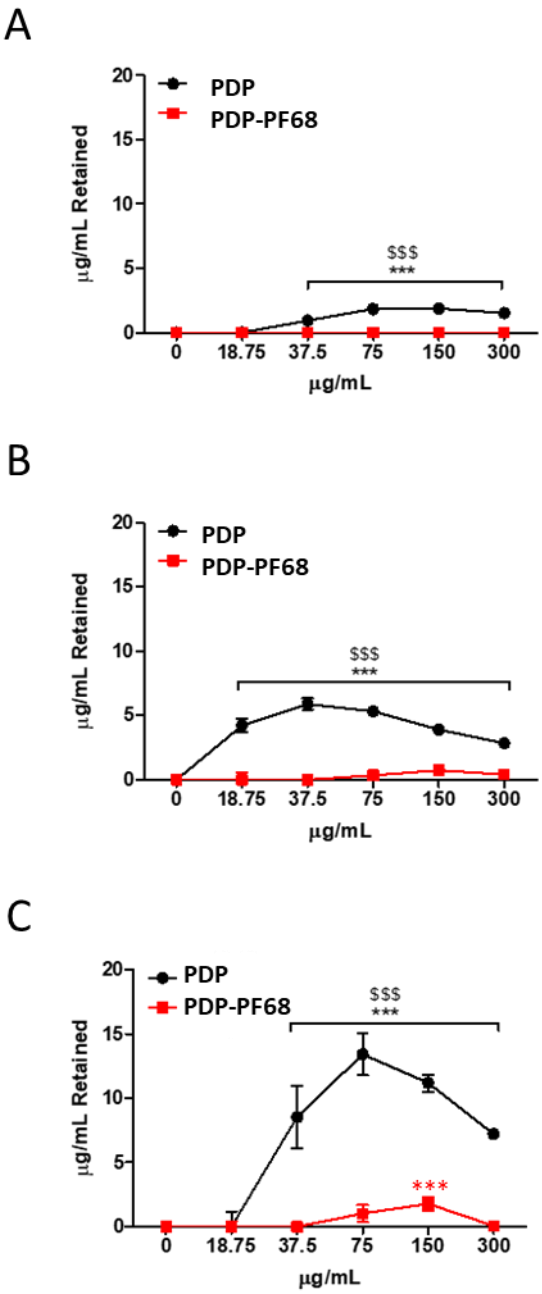

Figure 2.8 Uptake of PDP and PDP-PF68 NPs over time in C3A cells:Plate method.

Cells were exposed to PDP (black) or PDP-PF68 (red) NPs for 10 (A), 60 (B) and 1440 (C) minutes, at 18.75-300 µg/mL. Data are expressed as µg/mL retained (from appropriate standard curves) ± SEM (n=3). Significance indicated by ***=p< 0.001 compared with control, $$$=p< 0.001, when PDP NPs compared with PDP-PF68 NPs.

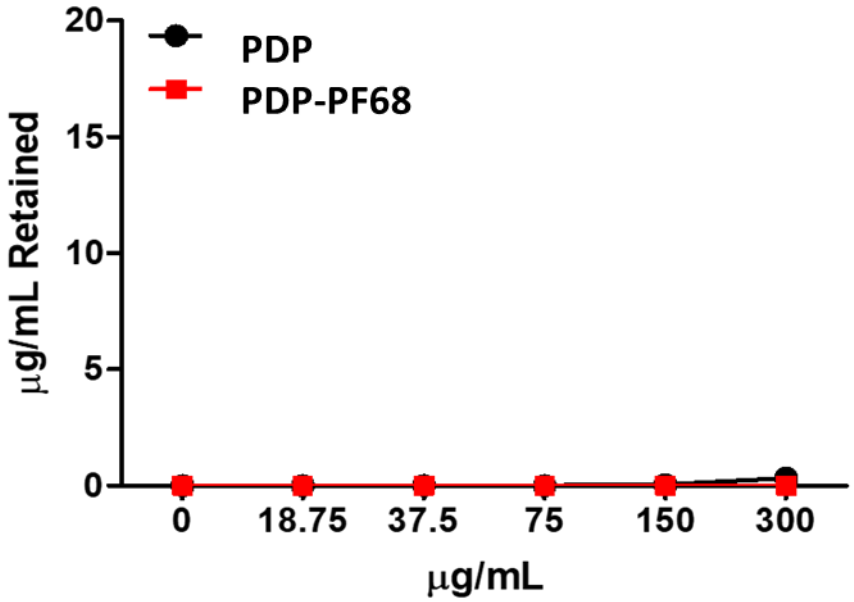

Figure 2.9 Uptake of PDP and PDP-PF68 NPs in C3A cells, at 4°C: Plate-based method.

Cells were exposed to PDP (black) or PDP-PF68 (red) NPs, at 18.75-300 µg/mL for 1440 minutes at 4°C. Data are expressed as µg/mL retained (from appropriate standard curves) (n=3).

2.3.4 PDP and PDP-PF68 NPs: Genotoxic effect on C3A cells

The genotoxic potential of PDP and PDP-PF68 NPs in C3A cells was assessed using the Comet assay in the presence and absence of Fpg to identify the contribution of oxidative stress to DNA damage observed. C3A cells were exposed to NPs at concentrations of 75 and 150 μg/mL for four hours.

Assessment of mean % of DNA in Tail was used to quantify NP-induced genotoxicity. PDP NPs did not induce DNA damage at the concentrations used, with or without Fpg (Figure 2.10). PDP-PF68 NPs induced a significant increase ($p< 0.05$-0.001) in DNA damage in C3A cells at both concentrations with and without Fpg (Figure 2.10B). Similar levels of DNA damage were seen for PDP-PF68 with and without Fpg at 75 μg/mL with a significant 2-fold increase in DNA damage ($p< 0.05$-0.005).

A significant 1.6-fold increase in DNA damage ($p< 0.05$) at a concentration of 150 μg/mL was observed in the absence of Fpg. For PDP-PF68 NPs, DNA damage was increased significantly ($p< 0.001$) in the presence of Fpg at 150 μg/mL, with a four-fold increase in DNA damage observed, compared with the untreated control. The PDP-PF68 NPs were significantly ($p< 0.01$-0.001) more genotoxic than the PDP NPs at 75 150 μg/mL with or without Fpg while at 150 μg/mL, a significant difference was only seen for with Fpg (Figure 2.10A/B). Notably, PF68 (alone) at a concentration representative of PF68 present in NP suspensions prepared did not induce DNA damage (Figure 2.10 C). The positive control H_2O_2 (60 μM) induced significant DNA damage ($p < 0.001$) with and without Fpg, with a higher level of significant DNA damage observed for cells treated with Fpg.

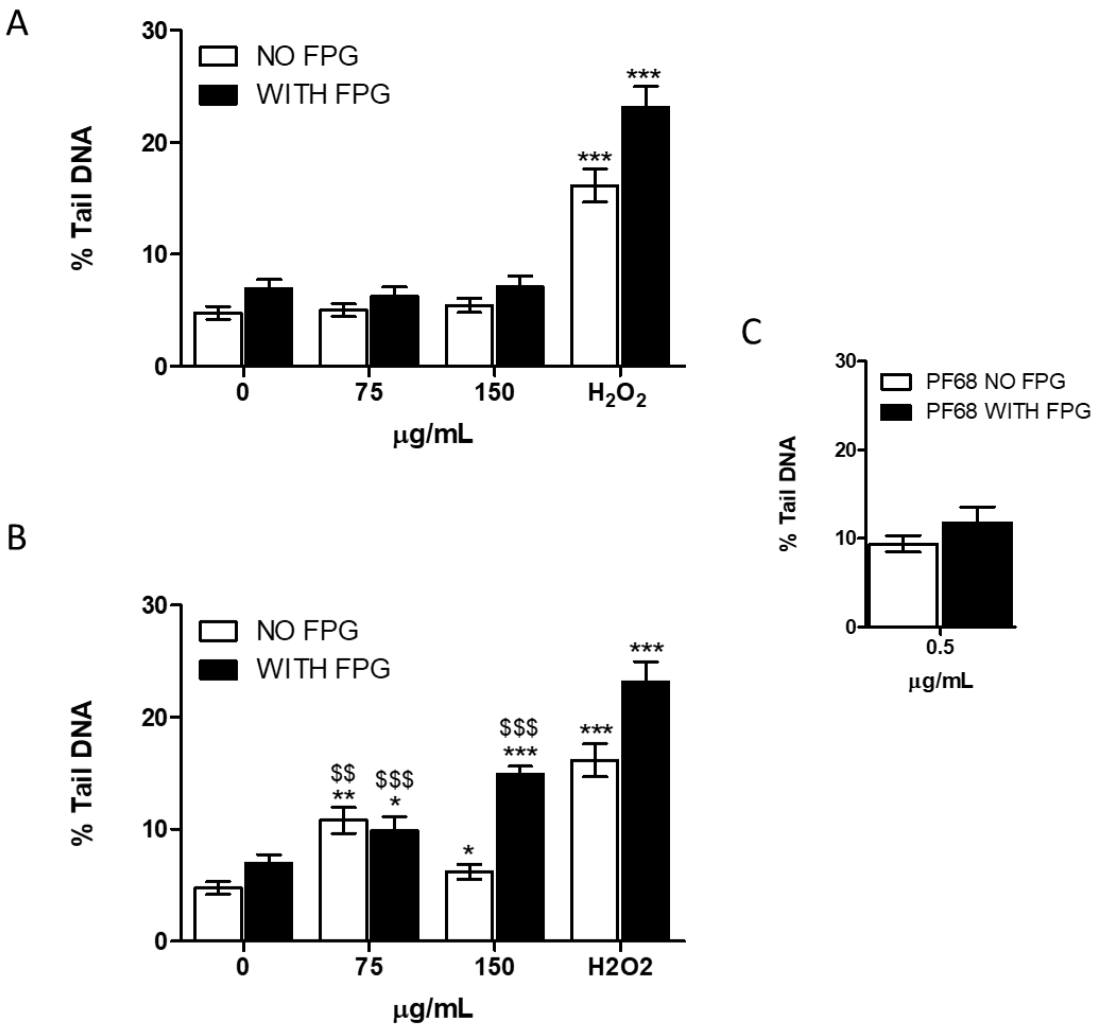

Figure 2.10 Genotoxicity of PDP and PDP-PF68 NPs in C3A cells: Comet assay. Cells were exposed to PDP (A) or PDP-PF68 (B) NPs at 75 and 150 µg/mL, 60 µM H_2O_2 (positive control) or HBSS (untreated control) or 0.5 µg/mL of PF68 (C) for four hours ± Fpg. Data are expressed as mean % Tail DNA ± SEM (n = 3). Significance was indicated by *** = p< 0.001, ** = p< 0.01 and * = p< 0.05, when compared with untreated control. $$$ = p< 0.001 and $$ = p< 0.01 when compared with PDP NPs at the same concentration.

2.3.5 PDP and PDP-PF68 NPs: Cytokine production in C3A cells

C3A cells were exposed to PDP and PDP-PF68 NPs for 24 hours, and production of IL-8, TNF-α, IL-ra and Gro-α were measured in the supernatant. There was a minimal yet significant decrease ($p<0.05$-0.001) seen in IL-8 production when C3A cells were exposed to PDP-PF68 NPs when compared to untreated cells. However, the low values suggest this was not biologically relevant (Figure 2.11A). There was no significant change in TNF-α production when cells where exposed to either NP (Figure 2.11B).

When C3A cells were exposed to PDP-PF68 NPs, there was a significant concentration-dependent increase ($p< 0.001$) in IL-1ra production from 75-300 µg/mL (Figure 2.12A). A similar significant increase ($p< 0.001$) was seen in Gro-α production for cells exposed to 150 and 300 µg/mL of PDP-PF68 NPs (Figure 2.12B). There appeared to no increase in IL-1ra or Gro-α production for cells exposed to PDP NPs.

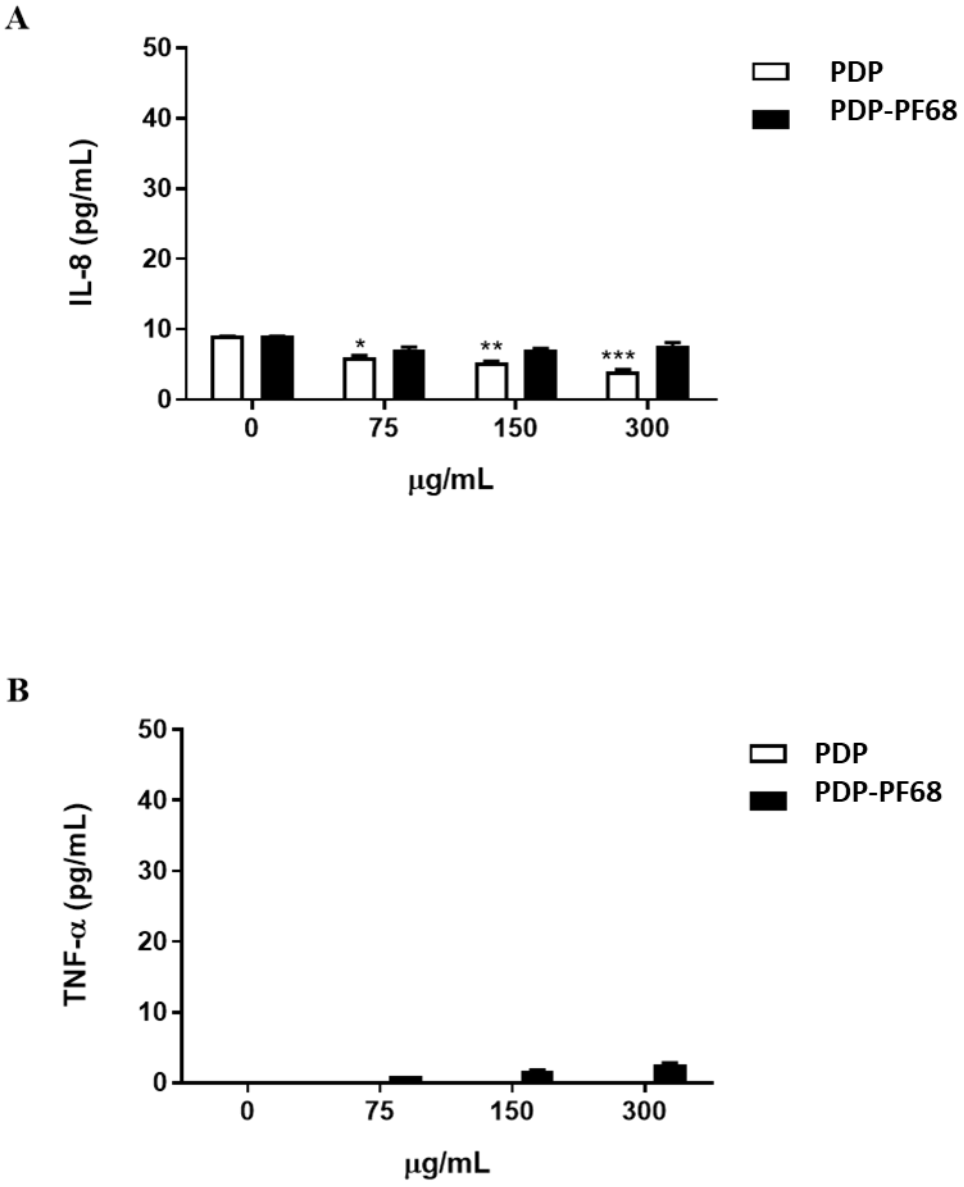

Figure 2.11 IL-8 and TNF-α production induced by PDP and PDP-PF68 NPs in C3A cells.

Cells were exposed to PDP or PDP-PF68 NPs for 24 hours at 75, 150 and 300 µg/mL, IL-8 (A) and TNF-α (B). Data are expressed as mean pg/mL ± SEM (n=3). Significance indicated by ***= $p< 0.001$, **= $p< 0.01$, *= $p< 0.05$ when compared with the untreated control.

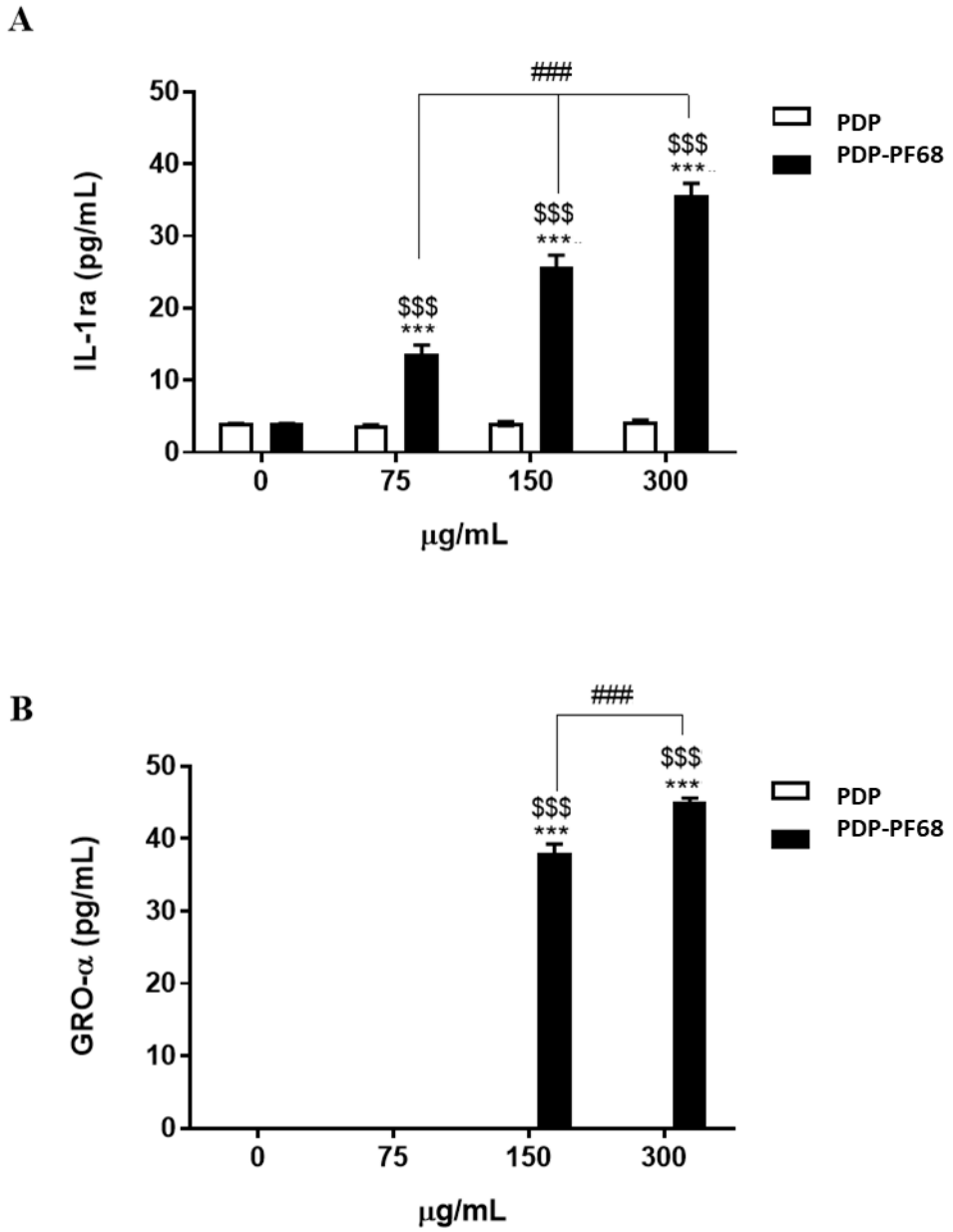

Figure 2.12 IL-1ra and Gro-α production induced by PDP and PDP-PF68 NPs in C3A cells.

Cells exposed to PDP and PDP-PF68 NPs for 24 hours at 75, 150 and 300 µg/mL, IL-1ra (A), Gro-α (B). Data are expressed as mean pg/mL ± SEM (n=3). Significance indicated by ***= p< 0.001, when compared with the untreated control. Significance indicated by $$$= p< 0.001 when compared with PDP NPs at the same concentration. Significance indicated by ###= p< 0.001 when comparing the same NP at different concentrations.

2.4 *Impact of PDP and PDP-PF68 NPs on J774 cells*

2.4.1 PDP and PDP-PF68 NPs: Cytotoxicity in J774 cells

J774 cells were exposed to PDP and PDP-PF68 NPs at 4.6-300 µg/mL for 24 hours and a benchmark concentration approach was used to assess cell viability (Wignall et al. 2014). The same three simultaneous fluorescence assays (AB, CFDA-AM, NR) used with the C3A cell line were applied. Both the AB and CFDA-AM assays indicated no biologically significant adverse effects on cell viability for either NP (Figures 2.13A/B). However, the NR assay, a marker of lysosome function, did indicate a significant decrease (***= $p < 0.001$) in viability for J774 cells exposed to PDP-PF68 NPs at 36% viability at 200 µg/mL and 10% viability at 300 µg/mL (Figure 2.13 C).

The EC_{20} values for the AB and CFDA-AM assays were above the highest concentrations of treatment. Therefore, no accurate EC_{20} values could be determined. Using the NR assay, it was possible to establish an EC_{20} for PDP-PF68 NPs of 153 µg/mL.

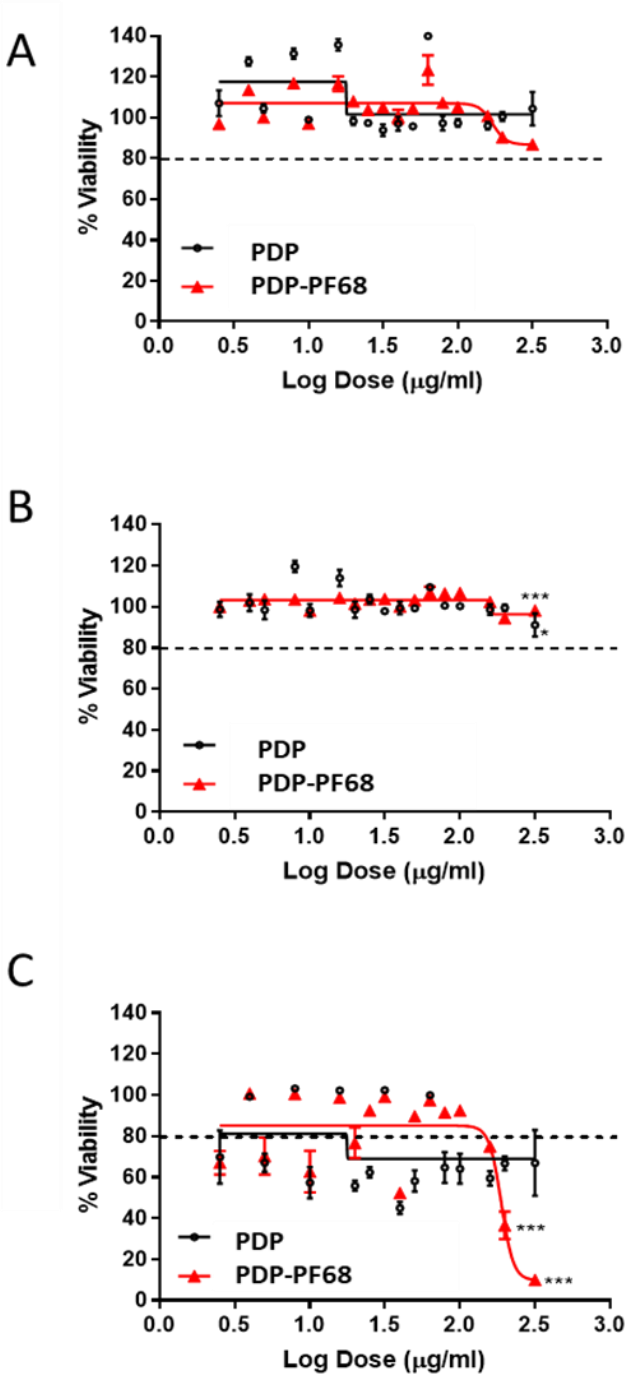

Figure 2.13 Cytotoxicity of PDP and PDP-PF68 NPs to J774 cells.

Cells were exposed to PDP (black) or PDP-PF68 (red) NPs (4.6-300 µg/mL) for 24 hours. Viability was measured via AB (A), CFDA-AM (B) and NR (C) assays. Data are expressed as mean % cell viability (i.e. % of untreated control) ± SEM (n=3). Significance indicated by ***= p< 0.001, compared control.

2.4.2 PDP and PDP-PF68 NPs: Uptake by J774 cells

Differences in the uptake of these NPs in C3A cells was most evident at 1440 minutes. Therefore, J774 cells were exposed to PDP-PF68 and PDP NPs at 100 µg/mL for 1440 minutes. Both NPs were readily taken up into the cytoplasm and compartmentalised in the cytoplasm surrounding the nucleus, potentially in organelles such as the lysosomes or endosomes. Although, neither NP appeared to enter the nucleus (Figures 2.14A/B).

Visually, there appears to be more uptake of the PDP NPs, and this can also be seen in the quantitative uptake analysis of the PDP NPs at 1440 minutes (Figure 2.15C). A significant increase ($p < 0.05$-0.001) in uptake was seen at 150 µg/mL for cells treated with PDP NPs for 10 and 60 minutes, while, above this concentration, there was less NP internalisation. There appears to be little internalisation of PDP-PF68 NPs at 10 and 60 minutes (Figures 2.15A/B). A significant increase ($p < 0.001$) in uptake can be seen, that is in a concentration dependent manner, up to 75 µg/mL for cells treated with both NPs for 1440 minutes, while there was less NP internalisation above this concentration (Figures 2.15C).

Interestingly, when J774 cells were incubated with these NPs at 4°C, there appears to be a significant ($p < 0.001$) internalisation of the PDP NPs up to 150 µg/mL, with less uptake at concentrations above this (Figure 2.16). There also appears to be some internalisation of PDP-PF68 NPs at 4°C, although, this is not significant. The internalisation of the PDP NPs is significantly higher ($p < 0.001$) than that seen for PDP-PF68 NPs at 37.5 -300 µg/mL.

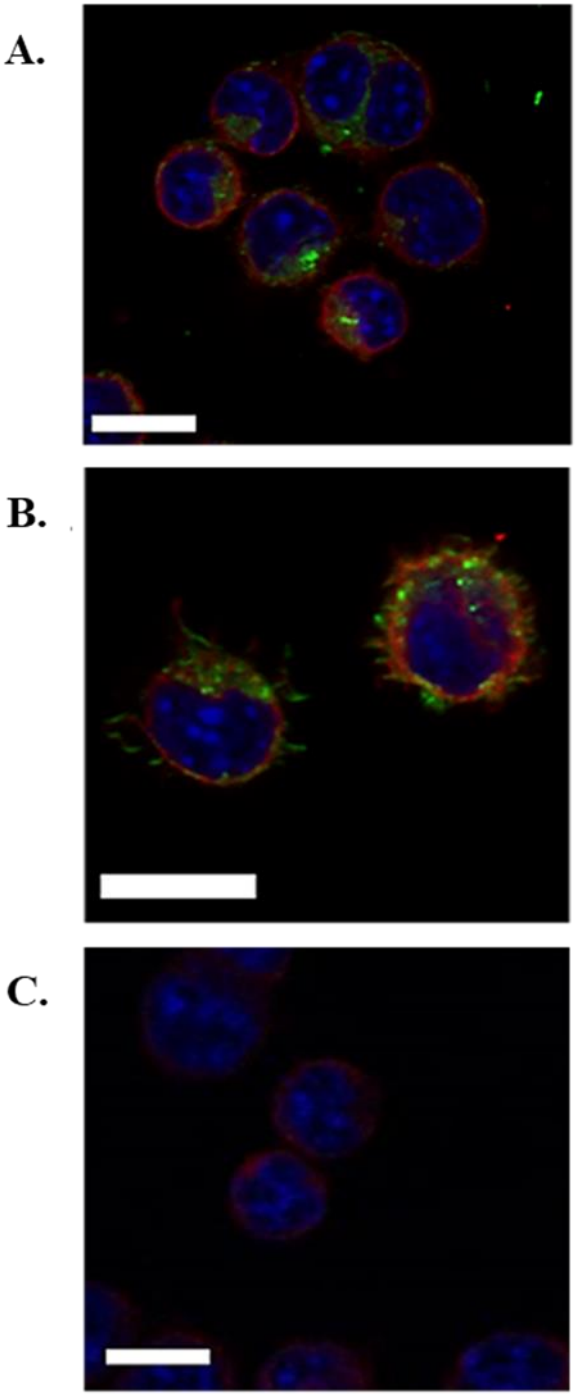

Figure 2.14 Uptake of PDP and PDP-PF68 NPs by J774 cells at 1440 minutes. Cells were treated with 100 μg/mL of PDP(A), PDP-PF68 NPs (B) or Complete Medium (C) for 1440 minutes. Representative images, tubulin (red), DNA (blue) (n=3), scale bar = 10 μm.

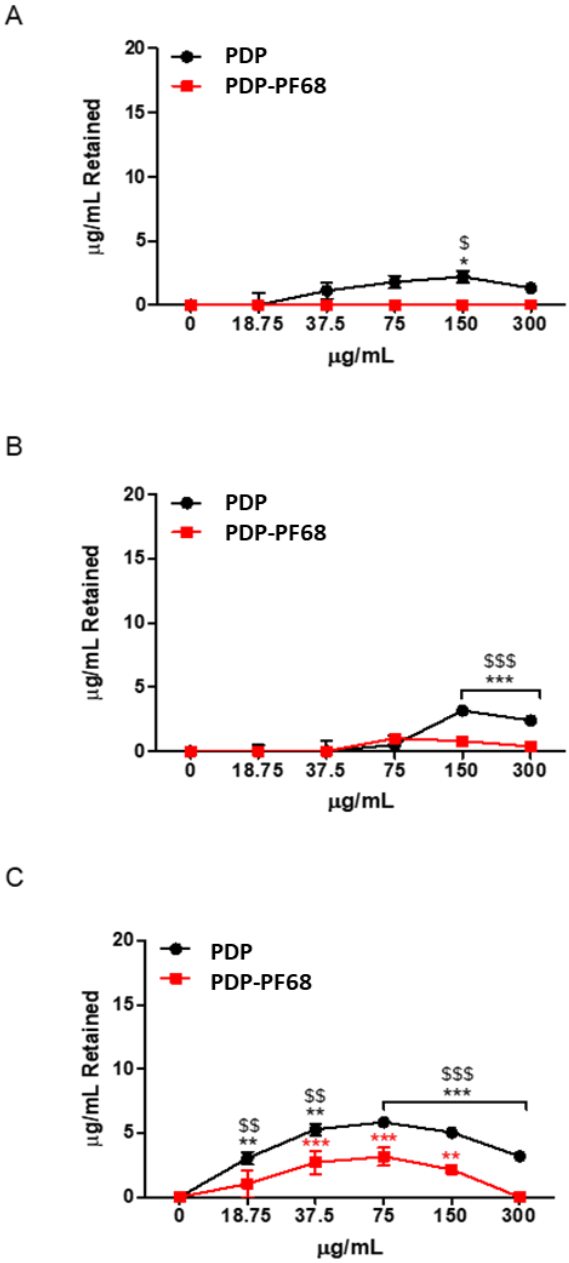

Figure 2.15 Uptake of PDP and PDP-PF68 NPs in J774 cells, over time: Plate method.

Cells were exposed to PDP (black) and PDP-PF68 (red) NPs for 10 (A), 60 (B) and 1440 (C) minutes, at 18.75-300 µg/mL. Data are expressed as mean µg/mL retained (from appropriate standard curves) ± SEM (n=3). Significance indicated by *= p< 0.05, **= p< 0.01, ***=p< 0.001 compared with untreated control. Significance indicated by $$=p< 0.01, $$$=p< 0.001, when PDP NPs compared with PDP-PF68 NPs at same concentration and timepoint.

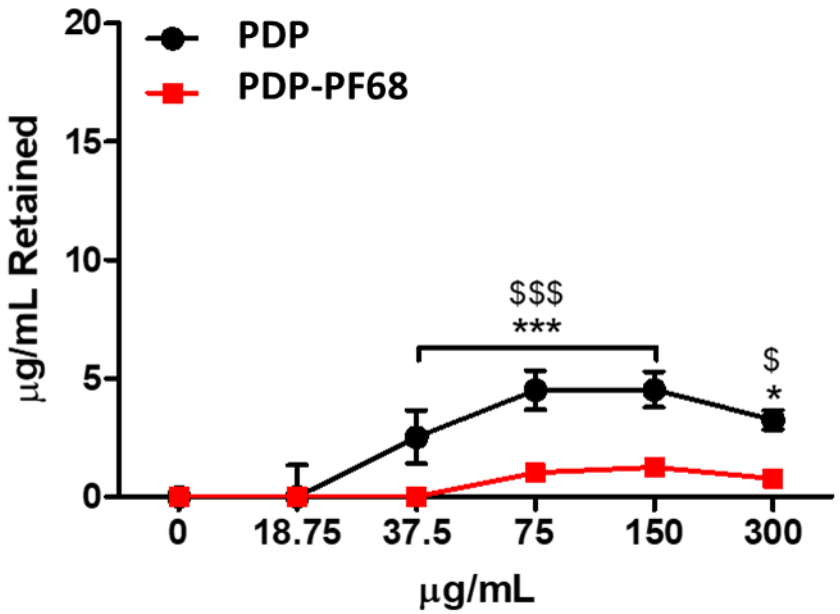

Figure 2.16 Uptake of PDP and PDP-PF68 NPs in J774 cells, 4°C: Plate method. Cells were exposed to PDP (black) or PDP-PF68 (red) NPs, at 18.75-300 µg/mL for 1440 minutes. Data are expressed as mean µg/mL retained (from appropriate standard curves) ± SEM (n=3). Significance indicated by ***= p< 0.001, *= p< 0.05, compared with untreated control. Significance indicated by $= p< 0.05, $$$= p< 0.001 for PDP NPs, compared with PDP-PF68 NPs at the same concentration.

2.5 Discussion

2.5.1 Overview of results

Before NP interaction with hepatocytes was assessed, it was essential to evaluate NP physiochemical characteristics that can influence these interactions, such as size and surface charge. The PDP-PF68 NPs were larger than the PDP NPs, as would be excepted as they had an adsorbed Pluronic coating. Both NPs had a negative surface charge that was not significantly different in Complete Medium, suggesting that charge may not differentially influence how the PDP-PF68 and PDP NPs interact with the cells. The cytotoxicity of the NPs was then assessed (via three assays) to compare the toxic potency of the PDP-PF68 and PDP NPs, and to identify sublethal concentrations of NPs to select when investigating the cellular response.

Data obtained demonstrated that a lack of biologically significant cytotoxicity was seen at the concentrations tested 24 hours post-exposure to C3A cells. Next, the uptake of NPs was imaged using confocal microscopy and quantified using a fluorescence plate reader. Uptake of the NPs increased in a time and concentration-dependent manner. Initially (10-240 minutes), NPs were compartmentalised within or between cells, suggesting localisation within cells' organelles (e.g. lysosomes, mitochondria) or structures similar to the bile canaliculi, as seen in previous studies (Johnston et al. 2010). However, at 24 hours post-exposure, PDP-PF68 NPs appeared to have become diffuse throughout the cells, while the majority of PDP NPs remained compartmentalised.

The genotoxicity of the NPs was assessed using the Comet assay. It was observed that the PDP-PF68 NPs stimulated DNA damage, whereas the PDP NPs were not genotoxic to C3A cells. No increased production of IL-8 or TNF-α by C3A cells was observed for C£A cells exposed to both NP types. However, there did appear to be an increase in the production of IL-1ra and Gro-α, by C3A cells exposed to PDP-PF68 NPs

Although these results suggest possible clinical usefulness for these NPs, there was evidence that adding a Pluronic coating enhances toxicity. This data could be used in the

design of safe nanomedicines in the future. Overall, these results indicate a panel of tests should be used to build a comprehensive picture of how these NPs affect the cell. Accordingly, safety testing should not rely solely on the assessment of the impact on cell viability.

2.5.2 Characterisation of PDP and PDP-PF68 NPs

This study focused on assessing size, shape, size distribution and surface charge via TEM and DLS. It is established that these parameters can influence the interactions of NPs with cells (Brown et al. 2001; Hirn et al. 2011; Schaeublin et al. 2012; Ke et al. 2014). Equally, the methods employed have previously been used in numerous studies to characterise NPs (e.g. Clift et al. 2011; Kermanizadeh et al. 2013; Brown et al. 2014). Using TEM, both NP types appear spherical and relatively monodispersed. The hydrodynamic diameter of PDP-PF68 NPs at T0 was significantly higher than for the PDP NPs, likely due to the presence of the adsorbed PF68 coating.

Several studies have shown that adding a surface coating can alter the hydrodynamic diameter of the NPs (Mulens-Arias et al. 2015; Mahaling & Katti 2016). For example, an increase in hydrodynamic diameter was seen when PF68 was adsorbed to Doxorubicin-loaded Poly(butyl cyanoacrylate) NPs (Petri et al. 2007).

Proteins present in the FBS of the Complete Medium can bind to the surface of NPs during incubation, and these proteins may influence NP size (Petri et al. 2007; Voigt et al. 2014). There was no significant difference between the hydrodynamic diameter of the NPs after 24 hours; this suggests that the sizes of both NPs were stable within the assay conditions. Stability can be an issue for nanomedicine production, as batchs produced will need to be near identical and be stabile long enough for batch safety testing to be performed as well as clinical application.

Zeta potential is a measurement of the electrostatic forces, at a defined distance from the NP's surface, and is used as an indicator of charge for particles in an aqueous dispersion (Brown et al. 2014). Zeta potential also indicates suspension stability or aggregation/agglomeration, with values above +30 mV or below −30 mV considered

stable (Silva et al. 2011). The zeta potential of both PDP and PDP-PF68 NPs were negative (-10 to -12 mV), however, they were not below -30 mV suggesting possibly low suspension stability and potential for agglomeration.

The PDI is ununited and calculated by dividing the standard deviation of the NP diameter by the average NP diameter, this can reflect the size distribution and stability of NP suspension. High PDI values (e.g. 0.5-1) can indicate a NP suspension with a broad size distribution or possible aggregation/agglomeration, while low values (e.g. <0.5) suggest a monodispersed population of NPs in the suspension (Cutts et al. 2015; Clayton et al. 2016). The low PDI values of both NPs, also suggests that NP suspensions are monodispersed, which agrees with the images of these NPs obtained by TEM. Since these NPs are intended for medical use, monodispersed and stable suspensions are necessary to ensure an accurate drug dose *in vivo* (Qian et al. 2010).

However, there was a higher PDI value for PDP-PF68 NPs compared with PDP NPs at both time points, suggesting that the PDP-PF68 NP suspension had marginally higher variability in size, less stability and therefore the PDP-PF68 NPs were more likely to aggregate/agglomerate than their PDP NP counterparts. This increased PDI may be due to the adsorbed coating being unstable. However, previous research indicated that a PF68 coating increases iron oxide NP and PLGA NP stability in saline solutions (Morales et al. 2005; Santander-Ortega et al. 2006).

The stability of the PDP NPs in Complete Medium containing 10% FBS remains constant over time, while there was a significant decrease in the PDI of PDP-PF68 NPs between 0 hours and 24 hours, suggesting that they had become more stable. Increases in dispersion stability over time were also seen at 24 hours for ZnO NPs in a cell culture medium, due to the presence of a protein corona (Semete et al. 2010). This suggests that components of the Complete Medium may form a different protein corona on the PDP-PF68 NPs compared with the PDP NPs, allowing increased stability over time for the PDP-PF68 NPs.

However, there are limitations to the methods used in this project. To establish NP hydrodynamic diameter, one of the most common methods used is DLS. This measures

the hydrodynamic diameter of NPs in suspension, and their size distribution. Even so, this technique uses computational algorithms which assume NPs are spherical and monodispersed in water. While TEM gives a visual representation of the size and size distribution of NPs, due to the low contrast of TEM, it can be challenging to image polymers and polymer coatings on NPs. Therefore measurements from TEM images may not be accurate (Zucker et al. 2012).

Ideally, additional measurement techniques would have been used to establish NP size directly in a biological medium, such as atomic force microscopy, a high-resolution imaging technique that physical measurement NPs using a scanning probe in any appropriate medium (Lin et al. 2014; Constantin et al. 2017). However, this technique would not provide higher resolution than that used in the current study, requires highly specialised equipment and is not as widely available as TEM (Win & Feng 2005; Klapetek et al. 2011; Wibroe et al. 2016).

2.5.3 Cytotoxicity of PDP and PDP-PF68 NPs

Data obtained showed that all three cytotoxicity assays gave similar results for both PDP and PDP-PF68 NPs. More specifically, the results demonstrated that both NPs were of relatively low toxicity in C3A cells, with less than a 20% reduction in cell viability observed at all concentrations tested, 24 hours post-exposure. Indeed, similar to previous studies which have demonstrated that biodegradable polymer NPs show low cytotoxicity in human hepatic (L02) and lung (A549/Calu-3) cells after 24 hours exposure (Cong et al. 2015; Maiolino et al. 2015). Low levels of cytotoxicity are ideally required for unloaded nanomedicines, as adverse side effects need to be limited in clinical applications, and the low cytotoxicity observed for both NPs suggests they could be clinically useful.

In the case of these PNPs that elicit low cytotoxicity, the benchmark concentration approach, that allowed for the addition of different concentrations to be assessed for cytotoxicity between replicates, did not provide additional information. Therefore, the benchmark concentration approach may not be a useful tool for safety profiling of low cytotoxicity PNPs as due to the additional investment in time and finances.

Previous studies investigating the toxicity of PNPs have used higher concentrations than those used here. For example, THP-1 macrophages were exposed to PF68-coated PLGA NPs at concentrations of 1-10 mg/mL, which had a significant impact on viability, membrane activity and cytokine production (IL-6) (Grabowski et al. 2015). Using a higher concentration of PDP and PDP-PF68 NPs may have had a cytotoxic outcome, and it may have been possible to determine EC_{20} for both NPs. However, as this study intended to reflect a more 'realistic' concentration range, the concentrations selected for *in vitro* testing were determined from calculations that reflected therapeutic application (Section 2.2.4).

Using three different assays for cytotoxicity of low toxicity PNPs may be redundant. It would be better in future to focus on the assay, such as AB, that has produced the most robust data, as well as previously been used in the cytotoxic testing of multiple engineered NPs.

2.5.4 Uptake of PDP and PDP-PF68 NPs

The current study used a combination of microscopy and a fluorescence plate reader to investigate uptake. The findings from both approaches were complementary. The plate based method was high throughput, which was beneficial in that it allowed the time and concentration dependence of NP uptake to be quantified. Therefore, the method developed in this study provides a quick, sensitive approach for screening fluorescent NP uptake by cells. While confocal microscopy provides useful information on NPs' intracellular fate, it cannot quantify uptake and takes a substantial investment of time. Such methods only apply to fluorescent NPs, with the investigation of the uptake of non-fluorescent NPs often more challenging.

Both methods showed an increase in NP uptake with time. These results agree with previous research, with uptake of PNPs (such as polystyrene) ranging from 20-200 nm within macrophages, kidney epithelial, hepatocytes and fibroblast cells increased over time (Davda & Labhasetwar 2002; Johnston et al. 2010; Nicolete et al. 2011; Firdessa et al. 2014). Also, the intracellular concentration of both NPs at 24 hours did not continue

to increase at higher concentrations. These observations may be related to the mild cytotoxic effects seen for these NPs at the higher concentrations, as fewer cells would be present, resulting in the lower fluorescent signal. The increased uptake with time suggests that, once administered, when NPs remain stable they could continue to circulate and deliver a therapeutic load for up to 24 hours.

The lower level of uptake observed for PDP-PF68 NPs were most likely due to the presence of the surface coating. A decrease in uptake of non-target cells is advantageous for nanomedicines, as many NPs are cleared rapidly in the liver and RES following administration (Ogawara et al. 2001). The reduced uptake seen for the PDP-PF68 NPs may indicate that these nanomedicines would circulate longer within the body, increasing the chance that NPs will reach target cells and potentially decrease the frequency of administration.

The contribution of active or passive uptake was also investigated by assessing uptake following treatment of cells with NPs at 4°C, as at 4°C the predominant form of uptake is passive (Firdessa et al. 2014). A lack of uptake of both NPs at 4°C indicated that C3A cells actively internalise both PDP and PDP-PF68 NPs. Moreover, it is preferable to have nanomedicines that are less likely to enter healthy cells. Therefore, limiting NPs entering cells via passive uptake could reduce non-specific uptake by healthy cells.

In the current study compartmentalisation of both PDP and PDP-PF68 NPs was seen at 10-240 minutes within the cells suggests localisation within organelles such as endosomes or lysosomes. In previous studies, the uptake of 20 nm polystyrene NPs in hepatocyte and macrophage cell lines had a similar pattern of compartmentalisation to that seen in the current study. Although NPs in hepatocyte cells appeared to localise in the endosomes and lysosomes, while in macrophage NPs appeared to prefer to localise in the mitochondria (Johnston et al. 2010; Firdessa et al. 2014).

Further research could be performed for these NPs in the current study to confirm the localisation of NPs within the organelles of C3A cells, using markers such as Lysotracker and Mitotracker to provide valuable information regarding the effects of PF68 coating on intracellular localisation. This information could be useful for intracellular clinical

targeted delivery of these NPs. Equally, markers such as FM4-64 could be used to label the endosomes fluorescently (Au et al. 2011). TEM is useful for observing localisation of many NPs such as silver NPs within cells. When using polymer NPs on the other hand, perhaps due to a similar density to the cells, it can be more difficult to differentiate between NPs and cell components.

The observation that the NPs accumulated between adjacent C3A cells may suggest NPs accumulating within bile canaliculi-like structures. Indeed, a similar observation was made when C3A cells were exposed to 20 nm polystyrene NPs in a previous study, with the fluorescent bile acid, cholyl lysyl fluorescein (CLF) used to confirm colocalisation of the NPs and bile (Johnston et al. 2010). This could indicate the active removal of NPs from the cells via bile, as has been observed *in vivo* (Guy et al. 1989; Kanakia et al. 2014). In the future, to investigate the possibility of PDP-PF68 NPs colocalising in bile canaliculi-like structures, CLF could be used *in vitro* (Milkiewicz et al. 2002; Johnston et al. 2010). Removal of NPs via the bile canaliculi could be clinically necessary, as this could reduce biopersistence in the liver, reducing the possibility of long-term adverse effects.

Both PDP and PDP-PF68 NPs are initially observed in the perinuclear region of cells and later diffused throughout the nucleus, which could indicate some form of targeting towards the nucleus (Akita et al. 2013). The nucleus has previously been targeted by liposomal NPs of similar size to PDP and PDP-PF68 NPs to deliver gene therapy (Akita et al. 2013). Since these NPs are intended for bioimaging or delivery of drugs, it may not be beneficial for these NPs to enter the nucleus and potentially interact with and damage the DNA. The localisation of these NPs in the nucleus could be further clarified using super-resolution microscopy technique (van der Zwaag et al. 2016).

Due to the enhanced biodegradable nature of the polymer used to produce both the PDP-PF68 and PDP NPs in the current study, it may be possible that these NPs degrade within the cells or extracellularly. Degradation profiles were performed over 90 days for the PDP NPs by collaborators at the University of Nottingham, with and without incubation with *Pseudomonas cepacia* lipase (0.2 mg/mL), a hydrolytic enzyme to identify biodegradability (Kakde et al. 2016). After 30 days' incubation in the hydrolytic enzyme

solution, there was only a marginal decrease in molar mass, while NPs without this enzyme remained stable. Therefore, extensive extracellular degradation within the experimental conditions over 24 hours was unlikely. After 90 days, the molar mass was decreased by half for NPs treated with the hydrolytic enzyme, suggesting that these NPs could potentially be broken down in the body and cleared. This is necessary for nanomedicines, as prolonged persistence may have detrimental effects on patients.

2.5.5 Cytokine production related to PDP and PDP-PF68 NPs

In this study, there was no increase in IL-8 production by cells exposed to both PDP-PF68 and PDP NPs. This is in line with other studies exposing macrophages to PF68-coated PLGA NPs, where no IL-8 production was observed (Grabowski et al. 2015). There appears to be a decrease in IL-8 production for PDP NPs; however due to low levels of IL-8 production, this is unlikely to be biologically relevant. C3A cells appear to produce little to no TNF-α when treated with the control or NPs, indicating these cells may be unresponsive. Nonetheless, a lack of IL-8 and TNF-α production could indicate that there was no significant pro-inflammatory response activated by these NPs.

Interestingly, there was a significant increase in IL-1ra and Gro-α in a concentration-dependent manner for PDP-PF68 NPs. IL-1ra is produced in the liver and *in vitro* in human hepatocytes in response to inflammation (Gabay et al. 1997). This anti-inflammatory cytokine competitively inhibits the pro-inflammatory cytokines, IL-1α and IL-1β, therefore halting an inflammatory cascade, reducing the inflammatory response (Duque & Descoteaux 2014). Studies have investigated NPs loaded with IL-1ra with the intention to treat inflammatory diseases such as osteoarthrosis (Agarwal et al. 2016). However, there are limited studies assessing IL-1rα production *in vitro* and *in vivo*. However, a significant increase in IL-1rα production was observed with the THP-1 (human macrophage) cell line exposure to TiO_2 NPs at 100 µg/mL (Kim et al. 2007). When osteoporosis patients were treated with 100 mg/day of alginate sodium NPs (approx. 200 nm), this also induced an increase in IL-1ra production (Qu et al. 2017).

Gro-α (also known as CXCL1) is a neutrophilic chemoattractant, known to stimulate epithelial cell growth (Coppé et al. 2010). Interestingly, the increase in Gro-α production

for cells exposed to PDP-PF68 NPs was similar to previous studies using other PNP which showed increased Gro-α mRNA expression and significant DNA damage when VK2 (vaginal epithelial) cells were exposed to 100 μg/mL PLGA-PEG NPs (approx. 50 nm diameter) (Wagner et al. 2017).

The stimulation of IL-1ra and Gro-α production may suggest that the PDP-PF68 NPs provoke an innate immune response (Moles et al. 2014). It has previously been shown that PF68 can elicit hypersensitive reactions *in vivo* via complementary activation, which, in turn, could lead to increased production of pro-inflammatory cytokines and further downstream effects such as genotoxicity (Moghimi et al. 2004). It would be of interest to investigate the production of other cytokines such as IL-6, that can be either pro-inflammatory or anti-inflammatory.

2.5.6 Genotoxicity of PDP and PDP-PF68 NPs

Genotoxicity would be a significant hurdle in nanomedicine development, as it could lead to the development of cancers and promote cell death. Although due to the limited volume and concentration of NPs the number of concentrations was limited to two and not the recommended three (OECD 2015). Although, these results could provide indication of potential genotoxicity of NPs, results most be considered preliminary.

Unlike PDP-PF68 NPs, PDP NPs did not appear to induce genotoxicity in C3A cells. The genetic damage caused by PDP-PF68 NPs appears to be mediated via oxidative stress, as DNA damage was heightened in the presence of Fpg. These results indicated that a PF68 coating may contribute to NP genotoxicity. Moreover, PF68 alone at relevant concentrations did not induce genotoxicity, indicating that this was a NP relevant issue. These results highlight the importance of establishing the safety of different nanoforms of the same core NP.

It was possible that when these PDP-PF68 NPs interact with C3A cells, ROS are produced. ROS is a crucial player in NP toxicity, and if levels exceed antioxidant levels within the cell, this may lead to oxidative damage (Nel et al. 2006). Prior studies of PF68 coated tri-block copolymers (PEO-PPO-PEO) NPs indicated a reduction in mitochondrial

membrane potential in Caco-2 cells (colon epithelial). The downstream effects of a reduction in the mitochondrial membrane could be ROS production (Ehrenberg et al. 1988).

It would be interesting to determine ROS production of these NPs in the future. ROS could be investigated using the fluorogenic dye 2', 7'-Dichlorodihydrofluorescein diacetate (DCFH-DA). The DCFH-DA dye enters cells and is rendered non-permeable to the cell membrane by esterases in the cell. In the presence of ROS, the dye will be rapidly oxidised to a highly fluorescent dye (Rota et al. 1999; Wilson et al. 2002). DNA damage was measured after four hours' exposure. Therefore, in the future, it would be useful to look at genotoxicity after 24 hours of NP exposure to reflect other endpoints used in the study (e.g. cytokine production). The measurement of NP genotoxicity using the Comet Assay can have limitations, and concerns have previously been raised regarding NP interference with measurement of this assay, however, this can be mitigated by suitable controls (Stone et al. 2009). Ideally, the results from the Comet Assay would be verified using additional genotoxic assays such as the robust micronuclei assay that quantifies the micronucleus produced in response to DNA damage.

2.5.7 Impact of PDP and PDP-PF68 NPs on J774 cells

The effects of PNP exposure on macrophages (J774) was briefly examined, to gain greater insight into the response of different cell lines to PNP toxicity. The AB and CFDA-AM assays did not suggest cytotoxicity for these NPs in J774 cells. Nonetheless, the NR assay did suggest an adverse effect on lysosome function by PDP-PF68 NPs at high NP concentrations. A previous study indicated that coating hexadecylcyanoacrylate NPs with PEG, which is an element of PF68, decreased toxicity in the J774 cell line, most likely mediated by PEG's steric repulsion reducing cell-NP interaction (Peracchia et al. 1999).

However, in the current study, PDP-PF68 NPs appear to be more cytotoxic than PDP NPs. PF68-coated poly (ε-caprolactone) NPs have been shown to reduce the viability of J774 cells by 60% at 100 µg/mL (Espuelas et al. 2003). Moreover, macrophage cells (THP-1) exposed to PF68-coated PLGA NPs induced a significant decrease in mitochondrial activity that was not seen for PLGA NPs or PF68 alone (Grabowski et al.

2015). These results indicate that macrophage cells may be adversely affected by a range of PNPs coated in PF68. It is noteworthy that the J774 cell line appears to be a more sensitive model, than the C3A cell line. The differences seen in the current study could be due to macrophages being specifically phagocytic cells, possibly altering the way these NPs are taken up, the amount internalised which is lower than hepatocytes and the intracellular localisation, compared with hepatocyte cells, which are predominantly non-phagocytic. Compartmentalisation of both NPs within the cells suggested localisation within organelles such as endosomes or lysosomes, this is similar to previous studies exposing J774 cells to 200 nm polystyrene PNPs (Clift et al. 2008; Clift et al. 2011).

Uptake of both NPs using microscopy and a fluorescence plate reader indicated higher internalisation of the PDP NPs by macrophages. The localisation was similar for both NPs, with cytoplasmic compartmentalisation and no apparent nucleus entry. These observations may suggest that the PF68 coating has the potential to decrease NPs uptake in J774 cells. This outcome would be preferred, as the addition of the PF68 coating was designed not only to increase NP stability but to decrease NP interactions with non-target cells, thus reducing clearance via the RES (Ogawara et al. 2001). These results could indicate that coating these NPs with PF68, helps increase circulation time, therefore allowing the drug cargo to reach the target, as well as increasing the time between treatment administrations.

For both the PDP and PDP-PF68 NPs at all time points, there appeared to be less NP uptake at concentrations above 75 µg/mL as this decrease was seen for both NPs and on PDP-PF68 had a cytotoxic effect, this may point to alternative reasons for less uptake at higher concentrations, perhaps exocytosis or intracellular degradation of NPs. Previous studies have seen iron (II,III) oxide NPs exocytose from macrophages via membrane vesicles (Serda et al. 2010). Additionally, a study using vascular smooth muscle cells observed that most endocytosed PLGA NPs were exocytosed to the cell's surface (Labhasetwar 2002). Therefore, the presence of PDP NPs on the surface of the J774 cells after 24 hours may suggest exocytosis of these NPs. This could be useful for certain nanomedicines as intracellular delivery of NP cargo may be needed, and therefore it can be important that nanomedicines escape membrane-bound organelles within the cell to reach their target site (Rots et al. 2003; Tkachenko et al. 2000; Maiolino et al. 2015.

Of interest is the significant uptake of the PDP NPs at 4°C at 1440 minutes, at a similar level to that seen at 37°C for 1440 minutes. This uptake at 4°C suggests that the PDP NPs can enter the J774 cells passively (Mu et al. 2012). This non-phagocytic means of uptake could be initiated by the physiochemical characteristics of the NPs, such as Van de Waals forces or surface charge, and may be influenced by the NPs' protein corona (Rimai et al. 2000). This passive entry of NPs such as seen with positivity charged PAMAM dendrimer NPs may rupture the cell's membrane (Leroueil et al. 2008). Further imaging of cells incubated at 4°C using Wortmannin, a phagocytosis inhibitor, could give greater insight into whether uptake of these NPs is a mix of active or passive mechanisms (Nie et al. 2011).

The pattern of internalised NPs in J774 cells compared with C3A cells differs in that PDP-PF68 NPs in C3A cells were diffuse throughout the cytoplasm and nucleus at 1440 minutes. Additionally, the PDP NPs in C3A cells had a mixture of compartmentalised and diffuse NPs at 24 hours. Differences can also be seen between C3A and J774 cells internalising NPs using the quantitative method. It appears that there was a higher internalisation of these NPs by C3A cells. However, as macrophages are professional phagocytic cells, these NPs would be expected to be taken up more readily by J774 cells (Shu et al. 2005; Tsai & Discher 2008). These differences in the internalisation pattern may indicate that J774 and C3A cells differentially take up and traffic these NPs, suggesting that a range of cells are relevant when assessing PNP safety before clinical use.

2.6 Conclusions

This study employed methods that allowed for investigation of the cellular toxicity and quantification of uptake of novel PDP-PF68 and PDP NPs. Results indicated that these NPs had relatively low cytotoxicity and that uptake was more efficient for the PDP NPs in C3A cells. The presence of a PF68 coating may alter the intracellular fate of the NPs and decrease cellular uptake. Results suggest that PDP NPs are relatively non-toxic. However, the addition of the PF68 coating to PDP NPs may enhance the PNPs toxicity, with PDP-PF68 NPs seen to stimulate IL-1ra and Gro-α production as well as

genotoxicity via an oxidative mechanism. This highlights the need for multiple endpoints and specific regulatory guidelines regarding nanomedicines.

The brief investigation of an additional cell line, J774, gave insights into the suitability of this cell line as a predictive model of PNP toxicity. This macrophage-like model was a more sensitive indicator of cytotoxicity than the C3A cells. However, PDP NP internalisation by J774 cells appears in this study to involve a passive mechanism not observed in C3A cells. This difference in uptake route could lead to a fundamentally different intracellular localisation and therefore downstream adverse effects of these NPs on cellular function. The use of primary hepatocytes in future experiments could also provide a greater understanding of any toxicity observed for these NPs. *In vivo* work could also provide invaluable information regarding biodistribution, clearance and systemic toxicity. The observations made in this study suggest genotoxicity could be used to inform future design of NPs and should encourage others to consider the effects of PNP coating on NP toxicity.

As hypothesised, both NPs had low cytotoxicity. Although there was less uptake of PDP-PF68 NPs, this did not link to reduced cytokine production or genotoxic effects. These results may be attributed to the coating altering how these NPs are internalised and trafficked once inside the cell. The results of this study suggest that, although these PNPs have low cytotoxicity, further investigations and considerations of an alternative NP coating would be necessary before this nanomedicine could be considered for use in a clinical setting.

The information from this study could be used to further develop the tier 1 and 2 of the testing strategies suggested (Figure 1.3). This could allow for the identification of indicators of toxicity for PNPs before progressing with more advanced *in vitro* testing or *in vivo* testing, where appropriate potential to reduce the investment and resources required for safety testing of PNPs. This information could be used by the generator of these PNPs to aid in designing with safety in mind.

Although cytotoxicity testing is required to establish non-lethal concentrations for further tests, when developing a testing strategy more than one assay may not be warranted as it

does not provide additional information needed to progress with testing. Additionally, PNP uptake did not provide as clear indication of toxicity and therefore may not need to be priorities or performed at multiple concentrations and time points in a PNP testing strategy. Again, cytokines can provide important information regarding cell health however when prioritising endpoints for testing the safety of PNPs, investigation of initial cytokines that are clear indicators of the safety of PNPs such as IL-8 and TNF-a could be performed before progressing to analysis of additional cytokines. Genotoxicity is probably the most impactful endpoint as when genotoxicity is observed it limited the potential of a PNP nanomedical progressing to the clinic. When testing for genotoxicity additional concentrations would provide future information as well as additional time points as both short and long exposures are suggested to capture the full scope of genotoxic impact of a NP (Yamani et al. 2017).

Chapter 3. *In vitro* assessment of the influence of copolymer chain length on NP safety using C3A hepatocytes.

3.1 Introduction

3.1.1 Designing safe PLGA-PEG PNPs for nanomedicine

In this study three different PLGA-PEG polymers were used to generate the PNPs: PEG2K-PLGA4K (4K NPs), PEG2K-PLGA15K (15K NPs) and PEG5K-PLGA55K (55K NPs). The PNPs were loaded with the non-toxic fluorescent conjugated polymer poly(2,5-di(3′,7′-dimethyloctyl) phenylene-1,4-ethynylene) (PPE) for bioimaging (Wu et al. 2013) (Figure 3.1).

The core of the PNPs in this study was composed of PLGA, one of the most common polymers used to generate PNPs due to FDA approval for clinical use (He et al. 2013; Dening et al. 2016). Previous studies suggest that PLGA NPs has low toxicity and are biocompatible and biodegradable. For example, when KMC-1 cells (bile duct epithelial) were exposed to PLGA NPs there were no changes in cell viability or cytokine production (TNF-α and IL-6) (Santos et al. 2013). Additionally, *in vivo,* following oral administration, PLGA NPs showed no histopathological changes in the liver and kidneys of exposed mice (Boitumelo Semete et al. 2010). However the by-products of PLGA NPs hydrolytic degradation, poly-lactic acid and polyglycolic acid, have been shown to cause cytotoxicity as well as TNF-α and ROS production by macrophage cells *in vitro* (Acharya & Sahoo 2011; Nie et al. 2012; Singh & Ramarao 2013).

The shell of the PNPs in this study was composed of PEG, an FDA-approved polymer for clinical use that has low toxicity (Cruz et al. 2011). PEG is hydrophilic, resulting in less opsonisation, decreased phagocytic recognition and increased circulation time (section 1.6 for more detail) (Alexis et al. 2008; Sheng et al. 2009; Jain et al. 2011). Moreover, the addition of PEG to PLGA NPs can improve the NPs usefulness as a nanomedicine as PEG increases PNP drug loading, solubility and stability (Danhier et al. 2009).

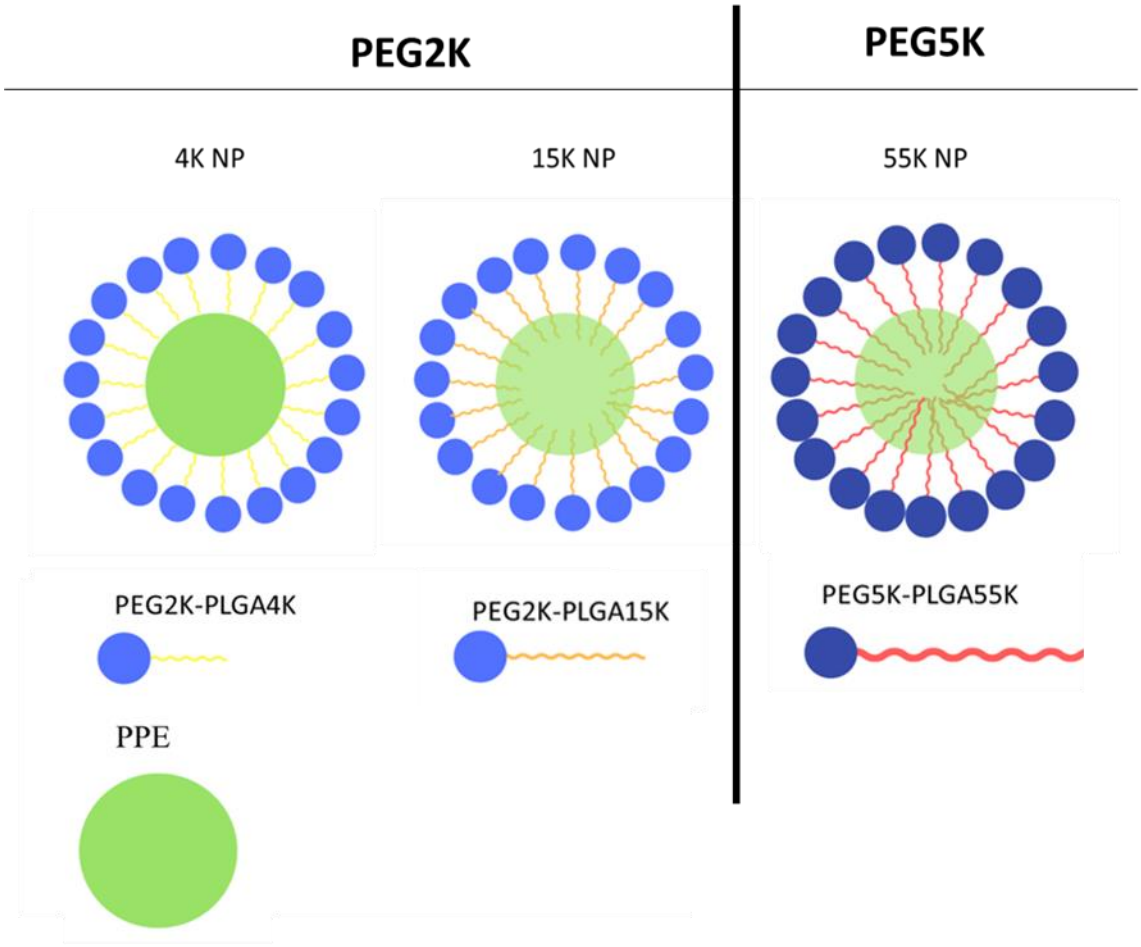

Figure 3.1 Scheme of PEG-PLGA NPs: 4K, 15K and 55K NPs.

Representation of PNPs used in this study. PNPs were made of polymer PEG2K (light blue), PEG5K (dark blue), PLGA4K (yellow), PLGA15K (orange), PLGA55K (red) and PPE (green).

3.1.2 The effect of altering polymer chain length on PNP safety

Three different chain lengths of PLGA and two different chain lengths of PEG were used in this study to generate 4K, 15K and 55K PNPs. Increasing polymer chain length has previously been shown to increase degradation time and decrease non-targeted NP uptake, both beneficial properties for NPs formulated to carry a fluorescent cargo such as PPE for bioimaging (Alexis et al. 2008; Dinarvand et al. 2011; Conde et al. 2014; Sharma et al. 2015). However, changes in polymer chain length can influence PNP toxicity.

When rabbit vascular smooth muscle cells were exposed to polyvinyl alcohol-PLGA NPs with varying PLGA chain lengths of 15-30K, there was no impact on viability (Westedt et al. 2007). Additionally, when Estradiol containing PLGA NPs were orally administered to Sprague Dawley rats, organs including the liver and lung appeared unaffected (Mittal et al. 2007).

However, longer PEG chain length can enhance NP stability and reduce cellular uptake, and could, therefore, reduce NP toxicity before they reach target cells. Furthermore, an increase in PEG chain length can increase PNP diameter (Gref et al. 2000; Ma et al. 2012). In a study comparing 2K and 5K PEG chain lengths *in vivo* using mice and rats, results indicated that a longer chain length leads to extended circulation (Bertrand et al. 2017). Furthermore, no TNF-α or IL-1β production was observed from macrophage cells exposed to chitosan-PEG NPs with 2K and 5K PEG chain lengths, although lower levels of internalisation were seen for chitosan-PEG NPs with 5K PEG chain lengths compared to 2K (Yang et al. 2017). Longer PEG chains as part of PLGA NPs can reduce serum protein adsorption and therefore serum-dependent phagocytosis (Yang et al. 2010).

Previous studies investigating the role of polymer chain length to PNP toxicity have focused on assessment of cytotoxicity, uptake and cytokine production. Using the complex polymer nanomedicines in this project, it was possible to assess the effects of polymer chain length on overall PNP toxicity. This could provide a more comprehensive assessment of PNP toxicity and a better understanding of the mechanism of PNP toxicity using a wider range of endpoints.

3.1.3 Study design and aims

The aim of this study was to assess the toxicity of PLGA-PEG PNPs of varied polymer chain lengths (4K, 15K and 55K PNPs) to hepatocytes *in vitro*. In addition to the endpoints investigated in Chapter 2 (cytotoxicity, cytokine production, cellular uptake, genotoxicity), this study investigated cellular ROS production, as well as liver-specific indicators of toxicity, urea and albumin.

In the cells of the liver, an increase in intracellular ROS could result in an imbalance of ROS and antioxidants, leading to indirect downstream effects such as DNA damage and metabolic changes in hepatocytes (Filippi et al. 2014; Evans et al. 2017). Previously, polymer NPs composed of PLGA and coated with PEI were observed to elicit ROS production in hepatocyte cells (HepG2) (Yu et al. 2014). Additionally, other studies using spheroid culture hepatic cells, indicate that polymer PAMAM dendrimer NPs could stimulate the production of ROS (Chen et al. 2016). ROS production mediated via polymer NPs has not been extensively investigate and could be an important marker of PNP toxicity, as has been observed for engineered NPs such as Ag and CuO NPs (Liu et al. 2016; Ahmad et al. 2016). Therefor it is important it investigate the ability of these PNPs to elicit a ROS response.

Reduction of urea and albumin production are markers of liver disease (Racine-Samson et al. 1996). This is an important endpoint *in vitro* as an indicator of hepatocyte health that has not been commonly investigated when assessing the toxicity of PNPs. Therefor this could be a useful marker for PNP toxicity, that warrant investigation. *In vivo* studies in mice and rats have shown a decrease in blood urea nitrogen (BUN) levels, an *in vivo* equivalent to urea synthesis, when exposed intravenously to various NPs (TiO_2, Ag, ZnO) < 300 nm (Wang et al. 2007; Faisst et al. 2010; Pan et al. 2012; Xu et al. 2013). In contrast, other *in vivo* studies in rats have shown that polymer based NPs such as PLGA NPs of < 500 nm failed to impact on BUN levels following oral and intravenous NP exposure (Italia et al. 2007; Moreno et al. 2010).

Similar observations of a marked reduction in urea and albumin synthesis together with increased ROS production were made in a previous *in vitro* study using primary

hepatocytes exposed to TiO_2 NPs < 900 nm (Natarajan et al. 2015). It was suggested that damage to the mitochondria, contributed to these liver-specific observations (Natarajan et al. 2015).

It is hypothesised that:

1. 4K, 15K and 55K NPs, at pharmacologically relevant concentrations would stimulate minimal cytotoxicity in C3A hepatocyte cells.

2. 4K, 15K and 55K NPs have increasing PLGA chain lengths, with increasing polymer chain length there would be a reduction in overall toxicity due to increased PNP stability.

3. 4K, 15K and 55K NPs would stimulate ROS production and activate a pro-inflammatory response in C3A hepatocyte cells.

4. 4K, 15K and 55K NPs would be internalised by C3A hepatocyte cells
    a. with less uptake observed for PNPs of longer polymer chain lengths.

5. 4K, 15K and 55K NPs at pharmacologically relevant concentrations would stimulate minimal genotoxicity in C3A hepatocyte cells.

6. 4K, 15K and 55K NPs would be capable of reducing albumin and urea production in C3A hepatocyte cells.
    a. with less of an impact observed for PNPs with longer polymer chain lengths.

In parallel to the assessment of PNP toxicity the physicochemical properties of the PNPs will be investigated via DLS and TEM. These batch produced NPs had short stability, low volume and low NP concentration. Therefore, it was not always possible to perform endpoints with a wide range of concentrations, in particular endpoints that require higher volumes such as genotoxicity.

3.2 Materials and methods

3.2.1 Preparation of 4K, 15K and 55K NPs

NPs were prepared at Heriot Watt University according to the method developed by Prof Lea Ann Dailey and Dr Thais Abelha of King's College London. The amphiphilic diblock copolymer PLGA–PEG was used to encapsulate the fluorescent, green-emitting conjugated polymer PPE. PLGA-PEG block copolymers of various molecular weights (PEG2K-PLGA4K (4K), PEG2K-PLGA15K (15K) and PEG5K-PLGA55K (55K)) were purchased from Sigma-Aldrich. A stock solution of each type of polymer was prepared at a concentration of 5 mg/mL in the solvent, Tetrahydrofuran (THF) (Sigma-Aldrich), in a glass vial. In a separate glass vial, the conducting polymer, PPE, was prepared at a concentration of 5 mg/mL in the THF.

Next, the PEG-PLGA copolymer solutions were combined with the PPE solution to a final volume of 1 mL in THF. The 4K and 15K solutions had final concentrations of 64.57 μg/mL (62 μL) of PPE and 645.82 μg/mL (620 μL) for PEG-PLGA, with a final polymer concentration (PLGA, PEG and PPE) of 0.710mg/mL. The 55K solution contained 45.83 μg/mL (44 μL) of PPE and 458.33 μg/mL (440 μL) of PEG-PLGA, giving a final polymer concentration (PLGA, PEG and PPE) of 0.504 mg/mL.

Each polymer solution (1 mL) was added dropwise to 4.8 mL of deionised water, under low, stirring conditions using a magnetic flea. Overnight stirring was kept at the lowest speed to allow complete evaporation of the THF. Any volume of water lost overnight was replaced, and NP suspensions were filtered using a sterile membrane syringe filter (pore size 200 nm) (Millipore), stored at 4°C and used within one month of preparation. For use in experiments, NPs were freshly diluted in cell culture medium and briefly vortexed.

3.2.2 Nanoparticle characterisation

NPs were characterised by DLS and TEM, as in Section 2.2.2. Additionally, the size stability of the NP suspensions were determined by monitoring changes in hydrodynamic diameter up for to one-month post-synthesis.

3.2.3 Cell culture

Human C3A hepatocellular carcinoma cells were cultured as in Section 2.2.3.

3.2.4 Cytotoxicity assay: Alamar Blue

A 96-well plate fluorescence-based assay assessed C3A cells viability following exposure to NPs using the AB assay as described in Section 2.2.5. NP interference with the AB assay was performed as in Section 2.2.5 with NPs prepared at concentrations of (4.6, 9.3, 18.7, 37.5, 75.0, 150 μg/mL). Inference results were only reported when positive.

3.2.5 Measurement of cytokine production

A multiplex sandwich ELISA was used to measure secretion of IL-8, IL-1ra, TNF-α, IL-1β and IL-6 from C3A cells exposed to NPs. Supernatants obtained from the cytotoxicity experiments (Section 3.2.4) were thawed and analysed using a human magnetic Luminex assay kit (R&D Systems), as in Section 2.2.9 and as per the manufacturer's instructions. All steps were carried out at RT and in subdued lighting conditions. Sublethal NP concentrations (31.25, 62.5 and 125 μg/mL) were assessed, as well as Complete Medium (negative control). Additionally, NPs' interference with this assay was established by adding the standard curves midpoint (SCM) concentration to 125 μg/mL NPs prepared in the same medium as the standard curve. Any interference observed was presented in results, if not presented interference was not observed.

3.2.6 Measurement of intracellular ROS production

A 96 well-plate fluorescence-based assay was used to determine C3A cells ROS production. Cells were exposed to UFCB a well-established mediator of ROS production as a positive control for ROS production with and without pre-treated with Trolox to establish the assay is functioning correctly (Brown et al. 2004). C3A cells were seeded into a 96-well plate at a concentration of 1.56×10^5 cells/cm^2 and incubated for 24 hours

at 37°C and 5% CO_2. Cells either remained in Complete Medium or were pre-treated with Trolox (100 µM in Complete Medium) for one hour at 37°C and 5% CO_2. Cells were then washed twice using PBS and exposed to NPs at sublethal concentrations (31.25, 62.5 and 125 µg/mL) or UFCB-Printex-90, 10 µg/mL (positive control) or Complete Medium (control) in triplicate for 1440 minutes at 37°C and 5% CO_2. Going forward all steps were performed in subdued lighting at RT.

Following NP treatment, cells were washed twice with HBSS (Sigma-Aldrich) and then incubated for five hours with 5 µM DCFH-DA (Sigma Aldrich) or methanol (without DCFH-DA) (100 µL) to assess the NPs potential for interference with DCFH-DA. This was measured in a SpectraMax M5 Microplate Reader at Ex/Em 495/529 nm. Data are expressed as mean fold change (from control) ± SEM. Interference was only reported when it was positive.

3.2.7 Quantification of NP uptake: plate method

A 96 well-plate fluorescence-based uptake assay was used to determine uptake of fluorescently loaded NPs by C3A cells at sublethal concentrations (1.9-125 µg/mL), as in Section 2.2.7. Data are expressed as average µg/mL of the retained NP suspension in the cell lysate, calculated from standard curves.

3.2.8 Assessment of NP uptake: confocal microscopy

Confocal microscopy was used to visualise NP uptake by C3A cells, as in Section 2.2.6. One timepoint (1440 minutes) was selected, based on the previously reported findings (Section 3.2.7) at one sublethal concentration of NPs of 125 µg/mL. Slides were stored at 4˚C until they were imaged using a Leica SP5 SMD laser-scanning confocal microscope (Edinburgh Super-Resolution Imaging Consortium).

3.2.9 Genotoxicity assessment: Comet assay

A 24-well plate-based assay was used to assess specific oxidative DNA damage and DNA strand breaks using the Fpg-modified Comet assay with the 24-well comet chip

(Trevigen) and the Fpg fragment length analysis using repair enzymes (FLARE) assay kit (Trevigen). Following this, cells were seeded and grown for 24 hours at 37°C and 5% CO_2 in 24-well plates (1.56 x10^5 cells/cm^2). These cells were washed twice in HBSS and exposed to NPs (62.5 and 125 μg/mL), Complete Medium (negative control), 60 μM hydrogen peroxide (H_2O_2, positive control) (Sigma-Aldrich). This was done in duplicate for 1440 minutes at 37°C and 5% CO_2. Due to the limited volume and concentration of NPs the number of concentrations assessed was limited to two and not the recommended three meaning these results most be considered preliminary (OECD 2015).

The cells were then washed twice with HBSS, trypsinised (Section 2.2.3) before being resuspended in Complete Medium (1 mL) and centrifuged at 2000 g for one minute. Subsequently, the supernatant was discarded, and the cells resuspended in ice-cold PBS (0.2 mL). The cells (100 μL) were then added to low melting point agarose (400 μL). The cell agarose suspension (25 μL) was next deposited onto a 24-well comet chip in duplicate. Slides were incubated on ice for 15 minutes before being transferred to a lysis solution for 12 hours at 4°C.

Following incubation, slides were immersed in the FLARE buffer for 30 minutes with three changes of buffer. Slides were next incubated with Fpg enzyme (1:75 dilution in the Fpg reaction buffer) or Fpg reaction buffer alone at 37°C for 30 minutes in a humidity chamber. Afterwards, they were transferred to an electrophoresis solution (300 mM sodium hydroxide, 200 mM EDTA, 2 L distilled water, pH 13) and incubated for 30 minutes at RT, with a single solution change. After this, slides were transferred to an electrophoresis tank containing an electrophoresis solution in a room with a temperature of 4°C. The solution was allowed to equilibrate for 20 minutes. Electrophoresis was performed for 40 minutes at 30 V and 300 mA. Next, slides were washed twice with deionised water and then once with 70% ethanol, each wash was five minutes. Slides were then dried for 15 minutes at 37°C before being stored at 4°C.

Samples were stained with GelRed (Biotum) to visualise DNA. Samples were imaged using a fluorescence microscope (Zeiss AX10 with an Allied Vision Technologies Stingray camera) connected to image-analysing software (Comet Assay IV, Perceptive Instruments, UK). Fifty measurements were taken for each slide per experiment. Data are

expressed as mean % Tail DNA ± SEM.

3.2.10 Measurement of urea production

The quantichrom urea assay kit (BioAssay Systems) was used to quantify C3A cells' urea production. Cells were seeded and grown for 24 hours at 37°C and 5% CO_2 in 96-well plates (1.56 x 10^5 cells/cm^2). Cells were exposed to NPs at a sublethal concentrations (31.25, 62.5 and 125 µg/mL) or Complete Medium (control) in triplicate for 24 hours at 37°C and 5% CO_2.

Following exposure, cell supernatants were collected and added to appropriate wells in a fresh black 96-well plate, including a set of standards to produce a standard curve (3.5 - 500 µg/dL) (50 µL). A working reagent (100 µL) was prepared from two components (Solution A: 10% sulphuric acid, 0.40% o-phthalaldehyde and 0.04% Brij 35 and Solution B: 0.08% Primaquine diphosphate, 22% sulphuric acid, 0.8% boric acid and 0.04% Brij 35) and added to all wells. The plates were incubated for 50 minutes at RT in subdued lighting conditions. Absorbance was measured in a SpectraMax M5 Microplate Reader at 430 nm. Data are expressed as average µg/dL of urea, calculated from the standard curve.

To determine the potential for NPs interference with this assays the NPs at 125 µg/mL were spiked with the SCM for the urea standards. Results were reported only when inference was observed.

3.2.11 Measurement of albumin production

Bromocresol green (Sigma Aldrich) was used to establish albumin production in C3A cells. Following seeding of cells and 24 hours' growth at 37°C and 5% CO_2 in 96-well plates (1.56 x 10^5 cells/cm^2), cells were exposed to NPs at sublethal concentrations (31.25, 62.5 and 125 µg/mL) or Complete Medium (control) in triplicate for 24 hours at 37°C and 5% CO_2.

Following exposure, cell supernatants were collected and added to the appropriate wells

of a fresh black 96-well plate, and a standard curve, 6.25-400 mg/dL of albumin from chicken-egg white (Sigma Aldrich) (50 µL). The Bromocresol green (0.066 mM in 100 mM Succinate Buffer (Sigma Aldrich), pH 4.2) solution (50 µL) was then added to all wells. The plates were incubated for five minutes and shaken at RT in subdued lighting. Absorbance was measured in a SpectraMax M5 Microplate Reader at 630 nm. Data are expressed as average mg/dL of albumin, calculated from the standard curve.

To determine the potential for NPs interference with this assays the NPs at 125 µg/mL were spiked with the SCM for the albumin standards. Results were reported only when inference was observed.

3.2.12 Statistical analysis

Experimental data were analysed using GraphPad Prism software. One-way ANOVA using Tukey post-test or two-way ANOVA, followed by the Bonferroni post-test were used to test significance which was set at $p< 0.05$. All experiments were repeated three times on different days unless otherwise stated.

3.3 Results

3.3.1 4K, 15K and 55K NPs: Physicochemical characterisation

Immediately after preparation, and 24 hours after incubation at 37°C and 5% CO_2, DLS was used to measure the hydrodynamic diameter, zeta potential and PDI of 4K, 15K and 55K NPs prepared in PRF Complete Medium (Figure 3.2). At both time points, both the 4K and 15K NPs had similar hydrodynamic diameters of ~140 nm and PDI values of ~0.2 (Figures 3.2 A/B). The hydrodynamic diameter of 55K NPs was at ~150 nm at both time points, which was significantly larger ($p < 0.05$) than those of both the 4K and 15K NPs (Figure 3.2A). After 24 hours' incubation, there was a significant decrease ($p < 0.05$) in the PDI of 55K (Figure 3.2B).

All NPs exhibited a slightly negative surface charge, ranging from -5 to -12 mV (Figure 3.2C). The zeta potential of 4K NPs was significantly less negative ($p < 0.001$) than those of both 15K and 55K NPs. On the other hand, 15K NPs showed a significant decrease in zeta potential following 24 hours' incubation. The size and morphology of the NPs were assessed using TEM. To closely resemble experimental conditions, all NPs were prepared in PRF Complete Medium for TEM imaging (Figure 3.3). All three NPs appear to have a mixed population of NPs, with the dominant NPs appearing to be 100-200 nm in diameter. Some NP agglomeration/aggregation was observed for all NPs.

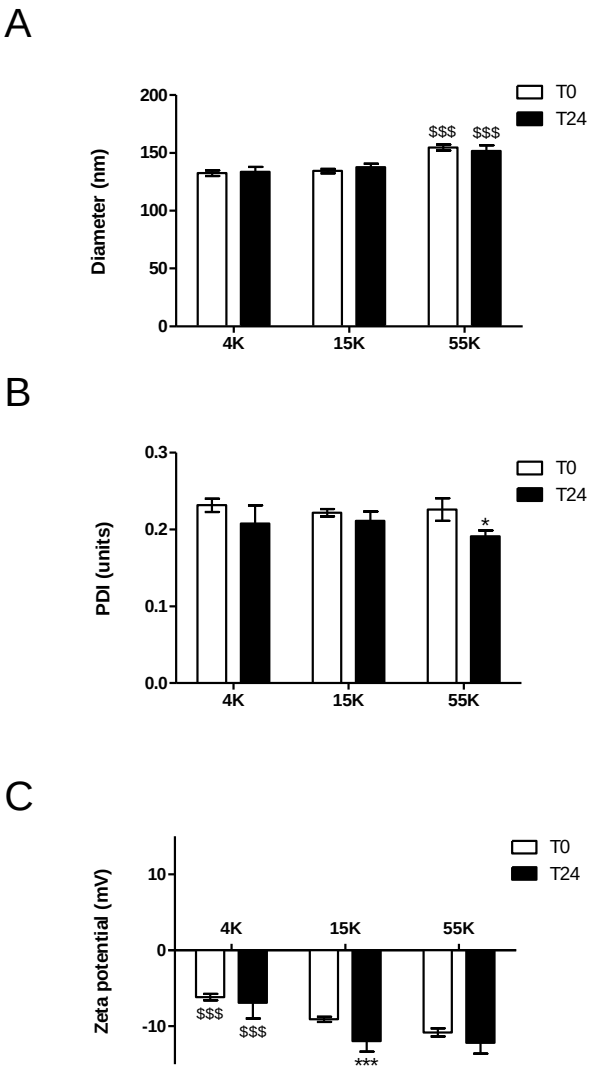

Figure 3.2 Characterisation of 4K, 15K and 55K NPs properties using DLS.

NPs (4K, 15K and 55K) were suspended in PRF Complete Medium (125 µg/mL). Hydrodynamic diameter (A), PDI (B) and zeta potential (C) were assessed at 0 (T0) and 24 hours (T24) post-incubation at 37°C, 5% CO_2 using DLS. Data are expressed as mean ± SEM (n=3). Significance indicated by *= p< 0.05 or ***= p< 0.001 when 0 and 24 hours compared. Significance indicated by $$$= p< 0.001 when 55K compared to 4K and 15K (A) or 4K compared to 15K and 55K (C).

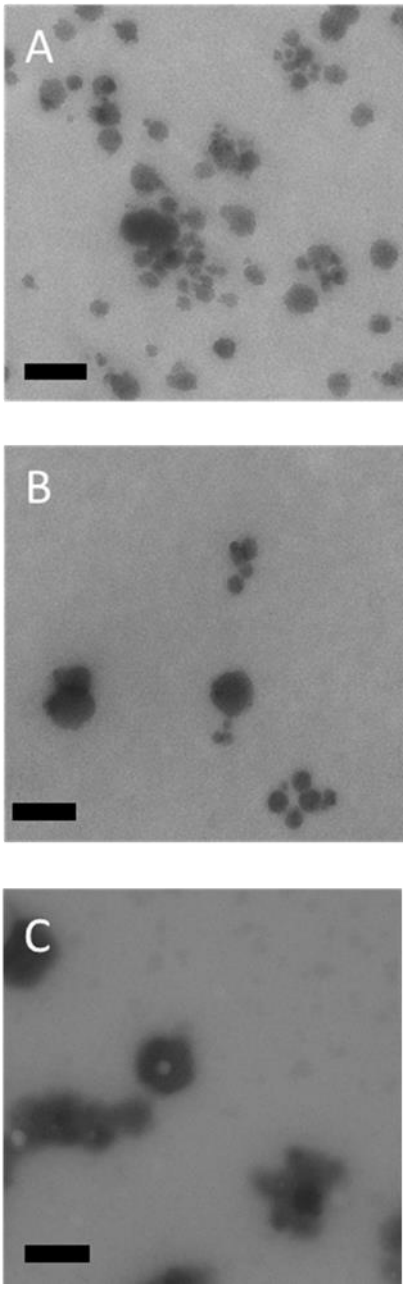

Figure 3.3 TEM characterisation of 4K, 15K and 55K NPs.

Images are of the 4K (A), 15K (B) and 55K NPs (C) when suspended in PRF Complete Medium at a concentration of 125 µg/mL and imaged using TEM. Representative images (n=3), scale bar, represents 200 nm.

3.3.2 4K, 15K and 55K NPs: Cytotoxicity

To investigate the effect of 4K, 15K and 55K NPs on cell viability, C3A cells were exposed to NPs at concentrations ranging from 4.7-150 µg/ mL, and the AB assay was used to measure the cells' metabolic activity (Figure 3.4). With all NPs, there was a concentration-dependent decrease in cell viability. A significant decrease in viability was observed for the 4K NPs at concentrations of 37.5 and 150 µg/mL. For the 15K NPs, a significant decrease in cell viability was observed at 150 µg/mL. However, for both the 4K and 15K NPs, viability did not decrease to levels below 80% and therefore was unlikely to be biologically relevant.

For the 55K NPs, cell viability decreased significantly ($p< 0.001$) at all concentrations except the lowest of 4.7 µg/mL (significance only indicated when value below 80% viability). A decrease in viability below 80% was only observed at the highest concentrations of 75 and 150 µg/mL. The reduction in the viability of cells exposed to the 55K NPs was significantly higher ($p< 0.01$) than that observed for the 4K or 15K NPs at 150 µg/mL. An EC_{20} value, indicating the concentration at which NP exposure causes 20% cell death, could not be calculated within the range of concentrations used for these NPs. EC_{20} calculations require a complete dose-response curve containing a top plateau (defined as 100) and a bottom plateau (defined as 0), when data do not have defined 100 and 0, then 20 is also undefined (Neubig et al. 2003). Although reading off the graph it may suggest that for 55K NPs at 37.5 µg/mL NP exposure causes 20% cell death (Figure 3.4).

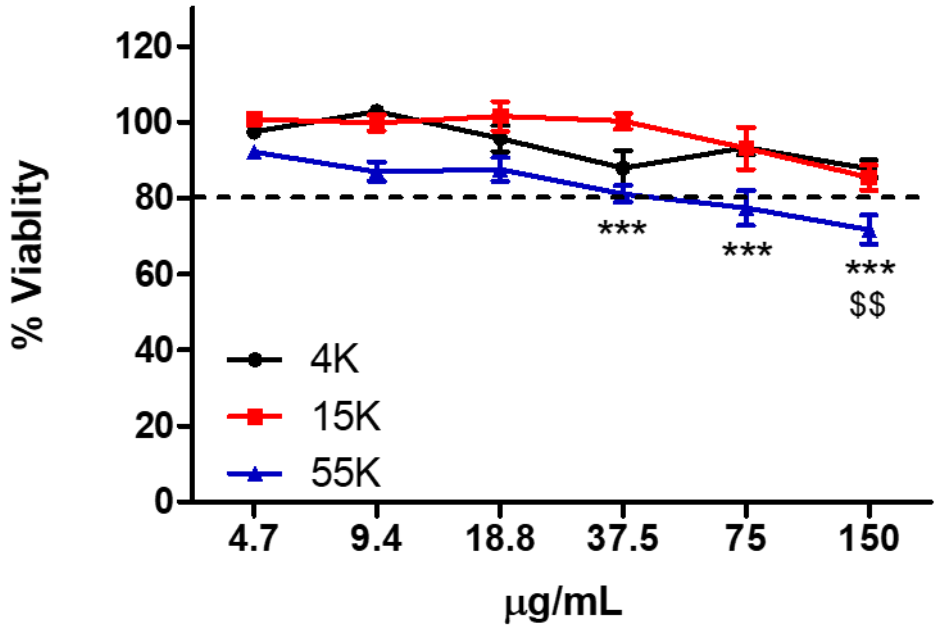

Figure 3.4 Cytotoxicity of 4K, 15K and 55K NPs to C3A cells.

Cells were exposed to 4K (black), 15K (red) and 55K NPs (blue) at 4.7-150 µg/mL for 24 hours. Percentage viability was measured via AB assay. Data are expressed as mean % viability (i.e. % of untreated control) ± SEM (n=3). Significance indicated by ***= $p< 0.001$ compared with untreated control. Significance indicated by $$= $p< 0.01$ when 4K/15K NP compared with 55K NPs.

3.3.3 4K, 15K and 55K NPs: Cytokine production

To determine any potential interference of NPs with cytokine measurement, all NPs at 125 µg/mL were incubated with a known concentration of cytokines equivalent to the SCM. The 55K NPs appeared to show a significant decrease in cytokine measurement of TNF- α, IL-6 and IL-1ra (Figure 3.5) ($p<0.01$ to $p<0.001$). However, both 4K and 15K NPs appeared to decrease significantly ($p<0.05$) the detection of IL-1ra. Although this interference was significant, it was ~5% or lower, suggesting cytokine detection would not be prevented.

Production of IL-8, IL-1ra, TNF-α, IL-1β and IL-6 cytokines from C3A cells was assessed following exposure to all NPs. For all NPs, there was no significant production of cytokines by C3A cells over background levels for TNF-α, IL-1β or IL-6. However, a significant ($p<0.01$ to $p<0.001$) decrease in IL-8 production was seen with all NPs (Figure 3.6A), although this was not significantly difference between the different NPs. Since the NPs did not interfere with the detection of IL-8 (Figure 3.5), the decrease observed can be assumed to accurately reflect the impact of these NPs on IL-8 production. Additionally, there appeared to be an increase in IL-1ra production for all NPs, but this was only significant for 4K NPs at 125 µg/mL (Figure 3.6B).

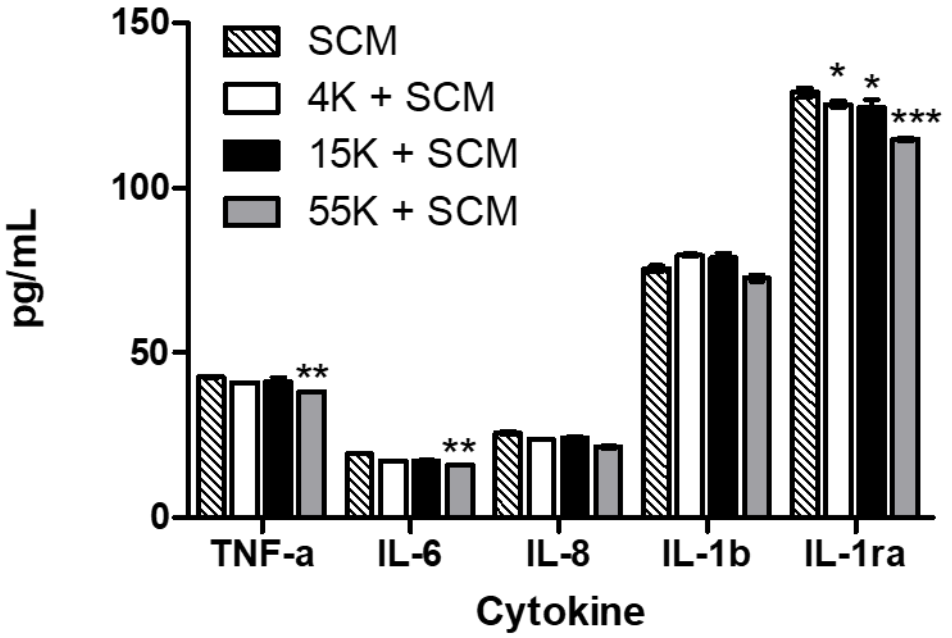

Figure 3.5 Optimisation of cytokine detection for 4K, 15K and 55K NPs.

The SCM concentration of each cytokine was incubated with 4K, 15K and 55K NPs prepared at 125 μg/mL in Complete Medium to observe interference of cytokine detection caused by NPs. Data are expressed as mean pg/mL ± SEM (n=3). Significance indicated by *= $p< 0.05$, **= $p< 0.01$ or *** = $p< 0.001$ when compared with SCM.

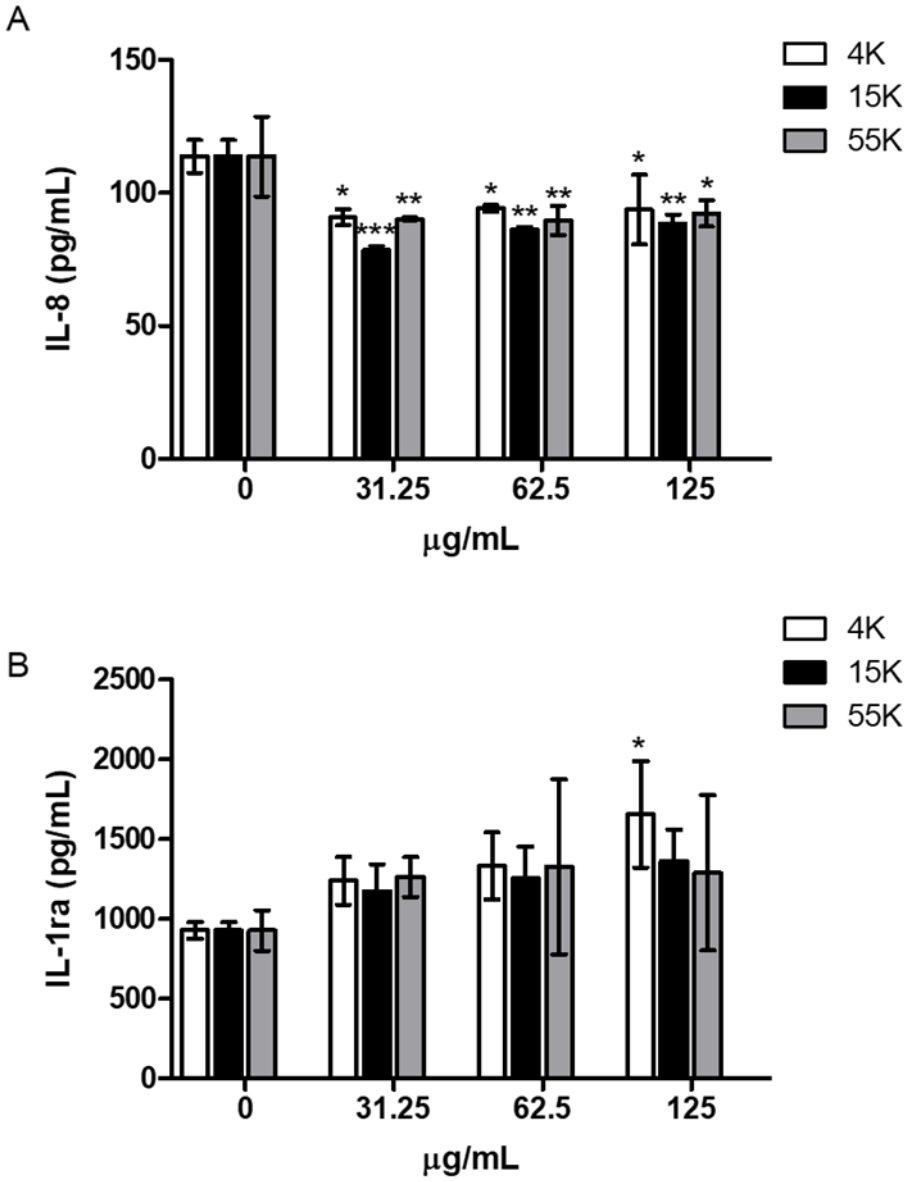

Figure 3.6IL-8 and IL-1ra production induced by the 4K, 15K and 55K NPs in C3A.

Cells were exposed to 4K, 15K and 55K NPs (31.25, 62.5 and 125 µg/mL) for 24 hours. Data are expressed as IL-8 (A) or IL-1ra (B) pg/mL ± SEM (n=3). Significance indicated by *= p< 0.05, **= p< 0.005 or *** = p< 0.001 compared with the untreated control.

3.3.4 4K, 15K and 55K NPs: Intracellular ROS production

To measure the ability of the 4K, 15K and 55K NPs to induce intracellular ROS production, the DCFH-DA assay was used. A significant increase ($p<0.001$) (~five-fold) in ROS production was observed for all NPs at all concentrations 24 hours post-exposure of C3A cells (Figure 3.7). There appears to be no dependence on NP concentration, suggesting all NPs at all concentrations induce the same level of ROS production. Although the 55K NPs at 125 µg/mL appeared to stimulate a significantly higher ($p<0.05$) level of ROS production when compared with both the 4K and 15K NPs at 125 µg/mL, albeit a small increase of ~ 20% (Figure 3.7C). UFCB (positive control) induced a significant increase ($p<0.001$) in ROS production (Figure 3.7).

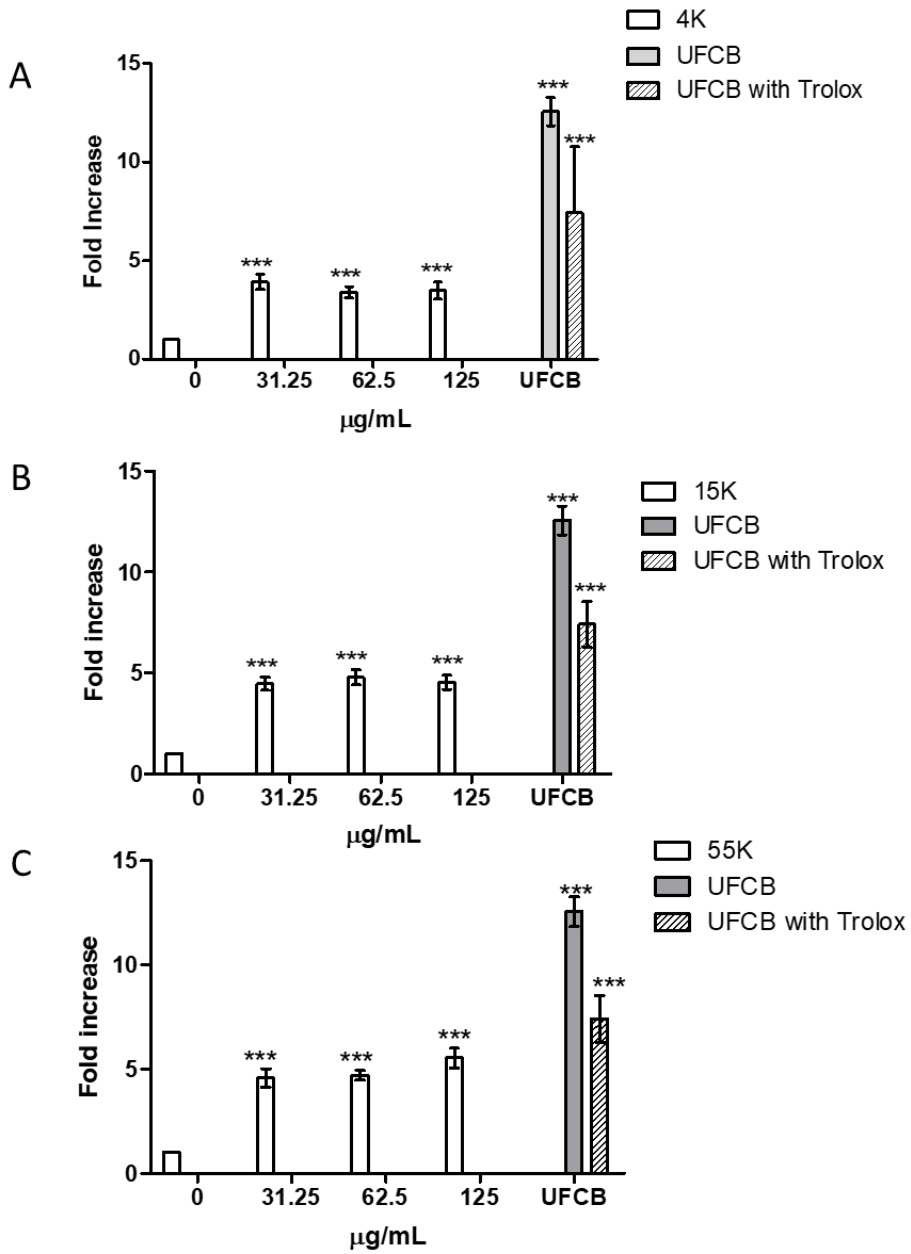

Figure 3.7 ROS produced by C3A cells exposed to 4K, 15K and 55K NPs: DCFH-DA assay.

Cells were exposed 4K (A) 15K (B) or 55K (C) at 31.25, 62.5 and 125 µg/mL and to UFCB (positive control) at 10 µg/mL for 24 hours. Data are expressed as mean fold change (from the untreated control) ± SEM (n=3). Significance indicated by ***=p< 0.001 compared with the untreated control.

3.3.5 4K, 15K and 55K NPs: Uptake

A fluorescent plate-based method was used to quantify the internalisation of the 4K, 15K and 55K NPs by C3A cells over time (10, 60 and 1440 minutes) at a range of concentrations (1.9-125 µg/mL). There appeared to be little or no internalisation of any of the NPs at any of the time points or concentrations investigated. The only detectable level of uptake observed was for 15K NPs at 125 µg/mL, 24 hours post-exposure (Figure 3.8).

NP internalisation at 24 hours post-exposure was also evaluated using confocal imaging, at a concentration of 125 µg/mL. There appeared to be the minimal uptake of all NPs (green) by C3A cells. The highest level of uptake was observed for 15K NPs, with a very limited number of NPs visible in the cytoplasm surrounding the nuclei in the cells (Figure 3.9).

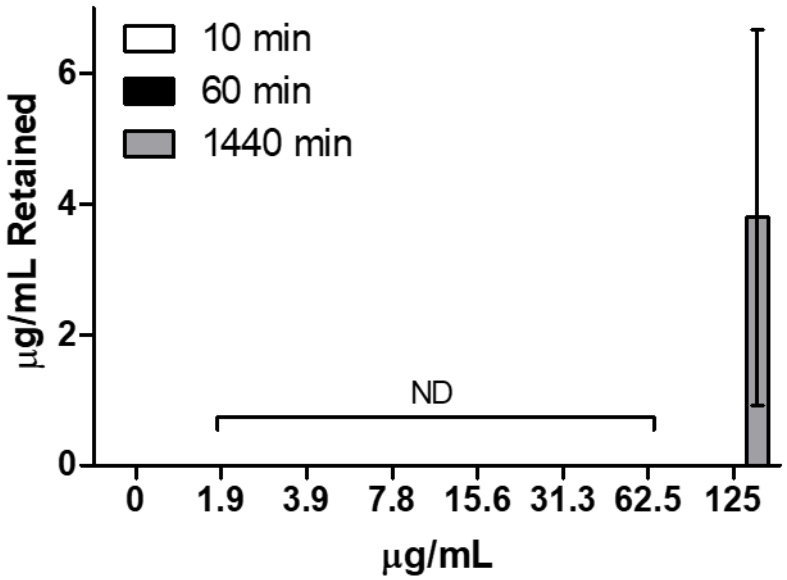

Figure 3.8 Uptake of 15K NPs in C3A cells, over time: Plate method.

Cells were exposed to the 15K NPs for 10 (white), 60 (black) and 1440 (grey) minutes at 1.9-125 µg/mL. Data are expressed as mean µg/mL retained (from appropriate standard curves) ± SEM (n=3). ND indicates non-detectable.

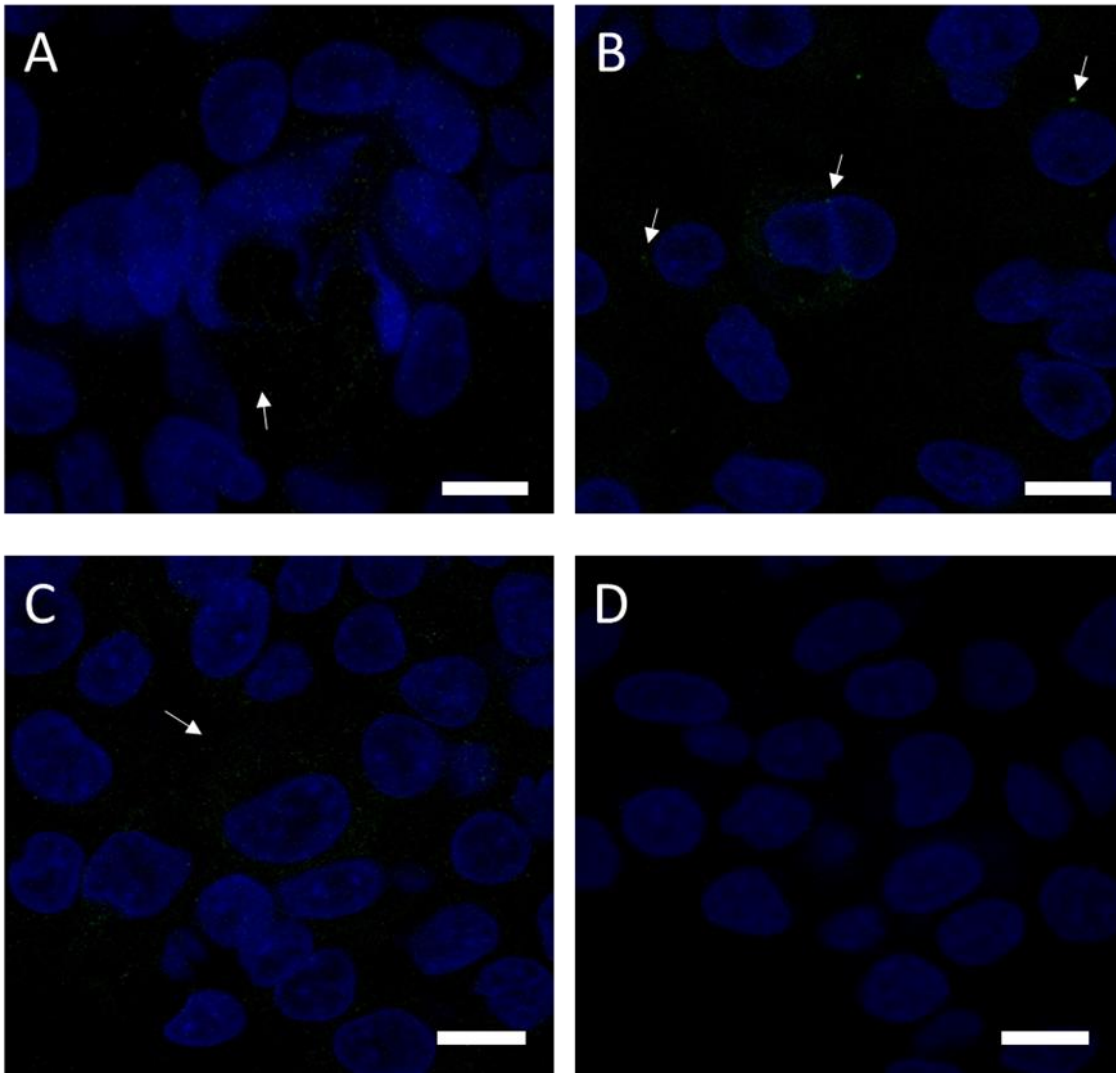

Figure 3.9 Uptake of the 4K, 15K and 55K NPs by C3A cells.

Cells were exposed to 125 µg/mL NPs (green), 4K (A), 15K (B), 55K (C) or Complete Medium (D) for 24 hours. DNA (blue). Representative images (n=3) scale bar represents 10 µm. Arrow points towards NPs (green).

3.3.6 4K, 15K and 55K NPs: Genotoxic effect

A semi-high throughput Comet assay was used to investigate the NPs' genotoxicity. C3A cells were exposed to all NPs for 24 hours at concentrations of 62.5 and 125 μg/mL, and the Fpg enzyme was used to determine the contribution of oxidative stress to any observed genetic damage.

There was no significant damage to DNA seen for all three NPs at both concentrations in the absence of Fpg (Figure 3.10). In the presence of Fpg, only the 15K NPs caused a small but significant increase ($p<0.05$) in DNA damage at 125 μg/mL. Additionally, when compared with the 4K and 55K NPs at the same concentration with Fpg, 15K NPs appeared to cause significantly more ($p<0.05$) DNA damage than the 4K and 55K NPs did. The positive control of H_2O_2 (60 μM) caused a significant increase ($p<0.001$) in DNA damage in the absence and presence of Fpg. In the presence of Fpg, the level of DNA damage was significantly higher ($p<0.001$) for H_2O_2, indicating that the assay had functioned as expected.

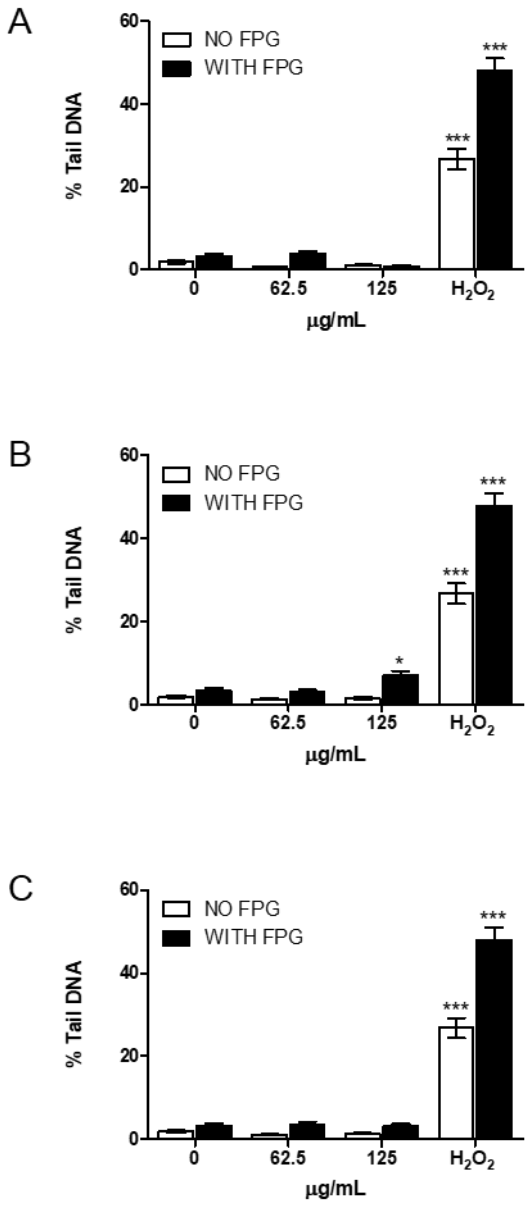

Figure 3.10 Genotoxicity of 4K, 15K and 55K NPs in C3A cells: Comet assay. Cells were exposed to 4K (A), 15K (B) and 55K (C) NPs at concentrations of 62.5 and 125 µg/mL, 60 µM H_2O_2 and Complete Medium for 24 hours ± Fpg. Data are expressed as mean % of DNA in tail ± SEM (n=3). Significance indicated by ***= $p< 0.001$, *= $p< 0.05$ compared with untreated control.

3.3.7 4K, 15K and 55K NPs: urea and albumin production

As a measure of hepatocyte function, urea and albumin production were investigated in cells treated with the 4K, 15K and 55K NPs following 24 hours exposure at three sublethal concentrations (31.25, 62.5 and 125 µg/mL). To determine the potential for NPs to interfere with these assays the NPs (125 µg/mL) were spiked with the SCM for both the urea and albumin standards. There did appear to be a significant reduction ($p < 0.001$) in urea measurement when the SCM was spiked with 4K and 15K NPs, both containing PEG2K as part of the polymer chain, as this reduced the measurement of urea by approx. ~ 40-50 %, therefore any reduction less than this cannot be considered to be a NP effect (Figure 3.11A). While there was no observed interference for 55K NPs which contains PEG5K as part of the polymer chain. There was no interference observed with the albumin production assay for any NPs (Figure 3.11 B).

A significant decrease ($p < 0.001$) in urea production was seen for cells exposed to all the NPs. The 55K NPs appeared to reduce significantly ($p<0.001$) the production of urea in a concentration-dependent manner (Figure 3.12A). Additionally, 4K NPs reduced urea production to non-detectable (ND) levels at the highest concentration of 125 µg/mL. Reduction in urea for the 15K NPs at all concentrations, and the 4K NPs at 31.25 and 62.5 µg/mL was likely to derive from interference, not NP toxicity. In contrast, there appeared to be no effect on albumin production by any of the NPs, at any of the concentrations tested (Figure 3.12B).

A previous *in vivo* (rat) study demonstrated that LPS downregulates urea cycle enzymes in the liver, making LPS a useful positive control for both urea and albumin production in hepatocytes (Tabuchi et al. 2000). When C3A cells were exposed to LPS, significant reductions ($p < 0.001$) in both urea and albumin production were observed (Figures 3.12A/B).

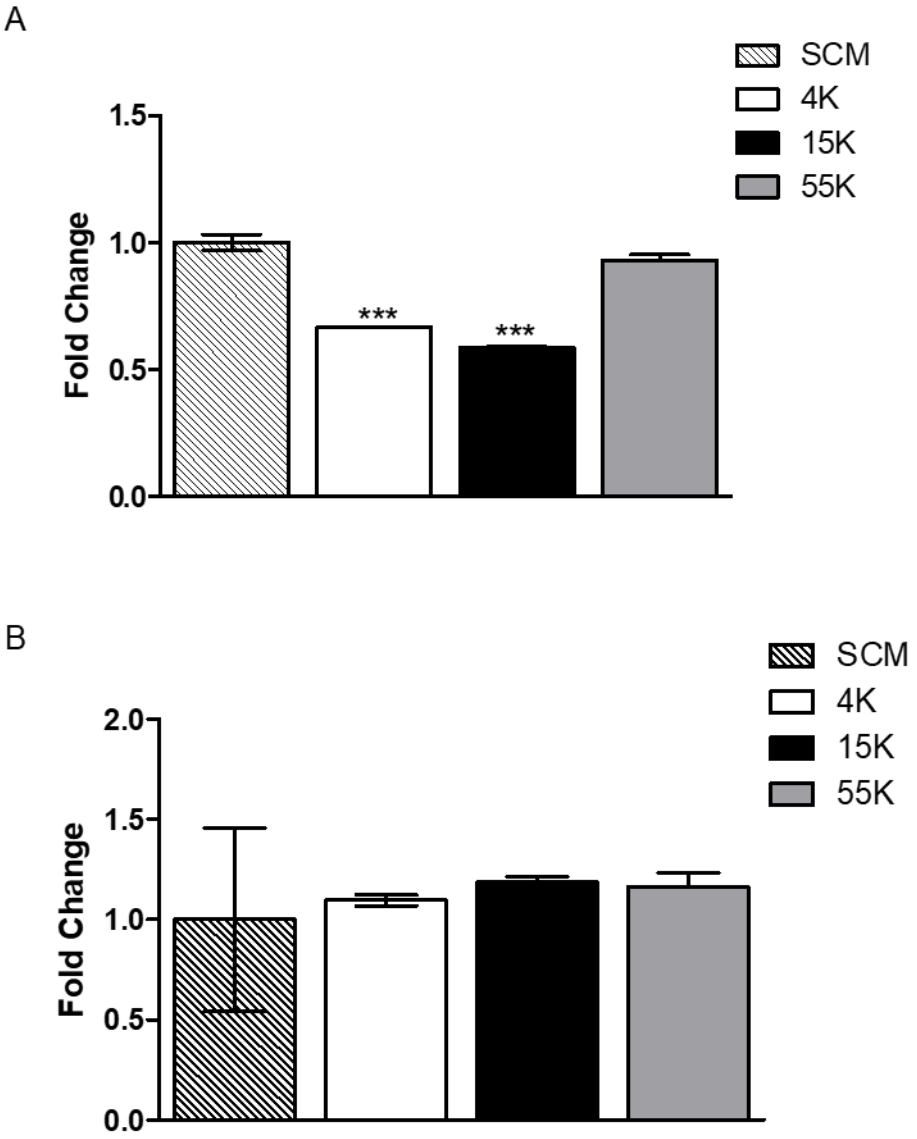

Figure 3.11 Interference of the 4K, 15K and 55K NPs with urea and albumin detection.

The SCM of urea or albumin standard curves was added to 4K, 15K and 55K NPs prepared at 125 μg/mL in Complete Medium for 24 hours at 37°C and 5% CO_2 to observe the interference of urea (A) and albumin (B) detection caused by NPs. Data are expressed as mean fold change ± SEM (n=3). Significance indicated by ***=p< 0.001 compared with SCM alone.

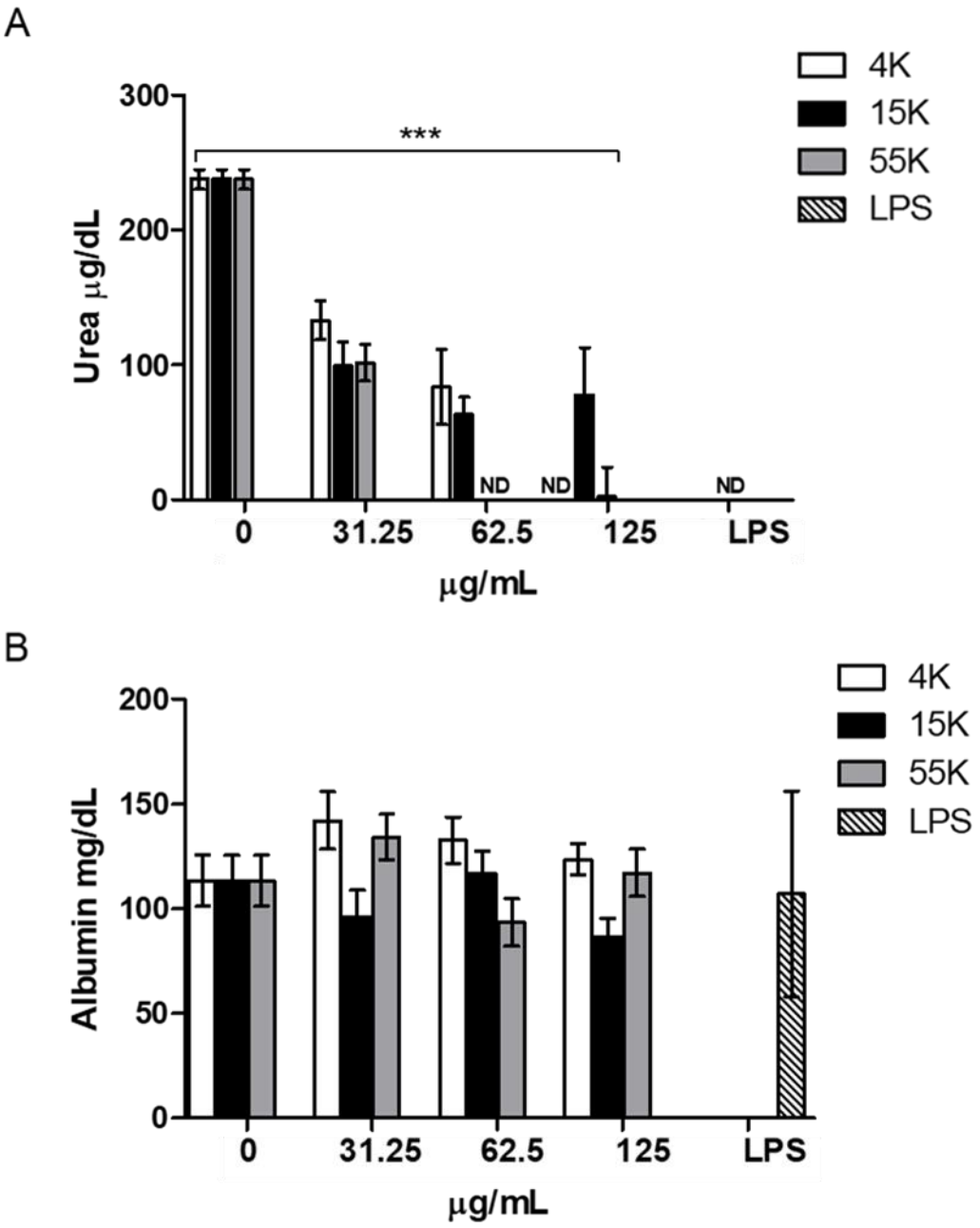

Figure 3.12 Urea and albumin production following exposure of C3A cells to 4K, 15K and 55K NPs.

Cells were exposed to the 4K, 15K and 55K NPs at 31.25, 62.5 and 125 µg/mL for 24 hours. Urea (A) and albumin (B). Data are expressed as mean urea µg/mL (A) or mean albumin mg/dL (B) ± SEM (n=3). Significance indicated by ***= $p<0.001$ when treated cells compared with untreated control. ND represents non-detectable.

3.4 Discussion

3.4.1 Overview of results

To understand the impact of varying polymer chain lengths on PLGA NP toxicity in C3A cells, NPs were first characterised using DLS and TEM to determine size, morphology and surface charge. Characterisation results indicated that all NPs were <150 nm in diameter and that the 4K and 15K NPs had no significant difference in size, while the 55K NPs appeared significantly larger. Following incubation at 37°C for 24h, there was no change in the size of any of the NPs, suggesting they remained stable throughout a 24 hour assay. All NPs had a negative surface charge. The zeta potential of the 15K NPs decreased after incubation at 37°C for 24h, which may have influenced the way these NPs interacted with cells.

Cytotoxicity assessment using the AB assay indicated that the 4K and 15K NPs did not affect C3A cell viability. The 55K NPs significantly decreased cell viability to below 80% at the highest concentration tested (150 µg/mL), indicating that NPs with longer PLGA chain lengths may negatively affect C3A cells viability. After this, the internalisation of NPs by cells was investigated. The internalisation of 4K and 55K NPs by C3A cells was negligible at the timepoints and concentrations investigated. However, very low levels of uptake of 55K NPs were observed at the highest concentration (125 µg/mL) after incubation for 24h.

Genotoxicity was assessed using the Comet assay. However, only the highest concentration of the 15K NPs caused a low level of genotoxicity in the presence of Fpg, suggesting that DNA damage was mediated by an oxidant mechanism. For all NPs, there was no production of TNF-α, IL-1β or IL-6 by cells, although there was a significant decrease in IL-8 production for cells exposed to all NPs, and a significant increase in IL-1ra was seen for cells exposed to 4K NPs at the highest concentration (125 µg/mL). The DCFH-DA assay was used to measure intracellular ROS production, and all the NPs induced an increase in ROS production by cells. However, there was little difference between the NPs.

Specific markers of hepatic damage (i.e. urea and albumin production) were investigated, and it was observed that for all NPs there was little effect on albumin production. There was, however, a significant decrease in urea production for all NPs. Nevertheless, the 4K and 15K NPs may interfere with the assay used to assess urea production.

Taken together, these results indicate that increasing PLGA chain length enhances polymer NP toxicity to C3A cells. This information could be used in the future to design polymeric NPs, design testing strategies to assess polymeric NP toxicity *in vitro* and feed into the development of legislation to protect human health from any risks polymeric NPs pose.

3.4.2 Characterisation of 4K, 15K and 55K NPs

The hydrodynamic diameter of all NPs was <150nm, as assessed using DLS. There was no change in hydrodynamic diameter over time for any of the NPs, suggesting that these NPs are relevantly stable throughout the experimental conditions (24 hours). The 55K NPs were significantly larger than the 4K and 15K NPs at both time points, most probably due to an increase in both PEG and PLGA chain length. These findings are in line with prior studies, which have shown that an increase in PEG chain length (the 4K and 15K NPs had a 2K PEG chain, the 55K had a 5K PEG chain) can increase PNP diameter (Gref et al. 2000; Ma et al. 2012).

TEM was also used to investigate NP size and morphology. The NP size observed using TEM appeared to reflect the measurements obtained using DLS, with the predominant population of NPs being ~100–200 nm in diameter. All three NPs appeared to have some degree of aggregation/agglomeration, and, for all samples, a mixed population of NP sizes was apparent. This could suggest degradation of the NPs before imaging or may also reflect the heterogeneous nature of NPs generated via the solvent displacement method. A study conducted by Fedatto Abelha et al. (2017), demonstrated that a microfluidic solvent displacement (MFSD) method used to synthesise polymeric NPs generated smaller, more uniform NPs than the more traditional solvent displacement methods. Thus, to translate these block copolymer NPs to the clinic, alternative manufacturing techniques, such as MFSD, could improve scalability, as well as NP uniformity (Hickey

et al. 2015).

Although TEM is often used to characterise NPs, polymeric NPs are known to be difficult to image with TEM. More specifically, the low density of PNPs produces low-contrast images, and the TEM preparation methods used can dry out NPs, causing distortion and artefacts (Renz et al. 2016). Therefore, to overcome these obstacles, other imaging modalities can be used, such as atomic force microscopy, which could allow visualisation and measurement of NP size in an appropriate biological medium (Constantin et al. 2017).

The charge of these NPs was slightly negative, which in line with previous studies showing that PEGylation of PLGA NPs generates NPs with slightly negative zeta potential (Li et al. 2001; Pamujula et al. 2012). It is established that PLGA has a negative charge (Yan et al. 2015). Previous studies have indicated that with increasing percentage of PEG in a polymer, there is a less negative zeta potential (Pamujula et al. 2012). Therefore, the finding that the 4K NPs have a less negative zeta potential compared with that of the 15K and 55K NPs, may be related to the higher percentage of PEG in the polymer used to prepare the 4K NPs (PEG2K-PLGA4K (4K NPs=33.3% PEG), PEG2K-PLGA15K (15K NPs=11.8% PEG); PEG5K-PLGA55K (55K NPs=8.3% PEG). Following incubation at 37°C for 24 hours, the 15K NPs had a significantly ($p< 0.01$) more negative zeta potential, perhaps due to the accumulation of a protein corona on their surface, or degradation of a proportion of the NPs. For example, proteins on the NP surface were previously shown to have an overall negative charge at pH7 (Tenzer et al. 2013). The low PDI of all these NPs points towards the high stability of these suspensions, a desirable characteristic for nanomedicines since this would allow for accurate dose administration *in vivo*.

Ideally, further characterisation of the physicochemical properties of these NPs would be performed to help identify which NP properties may confer toxicity. For example, the surface chemistry has been shown to influence NP toxicity (Voigt et al. 2014) and could be measured using a field emission scanning electron microscope (Bandyopadhyay et al. 2016). Analysis of the composition of the protein corona may also shed light on how or why these NPs interact with the cells differently, and could be investigated using Fluorine-19-labelled NPs and by measuring increases in NP radius and reduction in the

diffusion coefficient using Fluorine-19 diffusion nuclear magnetic resonance spectroscopy (Lazarovits et al. 2014; Carril et al. 2017).

3.4.3 Cytotoxicity of the 4K, 15K and 55K NPs

The AB assay was used to determine mitochondrial function as a measure of cell viability, due to its sensitivity and its established position in determining NP cytotoxicity *in vitro* (Zhang et al. 2011; Farcal et al. 2015; Brayden et al. 2015). Additional methods, such as the CFDA-AM and NR uptake assays, can also be used to determine cell viability, although using three different assays to assess the cytotoxicity of low toxicity PNPs may be unnecessary. From previous experiments (section 2.3.2) the Alamar Blue assay was seen to produce robust, reliable data.

. Neither the 4K nor the 15K NPs adversely affected cell viability, with viability above 80% at all concentrations tested, suggesting that these NPs are relatively non-toxic to C3A cells. While higher concentrations of NPs could have been tested to identify indicators of toxicity (e.g. EC_{20}), a maximal concentration of 150 µg/mL was chosen based on the administered dose of a commercially available nanomedicine, Genexol, as a reference point for calculating a top concentration for assay use and limited by NP concentration (Section 2.2.4). As seen for the polymer-based NPs tested in Chapter 2, and in line with previous studies from the wider scientific community, the results of this study indicate relatively low cytotoxicity conveyed by polymeric NPs (Yu et al. 2014; Chen et al. 2016).

However, the 55K NPs did appear to significantly decrease C3A cell viability when compared with untreated cells. More specifically, cell viability was reduced to 67% at the highest concentration tested (150 µg/ml). These results could suggest that increasing PLGA chain length enhances PNP toxicity. Another potential cause of increased 55K NP toxicity could be PLGA degradation products that can lead to the formation of acids and a change in pH, potentially negatively affecting cell viability. Interestingly, when PLGA is broken down, the by-products have previously induced cytotoxicity *in vitro* (Singh & Ramarao 2013). PLGA microspheres (50–100 µm) have previously induced a cytotoxic effect and inflammatory response in mice following subcutaneous injection (Kang et al.

2007). Therefore, the higher PLGA content in the 55K NPs may be responsible for the higher toxicity, as considerably more by-product could be produced compared with the 4K and 15K NPs.

The results could also suggest that increasing PEG chain length enhances PNP cytotoxicity. The 55K NPs (PEG5K-PLGA55K), while having the longest PLGA component to the polymer chain, also had the longest PEG component compared with the 4K and 15K NPs (PEG2K-PLGA4K, PEG2K-PLGA15K). These findings could be used when designing PEG-PLGA polymeric nanoparticles for nanomedicine to optimise their safety profile.

3.4.4 Cytokine production related to 4K, 15K and 55K NPs

PNPs can stimulate inflammatory responses *in vivo* and *in vitro* (e.g. Beyerle et al. 2009; Silva et al. 2016). To investigate the cytokine response to the 5K, 15K and 55K NPs after exposure for 24 hours, the production of TNF-α, IL-6, IL-8, IL-1β and IL-ra by C3A cells was measured.

All NPs appeared to decrease IL-8 production by C3A cells. Nonetheless, while statistically significant, the decrease in cytokine production was very low (<35 pg/mL), indicating that it may not be biologically relevant. There is limited research into IL-8 production in relation to PNP exposure, however existing research suggests that cytokine production is influenced by PNP size, surface charge and cell line. When respiratory epithelial cells (A549) were exposed to cationic polystyrene NPs (57 nm), a slight reduction in IL-8 production was observed (Thach & Finkelstein 2013). However, anionic polystyrene NPs (20 nm) induced a 17.2 fold up-regulation of the expression of the IL-8 gene in the human endothelial cell line (EA.hy926) treated, while 200 nm anionic polystyrene NPs did not affect expression of this gene (Fröhlich et al. 2014).

All NPs appeared to increase the production of anti-inflammatory cytokine IL-1ra. However only the 4K NPs at 125 µg/mL induced a significant increase. This suggests that the NPs may stimulate an anti-inflammatory response.

Although IL-1ra loaded within PNPs has been used to treat diseases such as liver failure (Xiao et al. 2013), there has been limited investigation of PNP-induced IL-1ra production *in vitro* and *in vivo*. In a human study, patients with the degenerative lumbar disease were orally administered Pluronic PNPs or alginate oligosaccharide NPs (<200 nm) for one month. After this time, according to patient blood samples, IL-1ra production appeared to be unaffected by Pluronic PNPs. However, a significant increase in IL-1ra production was seen for humans exposed to alginate oligosaccharide NPs (Qu et al. 2017). Additionally, an *in vitro* study demonstrated that silica oxide NPs (<100 nm) decreased IL-1ra production in human peripheral blood mononuclear cells (PBMC), while titanium dioxide NPs (<100 nm) were seen to increase IL-1ra production in PBMCs (Mendoza et al. 2014; Høl et al. 2018).

NPs can interfere with the detection of cytokines, due to protein adsorption on to the NP surface, which decreases the protein's detectability. For example, IL-8 has been observed to adsorb on to the surface of UFCB NPs, making the protein undetectable (Brown et al. 2010). Therefore, it is prudent to assess whether polymeric NPs interfere with the assays used to quantify cytokine production. When NP interference was investigated, all NPs caused a significant decrease in IL-1ra detection. The 55K NPs decreased TNF-α and IL-6 detection, meaning that any increase in cytokine production mediated by NPs may be under-represented.

3.4.5 ROS production related to 4K, 15K and 55K NPs

For NPs such as TiO_2 and ZnO, toxicity to hepatocytes *in vitro* has been linked to their ability to stimulate oxidative stress and thus has been commonly investigated *in vitro* (e.g. Kermanizadeh et al. 2012). However, cellular ROS production stimulated by PNPs has not been widely investigated. In this study, the potential for PNPs to generate ROS was investigated with the commonly used DCFH-DA assay. All three NPs stimulated a significant ROS response by hepatocytes, with a ~ five-fold increase in ROS production compared with the control.

Interestingly, a previous study indicated adequate uptake and retention of PLGA-PEI NPs, with little effect on viability (Yu et al. 2014). This, therefore, suggests that PNPs of

similar composition to the 4K, 15K and 55K NPs are capable of inducing ROS production without high levels of cytotoxicity.

Other studies using hepatic cells, as a spheroid culture, indicated that PAMAM dendrimer NPs could stimulate the production of ROS. Interestingly, this response was not seen to change with increasing NP concentration (Chen et al. 2016). As ROS production was the same at all concentrations for 4K, 15K and 55K NPs, this suggests that low concentrations of PNPs are capable of stimulating ROS production. These results highlight the need for safety profiling of PNPs using more than cytotoxicity testing alone to indicate toxicity. Induction of ROS production could lead to undesirable downstream effects, which could be a significant hurdle for nanomedicine development if the benefits do not outweigh the gains.

There did not appear to be a difference between the levels of ROS produced by the 4K and 15K NPs, although there was a significant increase in ROS production for cells treated with 55K NPs, albeit a small increase when compared with the 4K and 15K NPs. This could suggest that ROS generation depended on the polymer chain length of the 55K NPs. The 55K NPs have a significantly larger hydrodynamic diameter compared with both the 4K and 15K NPs. However as there was little difference between the ROS produced by these NPs suggesting that this ROS assay may not be sensitive enough for these PNPs. Alternative methods for assessing the involvement of oxidative stress in the toxicity of these PNPs could be used to understand further their impact on the C3A cells, such as measuring depletion of antioxidants (e.g. GSH), evaluating antioxidant activity (e.g. catalase, superoxide dismutase (SOD)) or identifying of markers of oxidative damage (e.g. marker of lipid peroxidation, Malondialdehyde (MDA)) (Gaiser et al. 2013; Johnston et al. 2018).

3.4.6 Uptake of the 4K, 15K and 55K NPs

The internalisation of these NPs was quantified using a semi-high throughput plate-based method that allows for assessment of the uptake of a panel of NPs, at multiple concentrations over time. It was not possible to detect uptake of any of the NPs at any of

the timepoints and concentrations tested, except for the 15K NPs at 125 µg/mL after exposure for 24 hours.

Previous studies have suggested that with increasing PEG chain length, there is a proportional decrease in NP opsonisation and NP-cell interactions (Alexis et al. 2008). This could allow for longer circulation time *in vivo*. Indeed, in the past, it has been noted that when administered via intravenous injection, PLGA-PEG NPs of 140 nm with a 5K PEG component were taken up by the liver half as much as PLGA-PEG NPs of the same size with a 2.5K PEG component (Bertrand et al. 2017). The 55K NPs have a 5K PEG component to their polymer chain compared with the 4K and 15K NPs, which have a 2K PEG component. Therefore, this could explain the particularly low level of uptake seen for the 55K NPs (Bertrand et al. 2017). Other studies have shown that NPs with shorter PLGA-containing polymer chains take less time to degrade than longer polymer chains. Therefore, it is possible that the 4K NPs degraded rapidly and therefore little uptake is observed (Sharma et al. 2015).

To further investigate NP uptake, confocal images were taken. Uptake was only evaluated at 24 hours post exposure, since this was the only timepoint at which internalisation of any NPs was observed. There appears to be little to no uptake of all of the NPs by C3A cells. However, some compartmentalisation of the 15K NPs was observed in the cytoplasm surrounding the nucleus. Quenching of conjugated polymers once they are suspended in cell culture medium has been previously observed, and can occur due to protein binding directly to the conjugated polymer changing the polymer structure (Herland & Inganäs 2007).

For example, in studies using PPE-loaded polymer NPs, it has been demonstrated that fluorescence was substantially quenched in the presence of 10% serum (Khanbeigi et al. 2015). This could suggest that the 10% FBS present in the C3A cell medium may quench PPE to below detectable levels. While it would be expected that the PEG of these NPs would lower protein-NP interactions, similar decreases in fluorescence have been seen for polymer NPs composed of PEGylated PPE (Khanbeigi et al. 2015).

While PPE is located within the 'core' of the PLGA-PEG NPs, it may be possible for serum proteins to interact, depending on the density of the PEG coating and the conformation of PPE within the polymer chains which could result in areas of PPE exposure (Fredenberg et al. 2011; Xu et al. 2015; Bertrand et al. 2017). Therefore, it would be relevant to investigate the effects of serum on the NP fluorescence in the future, since if this quenching persisted when NPs were administered *in vivo*, the NPs would have limited use in bioimaging. To further understand the uptake of these NPs with relation to coating, an alternative conjugated polymer such as the bright near infrared CN-PPV (poly(2,5-di(hexyloxy) cyanoterephthalylidene) could be used since this is less susceptible to quenching (Kemal et al. 2017).

3.4.7 Genotoxicity of 4K, 15K and 55K NPs

A semi-high throughput Comet assay was used to assess NP genotoxicity.. Due to the limited volume and concentration of these NPs the number of concentrations analysed was limited to two and not the recommended minimum of three, therefore although these data is a useful indicator of NP genotoxicity results should be considered preliminary (OECD 2015). There appeared to be no significant DNA damage for C3A cells exposed to the 4K and 55K NPs. However, a low level of DNA damage was observed in cells exposed to the 15K NPs.

These results could point towards the 15K NPs having the potential to induce DNA damage in hepatic cells. Interestingly, the 15K NPs had high levels of ROS and were the only NPs observed to be taken up by C3A cells. This could indicate that these NPs may be internalised by the cells to a greater extent than the 4K and 55K NPs and therefore had more opportunity to interact either indirectly or directly with the DNA, resulting in higher levels of DNA damage. This could be due to the difference in polymer chain length between these PNPs, altering the 15K NPs corona and how it interacts with the cells (Alexis et al. 2008). Additionally, when compared to 4K NPs ,15K NPs have an increase in overall polymer chain length, this increase has previously been noted to prolong degradation time, therefore it may be possible that 15K NPs have more opportunities to interact with the cells (Alexis et al. 2008; Dinarvand et al. 2011; Conde et al. 2014; Sharma et al. 2015). Further, when you compare 15K NPs with 55K NPs, 55K NPs have

an increase in PEG chain length as well as overall polymer chain length. This increase has already been seen to increase the diameter of 55K NPs and it may also have increased the NP stability and reduce cellular uptake, therefore, reduce the potential for 55K NPs to induced genotoxicity (Gref et al. 2000; Ma et al. 2012).

Using the Comet assay, similar levels of DNA damage were seen when mononucleated TK6 (human B-lymphoblastoid) cells and human PBMCs were exposed to 75 μg/cm^2 of PLGA-PEO, a polymer extremely similar to in composition to PLGA-PEG (Kazimirova et al. 2012; Zhang et al. 2014; Tulinska et al. 2015).
It is recommended that more than one assay be used to assess genotoxicity (Doak & Dusinska 2017). In the future, it would, therefore, be useful to investigate the genotoxic potential of these NPs using the micronucleus assay or perhaps a sister chromatid exchange assay. High genotoxicity in any nanomedicine would be prohibitive for use in the clinic since NPs with genotoxic potential may lead to the formation of cancers.

3.4.8 Urea and albumin production related to 4K, 15K and 55K NPs

Quantification of urea and albumin together can be used as a specific indicator of liver function (Watts et al. 1995). Following exposure of C3A cells to 4K, 15K and 55K NPs, it became evident that there was a decrease in the level of urea, but not albumin production. In the past, PLGA-PEG NPs have been seen to interfere in fluorescent assays via quenching of the detection dye's emission (Aranda et al. 2013). The 4K and 15K NPs were observed to interfere with the urea assay, highlighting the need to assess NP assay interference in parallel with the fluorescent-based assays.

However, at the highest concentration, the 4K NPs decreased urea production to below detectable levels (unrelated to NP interference), and 55K NPs were seen to significantly reduce urea production in a concentration-dependent manner, indicating that these NPs can affect hepatic function. The concentrations of 4K NPs used were previously shown not to affect viability, and results here indicate that these NPs are capable of significantly impairing hepatic functions. These results highlight that the use of viability assays alone may not be sufficient to assess the safety of polymer nanomedicines. The results suggest

that the 55K NPs have a stronger impact on hepatic function than the 4K NPs, which could be linked to the longer polymer chain present in these NPs.

3.5 *Conclusion*

This study used a range of approaches to investigate the toxicity of polymeric NPs to hepatocytes, including cytotoxicity, cytokine production, ROS production, genotoxicity, cellular uptake and urea and albumin production (as indicators of hepatocyte function). A hepatocyte cell line was investigated in this study; however, a more extensive range of cells should be considered in future studies. In particular, macrophages within the liver, Kupffer cells, are known to accumulate NPs and can be a sensitive model for assessing NP toxicity *in vitro* (Owens & Peppas 2006; Singh & Ramarao 2013; Brown et al. 2018). Therefore, to assess likely immune response in the liver, it would be important in the future to investigate the effects of these NPs on Kupffer cells. Furthermore, it is recommended that the response of primary cells is assessed in future studies to identify if cell lines provide a good prediction of PNP toxicity.

Previous studies have shown polymer NPs to have generally low toxicity both *in vitro* and *in vivo*. However, due to a focus on PNP efficiency and not PNP safety, other studies have not investigated the array of endpoints used in this investigation, which suggests that future studies should perform a more comprehensive *in vitro* assessment of PNP toxicity. A perceived lack of information on the translatability of *in vitro* to *in vivo* results for PNP safety profiling, together with clinical, regulatory guidelines requiring *in vivo* testing has resulted in PNP testing being performed primarily using *in vivo* models. The future use of *in vitro* assays to determine the safety profile of PNPs is essential, since commercially this will yield financial and time benefits. Furthermore, *in vitro* testing has the potential to reduce the number of animals needed for testing to align nanotoxicology testing with the 3Rs principles (Burden et al. 2017).

The varying length of the polymer chains used to generate these NPs may contribute to the toxic effects observed in this study. The 4K NPs cause lower levels of toxicity, while the 55K NPs significantly reduced cell viability. However, 55K NPs did significantly reduce urea production in a concentration-dependent manner compared to 4K and 15K

NPs. An understanding of which properties confer toxicity can feed into the design of future generations of NPs, and also support legislation development. Because these NPs are intended for medical applications, it is important to also assess their efficacy in order to conduct a risk-benefit analysis.

In this study, these NPs were loaded with fluorescent polymer PPE for bioimaging. Additional therapeutics could also be loaded for use in clinical applications. The nature of the cargo may influence NPs toxicity, and further assessment may be required. The usefulness of these NPs in a clinical setting may be promising, with relatively low levels of cytotoxicity and low levels of uptake by hepatocytes, meaning that if they were modified to target specific cells, there might be little accumulation in the liver, prolonging circulation time and increasing chances of NP-target cell interactions.

However, some of these results highlighted that there is still a need for a greater understanding of the toxicity of these PNPs with decreases in urea production suggesting there may be an adverse effect on hepatocyte cell health, although this would need to be investigated further *in vivo*. It is also evident that safety testing of PNPs should not just rely on cytotoxicity testing but should be performed using a broader panel of indicators of toxicity. This generates a greater understanding of the mechanism of action for PNP toxicity to inform future testing strategies to assess PNP toxicity and could be used in the future design of PNPs for clinical use. Toxicity testing in this study did point to longer polymer chain lengths being more toxic, the findings from the additional endpoints complemented these results, increasing confidence in these findings.

The observed results from this study could aid in the development of an in vitro testing strategy as highlighted in Figure 1.3. Identifying endpoints that will provide the most impactful information could both reduce the amount and time needed for safety testing of these polymer nanomedicines, meaning that they are available as safe and effective medical tools sooner.

With regards the developing a testing strategy the reduced number of cytotoxic assays provided adequate conclusions on PNP safety. Additionally, decreasing the timepoints of

confocal imaging, while using the semi high through put fluorescent plate method allowed for similar understanding of the impact of PNP uptake on safety. The most informative cytokine that provided a clear indication of PNP safety was IL-8 suggesting that initial cytokine screening with IL-8 could be performed before progressing to investigation of additional cytokines. Again, genotoxicity provided the most insight on potential safety concerns regarding the safety of these PNPs, although due to limited supply of PNPs it was not possible to perform additional concentrations or timepoints, these would still provide valuable safety information in a testing strategy. Unfortunate ROS measurement using DCFH-DA was not able to provide sufficient information regarding the oxidative impact of these PNPs, therefore additional endpoints may be required such as GSH. Although, albumin did not appear to provide information regarding the impact of these PNPs on liver cell health, measurement of urea did, however for this endpoint to be utilised with in a testing strategy a greater understanding of the impact of NPs on urea production would be required.

Chapter 4. *In vitro* assessment of the influence of a redox-reactive coating on copolymer NP safety using C3A hepatocytes

4.1 Introduction

4.1.1 Designing safe novel redox reactive PNPs for nanomedicine

The low solubility, instability and non-targeted nature of many therapies such as cancer-related drugs like Paclitaxel, has been a hurdle to their clinical application (Wiernik et al. 1986; Guo et al. 2011; Li et al. 2014). However, the opportunity to design PNPs with multiple functionalities can help overcome these challenges. One approach is to generate PNPs with elements that can allow controllable drug release in response to one or several intracellular or extracellular stimuli such as temperature, pH, light or redox potential (Han et al. 2015; Constantin et al. 2017; Yeh et al. 2018).

Previous research has shown that GSH levels within the cytosol and intracellular compartments such as the mitochondria and nucleus of cells can be higher in cancer cells than in normal cells (Griffith & Meister 1985; Lee et al. 1989; Gilbert 1990; Yao et al. 1995). This can be exploited in the clinic as NPs can be designed to release their cargo when there is a change in redox potential once inside the cell (Russo et al. 1986; Navath et al. 2009). Redox reactive NPs can respond to a change in redox potential and could be a promising new delivery agent for cancer therapies as they could provide effective targeting to cancer cells.

To date, redox reactive NPs have been assessed for their ability to deliver cancer drugs and genes using predominantly polymer and liposomal-based NPs (Kirpotin et al. 1996; Zalipsky et al. 1999; Petros et al. 2008; Takae et al. 2008). Redox reactive elements in the NPs, such as disulphide linkers, can be cleaved by GSH and allows for the targeted and controlled release of the cargo within cells (Holmgren 1979; Wang et al. 2011). The inclusion of disulphide linkers in NP delivery devices has been utilised in the development of FDA approved drugs such as Gemtuzumab ozogamicin, used in the treatment of myeloid lymphoma (Niculescu-Duvaz 2000; Hamann et al. 2002).

In this study, PLGA-PEG NPs were generated with (RR-NPs) and without (nRR-NP) a novel redox-responsive disulphide linker at an ethanoate ester between the PLGA core and PEG shell (Figure 4.1). Cleavage of the redox reactive disulphide linkers via

intracellular or extracellular thiols, such as GSH, is likely to stimulate the release of the PEG shell from the PLGA core, potentially resulting in a reduction in size or an increase in PNP agglomeration due to a decrease in NP stable and steric repulsion that were derived from the PEG coating (Lee et al. 1989; Yao et al. 1995; Gref et al. 2000; Tobío et al. 2000; Sun & Davis 2010). Additionally, cleavage of the disulphide linker at the ethanoate ester in PLGA generates new nucleophilic end groups that can increase the rate of PLGA degradation via hydrolysis, increasing the rate of RR-NP degradation, thereby promoting cargo release (Avgoustakis et al. 2002; Fomby & Cherlin 2011; Souza et al. 2015).

These relatively new PNPs with coatings/shells (e.g. PEG) that can be removed selectivley have great promise as targeted delivery agent. Using these complex polymer nanomedicines, it was possible to compare the toxicity of PNPs with a cleavable coated and PNPs without this element, allowing for the assessment the influence of cleavable coated polymer based nanomedicines on overall PNP toxicity.

The PNPs used in this study were loaded with the green fluorescent hydrophobic dye DiO (3,3'-dioctadecyloxacarbocyanine perchlorate) to mimic drug loading and allow for visualisation of NP uptake by cells. DiO together with DiL (1,1′- dioctadecyl-3,3,3′,3′-tetramethyl indocarbocyanine perchlorate) are widely used lipophilic tracers and share a similar structure (Muñoz-Barroso et al. 1998). DiL has been shown to have a low impact on viability, suggesting DiO would have similar low toxicity (Haldar & Uyetake 1992).

4.1.2 The effect of redox reactive elements on PNP safety

Redox-responsive PNPs have been observed to enhance cargo release in cancer cells in previous studies. For example, using respiratory epithelial cells (A549), disulphide linker containing poly(ε-caprolactone)-SS-poly(ethyl ethylene phosphate) NPs loaded with the chemotherapeutic doxorubicin, have been shown to be cleaved at the disulphide linker following internalisation, leading to NP disassembly and cargo release intracellularly (Tang et al. 2009). Additionally, polylysine PNPs containing a disulphide linker, used for gene delivery has demonstrated increased intracellular release and internalisation of DNA cargo in human liver cells (HuH7) in comparison to NPs lacking this disulphide linker.

In Human hepatocyte cells (QGY-7703), disulphide linker cleavage followed by NP dissociation was only seen intracellularly within endosomes/lysosomes for multi-layered redox active nanocomplexes used to deliver doxorubicin and siRNA, with no NP dissociation observed extracellularly (Han et al. 2015).

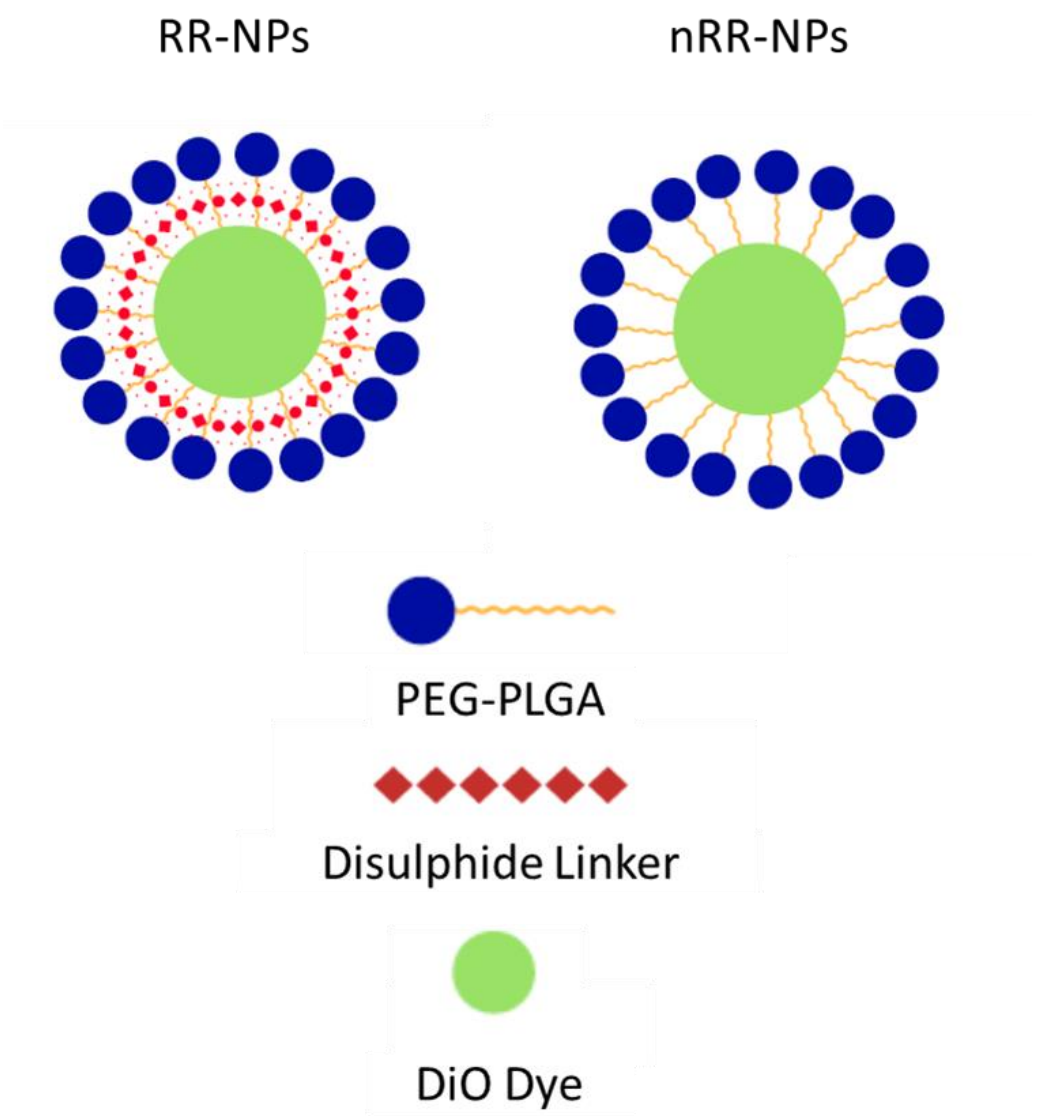

Figure 4.1 Scheme of RR-NPs and nRR-NPs.

Representation of the RR and nRR NPs used in this study. PNPs are made of the polymer PEG-PLGA, PEG (blue), PLGA (orange), disulphide linker (red), and fluorescent DiO dye (green).

Redox-responsive NPs can be targeted and increase drug delivery to cancer cells (Lee et al. 1989; Yao et al. 1995). For example, previous studies have used redox-responsive poly (oligo-L-arginine) PNPs for gene delivery to reduce atherosclerotic inflammation, in which endothelium α-2 adrenoceptors promoted targeted delivery following intravenous administration to mice (Ain et al. 2017). Other studies have used disulphide linker specific degradation (dithiothreitol) in biodegradable redox-responsive methoxy PEG-poly (lactic acid) PNPs to increase curcumin dye release by 3 times compared to non-redox-responsive NPs (Cao et al. 2015). This could indicate that these redox-responsive NPs have the potential to increase drug delivery. Interestingly, higher cellular uptake was observed for redox-responsive methoxy PEG-poly (lactic acid) PNPs *in vitro* following exposure of cervical cells (HeLa) for 24 hours (Cao et al. 2015).

4.1.3 Study aim and hypothesis

This study aimed to investigate the effects of the introduction of a redox-responsive disulphide linker on PNP toxicity via assessment of cytotoxicity, uptake, cytokine production, ROS production, genotoxicity, urea and albumin production as well as increases in intracellular calcium concentration.

It was hypothesised that:

1. RR-NPs and nRR-NPs, at pharmacologically relevant concentrations would stimulate minimal cytotoxicity in C3A hepatocyte cells.
2. RR-NPs and nRR-NPs would be internalised by C3A hepatocyte cells
    a. With less uptake observed for nRR-NPs.
3. RR-NPs and nRR-NPs would stimulate ROS production and activate a pro-inflammatory response in C3A hepatocyte cells.
4. RR-NPs and nRR-NPs at pharmacologically relevant concentrations would stimulate minimal genotoxicity in C3A hepatocyte cells.
5. RR-NPs and nRR-NPs would be capable of reducing albumin and urea production in C3A hepatocyte cells.
    a. With less of an impact observed for nRR-NPs.

6. RR-NPs and nRR-NPs would be capable of increase in intracellular calcium concentration in C3A hepatocyte cells.
    a. With less of an impact observed for nRR-NPs.

For all responses, it is hypothesised that RR-NPs would be less toxic than nRR-NPs due to the presence of the disulphide linker that would allow RR-NPs to degrade more readily once internalised within the cell, decreasing the potential NP-cell interactions and therefore potentially decreasing NP-specific toxicity to the cells. These NPS produced via multiple batches had short stability, low volume and low NP concentration, this resulted in limited concentrations used for some particularly endpoints that require higher volumes such as uptake via confocal imaging and genotoxicity.

4.2 Materials and methods

4.2.1 Nanoparticle synthesis

A non-redox active PLGA-PEG block copolymer (Figure 4.1 A) and a redox reactive PLGA-ss-PEG block copolymer were synthesised (Figure 4.1 B) by collaborators (Prof Cameron Alexander and Dr Claudia Conte) at the University of Nottingham.

NPs were loaded with DiO, a green fluorescent dye, using a double emulsion solvent evaporation method. Briefly, copolymer PLGA-PEG (10 mg) and DiO (0.1 mg) were dissolved in methylene chloride (1 mL), then probe sonicated (Sonicator 3000, Misonix) for 1 minute in a glass vial. Water (10 mL) containing 0.5% polyvinyl alcohol was then added and the suspension was probe sonicated for 3 minutes. To aid in solvent evaporation, the suspension was stirred without a lid for four hours at RT. The suspensions were then filtered through a membrane syringe filter (pore size: 450 nm) (Millipore) and centrifuged (17,000×g, 30 minutes, 4°C) to separate the free dye and surfactant from the suspension. To remove polyvinyl alcohol from the NP suspension, NPs were washed twice with sterile water. Finally, NPs were resuspended in sterile water (1 mL) and stored at 4°C and used within one month of preparation. Loading and entrapment efficiency was similar for both redox reactive and non-redox reactive NPs (Conte et al. 2018). For use in experiments, NPs were freshly diluted in cell culture medium and briefly vortexed.

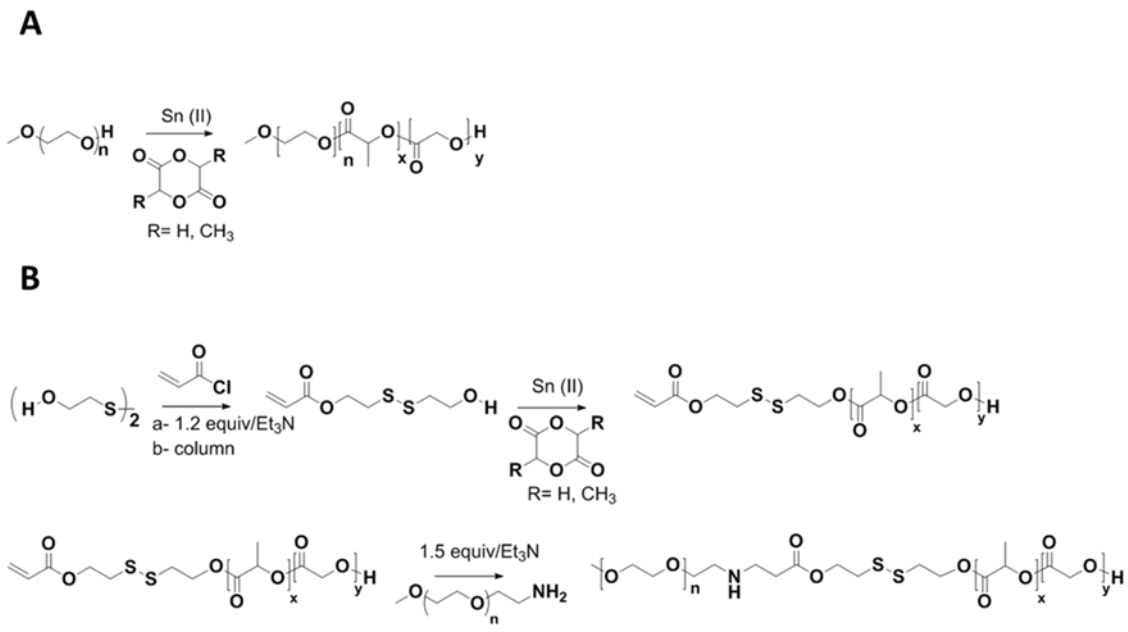

Figure 4.2 PLGA-PEG and PLGA-ss-PEG PNP polymer synthesis.

Chemical structure and polymer synthesis scheme of the non- redox active block copolymer, PLGA-PEG (A) and the redox active block copolymer, PLGA-ss-PEG (B) (Provided by Dr C. Conte).

4.2.2 Nanoparticle characterisation

Nanoparticles were characterised by DLS as described in section 2.2.2. TEM was performed by Dr Conte.

4.2.3 Cell culture

Human C3A hepatocellular carcinoma cell maintenance and seeding as described in section 2.2.3.

4.2.4 Cytotoxicity Assays: AB and NR

A 96-well plate fluorescent-based assay which simultaneously assessed the viability of C3A cells following exposure to NPs using AB and NR uptake assays was applied. The method was performed as described in section 2.2.5. NP interference with the AB assay was performed as in Section 2.2.5 with NPs prepared at concentrations of (5, 10, 25, 50, 100, 250 μg/mL). Inference results were only reported when positive.

4.2.5 Uptake Assay: Plate.

A 96 well-plate fluorescence-based uptake assay was used to quantify the uptake of fluorescently loaded NPs by C3A cells as described in section 2.2.7. Fluorescence was measured at Ex/Em 488/526 nm. NPs were prepared in cell lysate to produce a standard curve, ranging from 5-250 μg/mL

4.2.6 Uptake Assay: Confocal Microscopy.

Confocal microscopy was used to visualise NP uptake by C3A cells. A single time point (1440 minutes) was selected, based on the findings from the plate-based method (section 4.2.5). Cells were seeded onto 12 mm uncoated glass coverslips in 24-well plates at a concentration of 6.58 $x10^4$ cells/cm^2 and incubated at 37°C and 5% CO_2. Following 24 hours growth cells were exposed to a sub-lethal concentration of nanoparticles (125 μg/mL; as determined during cytotoxicity assays) or Compete Medium (control) for 1440

minutes at 37°C and 5% CO_2.

Cells were prepared for imaging as described in section 2.2.6. with DAPI staining omitted. Slides were stored at 4˚C until imaged using A Leica SP5 SMD gated-STED confocal laser scanning microscope and Leica Application Suite program.

4.2.7 Genotoxicity assessment: Comet assay

A Trevigen 24-well Comet Chip assay kit was used to assess oxidative DNA damage as described in section 3.2.9. NP concentrations of 125 and 250 µg/mL were used, as determined by the cytotoxicity assays.

4.2.8 Genotoxicity assessment: Micronucleus assay

The micronuclei assay is one of the most common genotoxicity assays, micronuclei formed by chromosomal fragmentation or chromosomal loss during nuclear division are used as markers for chromosomal damage (Heddle 1973). The cytokinesis-block micronucleus assay uses actin inhibitor (cytochalasin-B) during mitosis to produce a population of once-divided nuclei (binucleated cells), this increases accuracy as it counteracts changes in the rate of cell division that may occur due to genotoxic compound exposure (Umegaki & Fenech 2000; Fenech 2000). This assay has been utilised in previous studies when assessing the genotoxicity of PNPs (Kazimirova et al. 2012).

A 24-well based Micronucleus assay was used to assess DNA damage. C3A cells were seeded at a concentration of 1.56 x10^5 cells/cm^2 into 24-well plates and incubated at 37°C and 5% CO_2. Following 24 hours growth C3A cells were washed twice with PBS (Sigma-Aldrich) then exposed to nanoparticles (125 µg/mL) or Complete Medium (control) in duplicate for 24h at 37°C and 5% CO_2. Due to the limited volume and concentration of these NPs, analyse of one concentration was priorities, not the recommended three concentrations (OECD 2015). Although these data can be a useful indicator of NP genotoxicity, results should be considered preliminary.

Cells were washed twice with PBS and exposed to a cytokinesis blocker Cytochalasin B

(6 µg/mL, in Complete Medium) (Sigma-Aldrich) for 36 hours (Kirsch-Volders & Fenech 2001). Subsequently, the supernatant was discarded, the cells were washed twice with PBS and trypsinised (section 4.2.2). Following this, cells were centrifuged at 2000 g for 1 minute and washed another 2 times with PBS and resuspended in ice-cold PBS (0.5 mL). Cells were then added (100 µL) to a Cytospin (Shandon) and spun at 1500 g for 5 minutes. Slides were air-dried and fixed for 10 minutes in ice-cold 90% methanol.

Cells were stained with 20% Giemsa stain (VWR) for 6 minutes then washed twice with PBS. Following air drying for 4-5 hours, slides were dipped in Xylene (Sigma-Aldrich) for 10 seconds, allowed to dry and SlowFade Diamond Antifade mounting medium containing DAPI (ThermoFisher) was used to mount the coverslips onto glass slides. Binucleated cells were confirmed in the bright field, and the DAPI filter used to image micronuclei (Zeiss AX10 with Allied Vision Technologies Stingray camera). A total of 1000 binucleated cells were analysed, for each treatment. Data are expressed % micronucleus mean ± SEM.

4.2.9 Measurement of urea production

The QuantiChrom Urea assay kit (BioAssay Systems) was used as described in section 3.2.10 to establish urea production by C3A cells at sub-lethal NP concentrations of 62.5, 125 and 250 µg/mL.

To determine the potential for NPs interference with this assays the NPs at 250 µg/mL were spiked with the SCM for the urea standards. Results were reported only when inference was observed.

4.2.10 Measurement of albumin production

Bromocresol Green (Sigma Aldrich) was used as described in section 3.2.11 to establish albumin production in C3A cells at sub-lethal NP concentrations 62.5, 125 and 250 µg/mL as well as Complete Medium (negative control).

To determine the potential for NPs interference with this assays the NPs at 250 µg/mL

were spiked with the SCM for the albumin standards. Results were reported only when inference was observed.

4.2.11 Measurement of intracellular ROS production

ROS production by C3A cells was determined as described in section 3.2.6 at sub-lethal NP concentrations of 62.5, 125 and 250 µg/mL as well as Complete Medium (negative control).

4.2.12 Measurement of cytokine production

Secretion of IL-8, TNF-α, IL-6, IL-1ra and IL-1β from C3A cells exposed to NPs was measured using a multiplex sandwich ELISA as in section 3.2.5, at sub-lethal NP concentrations (62.5, 125 and 250 µg/mL) as well as Complete Medium (negative control). Additionally, interference of NPs with this assay was established by adding the SCM concentration to 250 µg/mL NPs prepared in the same medium as the standard curve and quantifying the concentration of cytokine via an ELISA.

4.2.13 Measurement of intracellular calcium

A 96 well-plate fluorescence-based assay was used to determine changes in intracellular calcium concentration following exposure of C3A cells to NPs. Fura-2-AM is a widely used radiometric dye to measure intracellular calcium. Once this dye penetrates the cell, esterases cleave the dye so it can no longer leave the cell. When Fura-2-AM is not bound to calcium, the Ex/Em is 380/510 nm. When Fura-2-AM is bound to calcium, the Ex/Em is 340/510 nm (Grynkiewicz et al. 1985).

C3A cells were seeded at a concentration of 1.56 $x10^5$ cells/cm^2 into 96-well well black plate with an optic bottom (Nunc) and incubated at 37°C and 5% CO_2. Following 24 hours growth, cells were washed twice with PBS.

The Fura-2 working solution was prepared; 5 µL of Fura-2-AM (1 mM in dimethyl sulfoxide (DMSO)) (Sigma Aldrich); 5 µL of 1M Probenecid (in sodium hydroxide) to

reduce dye leakage from the cells (Sigma Aldrich); 1 µL 20% Pluronic F127 (in DMSO) (Sigma Aldrich) to help disperse Fura-2-AM, and 5 mL Serum free MEM medium (Gibco, Invitrogen) containing 10 mM HEPES (Sigma Aldrich). The dye-free working solution was prepared as above without Fura-2-AM to allow for observation of NP interference. When interference was observed results were presented, if no interference present results will not be presented.

Cells were loaded with either the Fura-2 working solution (100 µL) or dye free working solution for 1 hour at 37°C and 5% CO_2. The cells were then washed once with HEPES containing FBS free Complete Medium. Basal fluorescence was measured with a SpectraMax M5 Microplate Reader at Ex/Em 340/510 nm and 380/510 nm, before adding 100 µL of NPs at a sub-lethal concentration (125 µg/mL prepared in Complete Medium), UFCB-Printex-90, 5 µg/mL prepared in Complete Medium or Complete Medium (Control) in triplicate. Fluorescence intensity was measured every 120 seconds for 36 minutes. Data are expressed as mean Ratio 340/380 ± SEM.

4.2.14 Statistical analysis

Experimental data were analysed using GraphPad Prism software. One-way ANOVA using Tukey post-test or two-way ANOVA followed by the Bonferroni post-test were used to test for statistical significance. Significance was set at $p < 0.05$. All experiments were repeated 3 times on different days unless otherwise stated.

4.3 Results

4.3.1 RR-NPs and nRR-NPs: Physiochemical characterisation

Immediately following preparation in PFR Complete Medium, and 24 hours post incubation at 37°C, 5% CO_2 both nRR-NPs and RR-NPs were of comparable size, with a hydrodynamic diameter of approx. ~60 nm (Figure 4.3A). The PDI values were relatively high (0.6-0.7) for both NP types at both time points (Figure 4.3B). The zeta potential of these NPs were slightly negative, ranging from -5 to -8 mV at both time points (Figure 4.3C). The zeta potential of RR-NPs after 24 hours is significantly more negative ($p<0.05$), indicates a change in surface charge over time.

TEM images of the nRR-NPs and RR-NPs (prepared in PBS) are presented in Figure 4.4 and were provided by Dr Conte. TEM images of RR-NPs appear to indicate 2 populations of NPs; one of ~ 50 nm in size with a low density indicated by lighter colour, and another of NPs that were ~ 100 nm in diameter, with higher density indicated by a darker colour. The nRR-NPs appear to be consistent in density, although there is some variation in size evident with NPs ranging from ~ 50 nm to 150 nm.

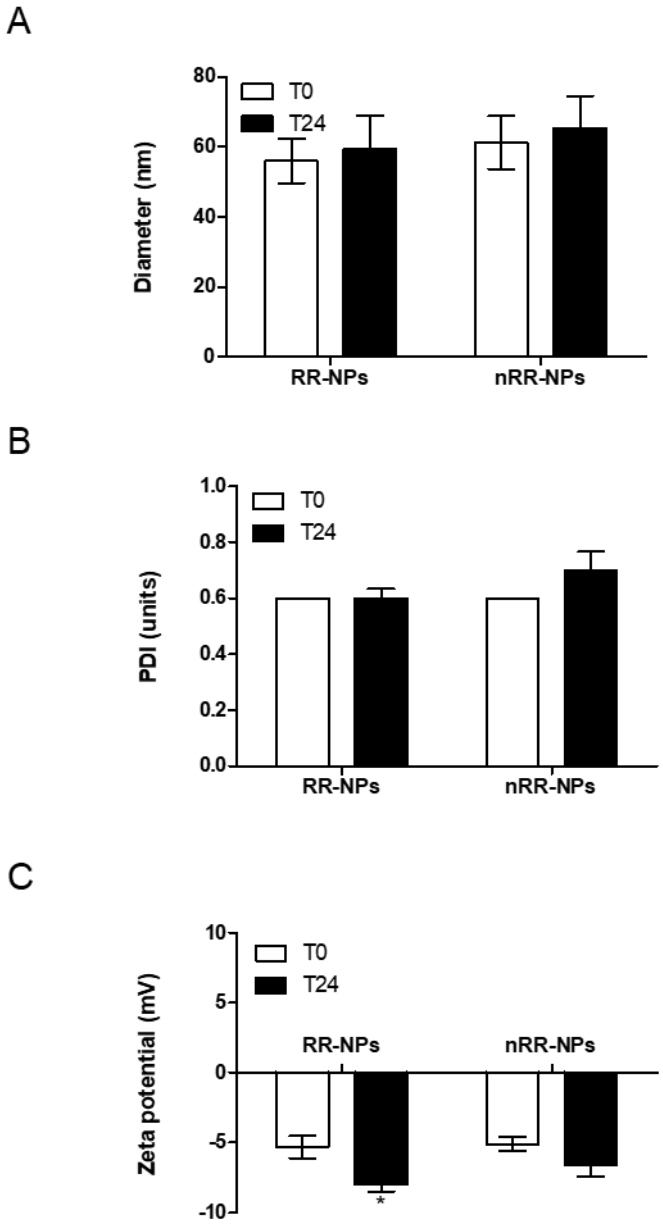

Figure 4.3 Characterisation of RR-NPs and nRR-NPs properties using DLS.
NPs (RR-NPs and nRR-NPs) were suspended in PFR Complete Medium (125 µg/mL). Hydrodynamic diameter (A), PDI (B) and zeta potential (C) assessed at 0 hours (T0) and 24 hours (T24) post incubation at 37°C, 5% CO_2. Data are expressed as mean ± SEM (n=3). Significant indicated by *= $p < 0.05$ when comparing T0 and T24.

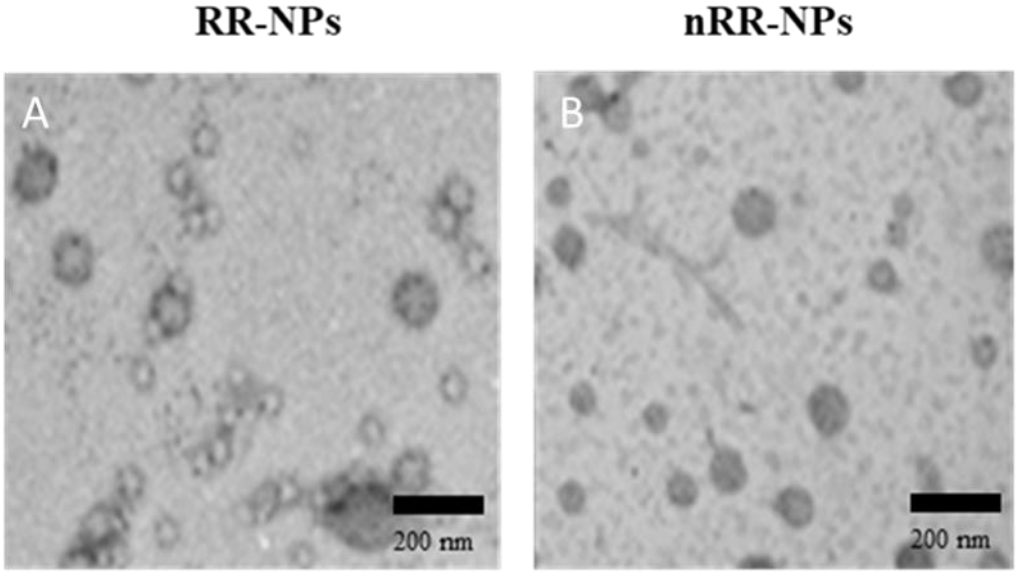

Figure 4.4 TEM characterisation of RR-NPs and nRR-NPs.

Images of RR-NPs (A) and nRR-NPs (B), suspended in PBS at 500 µg/mL. Representative images (n=3), Scale bar, represents 200 nm, presented and provided by Dr Conte.

4.3.2 RR-NPs and nRR-NPs: Cytotoxicity

To investigate the impact of RR-NPs and nRR-NPs on C3A cell viability, two fluorescent based assays were performed; the AB and NR assays (Figure 4.4). The CFDA-AM assay was found to be incompatible with these NPs. AB assay showed no significant reduction in viability for cells exposed to both RR-NPs and nRR-NPs when compared with the control, at all concentrations tested (Figure 4.4A). The NR assay showed no significant effects for either nRR-NPs or RR-NPs on cell viability (Figure 4.4B). An EC_{20}, the concentration where NP exposure leads to 20% cell death, could not be calculated for these NPs for either assay, suggesting that the NPs had relatively low cytotoxicity.

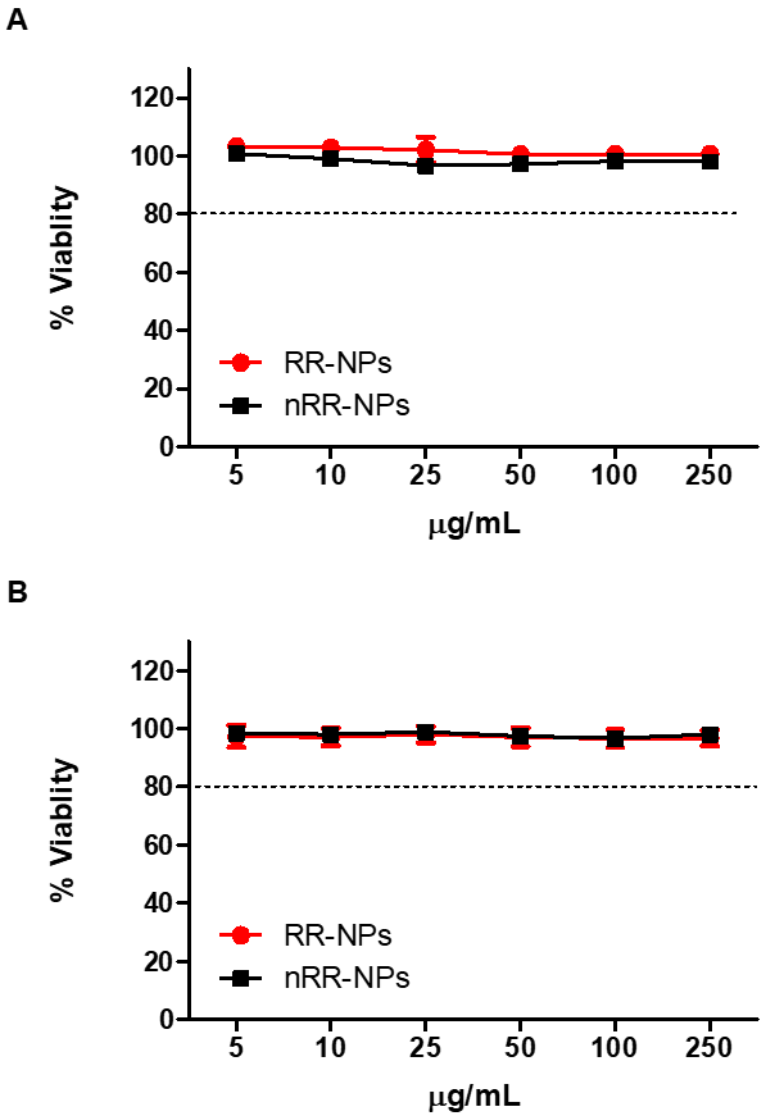

Figure 4.5 Cytotoxicity of RR-NPs and nRR-NPs to C3A cells.

Cells were exposed to RR-NPs (red) or nRR-NPs (black) at 5-250 µg/mL for 24 hours. Viability was measured via the AB (A) and NR (B) assays. Data are expressed as mean % viability (i.e. % of untreated control) ± SEM (n=3).

4.3.3 RR-NPs and nRR-NPs: Uptake

To quantify the internalisation of the nRR-NPs and RR-NPs by C3A cells, a plate-based method was used to quantify uptake over time (10, 60 and 1440 minutes), at a range of NP concentrations (5-250 µg/mL). There was a significant concentration and time-dependent increase ($p<0.001$) in NP internalisation for both RR and nRR-NPs (Figure 4.6). The highest level of uptake (~3.5 µg/mL retained) was observed for both NPs at a concentration of 250 µg/mL, following exposure for 1440 minutes. The uptake of RR-NPs was significantly higher ($p< 0.001$) than that of nRR-NPs.

Based on results from the plate-based method for evaluating uptake and observations made for other PNPs (sections 2.4.2 and 3.3.5), NP uptake was imaged using confocal microscopy at one-time point (1440 minutes) and a concentration of 125 µg/mL. Both NPs were internalised by C3A cells (Figure 4.7). However, uptake appears to be relatively low for both NPs, RR-NPs did appear to have marginally higher internalisation (Figure 4.7A). The NPs within the cells appear to be compartmentalised, potentially within organelles such as endosomes, lysosomes or mitochondria. There does not appear to be any NPs located on the surface or between the cells. Additionally, there appears to be no colocalization of these NPs with the tubulin cytoskeleton.

NP within the interior of the cell were confirmed in the xy-yz micrographs generated from z-stacks (Figure 4.8). Although there is no nuclear stain used, the nucleus was located using transillumination (denoted as N in Figure 4.7 and 4.8), and it can be observed that there is an absence of NP localisation within the nucleus of these cells.

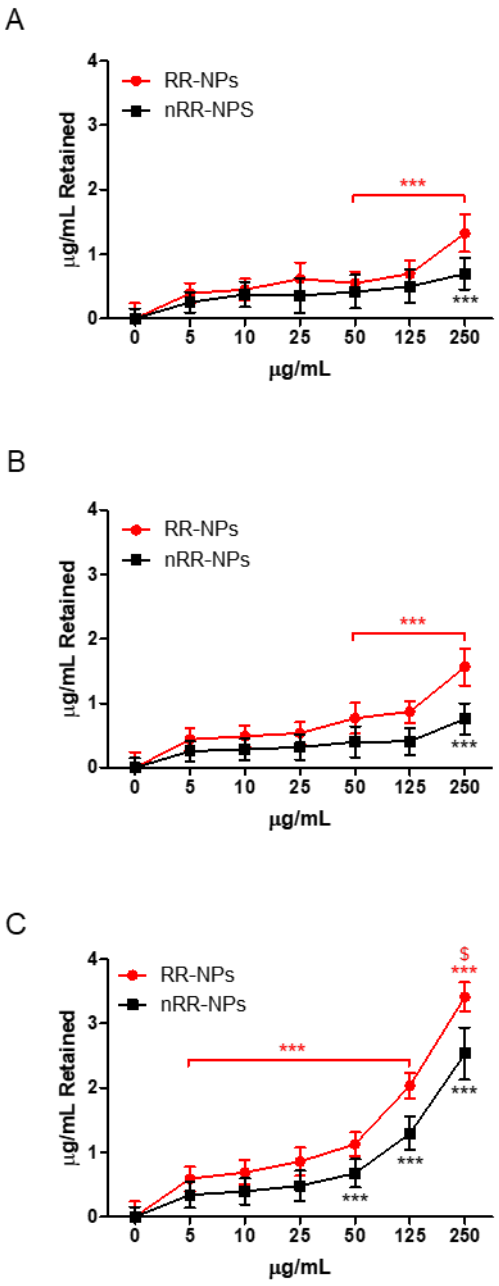

Figure 4.6 Uptake of RR-NPs and nRR-NPs by C3A cells, over time: Plate method.

Cells were exposed to RR-NPs (red) or nRR-NPs (black) for 10 (A), 60 (B) or 1440 (C) minutes, at 5-250 µg/mL. Data are expressed as mean µg/mL retained in cells (from appropriate standard curves) (n=3). Significance indicated by ***= $p < 0.001$ compared with control. Significance indicated by $ = $p < 0.05$ for RR-NPs compared with nRR-NPs at the same concentration and timepoint.

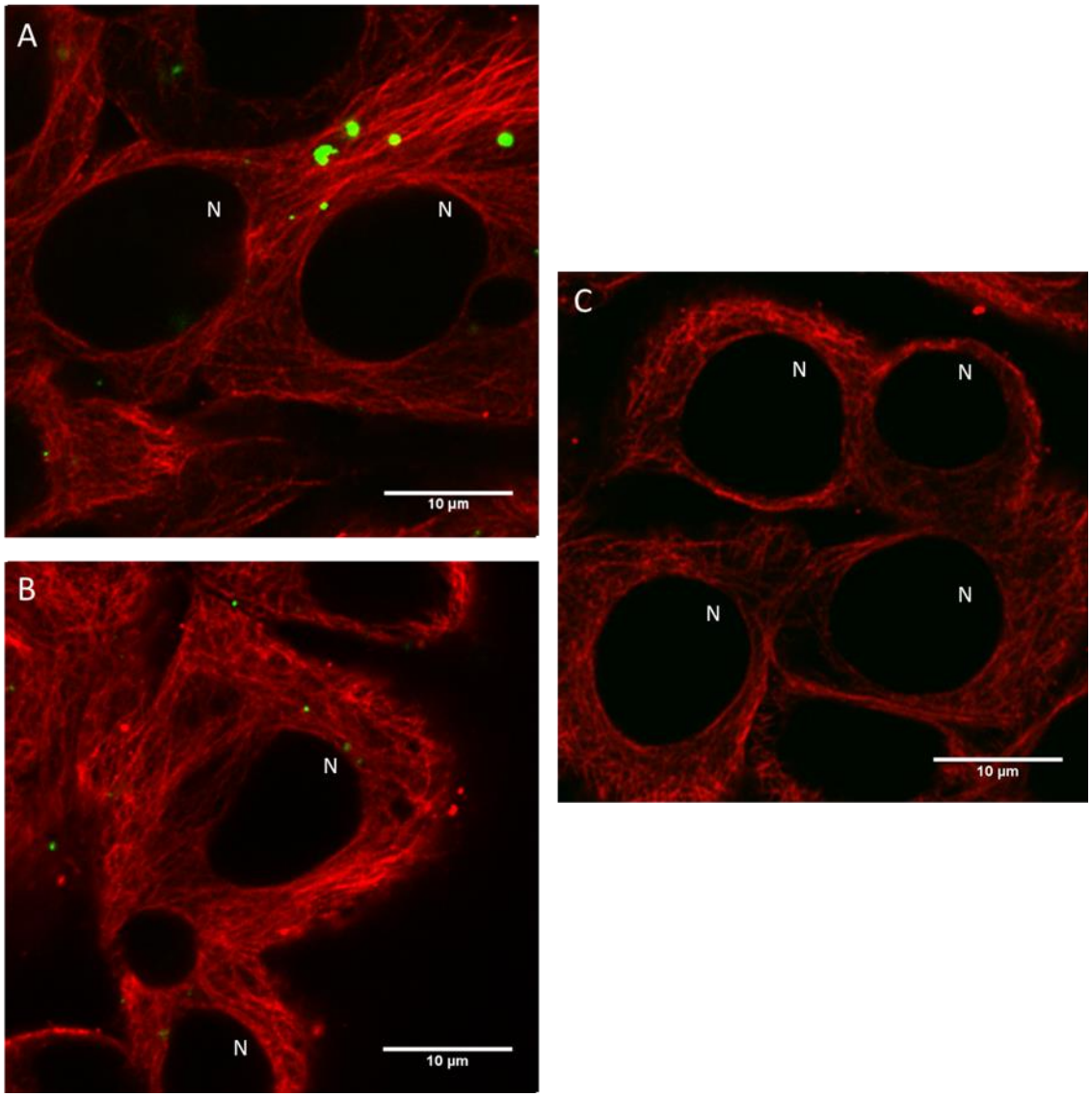

Figure 4.7 Uptake of RR-NPs and nRR-NPs by C3A cells.

Cells were treated with 125 µg/mL of RR-NPs (A), nRR-NPs (B) (green) or Complete Medium (C) for 1440 minutes. Representative images (n=3). Tubulin (red) and N indicates the location of the nucleus, scale bar =10 µm.

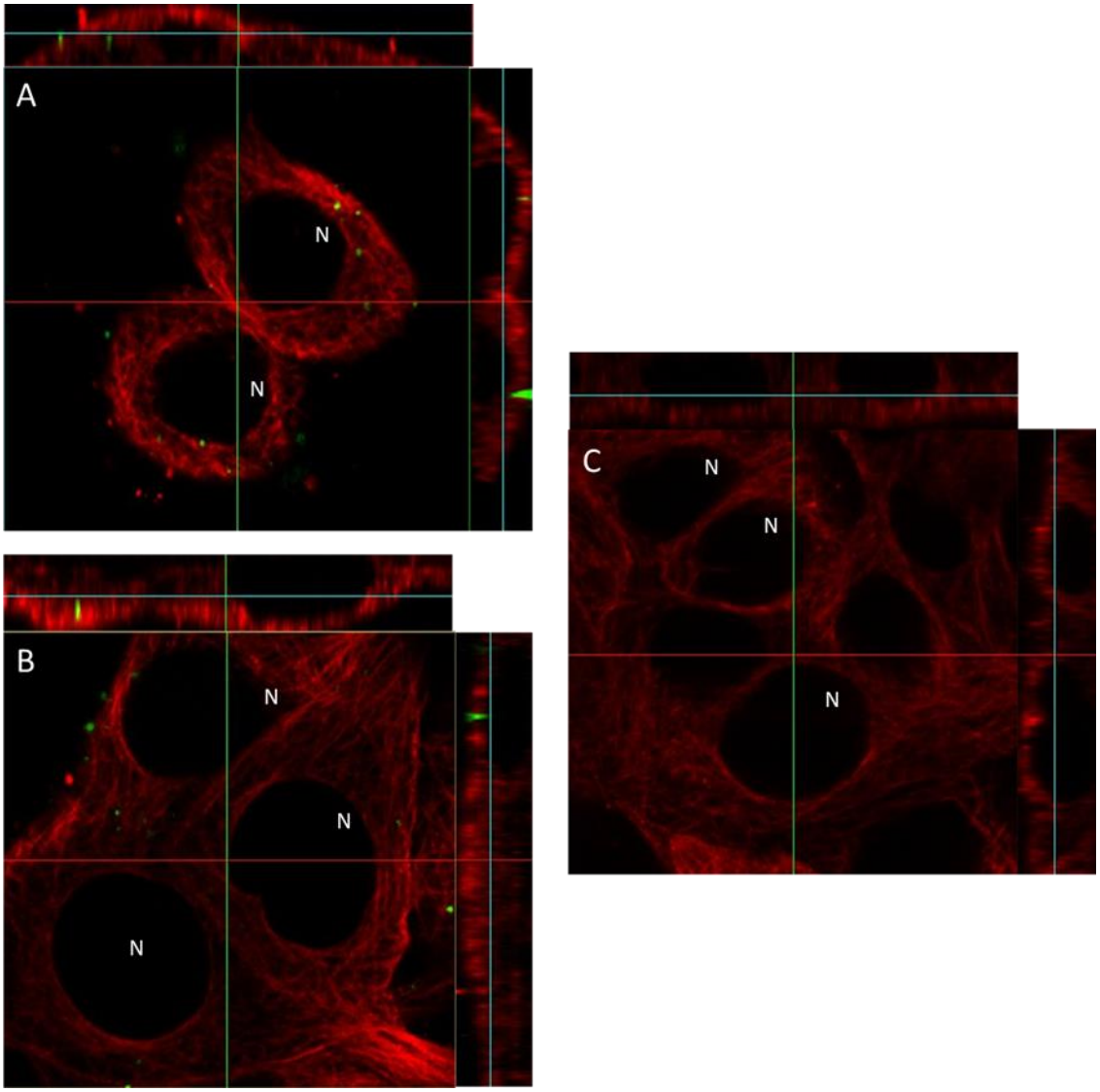

Figure 4.8 Uptake of RR and nRR-NPs by C3A cells: Z stacks.

Cells were treated with 125 µg/mL of RR-NPs (A), nRR-NPs (B) (green) or Complete Medium (C) for 1440 minutes, and xy and yz micrographs generated from z stacks. Representative images (n=3). Tubulin (red) and N indicates the location of the nucleus, scale bar =10 µm.

4.3.4 RR-NPs and nRR-NPs: Genotoxicity

The Comet assay was used to assess whether RR-NPs and nRR-NPs (125 µg/mL and 250 µg/mL for 24 hours) caused DNA damage in C3A cells. The potential contribution of oxidative stress was assessed by conducting the assay in the presence and absence of Fpg. The RR-NPs did not induce DNA damage, at either concentration tested, in the presence and absence of Fpg (Figure 4.8A). The nRR- NPs induced a significant increase ($p< 0.001$) in DNA damage in the presence of Fpg, with 25 and 27% DNA observed in the tail at concentrations of 125 and 250 µg/mL respectively, this was significantly higher ($p< 0.001$) than RR-NPs (Figure 4.8B). No DNA damage was observed following exposure of cells to nRR-NPs in the absence of Fpg. The positive control H_2O_2 stimulated a significant increase ($p< 0.001$) in DNA damage (~45-55% in the tail) in the presence and absence of Fpg. The Fpg treated samples had significantly higher ($p< 0.001$) DNA damage than H_2O_2 samples not treated with Fpg.

In this study, the micronucleus assay was also used to assess the genotoxicity of RR-NPs and nRR-NPs (125µg/mL for 24 hours) to C3A cells. Binucleated cells were confirmed using a light microscope to observe the Giemsa staining and formation of micronuclei, nuclear budding and nucleoplasm bridges observed. As seen previously in the Comet Assay, the RR-NPs do not appear to induce significant DNA damage (Figure 4.10A). However, the nRR-NPs induced a very low but significant increase ($p< 0.05$) in the % of micronuclei observed in binucleated cells (Figure 4.10B and C). There was no significant difference in nuclear budding or nucleoplasm bridge formation seen in cells treated with either RR-NPs or nRR-NPs.

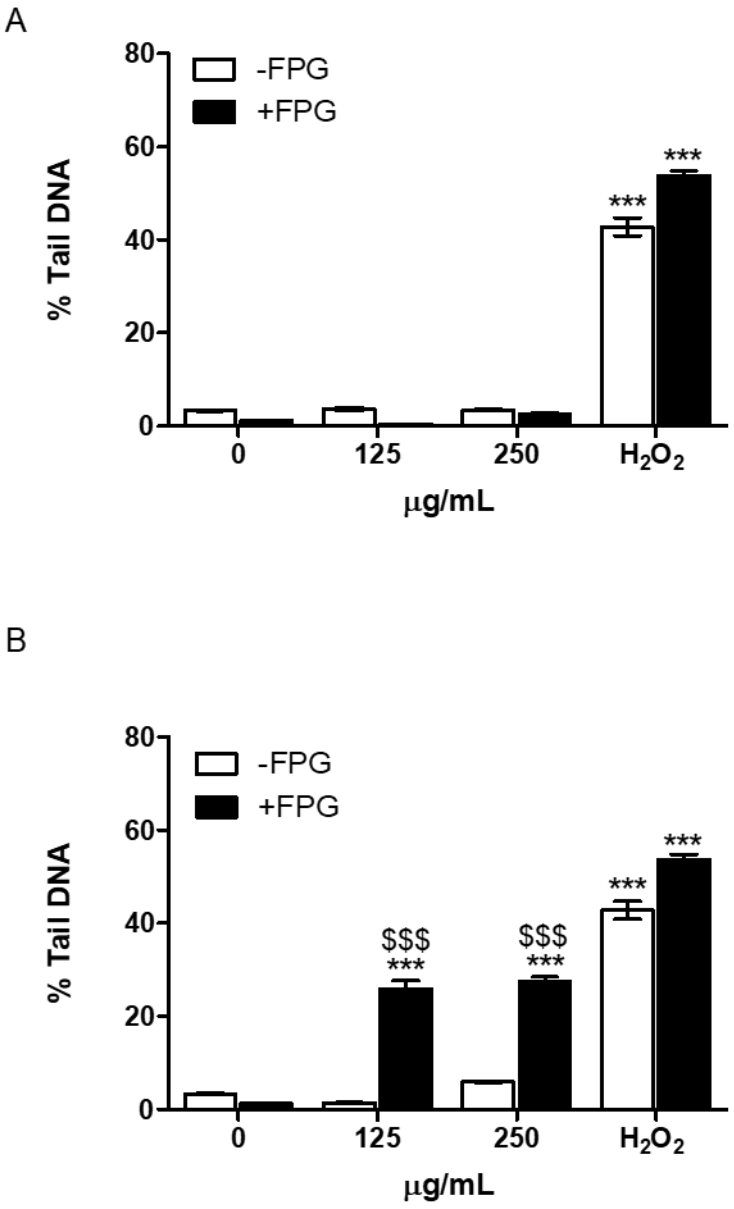

Figure 4.9 Genotoxicity of RR and nRR-NPs in C3A cells: Comet assay.

C3A cells were exposed to RR-NPs (A) or nRR-NPs (B) at 125 and 250 µg/mL for 1440 minutes, 60 µM H_2O_2 and Complete Medium ± Fpg. Data are expressed as mean %Tail DNA ± SEM (n=3). Significance indicated by *** = $p < 0.001$ compared with control. Significance indicated by $$$ = $p < 0.001$ for nRR-NPs compared to RR-NPs at the same concentration with Fpg.

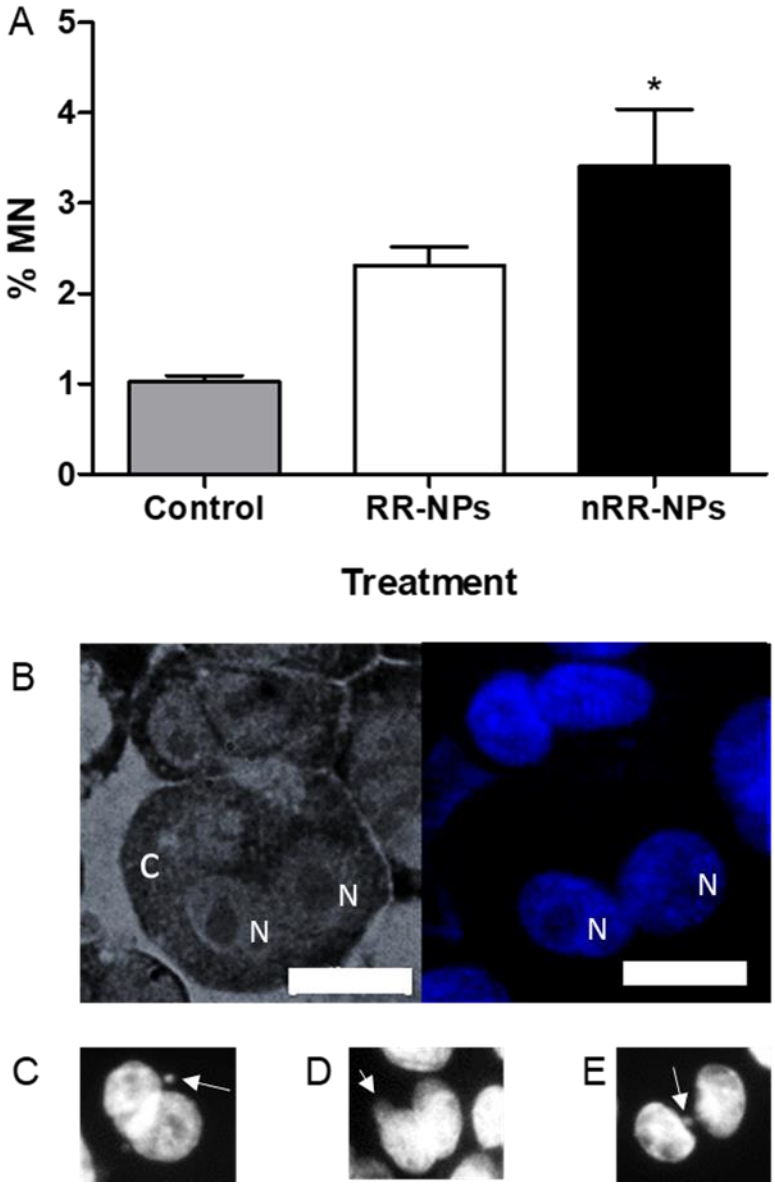

Figure 4.10 Genotoxicity of RR and nRR-NPs in C3A cells: Micronucleus assay. Cells were exposed to RR-NPs or nRR-NPs at 125 µg/mL, and Complete Medium (control), for 1440 minutes (A). Data are expressed as mean % MN ± SEM (n=3). Significance indicated by *= $p < 0.05$ when compared with untreated control. Representative images (n=3) of binucleated cells (B) (C= cytoplasm, N= nucleus), micronuclei (highlighted by arrow) (C), blebbing (D) and a nucleoplasm bridge (E). Scale bar represents 10 µm.

4.3.5 RR-NPs and nRR-NPs: Cytokine and ROS production

For both NPs, there was no significant production of IL-8, TNF-α, IL-1β and IL-6 by C3A cells. However, there was a significant increase ($p<0.01$) in the production of the anti-inflammatory cytokine IL-1ra (Figure 4.11B) at all concentrations for nRR-NPs ($p<0.01$) and at concentrations of 125 and 250 µg/mL for RR-NPs ($p<0.05$). Interference of RR-NPs and nRR-NPs with detection of cytokines was observed with an underestimation of IL-1ra by 15 and 8% respectively (Figure 4.11A).

C3A cells were exposed to RR-NPs and nRR-NPs at concentrations of 62.5, 125 and 250 µg/mL for 24 hours and intracellular ROS production assessed using the DCFH-DA assay. There was a significant increase ($p<0.001$) in ROS production seen for both RR-NPs and nRR-NPs at all concentrations, with a ~5-fold increase in fluorescence compared to the control (Figure 4.12A and B). The positive control UFCB (10 µg/mL) caused a significant increase in ROS production by cells (Figure 4.12C).

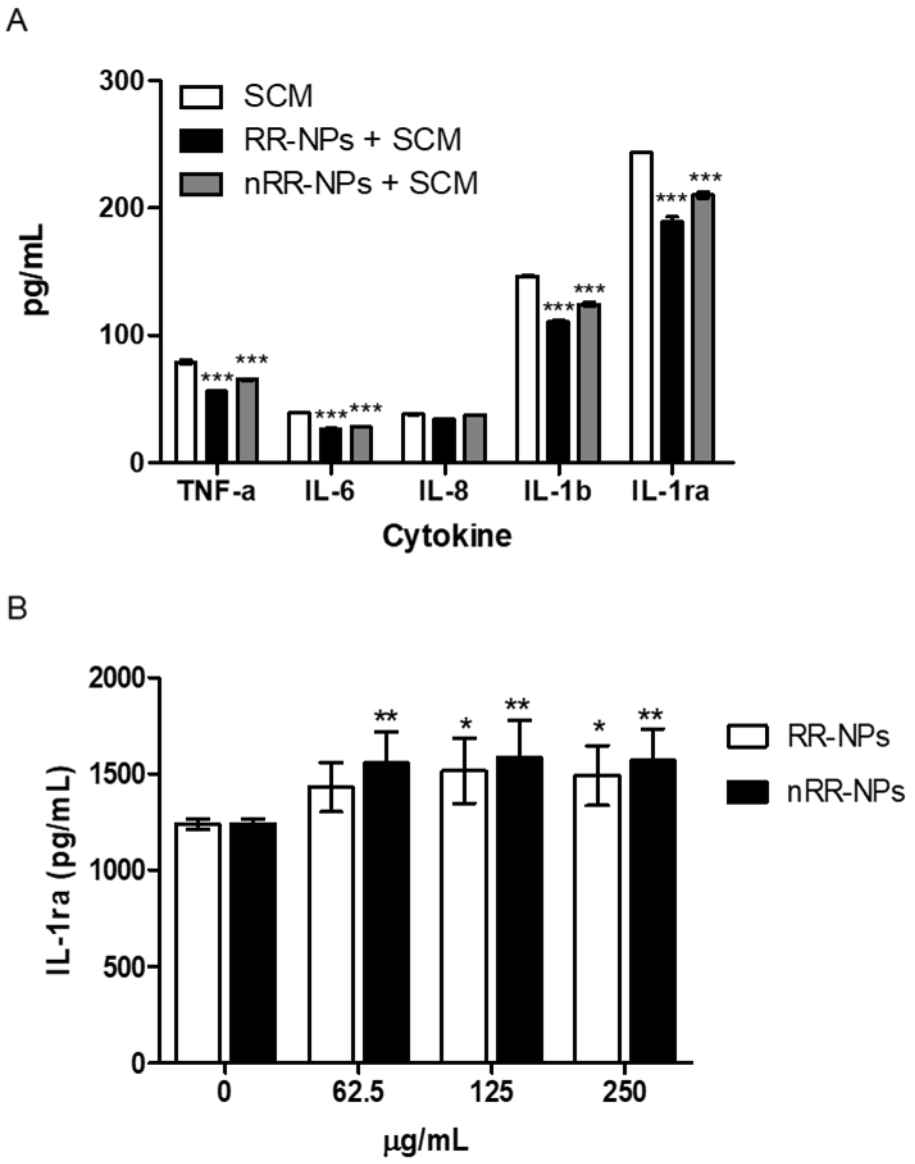

Figure 4.11 Optimisation of cytokine detection and IL-1ra production induced by RR-NPs and nRR-NPs in C3A cells.

The SCM concentration of each cytokine was incubated with RR-NPs or nRR-NPs (250 µg/mL), prepared in Complete Medium to observe interference of cytokine detection related to NPs (A). Cells were exposed to RR-NPs and nRR-NPs (62.5, 125 and 250 µg/mL) for 24 hours, IL-1ra(B). Data are expressed as mean (pg/mL) ± SEM (n=3). Significance indicated by ***= $p < 0.001$ when compared to SCM (A). Significance indicated by *= $p < 0.05$ and **= $p < 0.005$ when compared to untreated control (B).

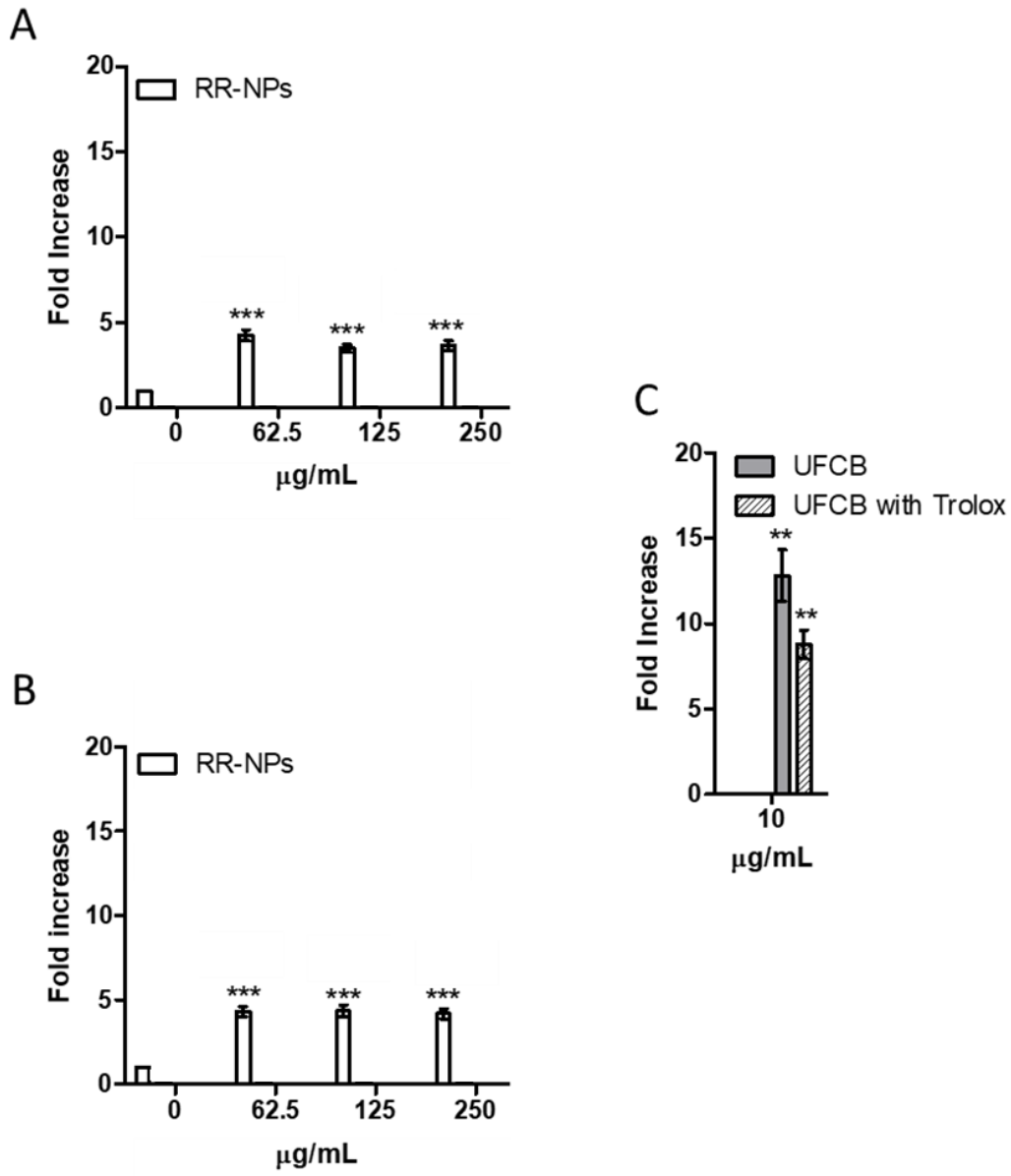

Figure 4.12 ROS production by RR-NPs and nRR-NPs in C3A cells: DCFH-DA assay.

Cells were exposed to RR-NPs (A) or nRR-NPs (B) at 62.5, 125 and 250 µg/mL or UFCB (10 µg/mL) for 24 hours. Data are expressed as fold increase in fluorescence (from the untreated control) ± SEM (n=3). Significance indicated by ***= $p < 0.001$ and **= $p < 0.005$ compared with untreated control.

4.3.6 RR-NPs and nRR-NPs: Urea and albumin production

Two essential hepatocyte functions; urea and albumin production were investigated following the exposure of C3A cells to NPs. Cells were treated with RR-NPs and nRR-NPs for 24 hours at three sub-lethal concentrations (62.5, 125 and 250 µg/mL).

Urea production was significantly reduced ($p < 0.005$-0.001) after exposure of cells to nRR-NPs, at all concentrations (Figure 4.13A). RR-NPs only decreased urea production at a concentration of 250 µg/mL. Similarly, albumin production was significantly reduced by cells exposed to nRR-NPs at concentrations of 125 and 250 µg/mL (Figure 4.13B). The RR-NPs were seen to reduce albumin production only at a concentration of 62.5 µg/mL.

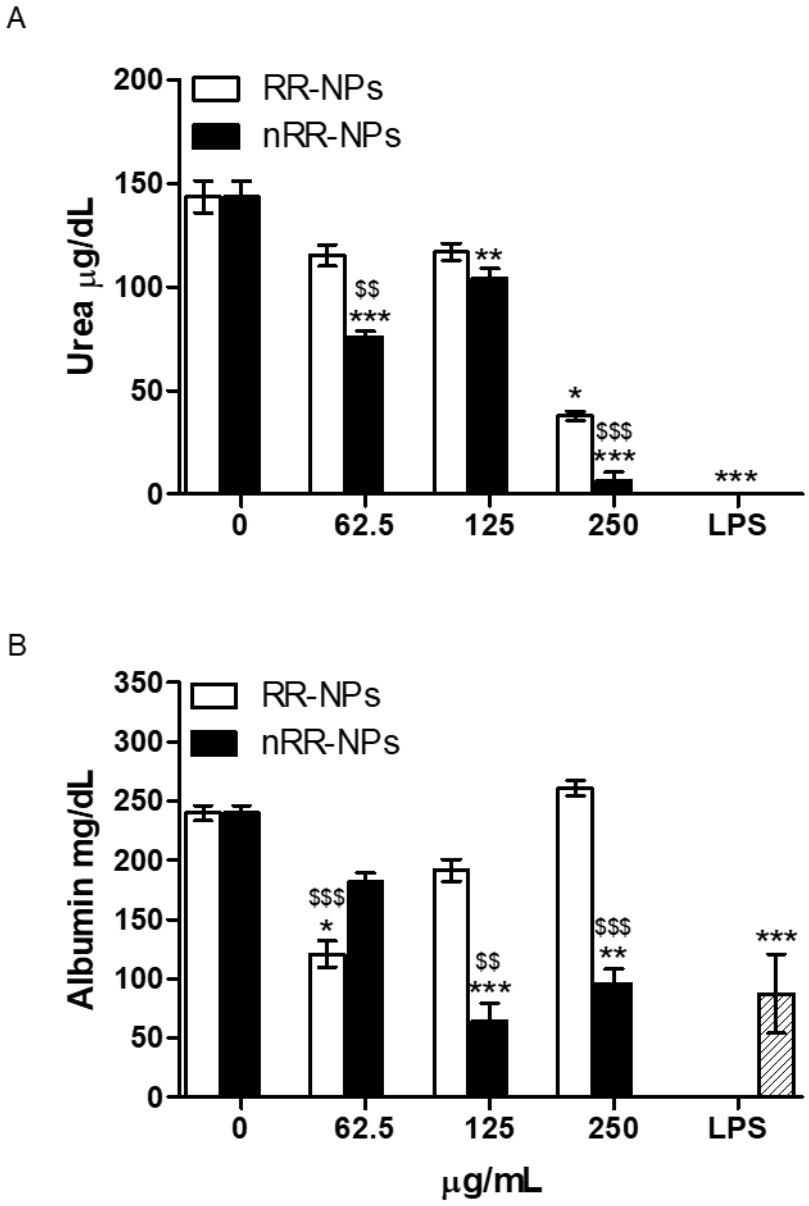

Figure 4.13. Urea and albumin production following exposure of C3A cells to RR-NPs and nRR-NPs.

Cells were exposed to RR-NPs and nRR-NPs at 62.5, 125 and 250 µg/mL for 24 hours and urea (A) and albumin (B). Data for urea expressed as mean µg/dL ± SEM(n=3). Data for albumin expressed as mean mg/dL ± SEM (n=3). Significance indicated by ***= p< 0.001, **= p< 0.005, *= p< 0.05 treatments compared with the untreated control. Significance indicated by $$$ = p< 0.001 when comparing nRR-NPs to RR-NPs at the same concentration.

4.3.7 RR-NPs and nRR-NPs: Intracellular calcium concentration

Fura-2 is a ratiometric dye that shifts excitation wavelength from 340 nm to 380 nm when bound with calcium, allowing accurate quantification of increases in $[Ca^{2+}]_i$ (Grynkiewicz et al. 1985). Fura-2 was used to monitor increases in $[Ca^{2+}]_i$ following exposure of C3A cells to RR-NPs and nRR-NPs at a concentration of 125 µg/mL for 30 minutes. UFCB (5 µg/mL) was included as a positive control.

The RR-NPs treatment resulted in significantly higher ($p < 0.001$) $[Ca^{2+}]_i$ compared to nRR-NPs and untreated control at 2-36 minutes (Figure 4.14). The nRR-NPs only significantly increased ($p<0.05$) $[Ca^{2+}]_i$ at 4 and 8 minutes. The UFCB treatment resulted in significantly higher $[Ca^{2+}]_i$ at 2-36 minutes, compared to the untreated control (Figure 4.14).

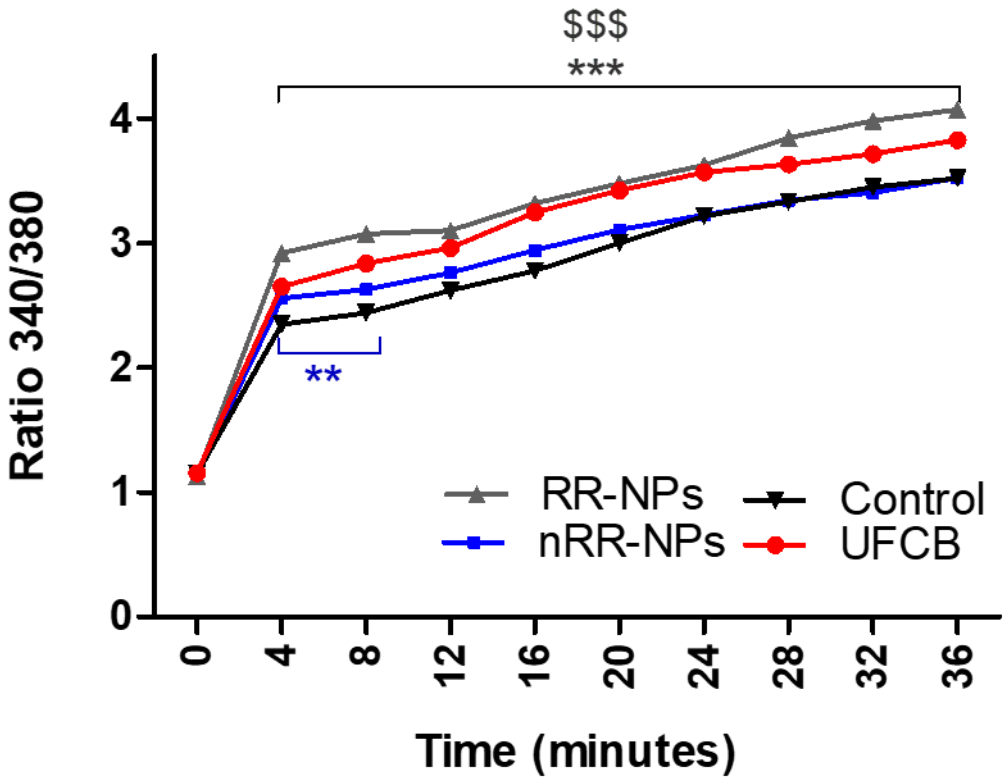

Figure 4.14 Intracellular calcium following exposure of C3A cells to RR-NPs and nRR-NPs.

Cells were exposed to RR-NPs, nRR-NPs (125 µg/mL), UFCB (5 µg/mL) or Complete Medium (control) for 36 minutes. Fura-2 was used to quantify increase in intracellular calcium concentration $[Ca^{2+}]_i$. Data are expressed as mean Ratio 340/380 ± SEM (n=3). Significance indicated by ***= p< 0.001 and **= p< 0.005 compared with the untreated control. Significance indicated by $$$= p< 0.001 compared with the nRR-NPs treatment.

4.4 Discussion

4.4.1 Overview of results

Before assessing the impact of the RR-NPs and the nRR-NPs on C3A cells, the physiochemical properties of the NPs such as size, morphology and surface charge were determined. Results indicated that RR-NPs and nRR-NPs were spherical, ~60 nm in diameter and had a slightly negative surface charge of ~ (-6) mV.

Following this, cytotoxicity was assessed, and it was observed that after 24 hours of exposure to RR-NPs and the nRR-NPs, there was no reduction in C3A cell viability observed. Next, NP uptake by C3A cells was assessed, and a concentration and time-dependent increase in NP internalisation as seen for both NPs. RR-NPs were internalised by cells to a greater extent than nRR-NPs.

To further investigate the safety of these NPs, genotoxicity was assessed, and results indicated that nRR-NPs induced greater DNA damage than RR-NPs, which was predominantly mediated by an oxidant mechanism. Furthermore, both NPs stimulated an increase in intracellular ROS production, although there was little difference between NPs. There was no increase in cytokine production for C3A cells exposed to both NPs, with the exception of IL-1ra, observed to be significantly increase compared to control when cells exposed to either NP.

Both NPs stimulated a decrease in urea and albumin production (markers of hepatocyte function), with the greatest effect observed for nRR-NPs. Finally, $[Ca^{2+}]_i$ was seen to increase for both NPs, with RR-NPs inducing a higher response than nRR-NPs.

Taken together these findings demonstrated that RR-NPs were less toxic than nRR-NPs. By performing a range of tests, a more detailed understanding of the *in vitro* toxicity of these NPs could be established and an insight into their mechanism of toxicity was obtained.

4.4.2 Characterisation of nRR-NPs and RR-NPs

The hydrodynamic diameter of RR-NPs and nRR-NPs were assessed immediately after preparation in cell culture medium and 24 hours post incubation at 37°C. The hydrodynamic diameter remained unchanged at both time points at ~60 nm, which suggests that both NPs are relatively stable up to 24 hours in cell culture conditions. TEM images confirmed that the NPs were spherical. The nRR-NPs were monodispersed, whereas RR-NPs appeared to have two different sized populations with some agglomerates present. Therefore it is possible that RR-NPs may have lost some of the PEG coating from the PLGA core resulting in a reduction in size or an increase in NP agglomeration, due to a lack of the steric repulsive forces of the PEG coating (Gref et al. 2000).

In the future to investigate PEG dissociation from these NPs, size exclusion chromatography could be used to differentiate between NPs with and without PEG via molecular mass (Spek et al. 2015). Imaging of PNPs using TEM can be difficult due to the harsh preparation methods, and the low density of the PNPs producing lower contrast images than those obtained for other NPs such as silver (Renz et al. 2016). Due to a less invasive preparation method, cryogenic scanning electron microscopy may be a suitable imaging alternative, with the added benefit of imaging hydrated NPs (Win & Feng 2005).

The relatively high PDI values for both NPs also suggests that the NPs are not monodispersed. Uniform and monodisperse NP suspensions are essential for nanomedicines to ensure accurate drug dosing (Venkataraman et al. 2011). Therefore, the synthesis of RR-NPs may require additional optimisation before they can be used in a clinical setting.

The zeta potentials of RR and nRR- NPs were slightly negative. After 24 hours incubation at 37°C, RR-NPs ween observed to become more negatively charged. However, this change was small and was therefore unlikely to have a biological effect. Previous studies have shown that PEGylated PLGA NPs have a less negative zeta potential than non PEGylated NPs, perhaps the more negative zeta potential observed for RR-NPs may be due to partial loss of PEG from the NP PLGA core (Li et al. 2001; Pamujula et al. 2012).

As collaborators were interested in targeting tumour cells, a degradation study was performed by the University of Nottingham in a biological medium that reflected the tumour microenvironment. Tumour cells can have elevated intracellular and extracellular GSH concentration compared to healthy cells (Lee et al. 1989; Edward et al. 1990; Yao et al. 1995; Sun & Davis 2010). Therefore, NPs were suspended in media containing GSH 10 mM, for 24 hours, to reflect the tumour microenvironment. Using TEM, it was evident that there was aggregation/disassembly of RR-NPS as NP shape and size had changed compared to nRR-NPs. This physical change of RR-NPs was most likely due to the cleavage of the disulphide linker between PLGA and PEG, which in turn reduced the stability of the RR-NPs.

This selective NP degradation would be clinically beneficial as it would ensure that NPs are targeted to tumour cells, and it could reduce the adverse effects of extended NP persistence within the body. In the future it could be useful to further characterise the size, shape and zeta potential of the NPs after incubation in media at a range of GSH concentrations, to provide more insight into how these NPs interact with different cells.

4.4.3 Cytotoxicity of nRR-NPs and RR-NPs

The viability of cells exposed to RR-NPs and nRR-NPs was assessed using the AB assay and the NR assay. The NR assay was performed in addition to the robust AB assay as when preliminary imaging was performed it appeared that NPs may be contained in organelles such as lysosomes and NR assay was had the potential for additional insight. Both assays gave similar results for both NPs, with less than 10% reduction in cell viability observed at all concentrations tested, 24 hours post exposure.

These results would suggest that RR-NPs and nRR-NPs have little effect on C3A cell viability. These results are similar to other studies, showing relatively low cytotoxicity of polymer-based NPs such as NPs generated from thermo-responsive and biocompatible polymer, Poly(N-vinylcaprolactam) (Vihola et al. 2005; Chronopoulou et al. 2013).

Cytotoxicity of RR-NPs and nRR-NPs was assessed at one-time point (24 hours) with a single NP exposure. Therefore, in the future to reflect the repeated administration of nanomedicines *in vivo*, it would be useful to assess toxicity following repeated exposures over a wider range of time points *in vitro*.

4.4.4 Uptake of nRR-NPs and RR-NPs

To investigate the internalisation of RR-NPs and nRR-NPs by C3A cells, a semi-high throughput plate-based method was used to quantify uptake, and confocal microscopy was used to visualise uptake. Both methods demonstrated that the uptake for both NPs was low and that uptake of RR-NPs was higher than that of nRR-NPs.

C3A cells are derived from carcinoma cells, that has the potential for higher intracellular and extracellular GSH compared to other non-hepatocyte cell lines (Lee et al. 1989; Yao et al. 1995; Sun & Davis 2010). Additionally, C3A cells are hepatocytes, which *in vivo* are responsible for synthesising the majority of newly circulating GSH (Griffith & Meister 1985; García-Ruiz et al. 1992). Therefore GSH levels outside C3A cells may be high enough to cleave the disulphide linkers in RR-NPs, thus removing the PEG from the PGLA NP core (Edward et al. 1990; Sun & Davis 2010). This may allow NPs to agglomerate or increase NP-cell interactions and uptake, due to increased NP hydrophobicity that has been shown to increase NP opsonisation (Gref et al. 2000; Ruge et al. 2012; Nocito et al. 2015; Pelaz et al. 2015). It may therefore be of interest in the future to perform a Rose Bengal adsorption assay that characterises the surface hydrophobicity of the NPs by observing changes in absorption in NP/ Rose Bengal solution (Muller et al. 1997; Doktorovova et al. 2012).

In the future, it would be useful to evaluate the total free GSH in the media of C3A cells over time in the presence and absence of the NPs. This could establish the contribution of extracellular GSH to increased RR-NP uptake as well as allow characterisation of NP properties such as size and zeta potential in the presence of GSH at a suitable concentration.

The pattern and level of NP uptake were in line with those published by our collaborator, where greater uptake was seen for RR-NPs than for nRR-NPs in alveolar epithelial cells (A549), although levels appear to be much lower in C3A cells (Conte et al. 2018).

Other studies have seen similarly low levels of uptake such as fluorescein-loaded PLGA NPs into human breast epithelial cells (MCF-10A neoT) alone or in coculture with Caco-2 cells (colon epithelial) 24 hours post exposure. (Kocbek et al. 2007). Moreover, polyester (PEG-polycaprolactone-poly(dimethylamino ethyl methacrylate) NPs with a hydrophobic core, much like the hydrophobic DiO dye loaded RR-NPs and nRR-NPs, observed similar uptake to RR-NPs and nRR-NPs, in hepatocyte cells (HepG2) (Han et al. 2015).

To further investigate the uptake of these NPs by C3A cells, confocal microscopy was used. A single time point, 24 hours, was selected to visualise NP uptake. This time point was selected as the plate-based method indicated the highest uptake of RR-NPs and nRR-NPs at 24 hours. The uptake of both NPs appears low, although RR-NPs appear to be taken up more readily than nRR-NPs. Although confocal microscopy has a resolution of approx. 250 nm. Therefore, it may not have been possible to visualise some of the NPs. Both NPs were compartmentalised, potentially in organelles such as the endosomes or lysosomes.

To gain greater insight into how the presence of the disulphide linker in RR-NPs effects the intracellular fate of these NPs, colocalisation with organelles such as the lysosome could be investigated using live confocal microscopy. The lysosome has been a prime candidate organelle for cleavage of disulphide linkers following internalisation due to the presence of gamma-interferon-inducible lysosomal thiol reductase (Phan et al. 2000; Arunachalam et al. 2000). Therefore, lysosomal labelling with the fluorescent LysoTracker dye could be used to investigate NP-lysosomal colocalization. As endosomes are another potential location of disulphide linker cleavage, NP localisation to the endosome could be established using a fluorescent label such as a fluorescent transferrin-conjugate or an endosome marker eg EEA-1 (Dautry-Varsat et al. 1983; Falcone et al. 2006; Firdessa et al. 2014).

Of benefit is that the findings from the plate-based method and confocal microscopy agreed. The plate-based method allows a semi high throughput screening of NPs uptake and can enable quantification of NP internalisation. However, it cannot provide information on intracellular localisation. This suggests that it was beneficial to use a combination of approaches when investigating NP-cell interactions.

4.4.5 Genotoxicity of nRR-NPs and RR-NPs

The Comet assay is commonly used to assess NP genotoxicity *in vitro*. Nonetheless, it can have a high level of variance (as reviewed by Rojas et al. 1999; Lee et al. 2004; Evans et al. 2017). To improve confidence in findings, use of more than one method to assess the genetic damage caused by NPs is desirable. In this study, the comet assay and MN assays were used to assess genotoxicity stimulated by RR-NPs and nRR-NPs. Different assays measure different endpoints; the comet assay measures transient DNA strand breaks and the MN assesses chromosomal damage. The combination of the two assays could allow for a more reliable indication of the genotoxic potential of NPs (Heddle 1973; Cook & Brazell 1976; Magdolenova et al. 2012). Due to the limited volume and concentration of these NPs, analyse of one concentration was priorities, not the recommended three concentrations (OECD 2015). Although these data can be a useful indicator of NP genotoxicity, results should be considered preliminary.

The RR-NPs did not stimulate DNA damage in C3A cells. However, nRR-NPs stimulated DNA damage, in both assays. The DNA damage observed appears to be mediated by an oxidative mechanism due to the higher level of DNA damage evident when using the lesion-specific repair Fpg enzyme in the Comet assay (Collins et al. 1996).

Prior studies using the sister chromatid exchange assay indicated that PLGA-PEG NPs with a similar composition to nRR-NPs, induced genotoxicity *in vitro* using Chinese hamster ovary cells (He et al. 2009). Additionally, *in vitro* studies using the Comet assay showed that PLGA-PEO NPs (PEO differs from PEG only in molecular weight) was genotoxic to primary rat hepatocytes as well as Kupffer cells (Cowie et al. 2015). Moreover, mononucleated TK6 (human B-lymphoblastoid) cells exposed to PLGA-PEO NPs have been seen to stimulate micronuclei formation, suggesting a potential to damage

DNA (Kazimirova et al. 2012). In contrast, there have been studies that show a lack of genotoxicity by PLGA NPs. For example, Setyawati et al. 2013 demonstrated that NP-mediated genotoxicity *in vitro* was dependent on cell type and NP surface coating such as PEG (Setyawati et al. 2013).

Therefore, it appears that nRR-NPs have the potential to cause mutations or genetic damage in the C3A cell line in not repaired. Moreover, the addition of a disulphide linker appears to reduce the potential of these NPs to cause genetic damage making them more attractive as a candidate nanomedicine. However, this finding would have to be further investigated in other cell types, and *in vivo*.

4.4.6 Cytokine production by RR-NPs and nRR-NPs

Assessment of cytokine production is commonly used to investigate the inflammatory response stimulated by NPs *in vitro* (Stone et al. 2009). The cytokines IL-8, IL-6, TNF-α, IL-1β and of IL-1ra were selected based on data from existing studies which have investigated cytokine production by C3A cells following exposure to NPs such as TiO_2, Ag, ZnO and carbon nanotubes (e.g. Kermanizadeh et al. 2012; Gaiser et al. 2013). Furthermore, PNPs have been seen to elicit a cytokine response in hepatocyte cell lines, with an increase in the production of IL-6, TNF-α observed previously (Bisht et al. 2011).

In alveolar epithelial cells (A549), IL-6 production was elevated when exposed to PNPs such as PEI NPs and PLGA/ polyvinyl alcohol NPs (Robbens et al. 2010; Grabowski et al. 2013). Additionally, C3A cells exposed to TiO_2 NPs increased mRNA expression of TNF-α, IL-1RI, IL-1β and IL-1ra receptors (Gaiser et al. 2013). Also, *in vivo*, TNF-α and IL-6 expression were elevated after oral exposure to PNPs such as polyurethane NPs and N-isopropylacrylamide-vinylpyrrolidone-acrylic acid NPs (Bisht et al. 2007; Silva et al. 2016). Interestingly, macrophage cell lines have also been seen to increase production of IL-1β when exposed to Ag or SiO_2 NPs (Carlson et al. 2008; Park & Park 2009). Although not often investigated the production of IL-1ra was increased by RAW cells exposed to CeO_2 hydroxyapatite NPs (Li et al. 2017). These studies highlight the importance of investigating cytokine production following exposure of cells to PNPs.

The only cytokine with increased production following exposure to both nRR-NPs and RR-NPs was the anti-inflammatory cytokine IL-1ra. Previous studies exposing monocytes and polymorphonuclear cells to PLGA-PEG NPs also failed to induce the production of pro-inflammatory (IL-1β, IL-6, TNF-α and IL-8) cytokines (Segat et al. 2011). Furthermore, although an increase in IL-6 was seen for hepatic cells exposed to polyethene imine NPs, these NPs failed to increase production of IL-8, the most common cytokine investigated for hepatocytes exposed to NPs (Robbens et al. 2010).

However, only one-time point was investigated for cytokine production, and there may have been the production of pro-inflammatory cytokines at earlier time points. Previous studies observed cytokine production such as IL-6, after 4 hours of exposure to hepatocytes (Brown et al. 2014). However, other studies have seen increases in cytokine production such as IL-8 using human liver microtissue following exposure to ZnO NPs for 24-312 hours (Kermanizadeh et al. 2014). Therefore in future studies, it would be informative to investigate cytokine production at a range of time points.

The results of this study suggest that the PNPs did not stimulate a pro-inflammatory response, although this would need to be confirmed *in vivo*. Notwithstanding, the observed increase in the anti-inflammatory cytokine IL-1ra could be an early indicator of low levels of cellular damage.

4.4.7 nRR-NPs and RR-NPs Intracellular ROS production

In this study, the potential for PNPs to generate intracellular ROS was investigated using the DCFH-DA assay. Both RR-NPs and nRR-NPs produced a similar ROS response at all concentrations, with a ~5-fold increase in ROS production compared to untreated cells. Previous studies have shown that PNPs can induce ROS production without affecting cell viability (Yu et al. 2014). This aligns with the findings of this study, where nRR-NPs stimulated DNA damage via an oxidant mechanism.

As elevation in ROS production has the potential to affect cell health negatively, it would be essential to understand the impact of this elevated ROS in more detail as it would not be a desirable attribute for a medical application. Prior studies using hepatocytes have

shown that an increase in ROS generation by NPs was strongly correlated with a decrease in GSH, suggesting that NPs may stimulate oxidative stress, interestingly, in turn, this may decrease the rate of RR-NP cleavage (Hussain et al. 2005). Therefore, it would be important in the future to investigate the levels or activities of antioxidants (e.g. GSH, catalase, SOD) in cells exposed to these NPs, as these antioxidants are essential in protection against oxidative stress through scavenging of ROS (Dewanjee et al. 2011).

Also, Kermanizadeh et al. demonstrated that NP-mediated cytokine production and genotoxicity in C3A cells were mediated by oxidants as pre-treatment with the anti-oxidant Trolox could protect against NP toxicity (Kermanizadeh et al. 2012). This approach could be employed in future studies to dissect out the role of ROS in PNP toxicity. To further investigate the role of oxidative stress in RR-NP and nRR-NP toxicity, dihydroethidium (DHE), a superoxide indicator that changes colour upon oxidisation, could be used (Filippi et al. 2014; Kung et al. 2015). Another method, electron spin resonance (ESR) uses a spectroscope to assess production of short-lived oxidants indirectly, and is typically used to assess acellular ROS production by NPs. This is achieved when oxidants bind with molecules such as alpha-phenyl N-tertiary-butyl nitrone to generate longer lived adducts with specific spectra that can be measured using ESR (Kadiiska et al. 1996; Sato et al. 2002; Žuvić-Butorac et al. 2005).

When cysteine thiols (e.g. in GSH) are exposed to ROS, sulfenic acid is formed, which in turn promote the formation of oxidant-mediated disulphide linkers (Claiborne et al. 1993; Rehder & Borges 2010). These oxidant-mediated disulphide linkers are distinct from structural disulphide linkers which are formed by a direct thiol-disulphide exchange reaction. To cleave oxidant-mediated disulphide linkers specific antioxidants are required such as thioredoxin or glutaredoxin (Holmgren 1979).While the structural disulphide bonds present in RR-NPs are designed to cleave in high redox environments (e.g. GSH) (Wang et al. 2011). Therefore, although the RR-NPs are redox reactive, it would not be expected that the increase in ROS production mediated by these NPs would increase cleavage of disulphide linker between PLGA and PEG.

However, a previous study demonstrated that some disulphide linkers had the potential to be cleaved by high levels of ROS, NPs were developed using anticancer prodrug

Paclitaxel and citronellol linked with varying lengths of disulphide linker (1-3 carbons). These disulphide linkers were observed to act as an oxidation-responsive element (Xiao et al. 2015; Luo et al. 2016; Sun et al. 2018). The RR-NPs in this study had a linker of 2 carbons, in the study performed by Sun et al. above it was observed that disulphide linkers containing 2 carbon bonds when exposed to either 10 mM dithiothreitol (similar to GSH) or 10 mM H_2O_2 both treatments resulted in similar levels of disulphide linker cleavage rate. Although these differ significantly in regards to location and composition of elements being linked, it is possible that ROS could cleave these disulphide bonds. However, this would need to be confirmed by exposing RR-NPs to H_2O_2 and analysising for sulfoxide, and sulphone production as these products are only produced when disulphide linkers are cleaved by ROS (Xiao et al. 2015; Luo et al. 2016; Sun et al. 2018).

The results of this study suggest that both RR-NPs and nRR-NPs may stimulate ROS production. However as there results were not dose dependent it is possible that this assay is not sensitive or reliable enough for these PNPs. Furthermore, assessment of the contribution of oxidative stress would require investigation of markers of oxidative stress such as the marker of lipid peroxidation, MDA (Ohkawa et al. 1979; Williams et al. 1998; Wheeler et al. 2001; Elchuri et al. 2005). Previous studies have indicated that NPs have the potential to induce increases in MDA production *in vitro* in hepatocyte cells (HepG2) exposed to silver NPs and *in vivo* in the livers of mice intravenously administered with cadmium telluride QDs (Oliveira et al. 2013; Zhang et al. 2015).

It was not possible to identify any current studies investigating the ROS production of PNP containing a disulphide linker. Also, it would be of interest in the future to look at mitochondrial antioxidant manganese superoxide dismutase (MnSOD) enzyme activity, as this enzyme can scavenge superoxide radical to protect the cells from damage caused by ROS. MnSOD could provide greater insight into the impact of RR-NPs and nRR-NPs on hepatocyte function, as well as provide insight relating to the elevated ROS levels observed (Gregory & Fridovich 1973).

4.4.8 Impact of nRR-NPs and RR-NPs on urea and albumin production

Following exposure of C3A cells to RR-NPs and nRR-NPs, a decrease in the levels of both urea and albumin were observed, indicating their potential to cause damage to hepatocytes. RR-NPs had a less pronounced effect.

In the current study RR-NPs and nRR-NPs did not appear to negatively impact on mitochondrial function according to the AB assay. However, alternative methods can be used to investigate mitochondrial function, such as the positively charged fluorescent dye tetramethylrhodamine, ethyl ester that is used as an indicator of mitochondrial membrane potential and readily accumulates in active mitochondria due to the mitochondria relative negative charge (Lammel et al. 2013).

Both these NPs appeared to affect hepatic function negatively. Although, results suggest that the disulphide linker in the RR-NP may have the potential to reduce adverse effects, therefore improving the safety profile of this NP as a nanomedicine.

4.4.9 nRR-NPs and RR-NPs effects on intracellular calcium concentration

Elevation of $[Ca^{2+}]_i$ in hepatocytes can occur as a response to cellular injury and has potential as a marker for nanomedicine induced hepatotoxicity (Trump et al. 1984; Tolosa et al. 2012; Jemnitz et al. 2017). In this study, Fura-2 was used to quantify increases in $[Ca^{2+}]_i$. Both NPs could increase $[Ca^{2+}]_i$, and RR-NPs stimulated a higher response than nRR-NPs.

These results are in line with other studies that had shown an increase in $[Ca^{2+}]_i$ when hepatocytes were exposed to PNPs such as PAMAM dendrimer NPs, while there was no impact on cell viability (Jemnitz et al. 2017). Interestingly, PEGylated PAMAM dendrimer NPs also elicited less of an increase in $[Ca^{2+}]_i$ in primary rat Kupffer cells (Jemnitz et al. 2017). Also, previous studies have shown that polystyrene NPs of < 100 nm were capable of inducing an increase in $[Ca^{2+}]_i$ in macrophage and neuroblasts (Brown et al. 2001; Meindl et al. 2015). Furthermore, PLGA NPs <100 nm increased intracellular calcium flux in both macrophage cells (RAW264.7) and human lung cells (BEAS-2B) (Zheng et al. 2015). Together these results indicate that polymer NPs can elicit an increase

in $[Ca^{2+}]_i$ in a range of cell lines and that NP physicochemical properties such as PEG coatings impact upon the magnitude of the response observed.

An increase in $[Ca^{2+}]_i$ can stimulate an array of downstream effects, such as apoptosis, cytokine production and membrane repair (Bement & Capco 1991; Steinhardt 1994; Terasaki et al. 1997; Shareia et al. 2009; Brown et al. 2010). To further investigate the effects of intracellular calcium and to confirm the observed increased $[Ca^{2+}]_i$ observed for RR-NPs and nRR-NPs it would be of interest to inhibit calcium signalling via calcium antagonists such as verapamil, which have previously been seen to decrease PM10 induced release of TNF-α protein related to increased $[Ca^{2+}]_i$ in human primary monocytes (Brown et al. 2013). However, although verapamil has been seen to have a protective effect on liver cells at low concentrations, it has also been observed to enhance the toxicity of specific compounds such as diclofenac in isolated hepatocytes (Schmitz et al. 1995; Szelag et al. 2003). Therefore endpoints investigated following calcium signalling inhibition may be difficult to distinguish from NP effect and toxic side effects of the calcium antagonists.

Cell membrane repair requires an influx of extracellular calcium, without this some forms of membrane repair cannot occur such as contraction and exocytosis (Bement & Capco 1991; Steinhardt 1994; Terasaki et al. 1997). It is possible that upon initial exposure RR-NPs cause injury to the membrane of C3A cells, therefore these cells could require an influx of extracellular calcium for repair. As there appears to be no extensive cell death observed perhaps this membrane damage was transient. This could be further studied by investigating the NP uptake over time using live imaging together with an appropriate cell stain such as Fura-2.

The results of the current study suggest that PNPs have the potential to increase $[Ca^{2+}]_i$, an endpoint that is not commonly investigated when assessing the safety of PNPs *in vitro*. Previous studies have indicated that ROS has a role in modulating $[Ca^{2+}]_i$ (Stone et al. 2000; Huang et al. 2010). To further investigate the contributions of ROS production to modulating $[Ca^{2+}]_i$ cells could be treated with an antioxidant such as Trolox which has previously been seen to effectively prevent NP induced calcium increase when macrophages were exposed to PEGylated QDs (Clift et al. 2010). However, in the current

study both RR-NPs and nRR-NPs appear to induce similar levels of ROS, suggesting that more than NP induced ROS alone plays a part in increasing $[Ca^{2+}]_i$. These results highlight the need to increase the understanding of the mechanism of toxicity of PNPs when used in nanomedicine.

4.5 Conclusion

This study used a range of methods to investigate the cellular toxicity of PLGA-PEG NPs with (RR-NPs) and without (nRR-NP) a novel redox-responsive disulphide linker including; uptake; genotoxicity; cytokine production; ROS production; urea and albumin production as well as increases in intracellular calcium concentration.

As hypothesised, both NPs had low cytotoxicity. There appeared to be a higher level of uptake of RR-NPs compared to nRR-NPs which was expected as the disulphide linker was designed to be degraded within a high GSH environment, which has previously been noted for cancer cell lines and in particular hepatocytes. Furthermore, the differential degradation rates of nRR-NPs and RR-NPs, as well as the disulphide linker in the RR-NPs may alter NP internalisation and trafficking within the cells, and therefore explain the differences in responses observed. Although, it would be expected that the NPs internalised to a greater extent would produce a greater toxic response. There was a marginally lower internalisation of nRR-NPs compared to RR-NPs, however the nRR-NPs should remain as intact NPs for longer within the cells than the GSH cleavable RR-NPs. Therefore, once inside the cell the nRR-NPs may have had more opportunity to interact with elements within the cell such as DNA leading to more genotoxic and stimulated a more prominent reduction in urea and albumin production than RR-NPs.

Both RR-NPs and nRR-NPs may increase ROS production and caused a moderate increase in IL-1ra production. Of interest was the increased $[Ca^{2+}]_i$ for both NPs but predominantly RR-NPs. Although in previous studies ROS has been linked to increased $[Ca^{2+}]_i$, there appears to be little difference in ROS production between RR-NPs and nRR-NPs, while there was a significant difference in intracellular $[Ca^{2+}]_i$ suggesting that in this situation other factors also influence $[Ca^{2+}]_i$. The relatively higher impact of nRR-NPs on urea and albumin production could be linked to differences in the cleavability of the PEG

shell of these PLGA NPs. The reduced degradation rate of nRR-NPs could delay degradation once internalised by cells compared to RR-NPs. This could lead to differences in how these NPs interact with the cells both extracellularly and intracellularly resulting in differential impacts of urea and albumin production.

As RR-NPs are the particles of interest in a medical application, these results are promising as it appears to indicate that the addition of the disulphide linker potentially increases the safety of these PLGA-PEG NPs. However, this would need further investigation in other cell lines and using *in vivo* studies. This information could be used in the design of future nanomedicines to increase safety while also increasing the targeting of the medically relevant NPs cargo.

The observations made during this study could contribute to refining a in vitro testing strategy for PNPs such as in tier 1 in Figure 1.3. Identifying the most informative endpoints has the potential to reduce in vitro testing required as well as in vivo, which has the potential to reduce the time and cost of bringing safe and useful nanomedicines to the patients.

Again, with a testing strategy in mind to determine PNP safety, limited cytotoxicity testing and PNP uptake assessment provided adequate information to make safety related decisions. Using two methodologies to assess genotoxicity provided a greater weight to the value of the genotoxic results and would be useful in a testing strategy for PNPs. Although concentrations and timepoints were limited due to the quantity of NPs available. For these PNPs cytokine production did not provide information regarding PNP safety. Additionally, ROS assessment via the DCFH-DA assay appeared to be an unsuitable indicator of the oxidative state of the cells. However, for these PNP both albumin and urea appear to be useful indicators of liver cell health. Although, greater understanding of how NPs impact on urea and albumin production would be require for this to be used successfully in a PNP testing strategy.

Chapter 5. General Discussion

5.1 Overview of project aims and objectives

Currently, due to the diversity of PNPs under development and lack of an in-depth understanding of their safety profile, the toxicity testing of a range of PNPs of varied physicochemical properties using evidence-based endpoints and physiologically relevant concentrations is needed for their successful clinical application. Obtaining a better understanding of the physicochemical properties of PNPs that confer toxicity and the cellular and molecular events which underlie any observed toxicity will inform future testing strategies used to assess PNP toxicity and ensure the safer design of future generations of PNPs.

The most commonly used and investigated PNPs for nanomedical use are spherical, micellar PNPs. These PNPs are usually composed of a hydrophobic "core" and a hydrophilic "shell". The PNP shell is the primary part of the PNP that comes into contact with cells, making it essential to investigate the impact of alterations of the micellar PNP shell on PNP safety. Accordingly, in this study, the toxicity of a panel of PNPs of varied shell composition was conducted to achieve a greater understanding of the influence of PNP physicochemical properties on their toxicity.

More specifically, a panel of PNPs of varying complexity were selected for investigation. PDP-PF68 PNPs had an adsorbed hydrophilic shell (PF68) which aimed to increase PNP stability and circulation time, for drug delivery via inhalation. The 4K, 15K and 55K PNPs had a chemically linked hydrophilic shell (PEG) and hydrophobic segment (PLGA) of varying lengths which aimed to increase PNP stability and circulation time, while improving the safety of these PNPs for bioimaging following intravenous administration. Also, RR-NPs had a chemically linked hydrophilic shell (PEG) that was responsive to a redox environment, making these PNPs specifically targeted to cancer cells and are intended for delivery via intravenous injection. Safety by design was used within each of the PNPs tested. More specifically, the hydrophilic polymer component shell of each of the PNPs was expected to increase PNP efficacy and safety, by increasing NP stability and circulation time for PDP-PF68 PNPs and 4K, 15K and 55K PNPs as well as increasing the targeting of PNPs such as for RR-NPs

Furthermore, when developing a testing strategy for assessing PNP safety, an understanding of the mechanisms underlying their toxicity is vital to identify which markers to prioritise when screening NP toxicity (Henderson et al. 2014; Boyles et al. 2015). Several *in vitro* studies have investigated the safety of PNPs but have used limited endpoints to assess toxicity. Also, only a limited range of cell models such as gut and breast cancer cells have been used. Therefore, there is an absence of information regarding the response of other cell types to PNPs. Accordingly, this study focused on assessing the response of the liver to address this knowledge gap and used a battery of tests to perform a thorough assessment of the hepatotoxicity for clinically relevant PNPs.

The overall aim of this project is to inform the development of evidence-based *in vitro* approaches to screen the toxicity of PNPs of varied physio-chemical properties. It is intended that the information obtained will inform the development of a tiered testing approach by allowing indicators of toxicity to be identified that can be used when screening PNP safety before progressing with *in vivo* testing, if deemed appropriate. This has the potential to reduce the resources required for testing these PNPs such as time, financial investment and animals, therefore becoming more in line with the principles of the 3Rs (replacement, refinement, and reduction of animal testing) (Burden et al. 2017). Also, it is envisioned that obtained data will inform the safe design of future generations of PNPs.

5.2 Hypothesis

It was hypothesised that PNPs would stimulate low cytotoxicity in C3A hepatocytes. Additionally, due to evidence from a large body of evidence for engineered NPs (metal, metal oxides), it was excepted that if any toxicity was observed it would be predominantly mediated by ROS and pro-inflammatory driven responses. It was expected that the physico-chemical properties of the PNPs would influence their toxicity such as PNP size, zeta potential, PDI, morphology and surface properties.

5.3 Overview of outcomes

A heat-map was generated to summarise results across all the tested PNPs (Table 5.1).

From the heat-map, there did not appear to be a consistent relationship between toxicity and the physicochemical characteristics of PNP such as hydrodynamic diameter, PDI or zeta potential. However, the NPs are all generated according to different preparation methods with varying polymers, and further research would be required to further probe the importance of physio-chemical characteristics to PNP toxicity. What is interesting is that the cytotoxicity assays (AB, CFDA and NR), which in previous studies have been the predominant method to assess PNP toxicity, appear to indicate little to no toxicity, while other endpoints such as genotoxicity suggest that further investigation of PNP safety may be required.

Ranking of PNP toxicity considered the findings from all assays. Interestingly, some assays were found to be consistently more sensitive to PNP toxicity than others. For example, assessment of PNP uptake by cells via quantitative and qualitative means did not appear to relate to the overall toxicity of PNPs. This may suggest that the level of PNP uptake observed for the PNPs under investigation to C3A cells had little impact on overall toxicity. To further investigate the uptake and intracellular fate of these PNPs in hepatocytes, it would be interesting to determine if these PNPs co-localise with cell organelles such as lysosomes or mitochondria using fluorescent probes such as Lysotracker or Mitotracker. As discussed in previous chapters it would also be useful to assess the mechanism of PNP uptake to allow for further relationships to be understood between PNP uptake and PNP safety. As hepatocytes are not professional phagocytes, and as the PNPs in this study are not targeted to hepatocytes, levels of uptake may not be high enough to elicit a toxic response. The response of other cell types such as macrophages that are likely to experience higher levels of PNP uptake should therefore be considered in the future to obtain a better understanding of how PNP uptake relates to toxicity.

Table 5.1 Heat-map of outcomes C3A cells (A/B), Ranking of PNP toxicity (C).

Endpoint results are coded according to the change from untreated control; no change-green, small change-yellow, moderate change-orange, larger change-red, incompatible assay-grey and assays not performed-white. Assays were weighted according to combined toxicity information obtained for all PNPs together with the assays sensitivity of predicting PNP safety. The weighted outcome was calculated as the sum of the weight of the assays 2= unacceptable safety impact, 1= acceptable safety impact and 0= undetermined impact on safety by PNPs (A/B). Table ranking from PNPs with lowest toxicity to highest toxicity according the weighted outcome (C).

A

End point*	PDP	PDP-PF68	4K	15K	55K	nRR-NPs	RR-NPs	
DLS (nm)	<150	<150	<150	<150	<150	<70	<70	
PDI	<0.3	<0.3	<0.3	<0.3	<0.3	<0.7	<0.7	
Zeta (mV)	<-12	<-12	<-7	<-12	<-12	<-7	<-7	
Polymer composition	PDeMS-PS	PDeMS-PS (PF68)	PEG2K-PLGA4K	PEG2K-PLGA15K	PEG5K-PLGA55K	PEG2K-PLGA6K	PEG2K-ss-PLGA6K	Wt. of Assay
AB								1
CFDA								1
NR								1
Comet assay								2
MN								2
ROS								1
IL-8								1
TNF-a								1
IL-1b								1
IL-6								1
Weighted outcome	1	2	1	3	2	4	2	

B

End point*	PDP	PDP-PF68	4K	15K	55K	nRR-NPs	RR-NPs	Wt. of Assay
Gro-a								0
IL-1ra								0
NP uptake								0
Urea								0
Albumin								0
$[Ca^{2+}]_i$ #								0
Weighted outcome	0	0	0	0	0	0	0	

C

Ranking	Lowest toxic	>	>	>	>	>	Highest toxic
PNP	PDP	4K	PDP-PF68	55K	RR-NPs	15K	nRR-NPs

Compared to untreated control					
No change	Slight change	Moderate change	Large change	Not compatible	Not performed

* =End point at 24 hours max change observed compared to untreated control

=36 minutes

Assay weight (Wt.) by inpact on PNP safety	
Undetermined	0
Acceptable	1
Unacceptable	2

Genotoxicity appears to be a sensitive marker of potential adverse effects of PNPs in C3A cells. However, as the number of NP concentrations that could be tested were limited results should be considered preliminary (OECD 2015). When both the comet assay and the MN assay were used to assess PNP genotoxicity similar results were observed indicating that both these assays are suitable to assess PNP toxicity in hepatocytes.

DNA damage for all PNPs appeared to be mediated via an oxidative mechanism, as a higher level of DNA damage was evident for Fpg treated samples, a specific measure of oxidised DNA base lesions (Collins et al. 1996). ROS production was increased following exposure of the hepatocytes to these materials, however, as ROS was also increased in cells that experienced no measurable DNA damage, the involvement of ROS production in PNP toxicity would need future investigation using additional markers for oxidative stress.

Interestingly alterations to the PNP shell differentially affected genotoxicity, indicating that when it comes to safety by design, the impact of the outer shell that comes into contact with the cells is essential to consider. Although, investigating the genotoxic potential of PNPs can be time-consuming as well as costly, if these PNPs are to be used as nanomedicines, it is an essential endpoint to investigate before progressing to *in vivo* studies.

When cellular ROS production was investigated it was elevated for all PNPs assessed regardless of PNP properties. This may indicate that the DCFH-DA assay is not suitable for assessment of ROS produced by PNP. Therefore, these results would require furthered investigation of other indicators of the oxidative state in the cell such as measurement of MDA, a by-product of lipid peroxidation (i.e. the oxidative degradation of the cells lipid membrane by free radicals) or the levels/activities of antioxidants such as SOD or glutathione peroxidase (GPx). If along with ROS and MDA elevation, the levels of the antioxidants (SOD or GPx) were observed to be decreased this could indicate oxidative stress. This oxidative stress, in turn, has the potential to damage DNA and alter metabolism in hepatocytes such as reduced urea production (Filippi et al. 2014; Evans et al. 2017; Sims et al. 2017).

The majority of cytokines analysed do not appear to be impacted by exposure of C3A cells to PNPs, except for IL-1ra and IL-8. Increased production of the anti-inflammatory protein, IL-1ra appears to be elevated regardless of PNP properties. These results therefore indicate that IL-1ra may be a good candidate to use during initial toxicity testing, along with IL-8.

What was interesting and in need of further investigation *in vivo* is the impact of PNPs on liver-specific markers such as urea production. This is a marker not commonly used within *in vitro* tests, especially with PNPs. However all PNPs investigated stimulated a decrease in urea production that was PNP concentration dependent. Therefore, additional studies using *in vivo* models could assess circulating levels of BUN to provide further insight into whether PNPs elicit liver damage. Here *in vivo* models would be useful as these PNPs may be cleared from the liver by Kupffer macrophage cells as well via hepatobiliary clearance, therefore potentially decreasing the adverse impact on hepatocytes (Tsai & Liu 2004).

$[Ca^{2+}]_i$ was a maker of interest as previous studies showed that elevated calcium was linked to NP toxicity. The semi-high throughput $[Ca^{2+}]_i$ assay developed during this study proved promising as changes in $[Ca^{2+}]_i$ were observed for RR-NPs using fewer resources and time needed for traditional imaged based measurement of $[Ca^{2+}]_i$. It would be interesting to investigate the impact of N-acetylcysteine (NAC) on $[Ca^{2+}]_i$, as previous studies have shown that increases in $[Ca^{2+}]_i$ could be negated by the addition of the antioxidant NAC (Stone et al. 2000; Huang et al. 2010). This could give additional insight into the role of PNP induced ROS in the increase in $[Ca^{2+}]_i$ by PNPs (Dubes et al. 2017).

The assays were weighted to aid in ranking with the combined toxicity information obtained for all PNPs and the sensitivity of the different assays employed to predicting PNP safety (Table 5.1 A/B). The results from this heatmap were used to rank the PNPs from lowest to highest overall toxicity as follows PDP NPs <4K NPs <PDP-PF68<55K NPs <RR-NPs <15K NPs <nRR-NPs (Table 5.1 C). It can be seen that for nRR-NPs the alteration of the PNP shell appears to have reduced PNP toxicity. In addition, the toxicity of PLGA-PEG PNPs may be influenced by PLGA chain length when PEG is of the same size chain length (4K,15K) with PNPs composed from longer polymer chain lengths of

greater toxicity. The nRR-NPs were typically more toxic than RR-NPs. Taken together, the results therefore suggest that the composition and surface properties of PNPs influence their toxicity.

5.4 Screening strategies

During pre-clinical development of PNPs it is important that safety by design is considered to produce effective as well as safe nanomedicines. Therefore, existing knowledge of NP toxicity can inform the design of PNPs to reduce the likelihood of adverse health effects manifesting in the clinic. This requires a comprehensive analysis of the physico-chemical properties of PNPs in the first tier of testing and thorough review of the literature (Figure 5.1). Next, it is suggested that *in vitro* screening (tier 2) be performed, using simple monocultures of cells (that represent a relevant target site) focusing on assessment of cytotoxicity, uptake, cytokine production, oxidative stress and genotoxicity (Figure 5.1). Testing can then progress to more advanced *in vitro* models and a more diverse array of endpoints, only with suitable candidate PNPs that have demonstrated low toxicity in earlier tiers of testing. Following an acceptable *in vitro* outcome candidate PNPs could then progress to *in vivo* analysis (Figure 5.1). Using a tiered testing strategy will ensure that testing of PNP safety is conducted in an evidence based and focused manner. This approach could reduce resources required for testing PNPs toxicity and the information gain could be used for the safer design of PNPs in the future.

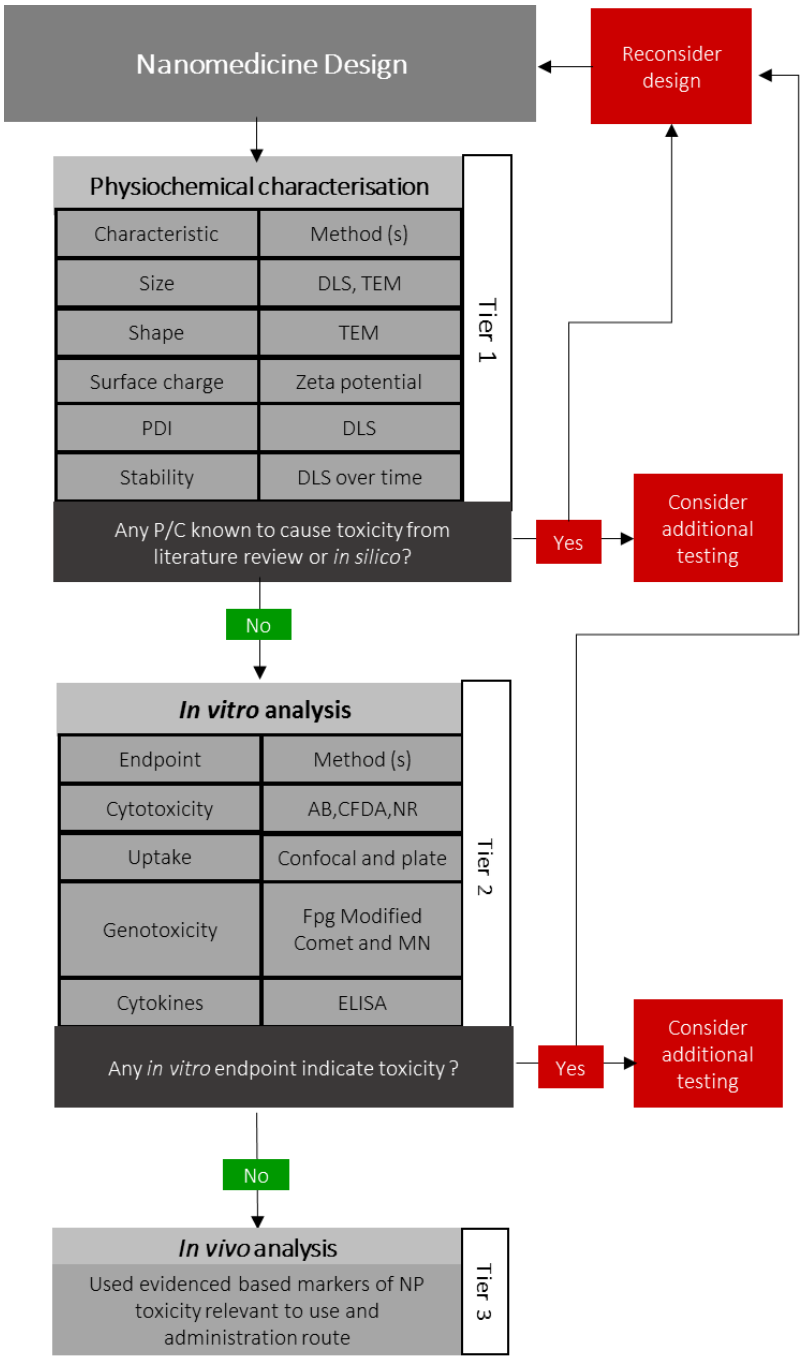

Figure 5.1 Expanded tiered testing strategy for assessment of nanomedicine safety. Expansion on the tiered testing approach suggested in Figure 1.3. Endpoint and method as for the PNPs tested in this study. Allowing for progression only with suitable NPs to *in vivo* analysis. Information generated from each step in the tiered testing strategy can prompt additional testing, design reconsideration or progression to the next tier of testing. This approach could reduce resources required for testing PNPs toxicity and information gain used for future safer design of PNPs.

The results from the PNPs examined in these projects in hepatocyte cells could be implemented to focus i*n vitro* screening for future generations of PNPs, by informing what endpoints are prioritised within tier 2 testing when considering PNP safety with in the liver (Figure 5.2).

When developing PNP nanomedicines it is key to consider genotoxicity, as when unacceptable levels of genotoxicity are observed, at therapeutically relevant concentrations, PNPs may not be useful as nanomedicines due to related adverse effects such as cancer. Figure 5.2 suggests an approach to PNP screening that starts by performing cytotoxicity testing (AB assay) to identify non-lethal concentrations of PNPs, followed by genotoxicity testing examined by both the Comet assay and the MN assay (4 and 24 hrs, at 3 or more concentrations). If results indicate unacceptable levels of genotoxicity, dependent on the application of these nanomedicines, the design of the PNPs may need to be reconsidered. If the results suggest low to no genotoxicity at clinically relevant concentrations, these PNPs could progress to the next endpoint.

Although ROS measurement via the DCFH-DA assay, was not suitable for these PNPs, it may be a useful endpoint for other PNPs, therefore genotoxicity testing could be followed by analysis of indicators of oxidative stress, via ROS and GSH measurement (e.g. MDA). Although the PNPs tested in this study appear to have limited impact on cytokine production, it is established that NPs can stimulate inflammatory responses *in vitro* and *in vitro,* and thus it is suggested to follow analysis of oxidative stress by focusing on the production of cytokines such as IL-8 in hepatocytes, although using other cell lines other cytokines such as TNF-α could be useful markers of an inflammatory response. When changes in IL-8 levels are observed in hepatocytes, additional cytokine analysis should be considered. When there is an absence of effect on cytokines it can be suggested to progress to the next phase of testing.

Although NP uptake is important to investigate for PNPs as it can influence their efficacy and safety of PNPs, there are currently not clear thresholds with regards to what level of PNP uptake or PNP retention within cells are associated with toxicity. Therefore, uptake studies should be performed during the screening of PNPs in pre-clinical development to obtain a better understanding of how uptake influences toxicity. The same can be said for

urea, albumin and [Ca^{2+}]$_i$, although these have all proven useful markers of liver cell health further understanding would be required for these endpoints to prove useful in a pre-clinical screening process as currently there are no clear thresholds to indicate these PNPs would be considered safe.

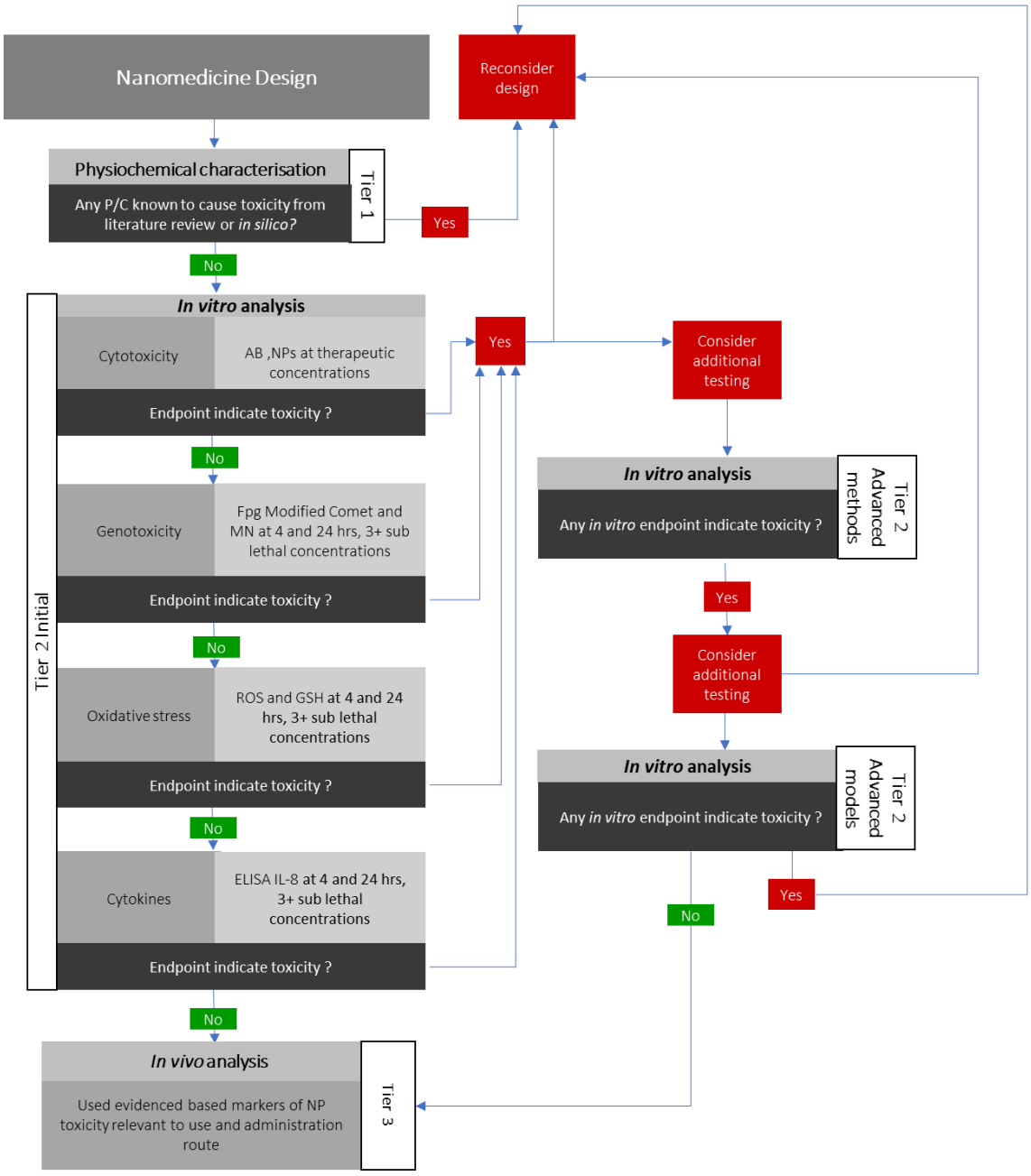

Figure 5.2 *In vitro* tiered testing strategy for assessment of nanomedicine safety. Expansion on the *in vitro* tier 2 testing approach suggested in Figure 5.1. Endpoint and method selection were informed by data collected for the PNPs tested in this study. This approach could be used to aid PNP safety by design and reduce resources required for i*n vitro* PNPs toxicity testing.

5.5 Future

This study focused on the investigation of impacts on hepatocytes and used the C3A cell line. Ideally primary human or animal cells would also be investigated. However these primary cells come with a high cost, high rate of variability and ethical implications associated with their use. In addition, previous studies have shown that the C3A cell line provides a good prediction of primary human or rat hepatocytes. However comparative studies would be useful to identify whether the cell line gives a good prediction of the response of primary cells. Assessment of the response of other toxicologically important cell lines to PNPs would also be beneficial. For example, assessment of the response of macrophages could provide additional information regarding the safety of these PNPs. As seen when the macrophage-like J774 cells were exposed to PDP and PDP-PF68 NPs. In addition, it would be of interest to investigate the response of neutrophils. More specifically, when hepatocytes are exposed to NPs, pro-inflammatory cytokines such as TNF-α, IL-8 or IL-1 and lipid peroxidation products can be released, promoting neutrophil accumulation and activation in the liver potentially causing excessive ROS production leading to inflammation and liver damage (Clark 1999; Leifeld et al. 2002; Antoniades et al. 2008; Kermanizadeh et al. 2013). It could also be of benefit to investigate the safety impact on target cells such as lung epithelial cells or intestinal epithelial cells, as well as additional target sites such as renal proximal tubule epithelial cells.

Cells used in this study were grown in monocultures. The use of 3-D cell models is increasing when investigating NP toxicity (Chen et al. 2016; Conte et al. 2018). InSphero is a 3-D cell culture system, consisting of hepatocytes together with Kupffer macrophage cells in a microtissue form. The presence of Kupffer (macrophage) cells is relevant as these cells are part of the RES that clear PNPs *in vivo*, and their presence may influence the toxicological impact observed (Bruderer et al. 2015). Therefore, these 3-D cell models could produce results that more closely reflect *in vivo* results. Additional advantages of these models are that they are long-lived, allowing for responses following longer term, repeated exposures to be investigated. Other advantages are that these models can be capable of active bile acid secretion to allow for monitoring of possible PNP elimination

(Hendriks et al. 2016). However, these microtissues do have limitations such as difficulty of high-resolution imaging as well as their high cost.

Although a human-derived hepatocyte cell line was used in this study, PNPs would benefit from *in vivo* safety profiling following initial *in vitro* screening. It is acknowledged that *in vivo* work is invaluable for information regarding PNP biodistribution, clearance and systemic toxicity, although there are concerns regarding the suitability of rodent models due to species differences and issues surrounding the reproducibility of findings (Bale et al. 2014; Johnston et al. 2018). However currently, *in vivo* models are essential tools to confirm *in vitro* findings before progressing to clinical trials in man. With time and increased research efforts, an increase in the translatability of *in vitro* to *in vivo* results may reduce *in vivo* testing even further.

5.6 Final conclusion

Commonly measured physiochemical properties such as NP diameter, PDI and zeta potential were difficult to distinguish as contributing factors to the toxicity of the PNPs investigated in this study. However, the PNP coating was identified to be the most influential property on PNP toxicity in this study. Therefore, coating modification appears to be a promising way to enhance PNP safety. This study used a battery of endpoints to assess PNP toxicity, and the findings will guide future testing strategies which investigate PNP safety. More specifically, the ability to distinguish between these PNPs via assays investigating genotoxicity, cytokine and urea production as well as via changes in intracellular calcium concentration suggest that the C3A *in vitro* model is useful in assessing PNP toxicity. Therefore, results from this project may allow for the prioritising of endpoints when assessing PNP toxicity. Although commonly used to investigate PNP toxicity it would appear that assessment of cytotoxicity, cellular uptake and cytokine production should not be used in isolation to assess PNP toxicity and that instead a more diverse range of endpoints are considered in the future.

When using a tiered approach to safety testing the toxicity of PNPs can be screened using a battery of endpoints before progressing to *in vivo* studies of PNPs. The utilisation of *in vitro* model has proven useful here to assess the safety of a panel of PNPs. With growing

use and interest of PNPs for medical use *in vitro* assays use will need to grow to save resources as well as align toxicity testing to the principles of the 3R's.

This study provides information on the hazards associated with a realistic level of PNP exposure. This data could be used in the future for risk assessment of PNPs where both the hazard and the level of exposure are taken into account. However, progressing the use of PNPs as nanomedicines is currently difficult as without method standardisation it can be challenging to compare toxicological data across studies. Additionally, a lack of specific regulations and guidelines for the safety testing of nanomedicines can make it challenging to have PNPs accepted by medical approval bodies such as the EMA and FDA. However, this is set to improve in the future as current European Union nanomedicine focused projects aim to developed risk management frameworks as well as standardised methods of safety testing.

References

Acharya, S. & Sahoo, S.K., 2011. PLGA nanoparticles containing various anticancer agents and tumour delivery by EPR effect. *Advanced Drug Delivery Reviews*, 63(3), pp.170–183. Available at: http://dx.doi.org/10.1016/j.addr.2010.10.008.

Acosta-, L.S. et al., 2012. Cytocompatible antifungal acrylic resin containing silver nanoparticles for dentures. , pp.4777–4786.

Agarwal, R. et al., 2016. Synthesis of self-assembled IL-1Ra-presenting nanoparticles for the treatment of osteoarthritis. *J Biomed Mater Res*, 104(3), pp.595–599.

Ahmad, J. et al., 2016. Differential cytotoxicity of copper ferrite nanoparticles in different human cells. *Journal of Applied Toxicology*, 36(10), pp.1284–1293.

Akita, H. et al., 2013. Particle tracking analysis for the intracellular trafficking of nanoparticles modified with African swine fever virus protein p54-derived peptide. *Molecular therapy : the journal of the American Society of Gene Therapy*, 21(2), pp.309–17. Available at: http://www.ncbi.nlm.nih.gov/pubmed/23164937.

Alexis, F. et al., 2008. Factors affecting the clearance and biodistribution of polymeric nanoparticles. *Molecular Pharmaceutics*, 5(4), pp.505–515.

Anderson, J.M. & Shive, M.S., 2012. Biodegradation and biocompatibility of PLA and PLGA microspheres. *Advanced Drug Delivery Reviews*, 64(SUPPL.), pp.72–82. Available at: http://dx.doi.org/10.1016/j.addr.2012.09.004.

Annangi, B. et al., 2014. Long-term exposures to low doses of cobalt nanoparticles induce cell transformation enhanced by oxidative damage. *Nanotoxicology*, 5390(Ii), pp.1–10. Available at: http://www.ncbi.nlm.nih.gov/pubmed/24713074.

Antoniades, C.G. et al., 2008. The importance of immune dysfunction in determining outcome in acute liver failure. *Journal of Hepatology*, 49(5), pp.845–861. Available at: http://dx.doi.org/10.1016/j.jhep.2008.08.009.

Aranda, A. et al., 2013. Dichloro-dihydro-fluorescein diacetate (DCFH-DA) assay: a quantitative method for oxidative stress assessment of nanoparticle-treated cells. *Toxicology in vitro : an international journal published in association with BIBRA*, 27(2), pp.954–63. Available at: http://www.ncbi.nlm.nih.gov/pubmed/23357416 [Accessed November 25, 2014].

Arts, J.H.E. et al., 2015. A critical appraisal of existing concepts for the grouping of

nanomaterials. *Regulatory Toxicology and Pharmacology*, 70(2), pp.492–506.

Arunachalam, B. et al., 2000. Enzymatic reduction of disulfide bonds in lysosomes: characterization of a gamma-interferon-inducible lysosomal thiol reductase (GILT). *Pnas*, 97(2), pp.745–750.

Arunkumar, R. et al., 2015. Biodegradable poly (lactic-co-glycolic acid)-polyethylene glycol nanocapsules: An efficient carrier for improved solubility, bioavailability, and anticancer property of lutein. *Journal of Pharmaceutical Sciences*, 104(6), pp.2085–2093.

Astete, C.E. & Sabliov, C.M., 2006. Synthesis and characterization of PLGA nanoparticles. *Journal of Biomaterials Science, Polymer Edition*, 17(3), pp.247–289. Available at: http://www.tandfonline.com/doi/abs/10.1163/156856206775997322 [Accessed December 4, 2014].

Athinarayanan, J. et al., 2014. Presence of nanosilica (E551) in commercial food products: TNF-mediated oxidative stress and altered cell cycle progression in human lung fibroblast cells. *Cell Biology and Toxicology*, 30(2), pp.89–100.

Au, L. et al., 2011. Quantifying the Cellular Uptake of Antibody-Conjugated Au Nanocages by Two-Photon Microscopy and Inductively Coupled Plasma Mass Spectrometry. , 4(1), pp.35–42.

Avalos, A. et al., 2014. Cytotoxicity and ROS production of manufactured silver nanoparticles of different sizes in hepatoma and leukemia cells. *Journal of Applied Toxicology*, 34(4), pp.413–423.

Bale, A.S. et al., 2014. Symposium report: Correlating in vitro data to in vivo findings for risk assessment. *Altex*, 31(1), pp.79–90.

Bandyopadhyay, S. et al., 2016. Conjugated Polymer Nanoparticle-Triplet Emitter Hybrids in Aqueous Dispersion: Fabrication and Fluorescence Quenching Behavior. *Macromolecular Rapid Communications*, 37(3), pp.271–277.

Barenholz, Y., 2012. Doxil®--the first FDA-approved nano-drug: lessons learned. *Journal of controlled release : official journal of the Controlled Release Society*, 160(2), pp.117–34. Available at: http://www.ncbi.nlm.nih.gov/pubmed/22484195 [Accessed July 16, 2014].

Barillet, S. et al., 2010. In vitro evaluation of SiC nanoparticles impact on A549 pulmonary cells: Cyto-, genotoxicity and oxidative stress. *Toxicology Letters*,

198(3), pp.324–330. Available at: https://www.sciencedirect.com/science/article/pii/S0378427410016012 [Accessed January 14, 2018].

Bement, W.M. & Capco, D.G., 1991. Analysis of inducible contractile rings suggests a role for protein kinase C in embryonic cytokinesis and wound healing. *Cell motility and the cytoskeleton*, 20(2), pp.145–157.

Benito-Miguel, M., Blanco, M.D. & Gómez, C., 2015. Assessment of sequential combination of 5-fluorouracil-loaded-chitosan-nanoparticles and ALA-photodynamic therapy on HeLa cell line. *Photodiagnosis and Photodynamic Therapy*, 12(3), pp.466–475. Available at: http://dx.doi.org/10.1016/j.pdpdt.2015.05.001.

Bertrand, N. et al., 2017. Mechanistic understanding of in vivo protein corona formation on polymeric nanoparticles and impact on pharmacokinetics. *Nature Communications*, 8(1). Available at: http://dx.doi.org/10.1038/s41467-017-00600-w.

Bexiga, M.G. et al., 2014. RNAi-mediated inhibition of apoptosis fails to prevent cationic nanoparticle-induced cell death in cultured cells. *Nanomedicine (London, England)*, 9(11), pp.1651–1664.

Bisht, S. et al., 2011. A polymeric nanoparticle formulation of curcumin (NanoCurc) ameliorates CCl 4-induced hepatic injury and fibrosis through reduction of pro-inflammatory cytokines and stellate cell activation. *Laboratory Investigation*, 91(9), pp.1383–1395. Available at: http://dx.doi.org/10.1038/labinvest.2011.86.

Bisht, S. et al., 2007. Polymeric nanoparticle-encapsulated curcumin ("nanocurcumin"): a novel strategy for human cancer therapy. *Journal of nanobiotechnology*, 5, p.3.

Boyles, M.S.P. et al., 2015. Multi-walled carbon nanotube induced frustrated phagocytosis, cytotoxicity and pro-inflammatory conditions in macrophages are length dependent and greater than that of asbestos. *Toxicology in Vitro*, 29(7), pp.1513–1528. Available at: http://www.sciencedirect.com/science/article/pii/S0887233315001484.

Bozzuto, G. & Molinari, A., 2015. Liposomes as nanomedical devices. *International Journal of Nanomedicine*, 10, pp.975–999.

Brayden, D.J. et al., 2015. High-content analysis for drug delivery and nanoparticle applications. *Drug Discovery Today*, 20(8), pp.942–957. Available at:

http://dx.doi.org/10.1016/j.drudis.2015.04.001.

Brown, D.M. et al., 2014. Cytotoxicity and Cytokine Release in Rat Hepatocytes, C3A Cells and Macrophages Exposed to Gold Nanoparticles—Effect of Biological Dispersion Media or Corona. *Journal of Biomedical Nanotechnology*, 10(11), pp.3416–3429.

Brown, D.M. et al., 2010. Interaction between nanoparticles and cytokine proteins: impact on protein and particle functionality. *Nanotechnology*, 21(21), p.215104. Available at: http://stacks.iop.org/0957-4484/21/i=21/a=215104?key=crossref.69fd8bcb040d3664ea4eed54a2497497.

Brown, D.M. et al., 2001. Size-dependent proinflammatory effects of ultrafine polystyrene particles: a role for surface area and oxidative stress in the enhanced activity of ultrafines. *Toxicology and applied pharmacology*, 175(3), pp.191–9. Available at: http://www.ncbi.nlm.nih.gov/pubmed/11559017 [Accessed November 8, 2014].

Brown, D.M. et al., 2013. The effects of PM10 particles and oxidative stress on macrophages and lung epithelial cells : modulating effects of calcium-signaling antagonists The effects of PM 10 particles and oxidative stress on macrophages and lung epithelial cells : modulating eff. , (March 2007), pp.1444–1451.

Brown, D.M., Donaldson, K. & Stone, V., 2002. Role of Calcium in the Induction of TNF α Expression by Macrophages on Exposure to Ultrafine Particles. , 46(June), pp.219–222.

Bruderer, R. et al., 2015. Extending the Limits of Quantitative Proteome Profiling with Data-Independent Acquisition and Application to Acetaminophen-Treated Three-Dimensional Liver Microtissues. *Molecular & Cellular Proteomics*, 14(5), pp.1400–1410. Available at: http://www.mcponline.org/lookup/doi/10.1074/mcp.M114.044305.

Brülisauer, L., Gauthier, M.A. & Leroux, J.C., 2014. Disulfide-containing parenteral delivery systems and their redox-biological fate. *Journal of Controlled Release*, 195, pp.147–154. Available at: http://dx.doi.org/10.1016/j.jconrel.2014.06.012.

Bulcão, R.P. et al., 2014. In vivo toxicological evaluation of polymeric nanocapsules after intradermal administration. *European Journal of Pharmaceutics and Biopharmaceutics*, 86(2), pp.167–177. Available at: http://dx.doi.org/10.1016/j.ejpb.2013.04.001.

Burden, N. et al., 2017. The 3Rs as a framework to support a 21st century approach for nanosafety assessment. *Nano Today*, 12, pp.10–13. Available at: http://dx.doi.org/10.1016/j.nantod.2016.06.007.

Cao, Y. et al., 2015. Triggered-release polymeric conjugate micelles for on-demand intracellular drug delivery. *Nanotechnology*, 26(11), p.115101. Available at: http://dx.doi.org/10.1088/0957-4484/26/11/115101.

Carlson, C. et al., 2008. Unique cellular interaction of silver nanoparticles: Size-dependent generation of reactive oxygen species. *Journal of Physical Chemistry B*, 112(43), pp.13608–13619.

Carril, M. et al., 2017. In situ detection of the protein corona in complex environments. *Nature Communications*, 8(1). Available at: http://dx.doi.org/10.1038/s41467-017-01826-4.

Cenni, E. et al., 2008. Biocompatibility of poly(d,l-lactide-co-glycolide) nanoparticles conjugated with alendronate. *Biomaterials*, 29(10), pp.1400–1411.

Chaudhari, K.R. et al., 2012. Opsonization, biodistribution, cellular uptake and apoptosis study of PEGylated PBCA nanoparticle as potential drug delivery carrier. *Pharmaceutical Research*, 29(1), pp.53–68.

Chen, D. et al., 2012. pH and temperature dual-sensitive liposome gel based on novel cleavable mPEG-Hz-CHEMS polymeric vaginal delivery system. *International Journal of Nanomedicine*, 7, pp.2621–2630.

Chen, D.B. et al., 2001. In vitro and in vivo study of two types of long-circulating solid lipid nanoparticles containing paclitaxel. *Chemical & pharmaceutical bulletin*, 49(11), pp.1444–7. Available at: http://www.ncbi.nlm.nih.gov/pubmed/11724235.

Chen, G. & Xu, Y., 2018. Biosynthesis of cerium oxide nanoparticles and their effect on lipopolysaccharide (LPS) induced sepsis mortality and associated hepatic dysfunction in male Sprague Dawley rats. *Materials Science and Engineering C*, 83(October 2017), pp.148–153. Available at: https://doi.org/10.1016/j.msec.2017.11.014.

Chen, Z. et al., 2016. Arginine–glycine–aspartic acid–polyethylene glycol–polyamidoamine dendrimer conjugate improves liver-cell aggregation and function in 3-d spheroid culture. *International Journal of Nanomedicine*, 11, pp.4247–4259.

Chithrani, B.D., Ghazani, A.A. & Chan, W.C.W., 2006. Determining the size and shape dependence of gold nanoparticle uptake into mammalian cells. *Nano Letters*, 6(4),

pp.662–668.

Cho, W.-S. et al., 2012. Differential pro-inflammatory effects of metal oxide nanoparticles and their soluble ions in vitro and in vivo; zinc and copper nanoparticles, but not their ions, recruit eosinophils to the lungs. *Nanotoxicology*, 6(1), pp.22–35. Available at: https://doi.org/10.3109/17435390.2011.552810.

Chronopoulou, L. et al., 2013. Chitosan-coated PLGA nanoparticles: A sustained drug release strategy for cell cultures. *Colloids and Surfaces B: Biointerfaces*, 103, pp.310–317. Available at: http://dx.doi.org/10.1016/j.colsurfb.2012.10.063.

Chung, E.J. et al., 2014. In vivo biodistribution and clearance of peptide amphiphile micelles. *Nanomedicine : nanotechnology, biology, and medicine*, pp.1–9. Available at: http://www.ncbi.nlm.nih.gov/pubmed/25194999 [Accessed November 21, 2014].

Claiborne, A. et al., 1993. Protein-sulfenic acid stabilization and function in enzyme catalysis and gene regulation. *FASEB journal : official publication of the Federation of American Societies for Experimental Biology*, 7(15), pp.1483–1490.

Clayton, K.N., Salameh, J.W. & Wereley, S.T., 2016. Physical characterization of nanoparticle size and surface modification using particle scattering diffusometry. , 054107, pp.1–14. Available at: http://dx.doi.org/10.1063/1.4962992.

Clift, M.J.D. et al., 2010. An investigation into the potential for different surface-coated quantum dots to cause oxidative stress and affect macrophage cell signalling in vitro. *Nanotoxicology*, 4(2), pp.139–149. Available at: http://www.ncbi.nlm.nih.gov/pubmed/20795892 [Accessed December 15, 2014].

Clift, M.J.D.D. et al., 2008. The impact of different nanoparticle surface chemistry and size on uptake and toxicity in a murine macrophage cell line. *Toxicology and applied pharmacology*, 232(3), pp.418–27. Available at: http://www.ncbi.nlm.nih.gov/pubmed/18708083 [Accessed November 17, 2014].

Clift, M.J.D.D. et al., 2011. The uptake and intracellular fate of a series of different surface coated quantum dots in vitro. *Toxicology*, 286(1–3), pp.58–68. Available at: http://www.ncbi.nlm.nih.gov/pubmed/21619910 [Accessed December 15, 2014].

Collins, a R., 2004. The comet assay for DNA damage and repair: principles, applications, and limitations. *Molecular Biotechnology*, 26(3), pp.249–261. Available at: http://www.ncbi.nlm.nih.gov/pubmed/15004294.

Collins, A.R. et al., 1996. Oxidative DNA damage to DNA: Do we have a reliable

biomarker? *Environmental Health Perspectives*, 104(104), pp.465–469.

Committee for Medicinal Products for Human Use & European Medicine Agency, 2013. Joint MHLW/EMA reflection paper on the development of block copolymer micelle medicinal products. , 44(January), p.EMA/CHMP/13099/2013.

Conde, J. et al., 2014. Revisiting 30 years of biofunctionalization and surface chemistry of inorganic nanoparticles for nanomedicine. *Frontiers in chemistry*, 2, p.48. Available at: http://www.pubmedcentral.nih.gov/articlerender.fcgi?artid=4097105&tool=pmcentrez&rendertype=abstract [Accessed November 10, 2014].

Cong, Y. et al., 2015. Alendronate-decorated biodegradable polymeric micelles for potential bone-targeted delivery of vancomycin. *Journal of Biomaterials Science, Polymer Edition*, 26(11), pp.629–643. Available at: http://www.embase.com/search/results?subaction=viewrecord&from=export&id=L604949230.

Conner, S.D. & Schmid, S.L., 2003. Regulated portals of entry into the cell. *Nature*, 422(6927), pp.37–44.

Connolly, M. et al., 2015. Comparative Cytotoxicity Study of Silver Nanoparticles (AgNPs) in a Variety of Rainbow Trout Cell Lines (RTL-W1, RTH-149, RTG-2) and Primary Hepatocytes. *International journal of environmental research and public health*, 12(5), pp.5386–405. Available at: http://www.mdpi.com/1660-4601/12/5/5386/htm.

Constantin, M. et al., 2017. Smart nanoparticles based on pullulan-g-poly(N-isopropylacrylamide) for controlled delivery of indomethacin. *International Journal of Biological Macromolecules*, 94(2017), pp.698–708. Available at: http://linkinghub.elsevier.com/retrieve/pii/S0141813016308236.

Conte, C. et al., 2018. Enhanced uptake in 2D- and 3D- lung cancer cell models of redox responsive PEGylated nanoparticles with sensitivity to reducing extra- and intracellular environments. *Journal of Controlled Release*, 277(March), pp.126–141. Available at: https://doi.org/10.1016/j.jconrel.2018.03.011.

Cook, P.R. & Brazell, I. a, 1976. CHARACTERIZATION OF NUCLEAR STRUCTURES CONTAINING SUPERHELICAL DNA Structures resembling nuclei but depleted of protein may be released by gently lysing cells in i-OMNaCl (Cook & Brazell , 1975 , 1976). These nucleoids sediment that is intact , supercoi. ,

324, pp.303–324.

Cooke, M.S. et al., 2003. Oxidative DNA damage: mechanisms, mutation, and disease. *FASEB journal : official publication of the Federation of American Societies for Experimental Biology*, 17(10), pp.1195–1214.

Coppé, J.P. et al., 2010. A human-like senescence-associated secretory phenotype is conserved in mouse cells dependent on physiological oxygen. *PLoS ONE*, 5(2).

Cowie, H. et al., 2015. Suitability of human and mammalian cells of different origin for the assessment of genotoxicity of metal and polymeric engineered nanoparticles. *Nanotoxicology*, 9(S1), pp.1743–5390.

Cressman, D.E. et al., 1996. Liver failure and defective hepatocyte regeneration in interleukin- 6-deficient mice. *Science*, 274, pp.1379–1383.

Cruz, L.J. et al., 2011. The influence of PEG chain length and targeting moiety on antibody-mediated delivery of nanoparticle vaccines to human dendritic cells. *Biomaterials*, 32(28), pp.6791–6803. Available at: http://dx.doi.org/10.1016/j.biomaterials.2011.04.082.

Cubillos-Ruiz, J.R. et al., 2009. Polyethylenimine-based siRNA nanocomplexes reprogram tumor-associated dendritic cells via TLR5 to elicit therapeutic antitumor immunity. *Journal of Clinical Investigation*, 119(8), pp.2231–2244.

Cui, Y. et al., 2011. Signaling pathway of inflammatory responses in the mouse liver caused by TiO2 nanoparticles. *Journal of Biomedical Materials Research - Part A*, 96 A(1), pp.221–229.

Cutts, S.M., Evison, B.J. & Pigram, P.J., 2015. Factors determining the stability , size distribution , and cellular accumulation of small , monodisperse chitosan nanoparticles as candidate vectors for anticancer drug delivery : application to the passive encapsulation of [14 C] -doxorubicin. , pp.67–80.

Danhier, F. et al., 2009. Paclitaxel-loaded PEGylated PLGA-based nanoparticles: In vitro and in vivo evaluation. *Journal of Controlled Release*, 133(1), pp.11–17. Available at: http://dx.doi.org/10.1016/j.jconrel.2008.09.086.

Dautry-Varsat, A., Ciechanover, A. & Lodish, H.F., 1983. pH and the recycling of transferrin during receptor-mediated endocytosis. *Proceedings of the National Academy of Sciences*, 80(8), pp.2258–2262. Available at: http://www.pnas.org/content/80/8/2258.short.

Davda, J. & Labhasetwar, V., 2002. Characterization of nanoparticle uptake by

endothelial cells. *International Journal of Pharmaceutics*, 233(1–2), pp.51–59.

Deng, J., Yao, M. & Gao, C., 2017. Cytotoxicity of gold nanoparticles with different structures and surface-anchored chiral polymers. *Acta Biomaterialia*, 53, pp.610–618. Available at: http://dx.doi.org/10.1016/j.actbio.2017.01.082.

Dening, T.J. et al., 2016. Oral nanomedicine approaches for the treatment of psychiatric illnesses. *Journal of Controlled Release*, 223, pp.137–156. Available at: http://linkinghub.elsevier.com/retrieve/pii/S0168365915302984.

Dewanjee, S. et al., 2011. Effective control of type 2 diabetes through antioxidant defense by edible fruits of Diospyros peregrina. *Evidence-based Complementary and Alternative Medicine*, 2011.

Dinarvand, R. et al., 2011. Polylactide-co-glycolide nanoparticles for controlled delivery of anticancer agents. *International journal of nanomedicine*, 6, pp.877–895.

Doak, S.H. & Dusinska, M., 2017. NanoGenotoxicology: present and the future. *Mutagenesis*, 32(1), pp.1–4.

Dobrovolskaia, M.A. & McNeil, S.E., 2013. Understanding the correlation between in vitro and in vivo immunotoxicity tests for nanomedicines. *Journal of Controlled Release*, 172(2), pp.456–466. Available at: http://dx.doi.org/10.1016/j.jconrel.2013.05.025.

Doktorovova, S. et al., 2012. Modified Rose Bengal assay for surface hydrophobicity evaluation of cationic solid lipid nanoparticles (cSLN). *European Journal of Pharmaceutical Sciences*, 45(5), pp.606–612. Available at: http://dx.doi.org/10.1016/j.ejps.2011.12.016.

Donaldson, K. et al., 2004. Nanotoxicology. *Occupational and Environmental Medicine*, 61(9), pp.727–728.

Dubes, V. et al., 2017. Calcium signalling induced by in vitro exposure to silicium dioxide nanoparticles in rat pulmonary artery smooth muscle cells. *Toxicology*, 375, pp.37–47. Available at: http://dx.doi.org/10.1016/j.tox.2016.12.002.

Duque, G.A. & Descoteaux, A., 2014. Macrophage cytokines: Involvement in immunity and infectious diseases. *Frontiers in Immunology*, 5(OCT), pp.1–12.

Durocher, I. & Girard, D., 2016. In vivo proinflammatory activity of generations 0–3 (G0–G3) polyamidoamine (PAMAM) nanoparticles. *Inflammation Research*, 65(9), pp.745–755.

Edlich, A. et al., 2017. Specific uptake mechanisms of well-tolerated thermoresponsive

polyglycerol-based nanogels in antigen-presenting cells of the skin. *European Journal of Pharmaceutics and Biopharmaceutics*, 116, pp.155–163. Available at: http://dx.doi.org/10.1016/j.ejpb.2016.12.016.

Edward et al., 1990. Cleavage of Disulfide Bonds in Endocytosed Macromolecules. , 265(31), pp.18780–18785.

Edwards-Jones, V., 2009. The benefits of silver in hygiene, personal care and healthcare. *Letters in Applied Microbiology*, 49(2), pp.147–152.

Ehrenberg, B. et al., 1988. Membrane potential can be determined in individual cells from the nernstain distribution of cationic dyes. *Biophys. J.*, 53(May), pp.785–794.

Elchuri, S. et al., 2005. CuZnSOD deficiency leads to persistent and widespread oxidative damage and hepatocarcinogenesis later in life. *Oncogene*, 24(3), pp.367–380.

EMA, 2012. *ICH guideline S2 (R1) on genotoxicity testing and data interpretation for pharmaceuticals intended for human use*,

Erickson, H.P., 2009. Size and shape of protein molecules at the nanometer level determined by sedimentation, gel filtration, and electron microscopy. *Biological Procedures Online*, 11(1), pp.32–51.

Espuelas, M.S. et al., 2003. Polymeric carriers for amphotericin B: In vitro activity, toxicity and therapeutic efficacy against systemic candidiasis in neutropenic mice. *Journal of Antimicrobial Chemotherapy*, 52(3), pp.419–427.

European Medicine Agency, 2013a. Reflection paper on surface coatings : general issues for consideration regarding parenteral administration of coated nanomedicine products. , 44(May), p.EMA/325027/2013.

European Medicine Agency, 2013b. Reflection paper on the data requirements for intravenous liposomal products developed with reference to an innovator liposomal product. *EMA/Committee for Human Medicinal Products 806058/2009/Rev. 02*, 44(February), pp.1–13.

Evans, S.J. et al., 2017. Critical review of the current and future challenges associated with advanced in vitro systems towards the study of nanoparticle (secondary) genotoxicity. *Mutagenesis*, 32(1), pp.233–241. Available at: http://www.ncbi.nlm.nih.gov/pubmed/27815329%5Cnhttps://academic.oup.com/mutage/article-lookup/doi/10.1093/mutage/gew054.

Fangueiro, J.F. et al., 2015. Current nanotechnology approaches for the treatment and management of diabetic retinopathy. *European Journal of Pharmaceutics and*

Biopharmaceutics, 95, pp.307–322. Available at: http://dx.doi.org/10.1016/j.ejpb.2014.12.023.

Farcal, L. et al., 2015. Comprehensive in vitro toxicity testing of a panel of representative oxide nanomaterials: First steps towards an intelligent testing strategy. *PLoS ONE*, 10(5), pp.1–34.

FDA, 2005. Guidance for Industry – Estimating the maximum safe starting dose in initial clinical trials for therapeutics in adult healthy volunteers. *US Department of Health and Human Services, Food and Drug Administration, Center for Drug Evaluation and Research*, (July), pp.1–30. Available at: downloads/Drugs/GuidanceComplianceRegulatoryInformation/Guidances/.

Fenech, M., 2000. The in vitro micronucleus technique. *Mutation Research - Fundamental and Molecular Mechanisms of Mutagenesis*, 455(1–2), pp.81–95.

Ferguson-Smith, A.C. et al., 1988. Regional localization of the interferon-beta 2/B-cell stimulatory factor 2/hepatocyte stimulating factor gene to human chromosome 7p15-p21. *Genomics*, 2(3), pp.203–208.

Filippi, C. et al., 2014. Toxicology of ZnO and TiO2 nanoparticles on hepatocytes: Impact on metabolism and bioenergetics. *Nanotoxicology*, 5390(November), pp.1–9. Available at: http://www.ncbi.nlm.nih.gov/pubmed/24708275.

Firdessa, R., Oelschlaeger, T. a & Moll, H., 2014. Identification of multiple cellular uptake pathways of polystyrene nanoparticles and factors affecting the uptake: relevance for drug delivery systems. *European journal of cell biology*, 93(8–9), pp.323–37. Available at: http://www.sciencedirect.com/science/article/pii/S017193351400106X.

Fischer, H.C. & Chan, W.C., 2007. Nanotoxicity: the growing need for in vivo study. *Current Opinion in Biotechnology*, 18(6), pp.565–571.

Florea, A.M., Yamoah, E.N. & Dopp, E., 2005. Intracellular calcium disturbances induced by arsenic and its methylated derivatives in relation to genomic damage and apoptosis induction. *Environmental Health Perspectives*, 113(6), pp.659–664.

Fomby, P. & Cherlin, A.J., 2011. Kinetically Controlled Cellular Interactions of Polymer-Polymer and Polymer-Liposome Nanohybrid Systems. , 72(2), pp.181–204.

Fredenberg, S. et al., 2011. The mechanisms of drug release in poly(lactic-co-glycolic acid)-based drug delivery systems - A review. *International Journal of Pharmaceutics*, 415(1–2), pp.34–52. Available at:

http://dx.doi.org/10.1016/j.ijpharm.2011.05.049.

Frohlich, E., 2012. The role of surface charge in cellular uptake and cytotoxicity of medical nanoparticles. *International Journal of Nanomedicine*, 7, pp.5577–5591.

Fröhlich, E. et al., 2014. Use of whole genome expression analysis in the toxicity screening of nanoparticles. *Toxicology and Applied Pharmacology*, 280(2), pp.272–284. Available at: http://www.sciencedirect.com/science/article/pii/S0041008X14002774.

Gabay, C. et al., 1997. Interleukin 1 Receptor Antagonist (IL-1Ra) Is an Acute-Phase Protein. , 99(12), pp.2930–2940.

Gabay, C., Lamacchia, C. & Palmer, G., 2010. IL-1 pathways in inflammation and human diseases. *Nature reviews. Rheumatology*, 6(4), pp.232–241.

Gaiser, B.K. et al., 2013. Effects of silver nanoparticles on the liver and hepatocytes in vitro. *Toxicological Sciences*, 131(2), pp.537–547.

Gaiser, B.K. et al., 2013. Effects of Titanium Dioxide Nanoparticles on the Liver and Hepatocytes in vitro. *Journal of Chemical Information and Modeling*, 53(9), pp.1689–1699.

George, S. et al., 2009. Use of a rapid cytotoxicity screening approach to engineer a safer zinc oxide nanoparticle through iron doping. *ACS Nano*, 4(1), pp.15–29.

Gerecke, C. et al., 2017. Biocompatibility and characterization of polyglycerol-based thermoresponsive nanogels designed as novel drug-delivery systems and their intracellular localization in keratinocytes. , 5390.

Gilbert, H.F., 1990. Molecular and cellular aspects of thiol-disulfide exchange. *Advances in enzymology and related areas of molecular biology*, 63, pp.69–172.

Gong, X. et al., 2015. Effect of matrine on primary human hepatocytes in vitro. *Cytotechnology*, 67(2), pp.255–265.

Grabowski, N. et al., 2015. Surface coating mediates the toxicity of polymeric nanoparticles towards human-like macrophages. *International journal of pharmaceutics*, 482(1–2), pp.75–83. Available at: http://dx.doi.org/10.1016/j.ijpharm.2014.11.042.

Grabowski, N. et al., 2013. Toxicity of surface-modified PLGA nanoparticles toward lung alveolar epithelial cells. *International Journal of Pharmaceutics*, 454(2), pp.686–694. Available at: http://dx.doi.org/10.1016/j.ijpharm.2013.05.025.

Graça, D. et al., 2017. Toxicity screening of a novel poly (methylmethacrylate) -Eudragit

nanocarrier on L929 fi broblasts. *Toxicology Letters*, 276(November 2016), pp.129–137. Available at: http://dx.doi.org/10.1016/j.toxlet.2017.05.017.

Gref, R. et al., 2000. "Stealth" corona-core nanoparticles surface modified by polyethylene glycol (PEG): Influences of the corona (PEG chain length and surface density) and of the core composition on phagocytic uptake and plasma protein adsorption. *Colloids and Surfaces B: Biointerfaces*, 18(3–4), pp.301–313.

Gregory, E.M. & Fridovich, I., 1973. Oxygen toxicity and the superoxide dismutase. *J Bacteriol*, 114(3), pp.1193–1197. Available at: http://www.ncbi.nlm.nih.gov/entrez/query.fcgi?cmd=Retrieve&db=PubMed&dopt=Citation&list_uids=4197269.

Griffith, O.W. & Meister, A., 1985. Origin and turnover of mitochondrial glutathione. *Proceedings of the National Academy of Sciences*, 82(14), pp.4668–4672.

Grynkiewicz, G., Poenie, M. & Tsien, R.Y., 1985. A new generation of Ca2+ indicators with greatly improved fluorescence properties. *Journal of Biological Chemistry*, 260(6), pp.3440–3450.

Guo, J. et al., 2011. Aptamer-functionalized PEG–PLGA nanoparticles for enhanced anti-glioma drug delivery. *Biomaterials*, 32(31), pp.8010–8020. Available at: http://linkinghub.elsevier.com/retrieve/pii/S0142961211007757.

Guy, R., L., H.R. & J., H.R., 2018. Hepatic metabolism of colloidal gold-low-density lipoprotein complexes in the rat: Evidence for bulk excretion of lysosomal contents into bile. *Hepatology*, 9(3), pp.380–392. Available at: https://doi.org/10.1002/hep.1840090307.

Haldar, K. & Uyetake, L., 1992. The movement of fluorescent endocytic tracers in Plasmodium falciparum infected erythrocytes. *Molecular and biochemical parasitology*, 50(1), pp.161–177.

Haldemann Heusler, R.C., Wight, E. & Marincek, B., 1995. Oral superparamagnetic contrast agent (ferumoxsil): tolerance and efficacy in MR imaging of gynecologic diseases. *Journal of magnetic resonance imaging : JMRI*, 5(4), pp.385–391.

Hamann, P.R. et al., 2002. Gemtuzumab ozogamicin, a potent and selective anti-CD33 antibody - Calicheamicin conjugate for treatment of acute myeloid leukemia. *Bioconjugate Chemistry*, 13(1), pp.47–58.

Han, L., Tang, C. & Yin, C., 2015. Biomaterials Dual-targeting and pH / redox-responsive multi-layered nanocomplexes for smart co-delivery of doxorubicin and siRNA.

Biomaterials, 60, pp.42–52. Available at: http://dx.doi.org/10.1016/j.biomaterials.2015.05.001.

Han, S. et al., 2015. Effects of hydrophobic core components in amphiphilic PDMAEMA nanoparticles on siRNA delivery. *Biomaterials*, 48, pp.45–55. Available at: http://dx.doi.org/10.1016/j.biomaterials.2015.01.026.

Hare, J.I. et al., 2017. Challenges and strategies in anti-cancer nanomedicine development: An industry perspective. *Advanced Drug Delivery Reviews*, 108, pp.25–38. Available at: http://dx.doi.org/10.1016/j.addr.2016.04.025.

Hatton, F.L. et al., 2014. Hyperbranched polydendrons: a new controlled macromolecular architecture with self-assembly in water and organic solvents. *Chemical Science*, 5(5), p.1844. Available at: http://xlink.rsc.org/?DOI=c4sc00360h [Accessed December 4, 2014].

He, B. et al., 2013. The transport pathways of polymer nanoparticles in MDCK epithelial cells. *Biomaterials*, 34(17), pp.4309–4326. Available at: http://dx.doi.org/10.1016/j.biomaterials.2013.01.100.

He, L. et al., 2009. In vitro evaluation of the genotoxicity of a family of novel MeO-PEG-poly(D,L-lactic-co-glycolic acid)-PEG-OMe triblock copolymer and PLGA nanoparticles. *Nanotechnology*, 20(45).

Heddle, J.A., 1973. A rapid in vivo test for chromosomal damage. *Mutation Research/Fundamental and Molecular Mechanisms of Mutagenesis*, 18(2), pp.187–190. Available at: http://www.sciencedirect.com/science/article/pii/0027510773900353.

Helma, C., Rautenberg, M. & Gebele, D., 2017. Nano-Lazar: Read across predictions for nanoparticle toxicities with calculated and measured properties. *Frontiers in Pharmacology*, 8(JUN), pp.1–11.

Hendriks, D.F.G. et al., 2016. Hepatic 3D spheroid models for the detection and study of compounds with cholestatic liability. *Scientific Reports*, 6(October), pp.1–12. Available at: http://dx.doi.org/10.1038/srep35434.

Herland, A. & Inganäs, O., 2007. Conjugated polymers as optical probes for protein interactions and protein conformations. *Macromolecular Rapid Communications*, 28(17), pp.1703–1713.

Hershfield, M.S. et al., 1987. Treatment of adenosine deaminase deficiency with polyethylene glycol-modified adenosine deaminase. *The New England journal of*

medicine, 316(10), pp.589–596.

Hickey, J.W. et al., 2015. Control of polymeric nanoparticle size to improve therapeutic delivery. *Journal of Controlled Release*, 219, pp.535–547. Available at: http://dx.doi.org/10.1016/j.jconrel.2015.10.006.

Høl, E. Kristoffersen, N. Gjerdet, A.P., Novel Nanoparticulate and Ionic Titanium Antigens for Hypersensitivity Testing.

Holmgren, A., 1979. Reduction of Disulfides by Thioredoxin. *The Journal of biological chemistry*, 254(18), pp.9113–9119.

Hoshino, Y. et al., 2012. The rational design of a synthetic polymer nanoparticle that neutralizes a toxic peptide in vivo. *Proceedings of the National Academy of Sciences of the United States of America*, 109(1), pp.33–8. Available at: http://www.pubmedcentral.nih.gov/articlerender.fcgi?artid=3252894&tool=pmcentrez&rendertype=abstract [Accessed November 27, 2014].

Huang, C. et al., 2010. Oxidative stress, calcium homeostasis, and altered gene expression in human lung epithelial cells exposed to ZnO nanoparticles. *Toxicology in vitro : an international journal published in association with BIBRA*, 24(1), pp.45–55. Available at: http://dx.doi.org/10.1016/j.tiv.2009.09.007.

Huang, K.T. et al., 2015. Titanium nanoparticle inhalation induces renal fibrosis in mice via an oxidative stress upregulated transforming growth factor-β pathway. *Chemical Research in Toxicology*, 28(3), pp.354–364.

Huang, S. et al., 2009. Disturbed mitotic progression and genome segregation are involved in cell transformation mediated by nano-TiO2 long-term exposure. *Toxicology and Applied Pharmacology*, 241(2), pp.182–194. Available at: http://dx.doi.org/10.1016/j.taap.2009.08.013.

Hühn, D. et al., 2013. Polymer-coated nanoparticles interacting with proteins and cells: Focusing on the sign of the net charge. *ACS Nano*, 7(4), pp.3253–3263.

Hussain, S.M. et al., 2005. In vitro toxicity of nanoparticles in BRL 3A rat liver cells. *Toxicology in Vitro*, 19(7), pp.975–983.

Hutter, E. & Maysinger, D., 2013. Gold-nanoparticle-based biosensors for detection of enzyme activity. *Trends in pharmacological sciences*, 34(9), pp.497–507. Available at: http://www.sciencedirect.com/science/article/pii/S0165614713001193 [Accessed November 20, 2014].

Iglesias, T., Cerain, A.L. De, et al., 2017. Evaluation of the cytotoxicity , genotoxicity

and mucus permeation capacity of several surface modi fi ed poly (anhydride) nanoparticles designed for oral drug delivery. *International Journal of Pharmaceutics*, 517(1–2), pp.67–79. Available at: http://dx.doi.org/10.1016/j.ijpharm.2016.11.059.

Iglesias, T., Irache, J.M., et al., 2017. Genotoxic evaluation of poly (anhydride) nanoparticles in the gastrointestinal tract of mice. *International Journal of Pharmaceutics*, 530(1–2), pp.187–194. Available at: http://dx.doi.org/10.1016/j.ijpharm.2017.07.066.

Iglesias, T., Dusinska, M., et al., 2017. In vitro evaluation of the genotoxicity of poly (anhydride) nanoparticles designed for oral drug delivery. *International Journal of Pharmaceutics*, 523(1), pp.418–426. Available at: http://dx.doi.org/10.1016/j.ijpharm.2017.03.016.

Iswarya, V. et al., 2016. Surface capping and size-dependent toxicity of gold nanoparticles on different trophic levels. *Environmental Science and Pollution Research*, 23(5), pp.4844–4858.

Italia, J.L. et al., 2007. PLGA nanoparticles for oral delivery of cyclosporine: Nephrotoxicity and pharmacokinetic studies in comparison to Sandimmune Neoral®. *Journal of Controlled Release*, 119(2), pp.197–206.

Iversen, T.G., Skotland, T. & Sandvig, K., 2011. Endocytosis and intracellular transport of nanoparticles: Present knowledge and need for future studies. *Nano Today*, 6(2), pp.176–185. Available at: http://dx.doi.org/10.1016/j.nantod.2011.02.003.

James, N.D. et al., 1994. Liposomal doxorubicin (Doxil): an effective new treatment for Kaposi's sarcoma in AIDS. *Clinical oncology (Royal College of Radiologists (Great Britain))*, 6(5), pp.294–296.

Jemnitz, K., Bátai-Konczos, A., et al., 2017. A transgenic rat hepatocyte - Kupffer cell co-culture model for evaluation of direct and macrophage-related effect of poly(amidoamine) dendrimers. *Toxicology in Vitro*, 38, pp.159–169.

Jemnitz, K., Bï¿½tai-Konczos, A., et al., 2017. A transgenic rat hepatocyte - Kupffer cell co-culture model for evaluation of direct and macrophage-related effect of poly(amidoamine) dendrimers. *Toxicology in Vitro*, 38(November), pp.159–169.

JH, K., 1994. Permanent human hepatocyte cell line and its use in a liver assist device (LAD). , 209(19), pp.365–380.

Jiang, L. et al., 2013. Cellular uptake mechanism and intracellular fate of hydrophobically

modified pullulan nanoparticles. *International Journal of Nanomedicine*, 8, pp.1825–1834.

Jin, H. et al., 2017. EGFR-targeting PLGA-PEG nanoparticles as a curcumin delivery system for breast cancer therapy. *Nanoscale*, 9(42), pp.16365–16374. Available at: http://xlink.rsc.org/?DOI=C7NR06898K.

Jin, H.J. et al., 2000. Thermal and mechanical properties of mandelic acid-copolymerized poly(butylene succinate) and poly(ethylene adipate). *Journal of Polymer Science, Part B: Polymer Physics*, 38(11), pp.1504–1511.

Jin, P. et al., 2012. Interactions between Al12X (X = Al, C, N and P) nanoparticles and DNA nucleobases/base pairs: Implications for nanotoxicity. *Journal of Molecular Modeling*, 18(2), pp.559–568.

Johnston, H. et al., 2015. Mechanism of neutrophil activation and toxicity elicited by engineered nanomaterials. *Toxicology in Vitro*, 29(5), pp.1172–1184. Available at: http://linkinghub.elsevier.com/retrieve/pii/S0887233315000922.

Johnston, H.J. et al., 2018. Adoption of in vitro systems and zebrafish embryos as alternative models for reducing rodent use in assessments of immunological and oxidative stress responses to nanomaterials. *Critical Reviews in Toxicology*, 48(3), pp.252–271. Available at: https://doi.org/10.1080/10408444.2017.1404965.

Johnston, H.J. et al., 2010. Evaluating the uptake and intracellular fate of polystyrene nanoparticles by primary and hepatocyte cell lines in vitro. *Toxicology and Applied Pharmacology*, 242(1), pp.66–78. Available at: http://www.ncbi.nlm.nih.gov/pubmed/19799923 [Accessed December 5, 2014].

Johnston, H.J. et al., 2015. Exploring the cellular and tissue uptake of nanomaterials in a range of biological samples using multimodal nonlinear optical microscopy. *Nanotechnology*, 26(50), p.505102. Available at: http://www.ncbi.nlm.nih.gov/pubmed/26584818.

De Jong, W.H. et al., 2013. Systemic and immunotoxicity of silver nanoparticles in an intravenous 28 days repeated dose toxicity study in rats. *Biomaterials*, 34(33), pp.8333–8343. Available at: http://dx.doi.org/10.1016/j.biomaterials.2013.06.048.

Joshi-Barve, S. et al., 2007. Palmitic acid induces production of proinflammatory cytokine interleukin-8 from hepatocytes. *Hepatology*, 46(3), pp.823–830.

Kadiiska, M.B. et al., 1996. Iron supplementation generates hydroxyl radical in vivo. *J Clin invest*, 98(4), pp.1966–1970.

Kakde, D. et al., 2016. Synthesis, characterization and evaluation of in vitro toxicity in hepatocytes of linear polyesters with varied aromatic and aliphatic co-monomers. *Journal of Controlled Release*, 244.

Kanakia, S. et al., 2014. Dose ranging, expanded acute toxicity and safety pharmacology studies for intravenously administered functionalized graphene nanoparticle formulations. *Biomaterials*, 35(25), pp.7022–7031. Available at: http://dx.doi.org/10.1016/j.biomaterials.2014.04.066.

Kanaras, A.G. et al., 2002. Thioalkylated tetraethylene glycol: A new ligand for water soluble monolayer protected gold clusters. *Chemical Communications*, 20, pp.2294–2295.

Kasper, J. et al., 2013. Interactions of silica nanoparticles with lung epithelial cells and the association to flotillins. *Archives of Toxicology*, 87(6), pp.1053–1065.

Kataoka, K., Harada, A. & Nagasaki, Y., 2001. Block copolymer micelles for drug delivery: Design, characterization and biological significance. *Advanced Drug Delivery Reviews*, 47(1), pp.113–131.

Kazimirova, A. et al., 2012. Genotoxicity testing of PLGA?PEO nanoparticles in TK6 cells by the comet assay and the cytokinesis-block micronucleus assay. *Mutation Research/Genetic Toxicology and Environmental Mutagenesis*, 748(1–2), pp.42–47. Available at: http://dx.doi.org/10.1016/j.mrgentox.2012.06.012.

Ke, X. et al., 2014. Role of non-covalent and covalent interactions in cargo loading capacity and stability of polymeric micelles. *Journal of Controlled Release*, 193, pp.9–26. Available at: http://dx.doi.org/10.1016/j.jconrel.2014.06.061.

Kemal, E. et al., 2017. Bright, near infrared emitting PLGA–PEG dye-doped CN-PPV nanoparticles for imaging applications. *RSC Adv.*, 7(25), pp.15255–15264. Available at: http://xlink.rsc.org/?DOI=C6RA25004A.

Kermanizadeh, A., Gaiser, B.K., et al., 2012. An in vitro liver model--assessing oxidative stress and genotoxicity following exposure of hepatocytes to a panel of engineered nanomaterials. *Particle and fibre toxicology*, 9(1), p.28. Available at: http://www.pubmedcentral.nih.gov/articlerender.fcgi?artid=3546021&tool=pmcentrez&rendertype=abstract [Accessed November 27, 2014].

Kermanizadeh, A., Pojana, G., et al., 2012. Assessment of Engineered Nanomaterials Using a Hepatocyte Cell Line: Cytotoxicity, Pro-Inflammatory Cytokines and Functional Markers. *Nanotoxicology*, 7(May), pp.1–13. Available at:

http://www.ncbi.nlm.nih.gov/pubmed/22263564 [Accessed December 2, 2014].

Kermanizadeh, A. et al., 2014. Hepatic toxicology following single and multiple exposure of engineered nanomaterials utilising a novel primary human 3D liver microtissue model. *Particle and Fibre Toxicology*, 11(1), p.56. Available at: http://www.particleandfibretoxicology.com/content/11/1/56.

Kermanizadeh, A., Pojana, G., et al., 2013. *In vitro* assessment of engineered nanomaterials using a hepatocyte cell line: cytotoxicity, pro-inflammatory cytokines and functional markers. *Nanotoxicology*, 7(3), pp.301–313. Available at: http://www.tandfonline.com/doi/full/10.3109/17435390.2011.653416.

Kermanizadeh, A. et al., 2015. Nanomaterial translocation–the biokinetics, tissue accumulation, toxicity and fate of materials in secondary organs–a review. *Critical Reviews in Toxicology*, 45(10), pp.837–872. Available at: https://doi.org/10.3109/10408444.2015.1058747.

Kermanizadeh, A., Gaiser, B.K., et al., 2013. Primary human hepatocytes versus hepatic cell line: assessing their suitability for in vitro nanotoxicology. *Nanotoxicology*, 7(7), pp.1255–71. Available at: http://www.ncbi.nlm.nih.gov/pubmed/23009365.

Khalil, N.M. et al., 2013. Pharmacokinetics of curcumin-loaded PLGA and PLGA-PEG blend nanoparticles after oral administration in rats. *Colloids and Surfaces B: Biointerfaces*, 101, pp.353–360. Available at: http://dx.doi.org/10.1016/j.colsurfb.2012.06.024.

Khanbeigi, R.A. et al., 2015. Interactions of stealth conjugated polymer nanoparticles with human whole blood. *J. Mater. Chem. B*, 3(12), pp.2463–2471. Available at: http://xlink.rsc.org/?DOI=C4TB01822B.

Kim, D.H. et al., 2007. Response of monocytes exposed to phagocytosable particles and discs of comparable surface roughness. *Biomaterials*, 28(29), pp.4231–4239.

Kim, D.W. et al., 2007. Multicenter phase II trial of Genexol-PM, a novel Cremophor-free, polymeric micelle formulation of paclitaxel, with cisplatin in patients with advanced non-small-cell lung cancer. *Annals of Oncology*, 18(12), pp.2009–2014.

Kim, J.Y. et al., 2010. In-vivo tumor targeting of pluronic-based nano-carriers. *Journal of Controlled Release*, 147(1), pp.109–117. Available at: http://dx.doi.org/10.1016/j.jconrel.2010.06.010.

Kim, T.Y. et al., 2004. Phase I and pharmacokinetic study of Genexol-PM, a Cremophor-free, polymeric micelle-formulated paclitaxel, in patients with advanced

malignancies. *Clinical Cancer Research*, 10(11), pp.3708–3716.

Kirsch-Volders, M. & Fenech, M., 2001. Inclusion of micronuclei in non-divided mononuclear lymphocytes and necrosis/apoptosis may provide a more comprehensive cytokinesis block micronucleus assay for biomonitoring purposes. *Mutagenesis*, 16(1), pp.51–58.

Klapetek, P. et al., 2011. Atomic force microscopy analysis of nanoparticles in non-ideal conditions. *Nanoscale Research Letters*, 6(1), p.514.

Kocbek, P. et al., 2007. Targeting cancer cells using PLGA nanoparticles surface modified with monoclonal antibody. *Journal of Controlled Release*, 120(1–2), pp.18–26.

Kohl, Y. et al., 2011. Preparation and biological evaluation of multifunctional PLGA-nanoparticles designed for photoacoustic imaging. *Nanomedicine: Nanotechnology, Biology, and Medicine*, 7(2), pp.228–237. Available at: http://dx.doi.org/10.1016/j.nano.2010.07.006.

Kong, B. et al., 2011. Experimental considerations on the cytotoxicity of nanoparticles. *Nanomedicine (London, England)*, 6(5), pp.929–941.

Koole, R. et al., 2008. Paramagnetic Lipid-Coated Silica Nanoparticles with a Fluorescent Quantum Dot Core: A New Contrast Agent Platform for Multimodality Imaging. *Proceedings 16th Scientific Meeting, International Society for Magnetic Resonance in Medicine*, Toronto, p.480. Available at: /MyPathway2008/0480.

Kreyling, W.G. et al., 2014. Air-blood barrier translocation of tracheally instilled gold nanoparticles inversely depends on particle size. *ACS Nano*, 8(1), pp.222–233.

Kreyling, W.G. et al., 2002. Translocation of ultrafine insoluble iridium particles from extrapulmonary organs is size dependent but very. *Journal of Toxicology and Environmental Health*, 65(20), pp.1513–1530.

Kung, M. ang et al., 2015. Enhanced reactive oxygen species overexpression by CuO nanoparticles in poorly differentiated hepatocellular carcinoma cells. *Nanoscale*, 7(5), pp.1820–1829. Available at: http://xlink.rsc.org/?DOI=C4NR05843G.

Labhasetwar, J.P. and V., 2002. Dynamics of Endocytosis and Exocytosis of Poly(D,L-Lactide-co-Glycolide) Nanoparticles in Vascular Smooth Muscle Cells. *Pharmaceutical Research*, 1621(June 2014), pp.36–43.

Lamacchia, C. et al., 2012. Mice deficient in hepatocyte-specific IL-1Ra show delayed resolution of concanavalin A-induced hepatitis. *European Journal of Immunology*,

42(5), pp.1294–1303.

Lammel, T. et al., 2013. Internalization and cytotoxicity of graphene oxide and carboxyl graphene nanoplatelets in the human hepatocellular carcinoma cell line Hep G2. *Particle and fibre toxicology*, 10(1), p.27. Available at: http://www.ncbi.nlm.nih.gov/pubmed/23849434.

Larsen, C.G. et al., 1989. Production of interleukin-8 by human dermal fibroblasts and keratinocytes in response to interleukin-1 or tumour necrosis factor. *Immunology*, 68(1), pp.31–6. Available at: http://www.pubmedcentral.nih.gov/articlerender.fcgi?artid=1385501&tool=pmcentrez&rendertype=abstract.

Larsen, M.T. et al., 2016. Albumin-based drug delivery: harnessing nature to cure disease. *Molecular and Cellular Therapies*, 4(1), p.3. Available at: http://www.molcelltherapies.com/content/4/1/3.

Laskin, J.J. & Sandler, A.B., 2004. Epidermal growth factor receptor: a promising target in solid tumours. *Cancer Treatment Reviews*, 30(1), pp.1–17. Available at: http://www.sciencedirect.com/science/article/pii/S0305737203002020.

Lazarovits, J. et al., 2014. Nanoparticle-blood interactions: the implications on solid tumour targeting. *Chemical communications (Cambridge, England)*, 51, pp.2756–2767. Available at: http://www.ncbi.nlm.nih.gov/pubmed/25502284.

Lee, E. et al., 2004. Use of the Tail Moment of the Lymphocytes to Evaluate DNA Damage in Human Biomonitoring Studies. , 132, pp.121–132.

Lee, F.Y. et al., 1989. Heterogeneity of glutathione content in human ovarian cancer. *Cancer research*, 49(19), pp.5244–5248.

Lehner, R. et al., 2012. Designing switchable nanosystems for medical application. *Journal of Controlled Release*, 161(2), pp.307–316. Available at: http://dx.doi.org/10.1016/j.jconrel.2012.04.040.

Leifeld, L. et al., 2002. Imbalanced intrahepatic expression of interleukin 12, interferon gamma, and interleukin 10 in fulminant hepatitis B. *Hepatology*, 36(4I), pp.1001–1008.

Lepedda, A.J. et al., 2014. Human Serum Albumin Cys 34 Oxidative Modifications following Infiltration in the Carotid Atherosclerotic Plaque. *Oxidative Medicine and Cellular Longevity*, 2014.

Leroueil, P.R. et al., 2008. Wide varieties of cationic nanoparticles induce defects in

supported lipid bilayers. *Nano Letters*, 8(2), pp.420–424.

Li, C. et al., 2014. Novel designed polyoxyethylene nonionic surfactant with improved safety and efficiency for anticancer drug delivery. , pp.2089–2100.

Li, G. et al., 2011. Polymeric micelles with water-insoluble drug as hydrophobic moiety for drug delivery. *Biomacromolecules*, 12(6), pp.2016–2026.

Li, K. et al., 2017. Incorporation of cerium oxide into hydroxyapatite coating regulates osteogenic activity of mesenchymal stem cell and macrophage polarization. *Journal of Biomaterials Applications*, 31(7), pp.1062–1076.

Li, N., Andre Nel, Tian Xia, Lutz Madler, N.L. & Li, N., 2006. Toxic Potential of Materials at the Nanolevel. , (February 2006), pp.622–628.

Lin, P.C. et al., 2006. Ethylene glycol-protected magnetic nanoparticles for a multiplexed immunoassay in human plasma. *Small*, 2(4), pp.485–489.

Liu, Y. et al., 2016. Copper nanoclusters trigger muscle cell apoptosis and atrophy in vitro and in vivo. *Journal of Applied Toxicology*, 36(3), pp.454–463.

Luo, C. et al., 2016. Self-Assembled Redox Dual-Responsive Prodrug-Nanosystem Formed by Single Thioether-Bridged Paclitaxel-Fatty Acid Conjugate for Cancer Chemotherapy. *Nano Letters*, 25(4), pp.368–379.

Ma, Y., Sadoqi, M. & Shao, J., 2012. Biodistribution of indocyanine green-loaded nanoparticles with surface modifications of PEG and folic acid. *International Journal of Pharmaceutics*, 436(1–2), pp.25–31. Available at: http://dx.doi.org/10.1016/j.ijpharm.2012.06.007.

Mahaling, B. & Katti, D.S., 2016. Understanding the influence of surface properties of nanoparticles and penetration enhancers for improving bioavailability in eye tissues in vivo. *International Journal of Pharmaceutics*. Available at: http://linkinghub.elsevier.com/retrieve/pii/S0378517316300539.

Mahmoud, E. & Wooley, K.L., 2013. Cytokines as biomarkers of nanoparticle immunotoxicity. *Chem Soc Rev. 2013*, 48(S), pp.5552–55766. Available at: http://xlink.rsc.org/?DOI=c3cs60064e.

Maiolino, S. et al., 2015. Biodegradable nanoparticles sequentially decorated with Polyethyleneimine and Hyaluronan for the targeted delivery of docetaxel to airway cancer cells. *Journal of Nanobiotechnology*, 13(1), pp.1–13. Available at: http://www.jnanobiotechnology.com/content/13/1/29.

Mao, C.Q. et al., 2011. A biodegradable amphiphilic and cationic triblock copolymer for

the delivery of siRNA targeting the acid ceramidase gene for cancer therapy. *Biomaterials*, 32(11), pp.3124–3133. Available at: http://dx.doi.org/10.1016/j.biomaterials.2011.01.006.

Marino, M.W. et al., 1997. Characterization of tumor necrosis factor-deficient mice. *Proceedings of the National Academy of Sciences*, 94(15), pp.8093–8098. Available at: http://www.pnas.org/cgi/doi/10.1073/pnas.94.15.8093.

Matsumura, Y. & Maeda, H., 1986. A new concept for macromolecular therapeutics in cnacer chemotherapy: mechanism of tumoritropic accumulatio of proteins and the antitumor agents Smancs. *Cancer research*, 46(12 Pt 1), pp.6387–6392.

Maynard, A.D. et al., 2006. Safe handling of nanotechnology. *Nature*, 444(7117), pp.267–269.

Maynard, A.D. & Aitken, R.J., 2016. "Safe handling of nanotechnology" ten years on. *Nature Nanotechnology*, 11(12), pp.998–1000. Available at: http://dx.doi.org/10.1038/nnano.2016.270.

Mei, L. et al., 2009. A novel docetaxel-loaded poly (ε-caprolactone)/Pluronic F68 nanoparticle overcoming multidrug resistance for breast cancer treatment. *Nanoscale Research Letters*, 4(12), pp.1530–1539.

Meindl, C. et al., 2015. Intracellular calcium levels as screening tool for nanoparticle toxicity. *Journal of Applied Toxicology*, 35(10), pp.1150–1159.

Mendoza, A. et al., 2014. Silica nanoparticles induce oxidative stress and inflammation of human peripheral blood mononuclear cells. *Cell stress & chaperones*, 19(6), pp.777–790.

Menemse KIREMITCI-GUMDERELGLU, G.D., 1999. Synthesis , Characterization and in Vitro Degradation of Poly (DL-Lactide)/ Poly (DL-Lactide-co-Glycolide). *Turkish Journal of Chemistry*, 23, pp.153–161.

Michael E. Werner, Natalie D. Cummings, Manish Sethi, E.C. & Wang, Rohit Sukumar, Dominic T. Moore, and A.Z.W., 2013. Preclinical Evaluation of Genexol-PM, a Nanoparticle Formulation of Paclitaxel, as a Novel Radiosensitizer for the Treatment of Non-Small Cell Lung Cancer. *Int J Radiat Oncol Biol Phys.*, 141(4), pp.520–529.

Milkiewicz, P. et al., 2002. Pathobiology and experimental therapeutics in hepatocellular cholestasis : lessons from the hepatocyte couplet model. , 614, pp.603–614.

Mittal, G. et al., 2007. Estradiol loaded PLGA nanoparticles for oral administration: Effect of polymer molecular weight and copolymer composition on release behavior

in vitro and in vivo. *Journal of Controlled Release*, 119(1), pp.77–85.

Moghimi, S.M. et al., 2004. Causative factors behind poloxamer 188 (Pluronic F68, Flocor)- induced complement activation in human sera. A protective role against poloxamer-mediated complement activation by elevated serum lipoprotein levels. *Biochimica et Biophysica Acta - Molecular Basis of Disease*, 1689(2), pp.103–113.

Moghimi, S.M. et al., 1994. Surface engineered nanospheres with enhanced drainage into lymphatics and uptake by macrophages of the regional lymph nodes. *FEBS Letters*, 344(1), pp.25–30.

Moles, A. et al., 2014. A TLR2/S100A9/CXCL-2 signaling network is necessary for neutrophil recruitment in acute and chronic liver injury in the mouse. *Journal of Hepatology*, 60(4), pp.782–791. Available at: http://dx.doi.org/10.1016/j.jhep.2013.12.005.

Molina, D.K. & DiMaio, V.J.M., 2012. Normal Organ Weights in Men: Part II—The Brain, Lungs, Liver, Spleen, and Kidneys. *The American Journal of Forensic Medicine and Pathology*, 33(4). Available at: http://journals.lww.com/amjforensicmedicine/Fulltext/2012/12000/Normal_Organ_Weights_in_Men__Part_II_The_Brain,.22.aspx.

Möller, W. et al., 2005. Ultrafine particles cause cytoskeletal dysfunctions in macrophages: role of intracellular calcium. *Particle and fibre toxicology*, 2, p.7. Available at: http://www.pubmedcentral.nih.gov/articlerender.fcgi?artid=1262770&tool=pmcentrez&rendertype=abstract [Accessed December 4, 2014].

Morales, M.A. et al., 2005. Magnetic studies of iron oxide nanoparticles coated with oleic acid and Pluronic block copolymer. *Journal of Applied Physics*, 97(10), pp.2005–2008.

Moreno, D. et al., 2010. Pharmacodynamics of cisplatin-loaded PLGA nanoparticles administered to tumor-bearing mice. *European Journal of Pharmaceutics and Biopharmaceutics*, 74(2), pp.265–274. Available at: http://dx.doi.org/10.1016/j.ejpb.2009.10.005.

Mu, Q. et al., 2012. Mechanism of cellular uptake of genotoxic silica nanoparticles. *Particle and Fibre Toxicology*, 9(1), p.29. Available at: http://particleandfibretoxicology.biomedcentral.com/articles/10.1186/1743-8977-9-29.

Muller, R.H. et al., 1997. Influence of fluorescent labelling of polystyrene particles on phagocytic uptake, surface hydrophobicity, and plasma protein adsorption. *Pharmaceutical research*, 14(1), pp.18–24.

Muñoz-Barroso, I. et al., 1998. Dilation of the human immunodeficiency virus-1 envelope glycoprotein fusion pore revealed by the inhibitory action of a synthetic peptide from gp41. *Journal of Cell Biology*, 140(2), pp.315–323.

Mura, S. et al., 2011. Influence of surface charge on the potential toxicity of PLGA nanoparticles towards Calu-3 cells. *International journal of nanomedicine*, 6, pp.2591–2605.

Mura, S. & Couvreur, P., 2012. Nanotheranostics for personalized medicine. *Advanced drug delivery reviews*, 64(13), pp.1394–416. Available at: http://www.ncbi.nlm.nih.gov/pubmed/22728642 [Accessed December 4, 2014].

Murali, K. et al., 2015. Uptake and bio-reactivity of polystyrene nanoparticles is affected by surface modifications, ageing and LPS adsorption: in vitro studies on neural tissue cells. *Nanoscale*, 7, pp.4199–4210. Available at: http://xlink.rsc.org/?DOI=C4NR06849A.

Muthu, M.S. et al., 2014. Nanotheranostics - application and further development of nanomedicine strategies for advanced theranostics. *Theranostics*, 4(6), pp.660–677.

Nadine Voigt, Petra Henrich-Noack,Sarah Kockentiedt, Werner Hintz, Jürgen Tomas, B.A.S., 2014. Toxicity of polymeric nanoparticles in vivo and in vitro Nadine. , 2(2), pp.1–22.

Narayanan, K. et al., 2013. Mimicking cellular transport mechanism in stem cells through endosomal escape of new peptide-coated quantum dots. *Scientific reports*, 3, p.2184. Available at: http://www.pubmedcentral.nih.gov/articlerender.fcgi?artid=3711047&tool=pmcentrez&rendertype=abstract.

Natanson, C. et al., 1989. Endotoxin and tumor necrosis factor challenges in dogs simulate the cardiovascular profile of human septic shock. *The Journal of experimental medicine*, 169(3), pp.823–832.

Natarajan, V. et al., 2015. Titanium dioxide nanoparticles trigger loss of function and perturbation of mitochondrial dynamics in primary hepatocytes. *PLoS ONE*, 10(8), pp.1–19.

Negrin, K.A. et al., 2014. IL-1 Signaling in obesity-induced hepatic lipogenesis and

steatosis. *PLoS ONE*, 9(9).

Neubig, R.R. et al., 2003. International Union of Pharmacology Committee on Receptor Nomenclature and Drug Classification . XXXVIII . Update on Terms and Symbols in Quantitative Pharmacology. , 55(4), pp.597–606.

Nicolete, R., Santos, D.F. Dos & Faccioli, L.H., 2011. The uptake of PLGA micro or nanoparticles by macrophages provokes distinct in vitro inflammatory response. *International Immunopharmacology*, 11(10), pp.1557–1563. Available at: http://dx.doi.org/10.1016/j.intimp.2011.05.014.

Niculescu-Duvaz, I., 2000. Technology evaluation: gemtuzumab ozogamicin, Celltech Group. *Current opinion in molecular therapeutics*, 2(6), pp.691–696.

Nie, S. et al., 2011. Thermoreversible pluronic® F127-based hydrogel containing liposomes for the controlled delivery of paclitaxel: In vitro drug release, cell cytotoxicity, and uptake studies. *International Journal of Nanomedicine*, 6(1), pp.151–166.

Nie, Y. et al., 2012. Investigation of PEG-PLGA-PEG Nanoparticles-based Multipolyplexes for IL-18 Gene Delivery. *Journal of Biomaterials Applications*, 26(8), pp.893–916.

Niemirowicz, K. et al., 2016. Magnetic nanoparticles as a drug delivery system that enhance fungicidal activity of polyene antibiotics. *Nanomedicine: Nanotechnology, Biology, and Medicine*, 12(8), pp.2395–2404.

Nocito, L. et al., 2015. The extracellular redox state modulates mitochondrial function, gluconeogenesis, and glycogen synthesis in murine hepatocytes. *PLoS ONE*, 10(3), pp.1–17.

Norris, C.A. et al., 2014. Synthesis of IL-6 by hepatocytes is a normal response to common hepatic stimuli. *PLoS ONE*, 9(4), pp.1–14.

O'Neal, D.P. et al., 2004. Photo-thermal tumor ablation in mice using near infrared-absorbing nanoparticles. *Cancer Letters*, 209(2), pp.171–176.

Oberdörster, G., Stone, V. & Donaldson, K., 2007. Toxicology of nanoparticles: A historical perspective. *Nanotoxicology*, 1(1), pp.2–25. Available at: http://informahealthcare.com/doi/abs/10.1080/17435390701314761 [Accessed October 31, 2014].

OECD, 2015. *Guidance Document on Revisions to OECD Genetic Toxicology Test Guidelines*,

Ogawara, K. ichi et al., 2001. Surface hydrophobicity of particles is not necessarily the most important determinant in their in vivo disposition after intravenous administration in rats. *Journal of Controlled Release*, 77(3), pp.191–198.

Ohkawa, H., Ohishi, N. & Yagi, K., 1979. Assay for lipid peroxides in animal tissues by thiobarbituric acid reaction. *Analytical Biochemistry*, 95(2), pp.351–358. Available at: http://www.sciencedirect.com/science/article/pii/0003269779907383.

Oliveira, E. et al., 2013. Synthesis of functionalized fluorescent silver nanoparticles and their toxicological effect in aquatic environments (Goldfish) and HEPG2 cells. *Frontiers in Chemistry*, 1(December), pp.1–11. Available at: http://journal.frontiersin.org/article/10.3389/fchem.2013.00029/abstract.

De Oliveira Tiera, V.A., Winnik, F.M. & Tiera, M.J., 2010. Interaction of amphiphilic derivatives of chitosan with DPPC (1,2-dipalmitoyl-sn-glycero-3-phosphocholine). *Journal of Thermal Analysis and Calorimetry*, 100(1), pp.309–313.

Owens, D.E. & Peppas, N. a., 2006. Opsonization, biodistribution, and pharmacokinetics of polymeric nanoparticles. *International Journal of Pharmaceutics*, 307(1), pp.93–102.

Pamujula, S. et al., 2012. Cellular delivery of PEGylated PLGA nanoparticles. *Journal of Pharmacy and Pharmacology*, 64(1), pp.61–67. Available at: https://www.ncbi.nlm.nih.gov/pmc/articles/PMC3319145/pdf/nihms-365512.pdf.

Pan, T.L. et al., 2012. Toxicological effects of cationic nanobubbles on the liver and kidneys: Biomarkers for predicting the risk. *Food and Chemical Toxicology*, 50(11), pp.3892–3901. Available at: http://dx.doi.org/10.1016/j.fct.2012.07.005.

Park, E.-J. & Park, K., 2009. Oxidative stress and pro-inflammatory responses induced by silica nanoparticles in vivo and in vitro. *Toxicology letters*, 184(1), pp.18–25. Available at: http://www.ncbi.nlm.nih.gov/pubmed/19022359 [Accessed December 9, 2014].

Park, E.J. et al., 2010. Repeated-dose toxicity and inflammatory responses in mice by oral administration of silver nanoparticles. *Environmental Toxicology and Pharmacology*, 30(2), pp.162–168. Available at: http://dx.doi.org/10.1016/j.etap.2010.05.004.

Pelaz, B. et al., 2015. Surface Functionalization of Nanoparticles with Polyethylene Glycol : E ff ects on Protein Adsorption and Cellular Uptake. , (7), pp.6996–7008.

Peracchia, M.T. et al., 1999. Stealth(®) PEGylated polycyanoacrylate nanoparticles for

intravenous administration and splenic targeting. *Journal of Controlled Release*, 60(1), pp.121–128.

Petri, B. et al., 2007. Chemotherapy of brain tumour using doxorubicin bound to surfactant-coated poly(butyl cyanoacrylate) nanoparticles: Revisiting the role of surfactants. *Journal of Controlled Release*, 117(1), pp.51–58.

Petros, R.A. et al., 2008. Reductively Labile PRINT Particles for the Delivery of Doxorubicin to HeLa Cells Reductively Labile PRINT Particles for the Delivery of Doxorubicin to HeLa Cells. , pp.2–4.

Phan, U.T., Arunachalam, B. & Cresswell, P., 2000. Gamma-interferon-inducible lysosomal thiol reductase (GILT): Maturation, activity, and mechanism of action. *Journal of Biological Chemistry*, 275(34), pp.25907–25914.

Platel, A. et al., 2016. Influence of the surface charge of PLGA nanoparticles on their in vitro genotoxicity, cytotoxicity, ROS production and endocytosis. *Journal of Applied Toxicology*, 36(3), pp.434–444.

Potočnik, J., 2011. Commission recommendation of 18 October 2011 on the definition of nanomaterial (2011/696/EU). *Official Journal of the European Union*, L275(June 2010), pp.38–40. Available at: http://scholar.google.com/scholar?q=related:iil0s0ZcGaYJ:scholar.google.com/&hl=en&num=20&as_sdt=0,5%5Cnfile:///Files/4B/4B0B3AFC-1EB5-44E3-B57E-E37E737BF1D0.pdf.

Qian, J. et al., 2010. Carboxyl-functionalized and bio-conjugated silica-coated quantum dots as targeting probes for cell imaging. *Journal of Nanoscience and Nanotechnology*, 10(3), pp.1668–75. Available at: http://www.ncbi.nlm.nih.gov/pubmed/20355555.

Qiu, L. et al., 2013. Phagocytic uptake and ROS-mediated cytotoxicity in human hepatic cell line of amphiphilic polyphosphazene nanoparticles. *Journal of Biomedical Materials Research - Part A*, 101 A(1), pp.285–297.

Qu, Y. et al., 2017. Oligosaccharide nanomedicine of alginate sodium improves therapeutic results of posterior lumbar interbody fusion with cages for degenerative lumbar disease in osteoporosis patients by downregulating serum miR-155. , pp.8459–8469.

Racanelli, V. & Rehermann, B., 2006. The liver as an immunological organ. *Hepatology*, 43(2 SUPPL. 1).

Racine-Samson, L. et al., 1996. The metabolic organization of the adult human liver: a comparative study of normal, fibrotic, and cirrhotic liver tissue. *Hepatology (Baltimore, Md.)*, 24(1), pp.104–113. Available at: http://www.ncbi.nlm.nih.gov/pubmed/8707247.

Radwan, M.A. et al., 2017. Oral administration of amphotericin B nanoparticles: Antifungal activity, bioavailability and toxicity in rats. *Drug Delivery*, 24(1), pp.40–50.

Raghavendra S. Navath1, 2, Yunus E. Kurtoglu1, Bing Wang2, 3, Sujatha Kannan3, R. & Romero2, and Rangaramanujam M. Kannan1, 2, 2008. Dendrimers-drug conjugates for tailored intracellular drug release based on glutathione levels. , 6(12), pp.247–253.

Rehder, D.S. & Borges, C.R., 2010. Cysteine sulfenic acid as an intermediate in disulfide bond formation and nonenzymatic protein folding. *Biochemistry*, 49(35), pp.7748–7755.

Reich, G., 1997. In Vitro Stability of Poly(D,L-lactide) and Poly(D,L-lactide)/Poloxamer Nanoparticles in Gastrointestinal Fluids. *Drug Development and Industrial Pharmacy*, 23(12), pp.1191–1200. Available at: https://doi.org/10.3109/03639049709146156.

Rennukka, M., Sipaut, C.S. & Amirul, A.A., 2014. Synthesis of poly(3-hydroxybutyrate-co-4-hydroxybutyrate)/chitosan/silver nanocomposite material with enhanced antimicrobial activity. *Biotechnology Progress*, 30(6), pp.1469–1479.

Renz, P. et al., 2016. Imaging of Polymeric Nanoparticles : Hard Challenge for Soft Objects. , pp.1879–1885.

Rimai, D.S., Quesnel, D.J. & Busnaina, A.A., 2000. The adhesion of dry particles in the nanometer to micrometer-size range. *Colloids and Surfaces A: Physicochemical and Engineering Aspects*, 165(1–3), pp.3–10.

Robbens, J. et al., 2010. Eco-, geno- and human toxicology of bio-active nanoparticles for biomedical applications. *Toxicology*, 269(2–3), pp.170–181.

Rojas, E., López, M. & Valverde, M., 1999. Single cell gel electrophoresis assay: Methodology and applications. *Journal of Chromatography B: Biomedical Sciences and Applications*, 722(1–2), pp.225–254.

Rota, C., Chignell, C.F. & Mason, R.P., 1999. Evidence for free radical formation during the oxidation of 2′-7′-dichlorofluorescin to the fluorescent dye 2′-7′-

dichlorofluorescein by horseradish peroxidase:Possible implications for oxidative stress measurements. *Free Radical Biology and Medicine*, 27(7–8), pp.873–881.

Rots, M.G. et al., 2003. Targeted cancer gene therapy: The flexibility of adenoviral gene therapy vectors. *Journal of Controlled Release*, 87(1–3), pp.159–165.

Ruge, C.A. et al., 2012. The interplay of lung surfactant proteins and lipids assimilates the macrophage clearance of nanoparticles. *PLoS ONE*, 7(7).

Russo, A. et al., 1986. Selective modulation of glutathione levels in human normal versus tumor cells and subsequent differential response to chemotherapy drugs. *Cancer research*, 46(6), pp.2845–8. Available at: http://www.ncbi.nlm.nih.gov/pubmed/2421885.

Sahay, G., Alakhova, D.Y. & Kabanov, A. V, 2010. Endocytosis of Nanomedicine. *Journal of Controlled Release*, 145(3), pp.182–195.

Saklatvala, J. & Dingle, J.T., 1980. Identification of catabolin, a protein fro synovium which induces degradation of cartilage in organ culture. *Biochemical and biophysical research communications*, 96(3), pp.1225–1231.

Santander-Ortega, M.J. et al., 2006. Colloidal stability of Pluronic F68-coated PLGA nanoparticles: A variety of stabilisation mechanisms. *Journal of Colloid and Interface Science*, 302(2), pp.522–529.

Santos, D.M. et al., 2013. PLGA nanoparticles loaded with KMP-11 stimulate innate immunity and induce the killing of Leishmania. *Nanomedicine: Nanotechnology, Biology, and Medicine*, 9(7), pp.985–995. Available at: http://dx.doi.org/10.1016/j.nano.2013.04.003.

Sato, K. et al., 2002. In vivo lipid-derived free radical formation by NADPH oxidase in acute lung injury induced by lipopolysaccharide: a model for ARDS. *The FASEB Journal*, 16(13), pp.1713–1720. Available at: https://doi.org/10.1096/fj.02-0331com.

Sato, Y. et al., 2017. Highly specific delivery of siRNA to hepatocytes circumvents endothelial cell-mediated lipid nanoparticle-associated toxicity leading to the safe and efficacious decrease in the hepatitis B virus. *Journal of Controlled Release*, 266(October), pp.216–225. Available at: https://doi.org/10.1016/j.jconrel.2017.09.044.

Schaeublin, N.M. et al., 2012. Does shape matter? Bioeffects of gold nanomaterials in a human skin cell model. *Langmuir*, 28(6), pp.3248–3258.

Schmitz, G., Lepper, H. & Estler, C.-J., 2018. Failure of Calcium Antagonistic Agents to Prevent Hepatotoxicity Induced by Diclofenac. *Pharmacology & Toxicology*, 77(1), pp.32–35. Available at: https://doi.org/10.1111/j.1600-0773.1995.tb01910.x.

Segat, D. et al., 2011. Proinflammatory effects of bare and PEGylated ORMOSIL-, PLGA- and SUV-NPs on monocytes and PMNs and their modulation by f-MLP. *Nanomedicine*, 6(6), pp.1027–1046. Available at: http://www.futuremedicine.com/doi/10.2217/nnm.11.30.

Semete, B. et al., 2010. In vivo evaluation of the biodistribution and safety of PLGA nanoparticles as drug delivery systems. *Nanomedicine: Nanotechnology, Biology, and Medicine*, 6(5), pp.662–671. Available at: http://dx.doi.org/10.1016/j.nano.2010.02.002 [Accessed December 5, 2014].

Semete, B. et al., 2010. In vivo uptake and acute immune response to orally administered chitosan and PEG coated PLGA nanoparticles. *Toxicology and Applied Pharmacology*, 249(2), pp.158–165. Available at: http://dx.doi.org/10.1016/j.taap.2010.09.002.

Senthilkumar, M., Mishra, P. & Jain, N.K., 2008. Long circulating PEGylated poly(D,L-lactide-co-glycolide) nanoparticulate delivery of Docetaxel to solid tumors. *Journal of drug targeting*, 16(5), pp.424–435.

Serda, R.E. et al., 2010. Logic-embedded vectors for intracellular partitioning, endosomal escape, and exocytosis of nanoparticles. *Small*, 6(23), pp.2691–2700.

Setyawati, M.I. et al., 2013. Cytotoxic and genotoxic characterization of titanium dioxide, gadolinium oxide, and poly(lactic-co-glycolic acid) nanoparticles in human fibroblasts. *Journal of Biomedical Materials Research - Part A*, 101 A(3), pp.633–640.

Sevimli, S. et al., 2015. The endocytic pathway and therapeutic efficiency of doxorubicin conjugated cholesterol-derived polymers. *Biomaterials science*, 3(2), pp.323–35. Available at: http://www.ncbi.nlm.nih.gov/pubmed/26218123.

Seyednejad, H. et al., 2011. Functional aliphatic polyesters for biomedical and pharmaceutical applications. *Journal of Controlled Release*, 152(1), pp.168–176. Available at: http://dx.doi.org/10.1016/j.jconrel.2010.12.016.

Shang, L. et al., 2011. One-Pot Synthesis of Near-Infrared Fluorescent Gold Clusters for Cellular Fluorescence Lifetime Imaging. *Small*, 7(18), pp.2614–2620.

Shareia A. et al., 2009. Plasma membrane recovery kinetics of a microfluidic intracellular

delivery platform. , 6(4), pp.247–253.

Sharma, S. et al., 2015. PLGA-based nanoparticles: A new paradigm in biomedical applications. *Trends in analytical chemistry*, 80, pp.30–40. Available at: http://dx.doi.org/10.1016/j.trac.2015.06.014.

Sharma, V., Anderson, D. & Dhawan, A., 2012. Zinc oxide nanoparticles induce oxidative DNA damage and ROS-triggered mitochondria mediated apoptosis in human liver cells (HepG2). *Apoptosis*, 17(8), pp.852–870.

Sheng, Y. et al., 2009. Long-circulating polymeric nanoparticles bearing a combinatorial coating of PEG and water-soluble chitosan. *Biomaterials*, 30(12), pp.2340–2348. Available at: http://dx.doi.org/10.1016/j.biomaterials.2008.12.070.

Shu, S., Liu, X. & Korn, E.D., 2005. Blebbistatin and blebbistatin-inactivated myosin II inhibit myosin II-independent processes in Dictyostelium. *Proceedings of the National Academy of Sciences*, 102(5), pp.1472–1477. Available at: http://www.pnas.org/cgi/doi/10.1073/pnas.0409528102.

Shubayev, V.I., Pisanic, T.R. & Jin, S., 2009. Magnetic nanoparticles for theragnostics. *Advanced Drug Delivery Reviews*, 61(6), pp.467–477. Available at: http://dx.doi.org/10.1016/j.addr.2009.03.007.

Shyh-Dar Li and Leaf Huang, 2011. Stealth Nanoparticles: High Density but Sheddable PEG is a Key for Tumor Targeting. , 145(3), pp.178–181.

Silva, A.H. et al., 2016. Toxicity and inflammatory response in Swiss albino mice after intraperitoneal and oral administration of polyurethane nanoparticles. *Toxicology Letters*, 246, pp.17–27. Available at: http://dx.doi.org/10.1016/j.toxlet.2016.01.018.

Silva, M. dos S. et al., 2011. Paraquat-loaded alginate/chitosan nanoparticles: Preparation, characterization and soil sorption studies. *Journal of Hazardous Materials*, 190(1–3), pp.366–374. Available at: http://dx.doi.org/10.1016/j.jhazmat.2011.03.057.

Simon, J.A., 2006. Estradiol in micellar nanoparticles: the efficacy and safety of a novel transdermal drug-delivery technology in the management of moderate to severe vasomotor symptoms. *Menopause (New York, N.Y.)*, 13(2), pp.222–231.

Simon, M. et al., 2011. Titanium dioxide nanoparticles induced intracellular calcium homeostasis modification in primary human keratinocytes. Towards an *in vitro* explanation of titanium dioxide nanoparticles toxicity. *Nanotoxicology*, 5(2), pp.125–139. Available at:

http://www.tandfonline.com/doi/full/10.3109/17435390.2010.502979.

Sims, C.M. et al., 2017. Redox-active nanomaterials for nanomedicine applications. *Nanoscale*, 9(40), pp.15226–15251.

Singh, R. et al., 2006. Tissue biodistribution and blood clearance rates of intravenously administered carbon nanotube radiotracers. *Proceedings of the National Academy of Sciences*, 103(9), pp.3357–3362. Available at: http://www.pnas.org/cgi/doi/10.1073/pnas.0509009103.

Singh, R.P. & Ramarao, P., 2013. Accumulated polymer degradation products as effector molecules in cytotoxicity of polymeric nanoparticles. *Toxicological Sciences*, 136(1), pp.131–143.

Soenen, S.J. et al., 2014. The effect of nanoparticle degradation on poly(methacrylic acid)-coated quantum dot toxicity: The importance of particle functionality assessment in toxicology. *Acta Biomaterialia*, 10(2), pp.732–741. Available at: http://dx.doi.org/10.1016/j.actbio.2013.09.041.

Solar, P. et al., 2015. Multifunctional polymeric nanoparticles doubly loaded with SPION and ceftiofur retain their physical and biological properties. *Journal of Nanobiotechnology*, 13(1), pp.1–12.

Spek, S. et al., 2015. Characterisation of PEGylated PLGA nanoparticles comparing the nanoparticle bulk to the particle surface using UV/vis spectroscopy, SEC, 1H NMR spectroscopy, and X-ray photoelectron spectroscopy. *Applied Surface Science*, 347, pp.378–385. Available at: http://dx.doi.org/10.1016/j.apsusc.2015.04.071.

Spencer, N.Y. et al., 2013. Hepatocytes produce TNF- following hypoxia-reoxygenation and liver ischemia-reperfusion in a NADPH oxidase- and c-Src-dependent manner. *AJP: Gastrointestinal and Liver Physiology*, 305(1), pp.G84–G94. Available at: http://ajpgi.physiology.org/cgi/doi/10.1152/ajpgi.00430.2012.

Steinhardt, 1994. Cell membrane resealing by a vesicular mechanism similar to neurotransmitter release.

Stone, V. et al., 2000. Increased calcium influx in a monocytic cell line on exposure to ultrafine carbon black. *European Respiratory Journal*, 15(2), pp.297–303.

Stone, V., Johnston, H. & Schins, R.P.F., 2009. Development of *in vitro* systems for nanotoxicology: methodological considerations. *Critical Reviews in Toxicology*, 39(7), pp.613–626. Available at: http://www.tandfonline.com/doi/full/10.1080/10408440903120975.

Sun-Woong Kang, Eui Ri Cho, Oju Jeon, B.-S.K., 2007. The Effect of Microsphere Degradation Rate on the Efficacy of Polymeric Microspheres as Bulking Agents: An 18-Month Follow-Up Study. *Journal of biomedical materials research. Part B, Applied biomaterials*, 83(2), pp.340–344.

Sun, W. & Davis, P.B., 2010. Reducible DNA nanoparticles enhance in vitro gene transfer via an extracellular mechanism. *Journal of Controlled Release*, 146(1), pp.118–127. Available at: http://dx.doi.org/10.1016/j.jconrel.2010.04.031.

Svenson, S., 2015. The dendrimer paradox – high medical expectations but poor clinical translation. *Chem. Soc. Rev.*, 44(12), pp.4131–4144. Available at: http://dx.doi.org/10.1039/C5CS00288E.

Szelag, A. et al., 2003. Influence of nifedipine, nitrendipine and verapamil at low concentration on antipyrine metabolism examined by extracorporeal rat liver perfusion Multidrug resistance in chronic lymphocytic leukemia. *Polish Journal of Pharmacology*, 55(2), pp.203–208. Available at: https://www.scopus.com/inward/record.uri?eid=2-s2.0-39349085570%7B&%7DpartnerID=40%7B&%7Dmd5=1848da9ad076ee42d74ef3ea809f6091.

Tabuchi, S. et al., 2000. Regulation of genes for inducible nitric oxide synthase and urea cycle enzymes in rat liver in endotoxin shock. *Biochemical and Biophysical Research Communications*, 268(1), pp.221–224.

Takae, S. et al., 2008. PEG-Detachable Polyplex Micelles Based on Disulfide-Linked Block Catiomers as Bioresponsive Nonviral Gene Vectors. *Journal of the American Chemical Society*, 130(18), pp.6001–6009. Available at: http://dx.doi.org/10.1021/ja800336v.

Tang, L. et al., 2009. Shell-Detachable Micelles Based on Disulfide-Linked Block Copolymer As Potential Carrier for Intracellular Drug Delivery Shell-Detachable Micelles Based on Disulfide-Linked Block Copolymer As Potential Carrier for Intracellular Drug Delivery. , pp.1095–1099.

Tang, W. et al., 2012. The cadmium-mercaptoacetic acid complex contributes to the genotoxicity of mercaptoacetic acid-coated CdSe-core quantum dots. *International Journal of Nanomedicine*, 7, pp.2631–2640.

Tenzer, S. et al., 2013. Rapid formation of plasma protein corona critically affects nanoparticle pathophysiology. *Nature Nanotechnology*, 8(10), pp.772–781.

Available at: http://www.nature.com/doifinder/10.1038/nnano.2013.181.

Terasaki, M., Miyake, K. & Mcneil, P.L., 1997. Large Plasma Membrane Disruptions Are Rapidly Resealed by Ca 2 + -dependent Vesicle–Vesicle Fusion Events. , 139(1), pp.63–74.

Thach, C.T. & Finkelstein, J.N., 2013. Cationic nanoparticles disrupt cellular signaling in a cholesterol dependent manner. *Toxicology in Vitro*, 27(4), pp.1277–1286. Available at: http://dx.doi.org/10.1016/j.tiv.2012.12.021.

Tkachenko, A.G. et al., 2003. Multifunctional gold nanoparticle-peptide complexes for nuclear targeting. *Journal of the American Chemical Society*, 125(16), pp.4700–4701.

Tobío, M. et al., 2000. The role of PEG on the stability in digestive fluids and in vivo fate of PEG-PLA nanoparticles following oral administration. *Colloids and Surfaces B: Biointerfaces*, 18(3–4), pp.315–323.

Tolosa, L. et al., 2012. Development of a multiparametric cell-based protocol to screen and classify the hepatotoxicity potential of drugs. *Toxicological Sciences*, 127(1), pp.187–198.

Trump, B.F. et al., 1984. Cell calcium, cell injury and cell death. *Environmental health perspectives*, 57, pp.281–287.

Tsai, R.K. & Discher, D.E., 2008. Inhibition of "self" engulfment through deactivation of myosin-II at the phagocytic synapse between human cells. *Journal of Cell Biology*, 180(5), pp.989–1003.

Tsai, T.H. & Liu, M.C., 2004. Determination of extracellular hesperidin in blood and bile of anaesthetized rats by microdialysis with high-performance liquid chromatography: A pharmacokinetic application. *Journal of Chromatography B: Analytical Technologies in the Biomedical and Life Sciences*, 806(2), pp.161–166.

Tulinska, J. et al., 2015. Immunotoxicity and genotoxicity testing of PLGA-PEO nanoparticles in human blood cell model. *Nanotoxicology*, 9(S1), pp.33–43. Available at: http://www.ncbi.nlm.nih.gov/pubmed/23859252.

Ul Ain, Q. et al., 2017. Amelioration of atherosclerotic inflammation and plaques via endothelial adrenoceptor-targeted eNOS gene delivery using redox-sensitive polymer bearing L-arginine. *Journal of Controlled Release*, 262(June), pp.72–86. Available at: http://dx.doi.org/10.1016/j.jconrel.2017.07.019.

Umegaki, K. & Fenech, M., 2000. Cytokinesis-block micronucleus assay in WIL2-NS

cells: a sensitive system to detect chromosomal damage induced by reactive oxygen species and activated human neutrophils. *Mutagenesis*, 15(3), pp.261–269. Available at: http://www.mutage.oupjournals.org/cgi/doi/10.1093/mutage/15.3.261.

Underhill, D. & Ozinsky, A., 2002. PHAGOCYTOSIS OF MICROBES: Complexity in Action. *Annual review of immunology*, 20(1), pp.825–852. Available at: http://arjournals.annualreviews.org/doi/abs/10.1146/annurev.immunol.20.103001.114744%5Cnpapers2://publication/uuid/4DBAAF71-54AF-4E3C-9B6A-1CC75560DCA7.

Vasconcelos, A. et al., 2015. Conjugation of cell-penetrating peptides with poly(Lactic-co-glycolic acid)-polyethylene glycol nanoparticles improves ocular drug delivery. *International Journal of Nanomedicine*, 10, pp.609–631.

Venkataraman, S. et al., 2011. The effects of polymeric nanostructure shape on drug delivery. *Advanced Drug Delivery Reviews*, 63(14–15), pp.1228–1246. Available at: http://dx.doi.org/10.1016/j.addr.2011.06.016.

Vidal, A.E. et al., 2001. Mechanism of stimulation of the DNA glycosylase activity of hOGG1 by the major human AP endonuclease: bypass of the AP lyase activity step. *Nucleic Acids Research*, 29(6), pp.1285–1292. Available at: https://academic.oup.com/nar/article-lookup/doi/10.1093/nar/29.6.1285.

Vihola, H. et al., 2005. Cytotoxicity of thermosensitive polymers poly(N-isopropylacrylamide), poly(N-vinylcaprolactam) and amphiphilically modified poly(N-vinylcaprolactam). *Biomaterials*, 26(16), pp.3055–3064.

Wagner, R.D. et al., 2017. Polyethylene glycol-functionalized poly (lactic acid-co-glycolic acid) and graphene oxide nanoparticles induce pro-inflammatory and apoptotic responses in Candida albicansinfected vaginal epithelial cells. *PLoS ONE*, 12(4), pp.1–21.

Wan, R. et al., 2017. Cobalt nanoparticles induce lung injury, DNA damage and mutations in mice. *Particle and Fibre Toxicology*, 14(1), pp.1–15.

Wang, J. et al., 2007. Acute toxicity and biodistribution of different sized titanium dioxide particles in mice after oral administration. *Toxicology Letters*, 168(2), pp.176–185.

Wang, T. et al., 2016. Biodegradable Self-Assembled Nanoparticles of Galactose-Containing Amphiphilic Triblock Copolymers for Targeted Delivery of Paclitaxel to HepG2 Cells. *Macromolecular Bioscience*, 16(5), pp.774–783.

Wang, T. et al., 2012. Cellular uptake of nanoparticles by membrane penetration: A study

combining confocal microscopy with FTIR spectroelectrochemistry. *ACS Nano*, 6(2), pp.1251–1259.

Wang, Y.C. et al., 2011. Redox-responsive nanoparticles from the single disulfide bond-bridged block copolymer as drug carriers for overcoming multidrug resistance in cancer cells. *Bioconjugate Chemistry*, 22(10), pp.1939–1945.

Watts, P. et al., 1995. The influence of medium composition on the maintenance of cytochrome P-450, glutathione content and urea synthesis: a comparison of rat and sheep primary hepatocyte cultures. *Journal of Hepatology*, 23(5), pp.605–612.

Weissig, V., Pettinger, T.K. & Murdock, N., 2014. Nanopharmaceuticals (part 1): products on the market. *International journal of nanomedicine*, 9, pp.4357–4373.

Westedt, U. et al., 2007. Poly(vinyl alcohol)-graft-poly(lactide-co-glycolide) nanoparticles for local delivery of paclitaxel for restenosis treatment. *Journal of Controlled Release*, 119(1), pp.41–51.

Wheeler, M.D. et al., 2001. Overexpression of Manganese Superoxide Dismutase Prevents Alcohol-induced Liver Injury in the Rat. *Journal of Biological Chemistry*, 276(39), pp.36664–36672.

Wibroe, P.P. et al., 2016. An integrated assessment of morphology, size, and complement activation of the PEGylated liposomal doxorubicin products Doxil®, Caelyx®, DOXOrubicin, and SinaDoxosome. *Journal of Controlled Release*, 221(2016), pp.1–8. Available at: http://dx.doi.org/10.1016/j.jconrel.2015.11.021.

Wignall, J.A. et al., 2014. Standardizing Benchmark Dose Calculations to Improve Science-Based Decisions in Human Health Assessments. , 122(5), pp.499–505.

Williams, M.D. et al., 1998. Increased Oxidative Damage Is Correlated to Altered Mitochondrial Function in Heterozygous Manganese Superoxide Dismutase Knockout Mice. , 273(43), pp.28510–28515.

Wilson, M., 2002. Interactions between Ultrafine Particles and Transition Metals in Vivo and in Vitro. *Toxicology and Applied Pharmacology*.

Win, K.Y. & Feng, S.-S., 2005. Effects of particle size and surface coating on cellular uptake of polymeric nanoparticles for oral delivery of anticancer drugs. *Biomaterials*, 26(15), pp.2713–2722.

Wu, C. & Chiu, D.T., 2013. Highly fluorescent semiconducting polymer dots for biology and medicine. *Angewandte Chemie (International ed. in English)*, 52(11), pp.3086–109. Available at: http://www.ncbi.nlm.nih.gov/pubmed/23307291 [Accessed

December 4, 2014].

Wuelfing, W.P. et al., 1998. Nanometer gold clusters protected by surface-bound monolayers of thiolated poly(ethylene glycol) polymer electrolyte. *Journal of the American Chemical Society*, 120(48), pp.12696–12697.

Xiao, J.Q. et al., 2013. Administration of IL-1Ra chitosan nanoparticles enhances the therapeutic efficacy of mesenchymal stem cell transplantation in acute liver failure. *Archives of Medical Research*, 44(5), pp.370–379. Available at: http://dx.doi.org/10.1016/j.arcmed.2013.06.004.

Xiong, S. et al., 2015. Size influences the cytotoxicity of poly (lactic-co-glycolic acid) (PLGA) and titanium dioxide (TiO2) nanoparticles Sijing. *Anal Chem.*, 25(4), pp.368–379.

Xu, J. et al., 2013. Acute Toxicity of Intravenously Administered Titanium Dioxide Nanoparticles in Mice. *PLoS ONE*, 8(8), pp.1–6.

Yamani, N. El et al., 2017. In vitro genotoxicity testing of four reference metal nanomaterials , titanium dioxide , zinc oxide , cerium oxide and silver : towards reliable hazard assessment. , (November 2016), pp.117–126.

Yang, A. et al., 2010. Influence of polyethyleneglycol modification on phagocytic uptake of polymeric nanoparticles mediated by immunoglobulin G and complement activation. *Journal of nanoscience and nanotechnology*, 10(1), pp.622–628.

Yang, C. et al., 2017. Impact of PEG Chain Length on the Physical Properties and Bioactivity of PEGylated Chitosan/siRNA Nanoparticles in Vitro and in Vivo. *ACS Applied Materials and Interfaces*, 9(14), pp.12203–12216.

Yang, D., Yu, L. & Van, S., 2011. Clinically relevant anticancer polymer paclitaxel therapeutics. *Cancers*, 3(1), pp.17–42.

Yang, Y. et al., 2014. Cytotoxicity of gold nanoclusters in human liver cancer cells. *International Journal of Nanomedicine*, 9(1), pp.5441–5448.

Yao, K.S. et al., 1995. Evidence for altered regulation of g-glutamylcysteine synthetase gene expression among cisplatin-sensitive and cisplatin-resistant human ovarian cancer cell lines. *Cancer Research*, 55(19), pp.4367–4374.

Yeh, H.P. et al., 2018. A New Photosensitized Oxidation-Responsive Nanoplatform for Controlled Drug Release and Photodynamic Cancer Therapy. *ACS applied materials & interfaces*, 10, p.acsami.8b05205. Available at: http://pubs.acs.org/doi/10.1021/acsami.8b05205%0Ahttp://www.ncbi.nlm.nih.gov/

pubmed/29863836.

Yokoyama, M. et al., 1990. Characterization and Anticancer Activity of the Micelle-forming Polymeric Anticancer Drug Adriamycin-conjugated Poly (ethylene glycol) -Poly (aspartic acid) Block Copolymer Characterization. *Cancer research*, 15(6), pp.1693–1700. Available at: http://cancerres.aacrjournals.org/content/50/6/1693%5CnE-mail.

Yoo, H.S. & Park, T.G., 2001. Biodegradable polymeric micelles composed of doxorubicin conjugated PLGA-PEG block copolymer. *Journal of Controlled Release*, 70(1–2), pp.63–70.

Yu, D. et al., 2014. Influence of surface coatings of poly(d,l-lactide-co-glycolide) particles on HepG2 cell behavior and particle fate. *Biointerphases*, 9(3), p.031015. Available at: http://avs.scitation.org/doi/10.1116/1.4894531.

Yu, J. et al., 2011. Effects of physicochemical properties of zinc oxide nanoparticles on cellular uptake. *Journal of Physics: Conference Series*, 304(1).

Yu, M. et al., 2012. Dextran and Polymer Polyethylene Glycol (PEG) Coating Reduce Both 5 and 30 nm Iron Oxide Nanoparticle Cytotoxicity in 2D and 3D Cell Culture. *International Journal of Molecular Sciences*, 13(12), pp.5554–5570. Available at: http://www.mdpi.com/1422-0067/13/5/5554/.

Yukawa, H. et al., 2014. Novel positively charged nanoparticle labeling for in vivo imaging of adipose tissue-derived stem cells. *PLoS ONE*, 9(11).

Zhang, L. & Eisenberg, A., 1995. Multiple Morphologies of "Crew-Cut" Aggregates of Polystyrene-b-poly (acrylic acid) Block Copolymers. *Science*, 268(5218), pp.1728–1731. Available at: http://www.sciencemag.org/content/268/5218/1728.short.

Zhang, Q. et al., 1998. Increase in gentamicin uptake by cultured mouse peritoneal macrophages and rat hepatocytes by its binding to polybutylcyanoacrylate nanoparticles. *International Journal of Pharmaceutics*, 164(1–2), pp.21–27.

Zhang, Q. et al., 2011. Uptake of gold nanoparticles in murine macrophage cells without cytotoxicity or production of pro-inflammatory mediators. *Nanotoxicology*, 5(September), pp.284–295.

Zhang, T. et al., 2014. Cytotoxic potential of silver nanoparticles. *Yonsei Medical Journal*, 55(2), pp.283–291.

Zhang, T. et al., 2015. Liver toxicity of cadmium telluride quantum dots (CdTe QDs) due to oxidative stress in vitro and in vivo. *International Journal of Molecular Sciences*,

16(10), pp.23279–23299.

Zucker, D. et al., 2012. Characterization of PEGylated nanoliposomes co-remotely loaded with topotecan and vincristine: Relating structure and pharmacokinetics to therapeutic efficacy. *Journal of Controlled Release*, 160(2), pp.281–289. Available at: http://dx.doi.org/10.1016/j.jconrel.2011.10.003.

Žuvić-Butorac, M. et al., 2005. EPR study of lipid phase in renal cortical membrane organelles from intact and cadmium-intoxicated rats. *Biochimica et Biophysica Acta - Biomembranes*, 1718(1–2), pp.44–52.

van der Zwaag, D. et al., 2016. Super Resolution Imaging of Nanoparticles Cellular Uptake and Trafficking. *ACS Applied Materials & Interfaces*, p.acsami.6b00811. Available at: http://pubs.acs.org/doi/abs/10.1021/acsami.6b00811.